Multi-Component Crystalline Systems based on Supramolecular Networks

A thesis presented for the degree of

Doctor of Philosophy

in the Faculty of Science

of the University of Strathclyde

by

Syed Atif Raza

Strathclyde Institute of Pharmacy and Biomedical Sciences

September, 2014

This thesis is a result of author's original research. It has been composed by the author and has not been previously submitted for an examination that has led to the award of a degree**.**

Signed:

Date:

Dedicated to my parents and wife Wajiha

Abstract

A series of selected essential hydrophobic amino acids, L-Valine, L-Leucine and L-Isoleucine were studied to prepare novel co-crystalline forms for comparison with their pure forms. The crystals of these amino acid complexes were characterised by various techniques including spectroscopy, thermal and X-ray diffraction. The analysis has confirmed the formation of three new co-crystals of L-Leucine-L-Isoleucine (compound 1), L-Valine-L-Leucine (compound 2) and L-Valine-L-Isoleucine (compound 3), the first co-crystals of naturally occurring hydrophobic amino acids with the same chirality.

The second experimental chapter describes the use of a Continuous Stirred Tank Crystalliser (CSTC) for bulk preparation of a multi-component system via an anti-solvent crystallisation process. The results indicate that the process conditions used to fabricate co-crystals of amino acids with anti-solvent crystallisation are reproducible with regard to the final product properties, purity and yield.

In the last theme, a host-guest complex is shown wherein the c(RGDfV), a cyclic pentapeptide [c(ArgGlyAspD-PheVal], forms an inclusion complex with β-cyclodextrin. In addition, the batch to batch variation between two batches of the pentapeptide procured from the same source is highlighted. The c(RGDfV) and the inclusion complex were characterised by differential scanning calorimetry, fourier transform infrared spectroscopy, circular dichroism, powder X-ray diffraction and nuclear magnetic resonance spectroscopy. Based on ^{1}H nuclear magnetic resonance (NMR) experiments, the possible mode of interaction of betacyclodextrin with the c(RGDfV) is proposed. Different methods to crystallise c(RGDfV) batch (B-1) and its self-assembly to form hydrogel is also presented.

Acknowledgments

I owe my deepest regards to my supervisor, Dr. Iain D.H. Oswald who was always there for encouragement, supervision and support from the day one and helped me to understand the subject. I am also obliged to Professor Alastair Florence for providing me the lab facilities to my satisfaction.

I am grateful to my second supervisor, Dr Dimitrios Lamprou for his support, guidance and sense of humour. My special thanks to Dr. Andrew Urquhurt and Dr. Jhon Obaji Igoli, Professor Alexander Gray for their valuable discussions and support in analysis of materials by AFM and NMR techniques respectively. I am grateful to Lisa McIntosh for helping me out with CD spectroscopy experiments and Naomi Briggs, Rajni Miglani for their assistance in powder X-ray diffraction studies. My sincere thanks are due to Ulrich Schacht and Jan Scfcik for collaboration for scale up of Amino acid co-crystals experiments and for their valuable comments and encouragements.

I am also thankful to Amit Delori and Ian Hutchison for their participation and inputs in group discussions. In addition, I would like to acknowledge all members of my research group, as well as faculty and staff for providing a friendly space and making my time in SIPBS so pleasing and memorable.

Financial support from University of the Punjab, Lahore, Pakistan is gratefully acknowledged.

And finally, my deepest regard and love to my family and friends who supported me throughout the years of studies.

Table of Contents

List of Figures

List of Tables

Abbreviations

AFM	Atomic force microscopy
API	Active pharmaceutical ingredient
β-CD	β-cyclodextrin
BCS	Biopharmaceutical Classification System
CIF	Crystallographic information file
COSY	Correlation Spectroscopy
c(RGDfV)	Cyclo[Arg-Gly-Asp-D-Phe-Val]
CSD	Cambridge Structural Database
DMF	Dimethylformamide
DMSO	Dimethylsulfoxide
DSC	Differential scanning calorimetry
FTIR	Fourier transform infrared spectroscopy
HMQC	Heteronuclear Multiple Quantum Coherence
MOF	Metallic organic frameworks
MRME	Mean residue molar ellipticity
MRW	Mean residue weight
MSMPR	Mixed-suspension, mixed-product removal
NMR	Nuclear magnetic resonance
NOESY	Nuclear Overhauser effect spectroscopy
OBC	Oscillatory baffled crystallisers
PFR	Plug flow reactors
PTFE	Polytetrafluoroethylene
PXRD	powder X-ray diffraction
SXD	Single crystal X-ray diffraction
TGA	Thermogravimetric analysis

CHAPTER 1

Introduction

1.1. Supramolecular Chemistry

Two American researchers Dr. Donald J. Cram, Dr. Charles J. Pedersen and a French scientist Dr. Jean-Marie Lehn established a field that exploits the fundamental role of the three dimensional shapes of molecules to their chemical and biological functions. They were awarded a Nobel prize and have laid the foundations of one of the vibrant and growing areas of research for which Lehn had suggested the term "supramolecular chemistry" (*Lehn, 1978*).

Supramolecular chemistry or "chemistry beyond the molecule" (*Steed and Atwood, 2000*) emphasizes the chemical systems that are developed from the assembly of two or more chemical entities held together by the weaker and reversible non-covalent interactions. Some of the non-covalent interaction types or bonding with their strength is summarised in Table 1.1 (*Hoeben et al, 2005*). The application of the important concepts in supramolecular networks like self-assembly, host-guest molecular recognition, mechanically-interlocked molecular structures, and dynamic covalent chemistry have made this field fascinating and a constantly expanding area of research (*Oshovsky, et al., 2007).*

Further, understanding non-covalent interactions (*El Kerdawy, et al., 2012*) which are vital in demonstrating many biological phenomena that depend on these intermolecular forces for structural organisation and specific function have generally laid the foundation for supramolecular research.

Table 1.1 Non-covalent intermolecular forces with their bonding strength.

Interaction Type	Energy (kJ/mol)
Hydrogen bonding	10 - 65
Dipole - Dipole	0 - 50
Hydrophobic effect	4 - 8
pi-pi interactions	0 - 50
van der Waals forces	< 5

A well-selected and thoughtful combination of supramolecular species often transforms a single component system with new and fascinating properties and performance when compared with the parent components. For example a 1:1 co-crystal (for definition of co-crystal see section 1.3.3) of indomethacin and saccharin has shown improved in vitro dissolution behaviour and bioavailability profile of the active pharmaceutical ingredient (API), indomethacin, in dogs (*Jung, et al., 2010*). Similarly, co-crystals of paracetamol with oxalic acid, naphthalene, theophylline and phenazine (*Karki, et al., 2009*) have better mechanical properties compared to pure paracetamol (Figure 1.1) thus offering a route to prepare new compressible forms of crystalline solids.

The chapter will briefly describe only those concepts related to supramolecular chemistry which are addressed in the experimental chapters of the thesis.

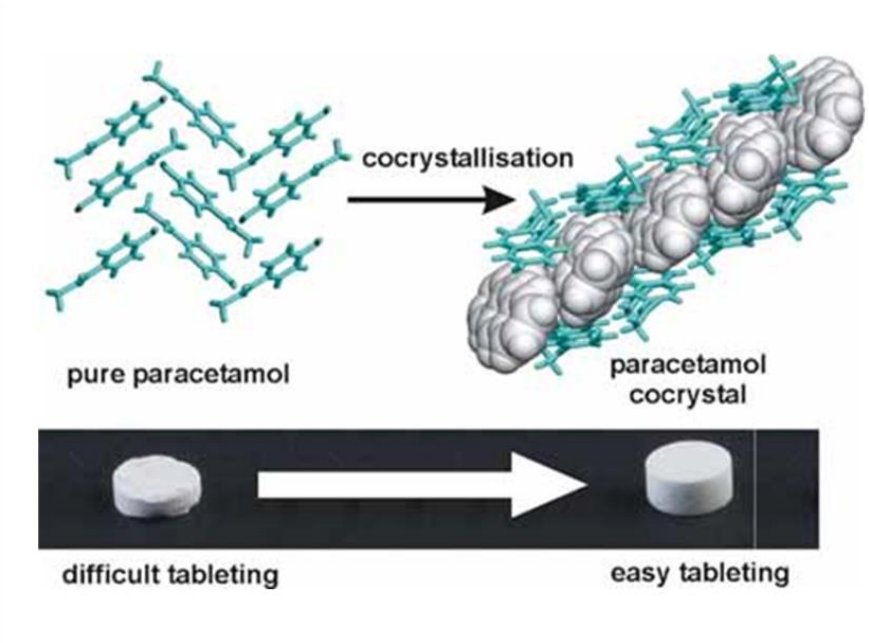

Figure 1.1 Co-crystal formation showing improved mechanical properties of paracetamol (*Karki et al., 2009*).

1.2. Molecular self-assembly

Molecular self-assembly is the heart core concept in the area of supramolecular chemistry (*Lehn, 1988*). It is a self-triggered phenomenon guided through noncovalent interaction by which molecules adopt a defined arrangement. The molecular self-assembly process can also be altered or induced in materials by provision of suitable thermodynamic and environmental controls (*Dhotel, et al., 2013*).

Generally the molecular self-assembly is classified in two categories. These are **intermolecular self-assembly** (Figure1.2a) and **intramolecular self-assembly** (Figure 1.2b). Molecular self-assembly is the basis of crystal engineering (which will be discussed in section 1.3.2) and also permits the formation of

superstructures such as micelles, membranes, vesicles and liquid crystals (*Ariga, et al., 2008*; *Rosen, 2004*).

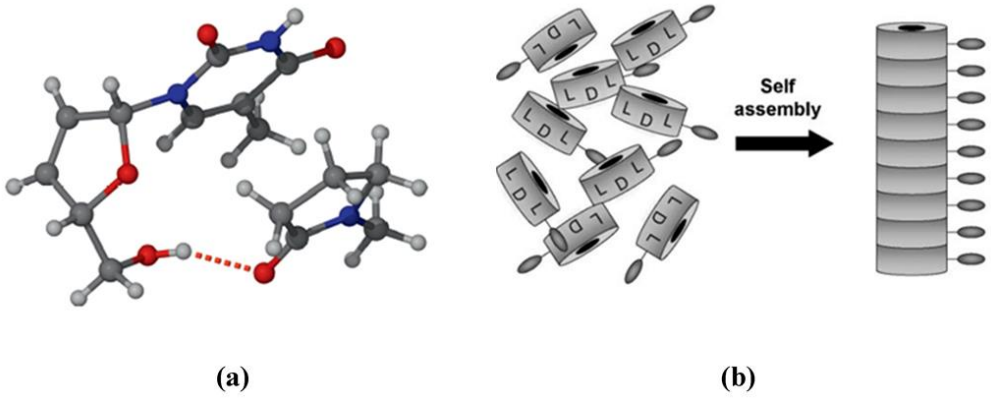

Figure 1.2 a). Co-crystal 1:1 stavudine N-methyl-2-pyrrolidinone (*Viterbo, 2000*) b). The specific assembly of alternating D- and L-amino acid cyclic peptide resulting in nanotubes (*Gazit, 2007*).

1.3. Crystalline solids

The properties such as physico-chemical, mechanical, pharmaceutical and therapeutic, etc., are often affected by the solid state of a compound (*Singhal, 2004*). Understanding crystal structure of the compound and intermolecular forces, especially the non-covalent bonding, give knowledge about the behaviour and the way of their interaction with similar and other types of molecules. The crystal structures are important and a direct method to unveil the information regarding chemical identity, molecular assembly and intermolecular interactions (*McKellar, 2012*). The three dimensional crystal structure provides a wealth of information in determining a suitable solid state form essential for an active pharmaceutical ingredient during the pre-clinical

drug development (*Cairns, 2009*), structure based drug design (*Ma, et al, 2013*) and bulk properties of the materials (*Upadhyay, et al, 2013*).

The solid state commonly exists in two forms which are generally recognised as amorphous substances and crystalline substances (Figure 1.3).

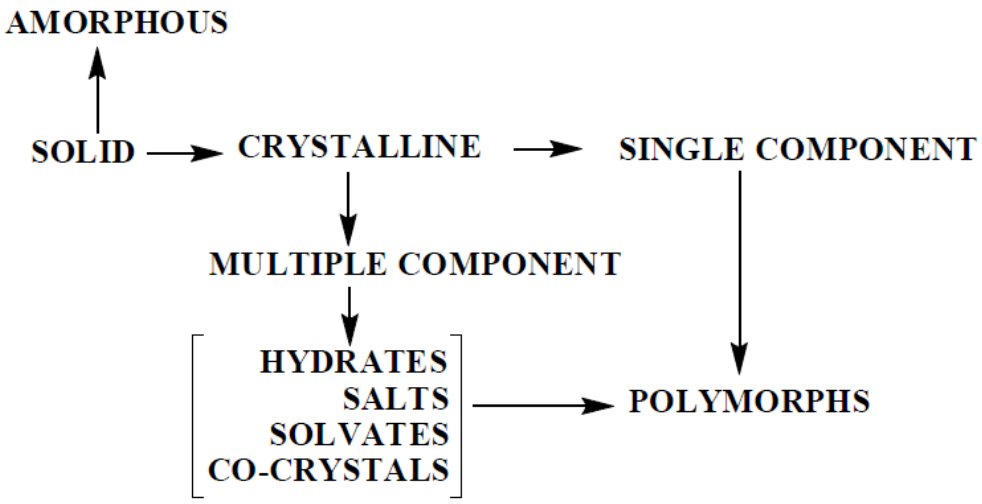

Figure 1.3 Solid form classification (*Sekhon, 2009*).

The amorphous state of a solid is regarded as a disordered material or a non-crystalline solid form which lack systematic long order arrangement of atoms and molecules in its structure (*Zallen, 1998).* Amorphous substances generally have high solubility, dissolution rate and bioavailability as compared to their crystalline counterparts making them ideal for pharmaceutical products but stabilising these products during various manufacturing processes and storage over a period of time can be quite difficult (*Alonzo et al., 2010*).

Crystalline forms are classified into one-component phase and multi-component phases (Figure 1.4) like solvate and hydrate (*Khankari & Grant,*

1995), salt (*Stahl and Wermuth,* 2002), eutectics (*Cherukuvada and Nangia 2014*) and co-crystal forms (*Desiraju 2013; Steed 2013; Aitipamula et al., 2012; Stahly, 2007*), where the rearrangement of the crystal packing is largely due to hydrogen bonding and other weak intermolecular forces. The covalent bonding between atoms and molecules is not altered but there is a probability to have polymorphs of single component or the multi-component phases. (*Aitipamula et al., 2014*).

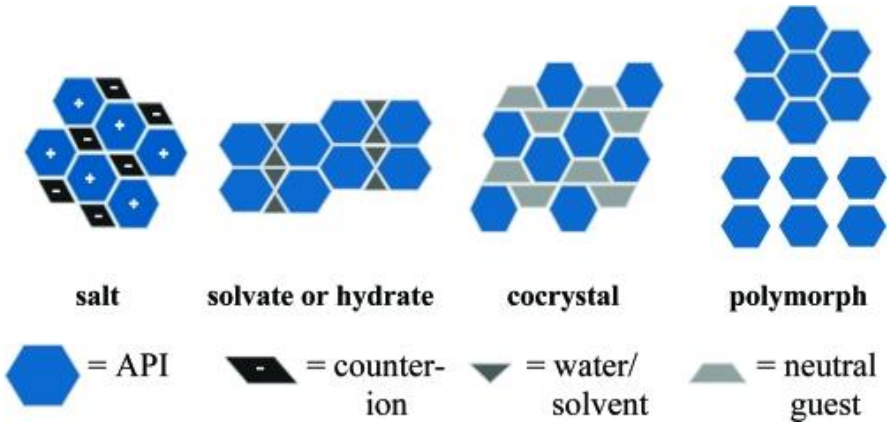

Figure 1.4 Common solid-state single and multi-component forms. (*Schultheiss and Newman, 2009*).

1.3.1. Polymorphism

Pharmaceutical manufacturers and researchers are keen to develop and design new pharmaceutical materials in order to overcome many challenges like drug solubility, stability and other pharmaceutical properties. It has been established that many substances exhibit a property to adopt more than one crystalline structure with the same chemical composition. This property of the substance is termed polymorphism (*Brittain, 2008*). Scientists are now realising the words

of wisdom which were shared by W.C. Mcrone in the early sixties regarding the importance of the phenomenon of polymorphism in research and agree with his statement "The numbers of crystalline forms or polymorphs that can be known of a compound are proportional to the time and resources dedicated to the investigation of them" *(as cited by Bernstein, 2002*).

Over the last three decades there has been an increasing awareness of the importance of polymorphism such that there has been an increasing number of reviews and monographs covering various topics of polymorphism, particularly in the area of pharmaceuticals. (*Rodrıguez-Spong, et al., 2004; Gavezzotti, 2007; Nangia, 2008; Brittan, 2010; Sarma et. al., 2011; Aitipamula et al, 2014*). The phenomenon also has a substantial impact on the economic and intellectual property issues relating to pharmaceutical products (*Trask, 2007*). For many reasons, further investigation of polymorphism is still required to understand this phenomenon and hence to control the crystallisation of a specific desired form (*Roy & Matzger, 2009*).

Polymorphism in materials has always motivated various industries like pharmaceutical, agrochemical, pigments, dyes, energetic materials and nutraceuticals etc., to identify an optimal physical form with desirable properties. The term active pharmaceutical ingredient (API) is mostly used by pharmaceutical manufacturers to represent a pharmacologically active drug substance (*Gardner, et al.,2004; Fabbiani, 2010*) and the physico-chemical studies of such substances is crucial and of considerable interest for the community for many decades to overcome the issues related with drug

stability, manufacturing, regulation, marketing and dealing with the issues of patent protection.(*Byrn, et al.,1995; Hilfiker, 2006; Steed, 2013*).

Polymorphs due to dissimilarity in their ionic or molecular assembly may experience different intermolecular forces and the crystal structures themselves will have different crystal energies (*Surov et al. 2014*). These structural differences or packing of molecules in crystals can cause an alteration in the physico- chemical properties of the material and can be directly related to drug substance and dosage form design including processing and manufacturing leading to a significant impact on product quality / performance like stability, dissolution, and bioavailability (*Gonzalez, et al., 2014*). Conversion of a desirable polymorphic form into an undesirable polymorphic form may cause an unnecessary delay in the product development, production suspension or it may end up in a situation leading to a product recall. Ritonavir, an antiviral compound used for the treatment of Acquired Immunodeficiency Syndrome (AIDS), failed its dissolution test because a more thermodynamically stable polymorph was identified that had a lower solubility. This new polymorph dominated the bulk product as well as in the formulation causing serious problems in manufacturing as well as its availability in the market (*Bauer, et al., 2001).* In this case, Norvir® was recalled until a more stable formulation using the new polymorph was developed.

Most pharmaceutical manufacturers formulate and market their products in solid state and cannot overlook the phenomenon of polymorphism and therefore, during the drug development phase, have started screening the drug substance more rigorously to avoid any unwanted appearance of a polymorphic

form throughout its shelf life. The early level investigation regarding physical and chemical properties can bypass manufacturing problems and help in the advancement to new strategies to develop a refined drug substance. Many new polymorphs have been discovered for those drugs which are considered as having one solid form making it a rule of thumb to screen the possible polymorphs of an active pharmaceutical ingredient before dosage form design.

1.3.2. Crystal engineering

For a successful release of a drug to the market place, it is imperative to develop strategies to prepare a stable physical form with the desired physical, chemical and therapeutic properties. Scientists in industry and in the field of polymorphism desire to achieve this control over crystallisation by investigating various strategies and principles of polymorph screening (*Byrn, et al., 1995*) before the release of the drug to the market. Pharmaceutical scientists are trying to find a solution to this problem and are exploring crystal engineering as a tool to design and construct the drug substance with a predefined structure and physico-chemical properties. Crystal engineering may be defined as "the understanding of intermolecular interactions in the context of crystal packing and utilization of such understanding in the design of new solids with desired physical and chemical properties" (*Desiraju, 1989*). The knowledge of supramolecular chemistry and how it applies to crystal architecture is one of the gateways to design and optimise a crystal form of the active pharmaceutical substance (*Desiraju, 2013*).

Pharmaceutical scientists are looking at this phenomenon of crystal engineering as an opportunity to develop new drug forms comprising of interesting and novel properties.

The Biopharmaceutical Classification System (BCS) class II drugs when administered orally exhibit low aqueous solubility and unsteady bioavailability resulting in poor safety and efficacy profiles. Different strategies have been in use for improving the pharmaceutical properties of drugs with low aqueous solubility like salt formation, hydrates, solublisation and micellisation (*Blagden, et al., 2007*). Crystal engineering in recent times provided various routes for the improvement in physical and chemical properties of drugs belonging to this BCS class II.

Crystal engineering is an interplay of hydrogen bond and other noncovalent intermolecular interactions to hold together two or more entities to form a desirable structure and properties *(Roesky and Andruh, 2003; Desiraju, 2010).* Crystal engineering is a multidisciplinary adventure taking organic chemistry and material science in particular on board and providing solutions to tune the properties of the crystal. The basis of crystal engineering lies in molecular engineering (*Hippel, 1962*) and later been given a new way of approaching the concept and that is supramolecular synthons (*Desiraju, 1995*). This is a unique relationship in between two molecules based upon their intermolecular forces which is tailored to combine the two molecules in a somewhat controlled manner (*Lehn, 1988*). Various studies in pharmaceutical and material sciences in particular have reported crystal engineering as a successful methodology of

preparing co-crystals with enhanced and tailored properties (*Thakuria, et al., 2013; Millar, et al., 2012; Yan et al 2011*).

1.3.3. Co-crystal

According to FDA guidance notes 2013 which classify pharmaceutical co-crystals in regulatory perspective as "Co-crystals are solids that are crystalline materials composed of two or more molecules in the same crystal lattice". This is a broad definition and in the literature many terms such as hydrates, solvates, salts, molecular complexes or adducts, inclusion complex etc., which are used to represent more or less same category of chemical combination and can be grouped in a family of multi-component systems (*Morissette, et al., 2004*).

There is some difference of opinion related to the arguments of using the term co-crystal or molecular complex (*Dunitz, 2003; Desiraju, 2003*) for a multi-component class of crystalline substances which is formed in between an active drug substance, whose properties are tuned or modified to a desired level by making a complex, with the screened guest molecule generally by non-covalent intermolecular forces.

A generally adopted definition of co-crystals is "A cocrystal is a multiple component crystal in which all components are solid under ambient conditions when in their pure form" (*Shan and Zaworotko, 2008*) however, Bond, A.D., has highlighted various examples from the literature that deviate from the general definition of co-crystal in one way or other but regarded as co-crystals by the authors. Based on his arguments he emphasised on that, the term co-crystal is fading as a flawless and a constant scientific explanation to such

multi-component systems and suggested that the term should be used only as an alternative expression for ‘‘multi-component molecular crystal’’ (*Bond, 2007*).

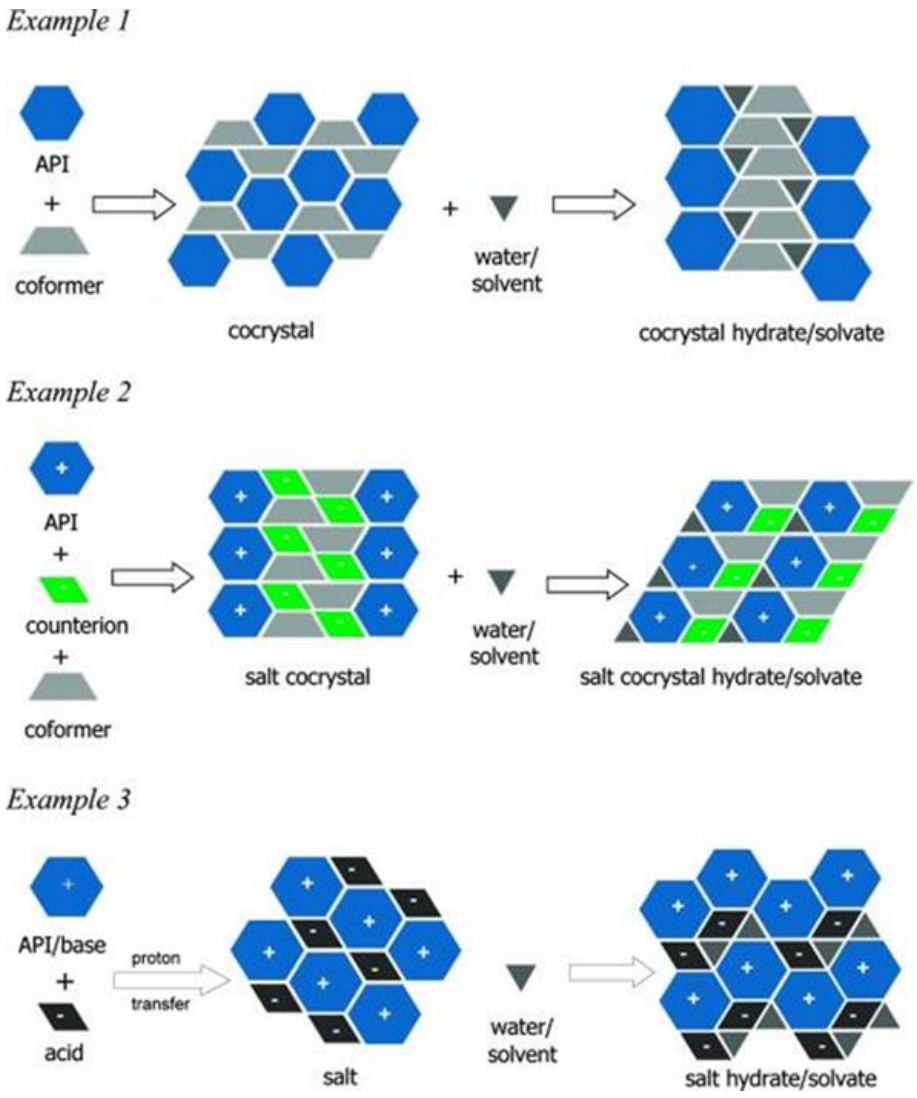

Figure 1.5 Examples of potential multi-component systems. (*Schultheiss and Newman, 2009*)

Schematic diagrams of three multi-component systems are presented in Figure 1.5. Literature still lacks a formal and universally accepted definition of co-

crystals despite being popular over the last few years. Many reviews and debates (*Aitipamula et al., 2012)* were initiated on its nomenclature and many researchers have postulated their version of co-crystal.

Beside all controversy we are interested in the formation of co-crystals or multicomponent systems. The main reason for preparing co-crystals or multi-component systems or molecular complexes is that these systems may change or alter physico-chemical or pharmaceutical properties such as crystal form, solubility, and stability etc. of a pharmacologically active ingredient without interfering in its pharmacological activity. For example various co-crystals of active pharmaceutical ingredients like itraconazole, norfloxacin, carbamazepine, meloxicam etc., have shown modification in dissolution profile when compared with their native state (*Thakuria, et al 2013*). In many other studies, co-crystal formation strategy illustrated the opportunity to give solution to issues related with physicochemical properties including solubility, stability and bioavailability (*Qiao, et al 2011*).

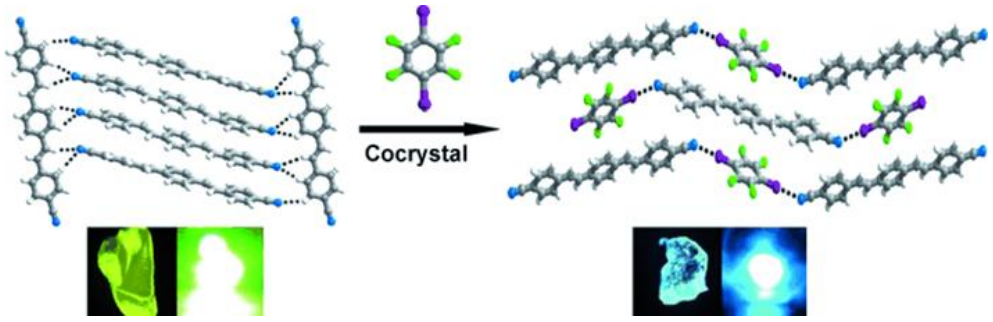

Figure 1.6 Co-crystal formation to change the optical properties of Stilbene type organic material (*Yan, et al., 2011*).

Co-crystallisation has also been exploited in material science to design or tune the properties of organic materials in solid state form for example in one case a supramolecular co-crystal method was successfully used to modify the optical properties of Stilbene derivatives (Figure 1.6) which are very attractive organic materials due to their optical and electrical properties (*Yan, et al., 2011*).

In another case, the crystal engineering approach presents a successful method to prepare energetic co-crystals of CL-20 (*Millar, et al., 2012*). The co-crystals highlighted the potential to fine tune the properties at the molecular level resulting in significant alteration in explosive performance of CL-20.

1.3.4. Supramolecular synthons and co-crystal design

Supramolecular systems through self-assembly from their entities into well organised "functional supramolecular architecture" (*Lehn, 1995*) provide a new route to construct novel materials (*Nangia, 2010*).

Supramolecular systems are the aggregates of molecules which are in contact with each other by noncovalent bonding like hydrogen bonds etc. and knowledge of these intermolecular forces, which direct molecular arrangement, geometry and conformation within the crystal is pivotal in co-crystal design, control and their applications. The supramolecular assembly can also be influenced by the size, shape (*Anderson, 2011*) and properties of the components in a co-crystal. The fundamental properties of specific intermolecular interactions can be used to design the three-dimensional ordered crystal structure. A strategy to design a co-crystal is with the use of a supramolecular synthon (*Desiraju, 1995; Merz. and Vasylyeva, 2010*), a

rational and objective liaison between supramolecular chemistry and organic synthesis. Supramolecular synthons are of the following two types (*Walsh, et al, 2003*);

1). Supramolecular homosynthons which involve similar self-complementary functional groups and

2). Supramolecular heterosynthons which are formed in between different but complementary functional groups.

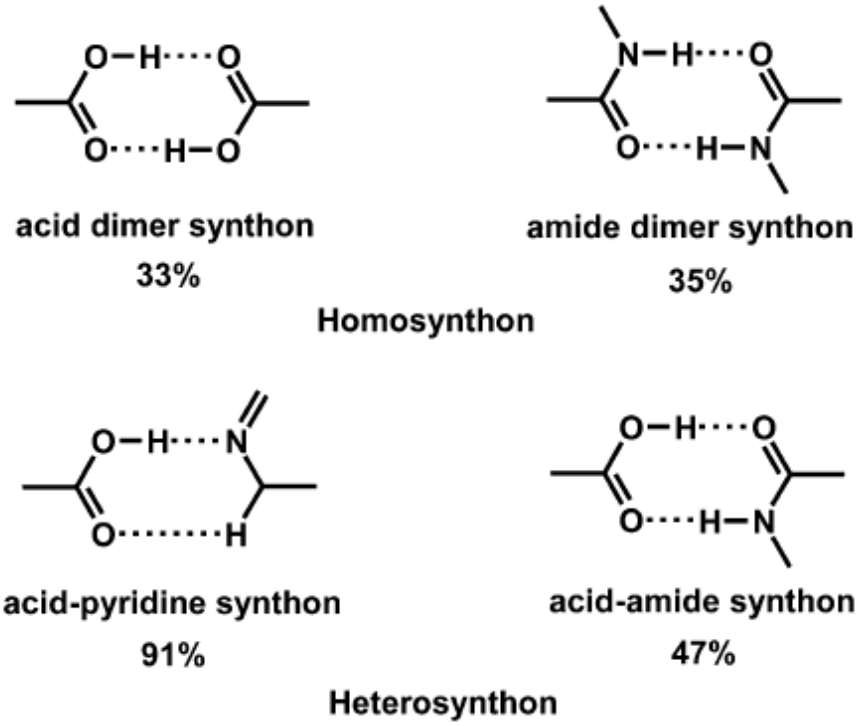

Figure 1.7 Examples showing likelihood of few supramolecular homosynthons and heterosynthons in the CSD (*Cherukuvada and Nangia 2014*).

Supramolecular homosynthons include the carboxylic acid and amide dimers whereas supramolecular heterosynthons include amide-acid, pyridine-hydroxyl

and pyridine-acid etc. Examples of a supramolecular homosynthons and heterosynthons are presented in Figure 1.7.

One can take advantage of the Cambridge Structural Database (*Groom and Allen, 2014*), a searchable repository of organic and inorganic crystal structures, to identify discrete and discontinuous structural units in a desired supermolecule that can be prepared from well-selected supramolecular synthons via co-crystallisation (*Wang, et al., 2014*). It is established based on CSD data that certain supramolecular synthons also called motifs (Figure 1.7) are more favourable within crystal structures compared to other less frequent patterns of interaction (*Cherukuvada and Nangia, 2014*).

The majority of patterns of interaction between molecules used in crystal engineering are constructed via non-covalent interactions like hydrogen bonding. The brief account of hydrogen bonding patterns has been extensively simplified by the using graph-set analysis to hydrogen bonding. The analysis is based on looking at the networking between molecules through hydrogen-bond motifs as very few parameters are required to explain the patterns of these hydrogen-bond motifs involved in networking (*Etter et al., 1990*).

A graph-set descriptor is written as Eq.1.1 (*Bernstein, et al., 1995*);

$$G^{a}_{d}(n) \qquad \text{Eq. 1.1}$$

Where,

G = the type of pattern, **a** = the number of hydrogen bond acceptors,
d = the number of donors, **n** = the number of atoms in the pattern.

There are four different types of pattern designator “G” namely, pattern “C” which represents an infinite chain, pattern “S” used for an intramolecular hydrogen bonding, “R” represent an intermolecular ring pattern and lastly pattern “D” narrate an interaction between two or more discrete entities.

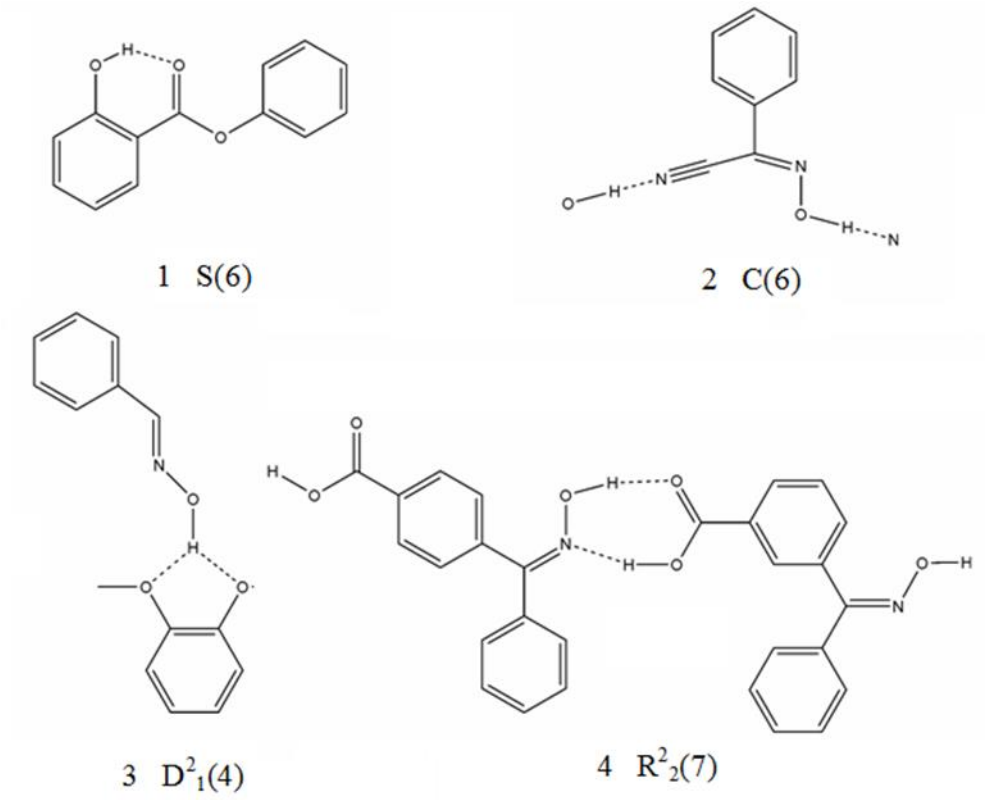

Figure 1.8 Hydrogen bonding pattern with the graph-set assignments.

Figure 1.8 presents each type of hydrogen bonding descriptor by an example (*Wood, 2008*) wherein, the intramolecular hydrogen bond pattern consisting of six atoms as in 1 would be specified as S(6) and similarly, the chain in 2 would be designated as C(6), for the six atoms involving the chain link pattern. In the

case, when there is only one donor and one acceptor in the motif generally, no subscript and superscript are specified. The letter D is designated to the hydrogen bond pattern when two or more distinct entities are involved as donor and acceptor as in 3 there is only one donor and two acceptors and graph set assignment would be given as $D^2_1(4)$. Lastly, the ring 4 as shown in the Figure 1.18. The pattern covers a total of seven atoms, consisting of two donors and two acceptors and therefore specified as $R^2_2(7)$.

1.3.6. Co-crystal preparation

In recent times many reviews have discussed co-crystal systems in general and that are of pharmaceutical interest in particular (*Brittain, 2012; Qiao, et al., 2011*). Various strategies have demonstrated successful routes for making co-crystals of API including slow evaporation, ultrasound (*Aher, 2010*), sublimation, solid state grinding (*Friscic and Jones, 2009; Delori, et al., 2012*), and solvent-drop grinding (*Friscic, et al., 2009*). A co-crystal of sulfamethazine and theophylline in a 2:1 molar ratio can be prepared by slow evaporation (*Lu and Rohani, 2010*). Solvent-drop grinding techniques proved to be successful in preparing co-crystal of meloxicam with succinic and maleic acids *(Myz, et al., 2009).* Studies also reported that a co-crystal prepared from solvent evaporation method can be formed by applying alternative methods of mechanochemistry which may reduce the cost of production significantly and considered to be green and dependable *(Weyna et. al., 2009).* In recent years novel methods such as (SCF) supercritical fluid (*Padrela et al, 2010*), and (HME) hot melt extrusion (*Paradkar, et al., 2010*; *Boksa et al, 2014*) for co-

crystal formation have been extensively studied. Indomethacin-saccharin co-crystals were prepared using supercritical fluid techniques and demonstrated the potential of producing micro and nano size particles (*Padrela et al, 2009*). Hot melt extrusion method was found to be an effective, scalable and green method to make co-crystals for Caffeine-Oxalic acid, Nicotinamide-trans cinnamic acid, Carbamazepine-Saccharin, and Theophylline-Citric acid (*Daurio et al., 2011***)**. The HME technique has shown great potential to prepare pharmaceutical co-crystal agglomerates of ibuprofen and nicotinamide in 1:1 ratio (*Dhumal et al., 2010*). The HME method demonstrated its utility as a scalable and solvent free technique to prepare co-crystals of pharmaceutical importance (*Maniruzzaman et al, 2012*).

1.4. Molecular self-assembly and peptide based hydrogels.

Over many years, researchers and scientists of various fields of physical, chemical and biological sciences have shown keen interest in supramolecular self-assembly. The discipline not only serves as a model for understanding molecular recognition and self-assembly but also investigated for designing extraordinary novel materials (*Lakshmanan, et al., 2012*) and biotechnological applications (*Loo, et al.,2012*).

1.4.1. Hydrogels

Gels are solid or jelly-like materials and they have been receiving considerable attention in recent years. A large number of molecules, particularly small molecules under suitable conditions, have the tendency to self-assemble in

solution. The self-assembly of these molecular gelators gives a three dimensional cross-linked network structure. The network formed by the gelating molecules has the capability to trap and immobilise a high content of solvent in the interstitial spaces, resulting in a gel (Figure 1.9).

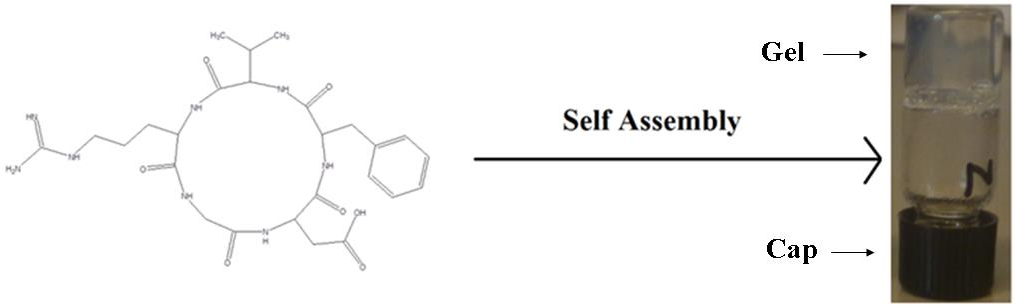

Figure 1.9 Structure of the c(RGDfV) a cyclic pentapeptide which self-assembles to form a hydrogel.

A hydrogel is comprised of three-dimensional network structures of low molecular weight (molecular gelators) organic compounds which do not dissolve in water. However, they swell and demonstrate an amazing capacity to immobilise a high load of water in the network matrix through intermolecular interactions between the network and water. The gel in which a mesh type network is formed through long, thin and flexible fibres are more efficient to hold the solvent molecules as compared to short fibres *(Maity, 2008*).

Hydrogel are categorised in many ways but usually classified as a chemical gel or a physical gel based on their cross linking nature (*Hoffman, 2012*). Chemical gels are permanent gels in which the cross-linked network is held due to stronger and stable covalent bonds whereas, the physical gel contains

molecular networks that are formed by weak intermolecular forces including hydrogen bonding or hydrophobic interactions (*Zhang et al., 2008*). Cross-linked networks based on non-covalent bonds are reversible, and can be disrupted as a response to a stimulus (Figure 1.10) which may be a physical, chemical or biochemical in nature (*Simoes et al., 2012*).

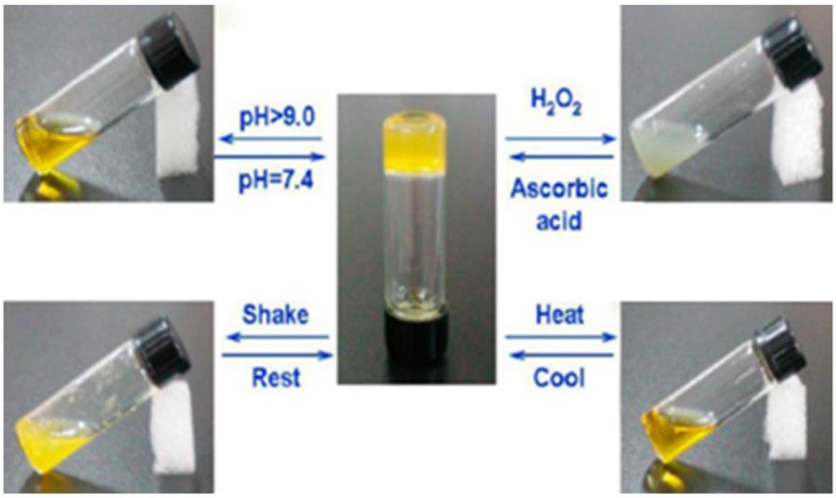

Figure 1.10. Supramolecular hydrogel demonstrating some reversible gel−sol transitions triggered by various physical and chemical stimuli (*Sun et al., 2013*).

Physical stimuli may include temperature (*Mah and Ghosh 2013*), UV light (*Zhao and Stoddart, 2009*) and mechanical stress (*Xia et al, 2013*) etc. whereas, chemical stimuli which can cause abrupt and significant changes in hydrogel properties include pH and chemical agents (*Krogsgaard et al, 2013; Sun et al., 2013*). Due to their extraordinary capability to entrap high water content and general biocompatibility, hydrogels are investigated in a variety of applications

such as drug delivery and biomedical applications (*Patel and Mequanint, 2011*).

1.4.2. Peptide based hydrogels

An attractive property of peptides and proteins is that they can self-assemble (depending on the sequence of amino acids) in water with specificity through noncovalent interactions. This fascinating property highlighted them as a considerable class of soft materials. Weak interactions particularly hydrogen bonding, hydrophobic interactions, and electrostatic interactions are the forces responsible for peptide self-assembly (*Smith et.al. 2008; Johnson et.al., 2011*). This feature is the basis for rational design of peptide-based supramolecular systems.

Like proteins, hydrogen-bonding can lead to the formation of ordered structures in peptide hydrogels which can be exploded into a primary, secondary, and tertiary structure to better understand the process of gel formation (Figure 1.11). The molecular level recognition of the aggregates determines the primary structure whereas, morphology of the aggregate such as α-helices, *β*-sheets and anti-parallel *β*-sheets represent the secondary structures. The tertiary structure defines the cross-linking of individual aggregates thus leading to macrostructures like gel formation. (*Skilling K. J et al. 2014*). Peptide-based hydrogels, in recent times have been explored extensively and specifically focussed on various classes of small peptide and polypeptide (*Panda and Chauhan, 2014*).

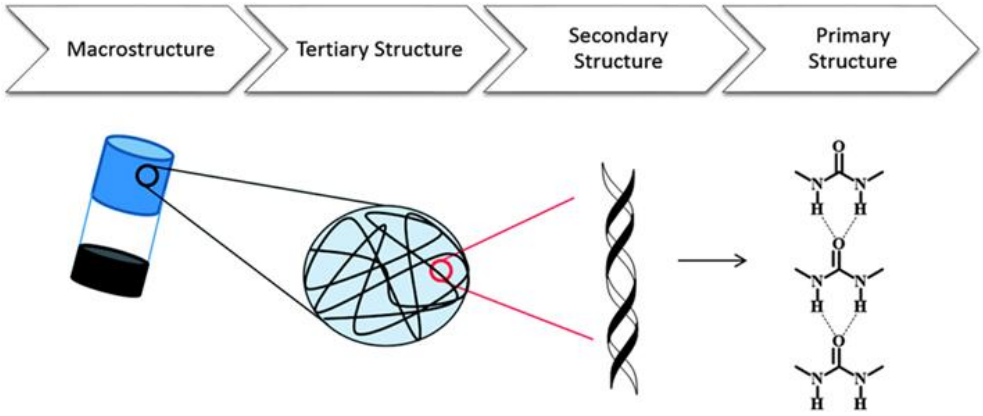

Figure 1.11 Schematic representation of gel formation (*Skilling, et al. 2014*).

Like hydrogels in general, many peptide hydrogels are responsive to various stimuli like pH (*Adams et.al., 2009*), temperature (*Perez et al., 2014*) and salt concentration (*Mishra et al., 2013*). Peptide-based hydrogels have demonstrated diversity in their self-assembling patterns leading to a range of ordered structures for example fibres, tapes, tubes, sheets and spheres, Figure 1.12. The understanding of architectural motifs, aggregation pattern, their morphology and their response to different stimuli provided a base for developing smart self-assembling peptides for various applications in biomedicine including wound healing, as a drug delivery system, tissue engineering and bio-inspired energy-related technologies (*Dasgupta et al. 2013; Ulijn et al., 2010*).

Another significance of generating knowledge about peptide and protein self-assembly is to understand protein unfolding processes which can be a major cause of degenerative diseases for example Alzheimer's (*Smith, 2009*).

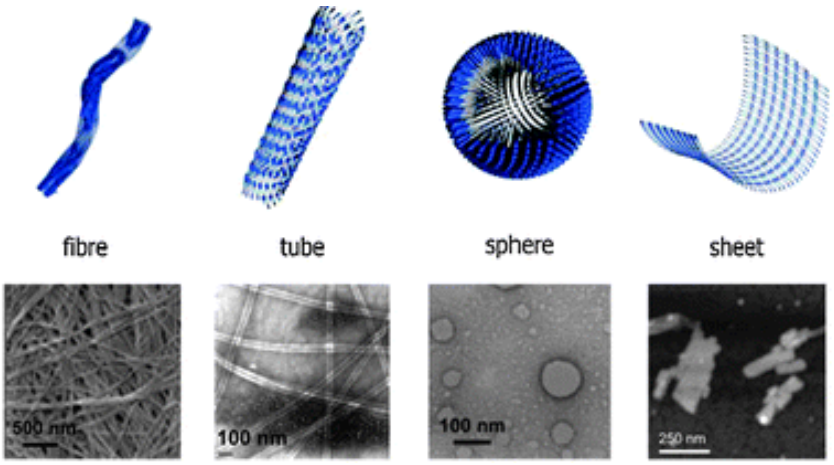

Figure 1.12 Structures observed through supramolecular peptide self-assembly (*Zelzer and Ulijn, 2010*)

1.5. Molecular recognition and complexation

The "molecular recognition" is generally regarded as "lock and key" principle presented by Emil Fischer in 1894. The recognition potential of the natural oligosaccharides and cyclic oligopeptide valinomycin were known by the 1950s whereas, Pedersen in 1967 reported the artificial molecule crown ether, showing the phenomenon of molecular recognition. Cram later on exploited this phenomenon and applied to a wide range of molecular systems and laid the foundation of a new field which he called, host–guest chemistry, where the complexes that are developed due to intermolecular forces other than covalent bonds and the terms used for the complimentary species as "host" or "guest" is arbitrary (*Ariga & Kunitake, 2006*). Cyclodextrins due to their insignificant toxicity and ability to enhance bioavailability of many hydrophobic drugs for example Doxorubicin, paclitaxel (anticancer agents), ibuprofen, indomethacin

(anti-inflammatory) make them suitable for their use in drug delivery systems (*Hu et al, 2014*).

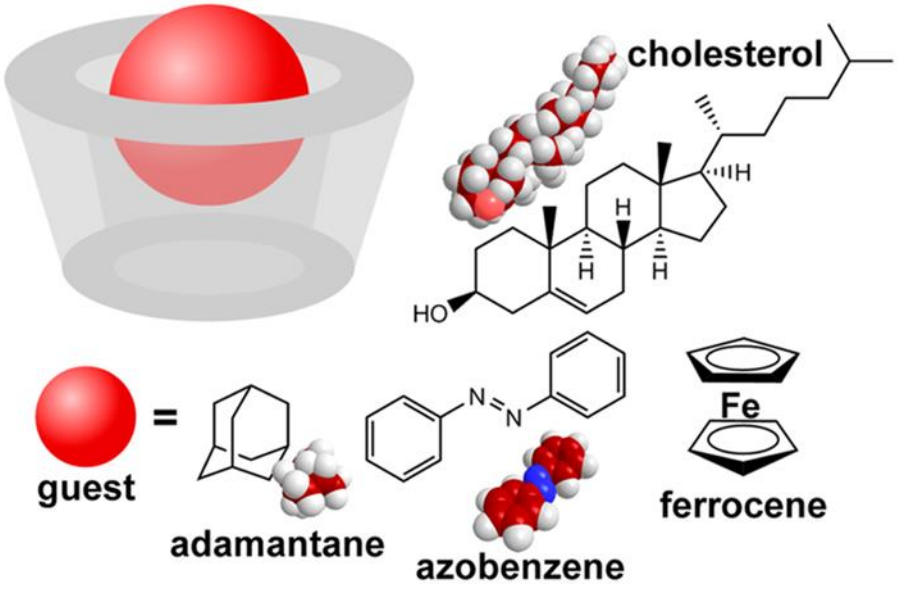

Figure 1.13 Host-guest inclusion complexes with β-CD (*Hu, et al., 2014*).

Some common guest molecules are presented in Figure 1.13 which form inclusion complexes with β-cyclodextrin (β-CD) include adamantane, azobenzene, ferrocene, cholesterol, etc.

Other popular host molecules include calixarenes (*Nimsea and Kim, 2013*), pillararenes (*Xue et al, 2012*), curcubiturils (*Kim et al., 2007*), crown ethers (*Zheng et al, 2012*) etc. Another rapidly growing class of supramolecular materials is metallic organic frameworks (MOF). These crystalline materials involve the interactions of an organic electron linker such as carboxylate or amine and inorganic counterpart metal cations for example Zinc. They can be

used as hosts for different guest molecules as their pore size and functionality are tuneable. MOFs have been investigated thoroughly in different applications including gas storage and drug delivery systems.

1.5.1. Cyclodextrin-based supramolecular architectures

Cyclodextrins (CDs) are natural cyclic oligosaccharides and commonly classified as α-cyclodextrin (α-CD), β-cyclodextrin (β-CD) and γ-cyclodextrin (γ-CD) which are prepared through enzymatic degradation of starch. Among these first generation cyclodextrins α-CD is composed of six, β-CD seven and γ-CD is composed of eight D-glucose units linked by α-1,4-linkages (*Dass and Jessup, 2000*). CDs are water soluble organic compounds and are easily available. The main properties of these cyclodextrins are listed in Table 1.2. CDs have the ability to host different hydrophobic organic molecules (guest) by making a complex. The principle underlying the complex formation is the supramolecular non-covalent interactions such as hydrogen bonding. The non-covalent interactions between water-soluble cyclodextrins hosts and hydrophobic guests allow the development of many supramolecular structures.

Cyclodextrin shape appears like a truncated cone due to the $^4C_1$ chair conformation of the glucose unit (Figure 1.14). All secondary hydroxyl groups [the O(2)-H and O(3)-H)] and the primary hydroxyl groups [O(6)-H] are situated opposite to each other. The cavity is relatively hydrophobic because of the presence of C-3 C-H groups, C-5 C-H groups and glycosidic oxygen atoms (*Jones et al., 1984*).

Table 1.2 Properties of α, β and γ Cyclodextrin (*Martin Del Valle, 2004*).

Property	α Cyclodextrin	β Cyclodextrin	γ Cyclodextrin
No. of glucopyranose units	6	7	8
Molecular weight (g/mol)	972	1135	1297
Solubility in water 25ºC	14.5	1.85	23.2
Outer diameter (Å)	14.6	15.4	17.5
Cavity diameter (Å)	4.7 – 5.3	6.0 – 6.5	7.5 – 8.3
Height of torus (Å)	7.9	7.9	7.9
Cavity volume ($Å^3$)	174	262	427

The cyclodextrin derivatives can also be prepared to modify the properties such as solubility, reduction of toxicity etc., of the natural cyclodextrin by the

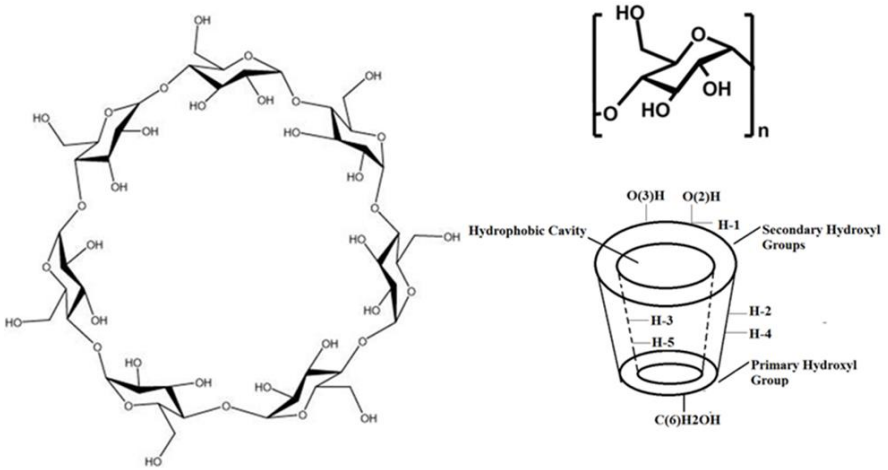

Figure 1.14 The molecular structure and shape of β-cyclodextrin.

displacement reaction at oxygen atom of the hydroxyl group at the primary and secondary positions (*Khan et al., 1998*). The host-guest complex formation between CDs and various drug moieties have been explored in context of supramolecular chemistry and their binding constants, enthalpy and entropy analysis have been well studied (*Connors, 1997*).

Among these natural CDs, β-CD is popular because of its advantages being relatively cheap and easy availability. In addition, the hydrophobic pocket size is appropriate for a variety of guest molecules (*Sambasevam, et al., 2013*).

The extraordinary capability of β-CD to entrap completely or partially a wide range of organic molecules such as drugs, steroids (*Yanez, et al., 2007*), pigments (*Melo, et al., 2003*), dyes (*Al-Rawashdeh, et al., 2013*) and peptides (Lula, et al., 2011) via inclusion complex formation may modify the properties such as physico-chemical, biochemical, photochemical properties etc., of the guest molecules.

1.6. References

Adams, D.J., Butler, M.F., Frith, W.J., Kirkland, M., Mullen, L., & Sanderson, P. (2009). A new method for maintaining homogeneity during liquid–hydrogel transitions using low molecular weight hydrogelators. *Soft Matter*. *5*, 1856.

Aher, S., Dhumal, R., Mahadika, K., Paradkar, A., & York P. (2010). Ultrasound assisted cocrystallization from solution (USSC) containing a non-congruently soluble cocrystal component pair: Caffeine/maleic acid. *European Journal of Pharmaceutical Sciences. 41,* 597–602.

Aitipamula S., Banerjee R., Bansal A.K., Biradha K., Cheney M.L., Choudhury A.R. … & Zaworotko M.J. (2012). Polymorphs, Salts, and Cocrystals: What's in a Name? *Crystal Growth & Design*. *12,* 2147−2152.

Aitipamula S., Chowa P.S. & Tan R.B.H. (2014). Polymorphism in cocrystals: a review and assessment of its significance. *CrystEngComm. 16*, 3451-3465.

Alonzo, D.E., Zhang, G.G.Z., Zhou, D., Gao, Y., & Taylor, L.S. (2010). Understanding the Behavior of Amorphous Pharmaceutical Systems during Dissolution. *Pharmaceutical Research*. *27*(4), 608-618.

Al-Rawashdeh, N.A.F., Al-Sadeh, K.S., & Al-Bitar, M.B. (2013). Inclusion Complexes of Sunscreen Agents with β-Cyclodextrin: Spectroscopic and Molecular Modeling Studies. *Journal of Spectroscopy*. Vol.2013.

Anderson, K.M., Probert, M.R., Goeta, A. E., & Steed, J. W. (2011). Size does matter—the contribution of molecular volume, shape and flexibility to the formation of co-crystals and structures with $Z' > 1$. *CrystEngComm*. *13*, 83-87.

Ariga, K., Hill, J.P., Lee, M.V., Vinu, A., Charvet, R., & Acharya, S. (2008). Challenges and breakthroughs in recent research on self-assembly. *Science and Technology of Advanced Materials.* 9.

Ariga, K., & Kunitake, T. (2006). Chemistry – Fundamentals and Applications. Springer-Verlag Berlin Heidelberg.

Bauer, J., Spanton, S., Henry, R., Quick, J., Dziki, W., Porter, W., & Morris, J. (2001). Ritonavir: An Extraordinary Example of Conformational Polymorphism. *Pharmaceutical Research. 18*(6).

Bernstein, J. (2002). Polymorphism in Molecular Crystals (ed.). Oxford: Oxford University Press.

Bernstein, J., Davis, R.E., Shimoni, L., & Chang N-L. (1995). Patterns in Hydrogen Bonding: Functionality and Graph Set Analysis in Crystals. *Angewandte Chemie International Edition in English., 34*, 1555-1573.

Blagden, N., de Matas, M., Gavan, P.T., & York, P. (2007). Crystal engineering of active pharmaceutical ingredients to improve solubility and dissolution rates. *Advanced Drug Delivery Reviews. 59*, 617-630.

Boksa, K., Otte, A., & Pinal, R. (2014). Matrix-Assisted Cocrystallization: The Simultaneous Production and Formulation of Pharmaceutical Cocrystals by Hot-Melt Extrusion. *Journal of Pharmaceutical Science. 103*(9), 2904-10.

Bond, A.D. (2007). What is a co-crystal? *CrystEngComm. 9,* 833–834.

Brittain., H. G. (2012). Cocrystal Systems of Pharmaceutical Interest: 2011. *Crystal Growth and Design*. *12*, 5823−5832.

Brittain, H. G. (2011). Polymorphism and Solvatomorphism 2009. *Journal of Pharmaceutical Sciences*. *100*(4),1260-79.

Brittain., H. G. (2008). "Polymorphism and Solvatomorphism 2006". *Journal of Pharmaceutical Sciences. 97* (9), 3611-36.

Byrn, S., Pfeiffer, R., Ganey, M., Hoiberg C., & Poochikian, G. (1995). Pharmaceutical Solids: A Strategic Approach to Regulatory Considerations. *Pharmaceutical Research. 12* (7), 945-954.

Cairns, P. W. (2009). Classical methods of preparation of polymorphs and alternative solid forms. In Brittain, H. G. (Ed.), *Polymorphism in pharmaceutical solids*. Informa Healthcare, New York.

Cherukuvada, S. & Nangia, A. (2014). Eutectics as improved pharmaceutical materials: design, properties and characterization. *Chemical Communication. 50,* 906-923.

Connors, K.A. (1997). The Stability of Cyclodextrin Complexes in Solution. Chemical Reviews. 97, 1325-1357.

Dasgupta, A., Mondal, J.H. & Das, D. (2013). Peptide hydrogels. *RSC Advances. 3,* 9117–9149.

Dass, C.R., Jessup, W. (2000). Apolipoprotiens A-I, Cyclodextrins and liposomes as potential drugs for the reversal of atherosclerosis. *Journal of Pharmacy and Pharmacology*. *52*, 731– 61.

Daurio, D., Medina, C., Saw, R., Nagapudi, K., & Alvarez-Núñez, F. (2011). Application of Twin Screw Extrusion in the Manufacture of Cocrystals, Part I: Four Case Studies. *Pharmaceutics. 3*, 582-600.

Delori, A., Friscic, T., & Jones, W. (2012). The role of mechanochemistry and supramolecular design in the development of pharmaceutical materials. *CrystEngComm. 14*, 2350.

Desiraju, G.R. (2013). Crystal Engineering: From Molecule to Crystal. *Journal of the American Chemical Society. 135*, 9952−9967.

Desiraju, G.R. (2010). Crystal engineering: A brief overview. *Journal of Chemical Science. 122*(5), 667–675.

Desiraju, G.R. (2003). Crystal and co-crystal. *CrystEngComm. 5*, 466 - 467.

Desiraju, G.R. (1995). Supramolecular Synthons in Crystal Engineering-A New Organic Synthesis. *Angewandte Chemie International Edition in English. 34*(21), 2311-2327.

Dhotel, A., Chen, Z., Delbreilh, L., Youssef, B., Saiter, J-M., & Tan L. (2013). Molecular Motions in Functional Self-Assembled Nanostructures. *International Journal of Molecular Science. 14*, 2303-2333.

Dhumal, R.S., Kelly, A.L., York, P., Coates, P.D., & Paradkar, A. (2010). Cocrystalization and Simultaneous Agglomeration Using Hot Melt Extrusion. *Pharm Res. 27*, 2725–2733.

Dunitz, J.D. (2003). "Crystal and co-crystal: a second openion." *CrystEngComm. 5*, 506.

El Kerdawy, A., Wick, C.R., Hennemann, M., & Clark, T. (2012). Predicting the Sites and Energies of Noncovalent Intermolecular Interactions Using Local Properties. *Journal of Chemical Information and Modeling*. *52*, 1061−1071.

Etter, M.C., MacDonald J.C., & Bernstein J. (1990). Graph-Set Analysis of Hydrogen-Bond Patterns in Organic Crystals. Acta Crystallographica. B*46*, 256-262.

Fabbiani, F.P.A., in Boldyreva, E.V., & P. Dera, P. (eds.), (2010). High-Pressure Crystallography. Fundamentals and Applications, Springer.

Friscic, T., Childs, S.L., Rizvi, S.A.A., & Jones, W. (2009). The role of solvent in mechanochemical and sonochemical cocrystal formation: a solubility-based approach for predicting cocrystallisation outcome. *CrystEngComm. 11*, 418-426.

Friscic, T. & Jones, W. (2009). Recent advances in understanding the mechanism of cocrystal formation via grinding. *Crystal Growth & Design*. *9*, 1621-1637.

Gardner C.R., Walsh, C.T., & Almarsson O. (2004). Drugs as materials: valuing physical form in drug discovery. *Nature Reviews, Drug Discovery*. *3*(11): 926-934.

Gavezzotti, A. (2007). "A Solid-State Chemist's View of the Crystal Polymorphism of Organic Compounds." *Journal of Pharmaceutical Sciences. 96*(9), 2232–2241.

Gazit, E. (2007). Self-assembled peptide nanostructures: the design of molecular building blocks and their technological utilization. *Chemical Society Reviews. 36,* 1263–1269.

Gonzalez, E.G.S, Mulia, L.Y., Abad, V.J.H., Jung, H., & Cook, H.J. (2014). The influence of polymorphism on the manufacturability and *in vitro* dissolution of sulindac-containing hard gelatin capsules. *Pharmaceutical Development and Technology. 0 0*,0, 1-8.

Groom, C.R., & Allen, F.H. (2014). The Cambridge Structural Database in Retrospect and Prospect. *Angewandte Chemie International Edition in English., 53,* 662 – 671.

Hilfiker, R. E.d. (2006). Polymorphism; in the pharmaceutical industry, Wiley-VCH Verlag GmbH & Co. KGaA.

Hippel, A.R. (1962). "Molecular Designing of Materials." Science. *138* (3537), 91-108.

Hoeben, F.J.M., Jonkheijm, P., Meijer, E.W., & Schenning, A.P.H.J. (2005). About Supramolecular Assemblies of π-Conjugated Systems. *Chemical Reviews. 105*, 1491−1546.

Hoffman, A.S. (2012). "Hydrogels for biomedical applications". *Advanced Drug Delivery Reviews. 64,* 18‑23.

Hu, Q.D., Tang, G.P., & Chu, P.K. (2014). Cyclodextrin-Based Host-Guest Supramolecular Nanoparticles for Delivery: From Design to Applications. *Accounts of Chemical Research. 47*, 2017−2025.

Johnson, E.K., Adams, D.J., & Cameron, P.J. (2011). Peptide based low molecular weight gelators. *Journal of Materials Chemistry. 21*, 2024.

Jones, S.P., Grant, J.W., Hadgraft, J., Parr, G.D. (1984). Cyclodextrin in the pharmaceutical sciences part I: Preparation, structure and properties of cyclodextrins and cyclodextrin inclusion compounds. *Acta Pharm. Technol. 30,* 213-223.

Jung, M.S., Kim, J.S., Kim, M.S., Alhalaweh, A., Cho, W., Hwang, S. J., & Velaga, S.P. (2010). Bioavailability of indomethacin-saccharin cocrystals. *Journal of Pharmacy and Pharmacology* **.** *62*(11), 1560-1568.

Karki, S., Friščić, T., Fábián, L., Laity, P.R., Day, G.M., & Jones, W. (2009). Improving Mechanical Properties of Crystalline Solids by Cocrystal Formation: New Compressible Forms of Paracetamol. *Advanced Materials. 21*, (38-39), 3905-3909.

Khan, A.R., Forgo, P., Stine, K.J., & D'Souza, V.T. (1998). Methods for selective modifications of cyclodextrins. *Chemical Reviews. 98*, 1977**.**

Khankari, R.K., & Grant, D.J.W. (1995). "Pharmaceutical hydrates." *Thermochimica Acta. 248*, 61-79.

Kim, K., Selvapalam, N., Ko, Y.H., Park, K.M., Kim, D., & Kim, J. (2007). Functionalized cucurbiturils and their applications. *Chemical Society Reviews*. 36, 267-279.

Krogsgaard, M., Behrens, M.A., Pedersen, J.S., & Birkedal, H. (2013). Self-Healing Mussel-Inspired Multi-pH-Responsive Hydrogels. *Biomacromolecules. 14*, 297−301.

Lakshmanan, A., Zhang, S., & Hauser, C.A.E. (2012). Short self-assembling peptides as building blocks for modern nanodevices. *Trends in Biotechnology. 30,* (3).

Lehn, J.M. (1978) Cryptates: inclusion complexes of macropolycyclic receptor molecules. *Pure and Applied Chemistry. 50*, 871–892.

Lehn, J.M. (1988). Supramolecular chemistry - scope and perspectives molecules, supermolecules, and molecular devices. *Angewante. Chemie, International Edition English. 27*, 89-112.

Lehn, J.M. (1995). "Supramolecular Chemistry: Concepts and Perspectives, VCH. Weinheim.

Loo, Y., Zhang, S., & Hauser, C.A.E. (2012). From short peptides to nanofibers to macromolecular assemblies in biomedicine. *Biotechnology Advances. 30*, 593–603.

Lu, J., & Rohani, S. (2010). Synthesis and Preliminary Characterization of Sulfamethazine-Theophylline Co-Crystal. *Journal of Pharmaceutical Sciences. 99*(9): 4042–4047.

Lula, I., de Sousa, F.B., Denadai, A.M.L., Ianzer, D., de Camargo, A.C.M., Santos, R.A.S., & Sinisterra, R.D. (2011). Study of the BPP7a Peptide and its beta -Cyclodextrin Complex: Physicochemical Characterization and Complete Sequence Specific NMR Assignments. *Journal-Brazillian Chemical Society. 2*(9), 1765-1773.

Ma, Z., Liu, H., & Wu, B. (2013). Structure-based drug design of catechol-O-methyltransferase inhibitors for CNS disorders. *British Journal of Clinical Pharmacology. 77*(3), 410–420.

Mah, E., & Ghosh, R. (2013). Thermo-Responsive Hydrogels for Stimuli-Responsive Membranes. *Processes. 1*, 238-262.

Maity, G.C. (2008) Supramolecular Hydrogels. *Journal of Physical Sciences*. *12*, 173-186.

Maniruzzaman, M., Joshua, S., Boateng, J.S., Snowden, M.J., & Douroumis, D. (2012). A Review of Hot-Melt Extrusion: Process Technology to Pharmaceutical Products. *ISRN Pharmaceutics*. *Vol. 2012*, 436763.

Martin Del Valle E.M. (2004). Cyclodextrins and their uses: a review. *Process Biochemistry*. 39, 1033–1046.

McKellar, S.C. (2012). Crystal Engineering Approaches to Solid-State Pharmaceutical Systems. Thesis, University of Strathclyde.

Melo, P.S., Justo, G.Z., de Azevedo, M.B.M., Duran, N., & Haun, M. (2003). Violacein and its b-cyclodextrin complexes induce apoptosis and differentiation in HL60 cells. *Toxicology*. 186, 217-225.

Merz, K., & Vasylyeva, V. (2010). "Development and boundaries in the field of supramolecular synthons" *CrystEngComm. 12*, 3989-4002.

Millar, D.I.A., Maynard-Casely, H.E., Allan, D.R., Cumming A S, Lennie A R, Mackay A J, Oswald I D H, Tang C C and Pulham C R (2012). Crystal engineering of energetic materials: Co-crystals of CL-20. *CrystEngComm*. 14, 3742.

Mishra, A., Chan, K.H., Reithofer, M.R., & Hauser, C.A.E. (2013). Influence of metal salts on the hydrogelation properties of ultrashort aliphatic peptides. *RSC Advances*. 3, 9985.

Myz, S.A., Shakhtshneider, T.P., Fucke, K., Fedotov, A.P., Boldyreva, E.V., Boldyreva, V.V., Nadezhda, I., & Kuleshovad, N.I. (2009). Synthesis of co-crystals of meloxicam with carboxylic acids by grinding. *Mendeleev Commununications*. *19*, 272–274.

Nangia, A. (2010). Supramolecular chemistry and crystal engineering. *Journal of Chemical Science. 122* (3), 295–310.

Nangia, A. (2008). Conformational Polymorphism in Organic Crystals. *Accounts Of Chemical Research*. *41*(5), 595-604.

Nimsea, S.B. & Kim, T. (2013). Biological applications of functionalized calixarenes. *Chemical Society Reviews. 42*, 366.

Oshovsky, Gennady V., Reinhoudt, David N. and Verboom, W. (2007), Supramolecular Chemistry in Water. *Angewandte Chemie International Edition. 46*, 2366–2393.

Padrela, L., Rodrigues, M.A., Velaga, S.P., Matos, H.A. & Azevedo E.G. (2010). Screening for pharmaceutical cocrystals using the supercritical fluid enhanced atomization process. *Journal of Supercritical Fluids. 53*, 156–164.

Padrela, L., Rodrigues, M.A., Velaga, S.P., Matos, H.A. & Azevedo E.G. (2009). Formation of indomethacin–saccharin cocrystals using supercritical fluid technology. *European Journal of Pharmaceutical Sciences*. *38*, 9–17.

Panda, J.J. & Chauhan V S. (2014). Short peptide based self-assembled nanostructures: implications in drug delivery and tissue engineering. *Polymer Chemistry*. 5, 4418-4436.

Paradkar, A.R., Kelly, A.L., Coates, P.D., & York, P. (2010). Method and product. WO. 2010;013035:A1.

Patel, A., & Mequanint, K. (2011). Hydrogel Biomaterials, Biomedical Engineering - Frontiers and Challenges, Prof. Reza Fazel (Ed.), ISBN: 978-953-307-309-5, InTech, DOI: 10.5772/24856. Available from: http://www.intechopen.com/books/biomedical-engineering-frontiers-and-challenges/hydrogel-biomaterials.

Perez, C.M.R., Rank, L.A., & Chmielewski, J. (2014). Tuning the thermosensitive properties of hybrid collagen peptide–polymer hydrogels. *Chem. Commun. 50*, 8174-8176.

Qiao N, Li M , Schlindwein W, Malek N, Davies A, Trappitt G (2011). Pharmaceutical cocrystals: An overview. *International Journal of Pharmaceutics. 419*, 1‑2, 1‑11

Rodriguez-Spong,B., Price, C.P., Jayasankar, A.,Matzger,A.J., Rodriguez-Hornedo, N. (2004). General principles of pharmaceutical solid polymorphism: a supramolecular perspective. *Advanced Drug Delivery Reviews. 56,* 241– 274.

Roesky, H.W., & Andruh, M. (2003). The interplay of coordinative, hydrogen bonding and p_/p stacking interactions in sustaining supramolecular solid-state architectures. A study case of bis(4-pyridyl)- and bis(4-pyridyl-N-oxide) tectons. *Coordination Chemistry Reviews*. *236*, 91-119.

Rosen, M.J. (2004). *Surfactants and interfacial phenomena*. Hoboken, NJ: Wiley-Interscience.

Roy, S., & Matzger, J. (2009). Unmasking a Third Polymorph of a Benchmark Crystal-Structure-Prediction Compound. *Angewandte Chemie International Edition English. 48(45): 8505–8508.*

Sambasevam, K.P., Mohamad, S., Sarih, N.M., & Ismail, N.A. (2013). Synthesis and Characterization of the Inclusion Complex of β-cyclodextrin and Azomethine. *International Journal of Molecular Sciences.*14, 3671-3682.

Sarma, B., Chen, J., Hsi, H., & Myerson, A.S. (2011). Solid forms of pharmaceuticals: Polymorphs, salts and cocrystals. *Korean Journal of Chemical Engineering. 28*(2), 315-322.

Sekhon, B.S. (2009). Pharmaceutical co-crystals - a review. *ARS Pharmaceutica*. *50*(3), 99-117.

Schultheiss, N., & Newman, A. (2009). Pharmaceutical Cocrystals and Their Physicochemical Properties. *Crystal Growth & Design. 9*(6), 2950–2967.

Shan, N., & Zaworotko, M.J. (2008). The role of cocrystals in pharmaceutical Science. *Drug Discovery Today*. *13,* 440-446.

Simoes, S., Figueiras, A., & Veiga, F. (2012). Modular Hydrogels for Drug Delivery. *Journal of Biomaterials and Nanobiotechnology. 3,* 185-199.

Singhal, D., & Curatolo, W. (2004). Drug polymorphism and dosage form design: a practical perspective. *Advanced Drug Delivery Reviews. 56,* 335–347.

Skilling, K.J., Citossi, F., Bradshaw, T.D., Ashford M, Kellama, B., & Marlow, M. (2014). Insights into low molecular mass organic gelators: a

focus on drug delivery and tissue engineering applications. *Soft Matter*. *10*, 237–256.

Smith, D.K. (**2009).** Lost in translation? Chirality effects in the self-assembly of nanostructured gel-phase materials. *Chemical Society Reviews, 38,* 684.

Smith, A., Williams, R., Tang, C., Coppo, P., Collins, R., Turner, M., Saiani, A., & Ulijn, R. (2008). *Advanced Materials, 20,* 37.

Stahly, G.P. (2007). Diversity in Single-and Multiple-Component Crystals. The Search for and Prevalence of Polymorphs and Cocrystals. *Crystal Growth & Design. 7,* 1007-1026.

Stahl, P.H., & Wermuth, C.G. (2002). Handbook of pharmaceutical salts : properties, selection, and use. New York, Weinheim ; VHCA .Wiley-VCH.

Steed, J.W. (2013). The role of co-crystals in pharmaceutical design. *Trends in Pharmacological Sciences. 34,* No. 3.

Steed, J.W., & Atwood, J.L. (2000). Supramolecular chemistry. John Wiley & Sons, Ltd, Chichester.

Sun, Z., Li, Z., He, Y., Shen, R., Deng, L., Yang, M., Liang, Y., & Zhang, Y. (2013). Ferrocenoyl Phenylalanine: A New Strategy Toward Supramolecular Hydrogels with Multistimuli Responsive Properties. *Journal of American Chemical Society. 135*, 13379−13386.

Surov, A.O., Solanko, K.A., Bond, A.D., Brandl, A.B., & Perlovich, G.L. (2014). Polymorphism of felodipine co-crystals with 4,4′-bipyridine. *CrystEngComm. 16,* 6603-6611.

Trask, A.V. (2007). An overview of Pharmaceutical co-crystals as intellectual property. *Molecular Pharmaceutics.* 4, 301–309.

Thakuria, R., Delori, A., Jones, W., Lipert, M.P., Roy, L., & Rodríguez-Hornedo, N. (2013). Pharmaceutical cocrystals and poorly soluble drugs. *International Journal of Pharmaceutics. 453,* 1, 10–125.

Upadhyay P., Khomane, K.S., Kumar, L., & Bansal, A.K. (2013). Relationship between crystal structure and mechanical properties of ranitidine hydrochloride polymorphs. *CrystEngComm. 15,* 3959-3964.

Ulijn, R.V., & Woolfson, D.N. (2010). Peptide and protein based materials in 2010 : from design and structure to function and application. *Chemical Society Reviews. 39*(9), 3349.

Viterbo, D., Milanesio, M., Hernandez, R.P., Tanty, C,R., Gonzalez, I.C., Carrazanad, M.S., & Rodriguez, J.D. (2000) 2',3'-Didehydro-3'-deoxythymidine N-methyl-2-pyrrolidone solvate (D4TNMPO). *Acta Crystallographica. Sect. C* 56, 580–581.

Walsh, R.D.B., Bradner, M.W., Fleischman, S., Morales, L.A., Moulton, B., Rodríguez-Hornedo, N., & Zaworotko, M.J. (2003). Crystal engineering of the composition of pharmaceutical phases. *Chemical Communications*. 186.

Wang, J.R., Ye, C., & Mei, X. (2014). Structural and physicochemical aspects of hydrochlorothiazide co-crystals. *CrystEngComm. 00*, 1-8.

Weyna, D.R., Shattock, T., Vishweshwar, P., & Zaworotko, M.J. (2009). Synthesis and Structural Characterization of Cocrystals and Pharmaceutical Cocrystals: Mechanochemistry vs Slow Evaporation from Solution. *Crystal Growth & Design, 9*(2), 1106-1123.

Wood, P.A. (2008). The Effect of High Pressure on Crystal Structure Topology. Thesis, University of Edinburgh.

Xia, L.W., Xie, R., Ju, W.J., Wang, W., Chen, Q., & Chu, L.Y. (2013). Nano-structured smart hydrogels with rapid response and high elasticity. *Nature Communications. 4.* Article number:2226.

Xue, M., Yang, Y., Chi, X., Zhang, Z., & Huang, F. (2012). Pillararenes, a new class of macrocycles for supramolecular chemistry. *Accounts of Chemical Research. 45*(8), 1294–130.

Yan, D., Delori, A., Lloyd, G.O., Friscic, T., Day, G.M., Jones, W., Lu, J., Wei, M., Evans, D.G., & Duan, X. (2011). A cocrystal strategy to tune the luminescent properties of stilbene type organic solid-state materials. *Angewandte Chemie International Edition. 50,* 12483 –12486.

Yanez, C., Basualdo, J., Jara-Ulloa, P., & Squella, J.A. (2007). Inclusion complexes of estrone and estradiol with b-cyclodextrin: Voltammetric and HPLC studies. *Journal of Physical Organic Chemistry.* 20, 499.

Zallen, R., Ed. (1998). The Physics of Amorphous Solids, Berlin, Wiley-VCH.

Zelzer, M., & Ulijn, R.V. (2010). Next-generation peptide nanomaterials: molecular networks, interfaces and supramolecular functionality. *Chemical Society Reviews. 39*, 3351–3357.

Zhao, Y.L., & Stoddart, J.F. (2009). Azobenzene-Based Light-Responsive Hydrogel System. *Langmuir. 25* (15), 8442–8446.

Zhang, Z., Chao, T., & Jiang, S. (2008). Physical, Chemical, and Chemical-Physical Double Network of Zwitterionic Hydrogels. *Journal of Physical Chemistry B, 112* (17), 5327–5332.

Zheng, B., Wang, F., Dong, S., & Huang, F. (2012). Supramolecular polymers constructed by crown ether-based molecular recognition. *Chemical Society Reviews. 41*, 1621–1636.

Chapter 2

Aims and Objectives

2.1. Aims

The collective aim of this thesis is to develop an understanding of multi-component systems based on supramolecular chemistry particularly self-assembly and molecular recognition. These multi-component systems are of considerable importance in many areas particularly in pharmaceutical industry. The addition of a different entity or a component in crystal structures can radically alters the properties of a solid in a systematic way therefore, their study is of great interest to develop basic knowledge of the factors that affect the formation of multi-component crystal structures under various conditions. To address the theme the thesis emphasized on two multi-component systems. One system is based on the co-crystallisation of naturally-occurring amino acids to form co-crystals, while the other explain the inclusion phenomenon involving a host (β-cyclodextrin) and a guest c(RGDfV) a cyclic penta-peptide. A potential outcome from this research is to propose novel co-crystals of hydrophobic homochiral naturally occurring amino acids. Further, to present continuous crystallisation, an emerging route to prepare solid forms, as a robust, reproducible and viable method to translate laboratory scale research to the large scale bulk preparation of these molecular complexes.

2.2. Objectives

In the following sections, the main objectives of this study are presented on chapter basis.

2.2.1. Co-crystallisation of homochiral (L-L) amino acids

(i) Preparation, characterisation and crystal structure determination of co-crystals of L-Leucine and L-Isoleucine to understand how zwitterions are held together in the crystalline state and how many conformations of the side chains in the molecules are affected in comparison with their parent components.

(ii) Preparation, characterisation and crystal structure determination of co-crystals of L-Leucine and L-Valine to understand how zwitterions are held together in the crystalline state and how many conformations of the side chains in the molecules are affected in comparison with their parent components.

(iii) Preparation, characterisation and crystal structure determination of co-crystals of L-Valine and L-Isoleucine to understand how zwitterions are held together in the crystalline state and how much conformations of the side chains in the molecules are affected in comparison with their parent components.

2.2.2 Bulk preparation of homochiral amino acids co-crystals.

(i) Continuous production of amino acid co-crystals via rapid anti-solvent crystallisation.

(ii) Bulk characterisation of the co-crystals to ensure phase purity and its comparison with the single crystals.

(iii) Study of steady state operation through the particle size distribution and process yield.

(iv) Solubility studies of the bulk powder of co-crystals.

2.2.3. Host–guest complexation of β-Cyclodextrin with c(RGDfV)

(i) Preparation and characterisation of Inclusion complex of β-cyclodextrin with c(RGDfV).

(ii) ^{1}H NMR study of the inclusion complex to understand the mechanism of host-guest interaction and to determine the stoichiometry of the complex.

(iii) In a similar fashion, to develop a method for crystallisation of the pure penta-peptide [c(RGDfV)] and of inclusion complex of the penta-peptide with Beta cyclodextrin towards determining the X-ray structures of these solid state forms.

CHAPTER 3

Instrumentation

3.1 Introduction

This chapter provide a brief overview of the instrumental techniques used throughout this thesis. The general theories behind the instruments and how they work will be discussed. Major characterisation methods used in the thesis include thermal analysis (DSC and TGA), which co-relates the response of substances to heat; vibrational spectroscopies (FTIR, Raman) to identify local structural information, *e.g.* functional groups (*Hollas, 1996*); Circular dichroism spectroscopy (CD) to observe the conformational changes in biomolecules (*Fiedler. et. al., 2013*); Nuclear magnetic resonance spectroscopy (NMR) to elucidate the structure of molecules and can be used on analytical applications (*López-Cebral. et al.2014*). Atomic force microscopy (AFM) for surface topography (*Seo and Jhe, 2008*); Scanning electron microscopy (SEM) that provides a three-dimensional profile of a material and aids in its characterisation (*Liu. 2010*); and last but not least diffraction techniques such as single crystal X-ray diffraction (SXD) and powder X-ray diffraction (PXRD) that give longer range order information *e.g.* molecular packing arrangements (*Giacovazzo, et. al.2002*).

The specific details of the instrumental parameters used in the experiments will be addressed in the specific chapters.

3.2. Analytical techniques

The crystalline product obtained, using the crystallisation methods previously described, were analysed in several ways including thermal analysis, DSC, TGA and spectroscopic methods as outlined below.

3.2.1. Thermal analysis

Thermoanalytical techniques comprises all those that determined the physical and energetic properties of a material as a function of an applied temperature (*Brittain, 1995*). Differential scanning calorimetry (DSC) and thermal gravitational analysis (TGA) are two of the most common thermal analysis techniques used in pharmaceutical research, due to simplicity in use and broad range of applications. Thermal analysis methods provide detailed information on thermodynamic properties about new entities in the early stages of drug discovery and development (*Clas, et al., 1999*).

3.2.1.1. Differential scanning calorimetry (DSC).

Differential scanning calorimetry gives detailed information on the relationship between temperature and physical properties like specific heat capacity, glass transition, heat of fusion, melting point etc. (*Pyramides, 1995*) and can provide information on significant changes in phase such as crystallisation and polymorphic transitions (*Zhang. et al., 2003*).

The underlying principle of DSC technique is to measure the difference between the heat flow that occurs between reference and a sample that undergoes some physical change when heat is absorbed or released.

Figure 3.1 Differential Scanning Calorimeter (DSC) lab source.

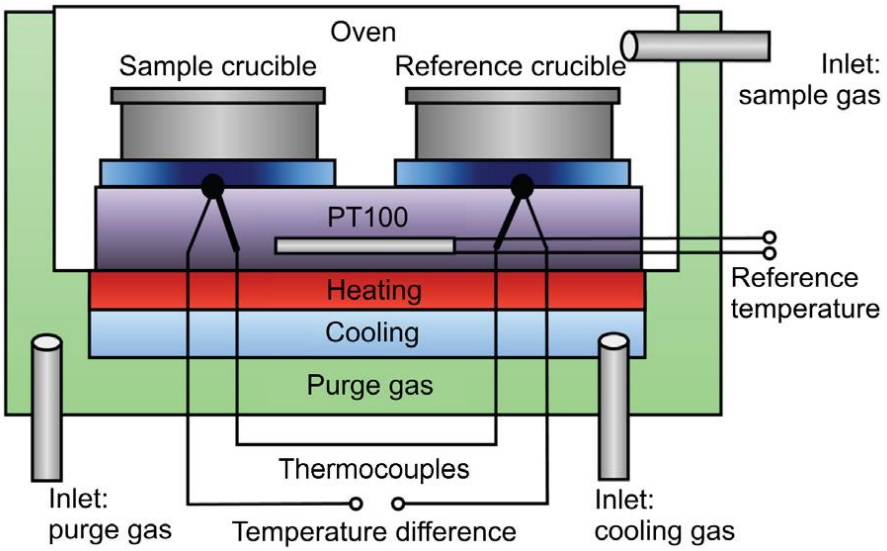

Figure 3.2 Schematic diagram of differential scanning calorimetry (*Elkordy, 2013*).

To perform a basic DSC experiment on a sample, 1-7 mg of material is placed in an Aluminium sample pan. An identical pan which does not contain any sample is used as a reference. The sample and reference pans are placed in a

furnace on heating stage linked with measurement thermocouples as shown in Figure 3.2. Depending upon the experiment requirements, controlled environment over the sample is achieved by an inert gas like nitrogen or a reactive gas such as oxygen which flows over the sample and passed out through an exhaust. The difference in the externally applied energy, required to equate the temperature of the sample with that of the reference, would be the amount of additional heat absorbed during an endothermic process (melting) or released during an exothermic event (crystallisation) by the sample.

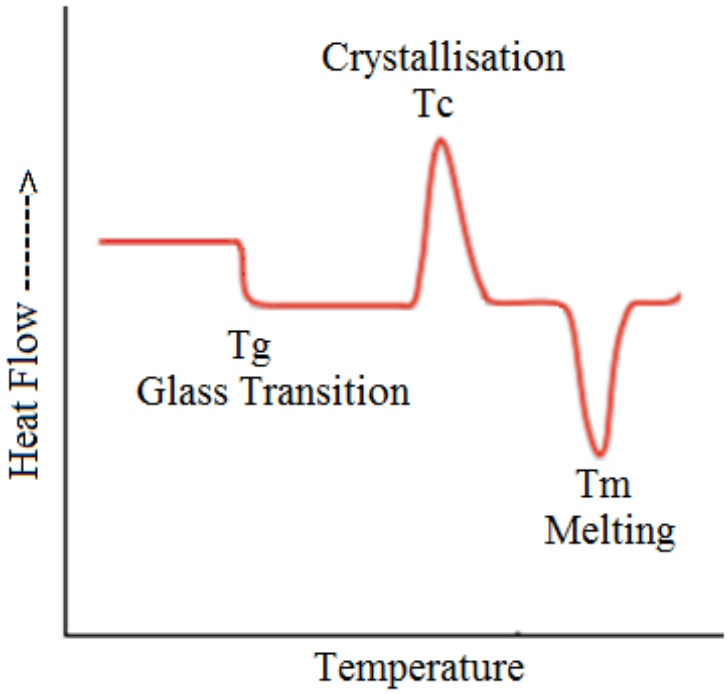

Figure 3.3 Scheme showing the glass transition (Tg), melting point (Tm) and crystallisation (Tc).

Any changes in material as a function of temperature (Figure 3.3) can be visualised from the thermogram or DSC curve as endotherms, exotherms and glass transitions. The DSC technique is extensively employed in various

applications such as chemical analysis, drug analysis, polymers, food science etc.

3.2.1.2. Thermogravimetric analysis (TGA)

Thermal gravimetric analysis is primarily used for the characterisation of materials that show a weight gain (oxidation / absorption) or decrease in weight due to loss of moisture or volatile constituents and may be because of decomposition of the sample. Schematic diagram of furnace set up used in TG instrument is shown in Figure 3.4.

In a routine TGA experiment the sample is added to a platinum pan or any other suitable inert pan which then accurately weighed. The quantity of the sample for experiment generally varies but may go upto 20mg depending upon the nature of the sample. The pan is then introduced into a furnace and heated until decomposition or loss of one of the constituent of the sample during the experimental run. A calibrated, highly sensitive and precise scale is used to measure any change in mass of a sample. A suitable gas for the prescribed experiment is passed through the furnace cell to make sure that the atmosphere is inert or reactive and to purge any volatile substance formed during the experiment. The weight loss or weight gain is recorded throughout the experiment and a trace of % weight against temperature is generated. In thermal decomposition the weight of the sample decreases and may form gaseous product or a residue of char. The typical descending TG curve indicates that a weight loss occurred over increasing temperature (Figure 3.5).

The curve gives a wealth of information including sample composition, thermal stability and kinetic parameters of thermal decomposition.

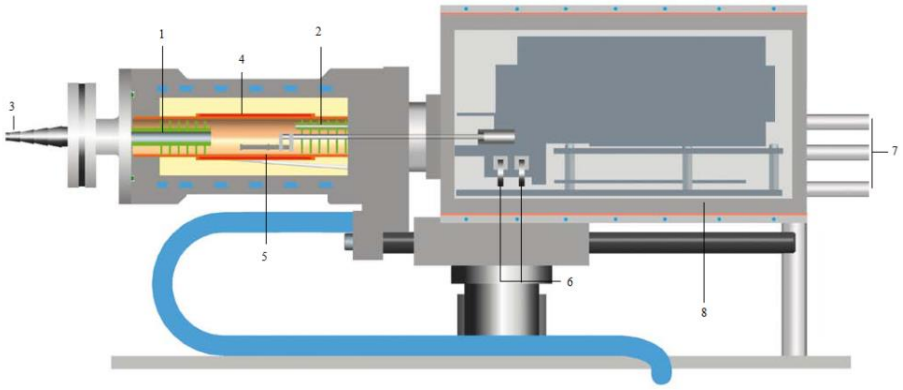

Figure 3.4 A schematic representation of a TGA instrument. 1 Baffles, 2 Reactive gas capillary, 3 Gas outlet, 4 Furnace heater, 5 Furnace temperature sensor, 6 Adjustment ring weights, 7 Protective and purge gas connector, 8 Thermostated balance chamber (www.mt.com/ta-handbooks)

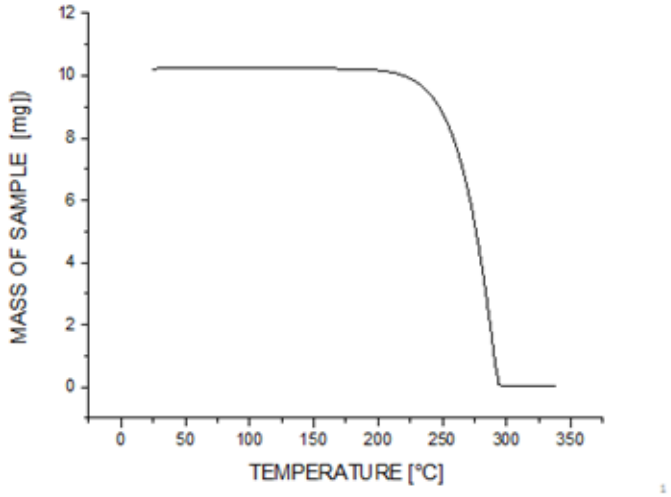

Figure 3.5 An example of typical TGA curve.

3.2.2. Spectroscopic methods

Spectroscopy defines the interplay between electromagnetic radiation and the sample. The technique provides valuable information for the identification and characterisation of substances. There are many spectroscopic techniques but all shares the basic underlying principle of exposing the sample to a beam of an electromagnetic radiation of a specific wavelength and response of the molecules of the sample to these radiation provide information about the structure and properties of the sample.

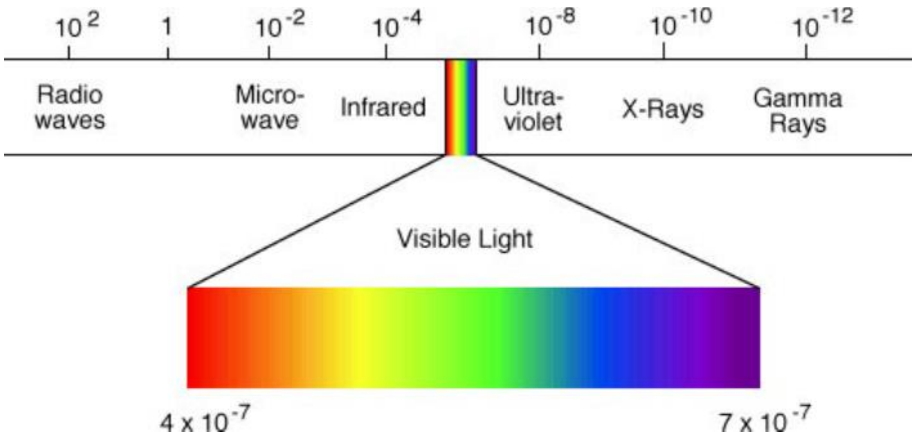

Figure 3.6 Electromagnetic spectrum.

The spectroscopic techniques utilise different ranges of the electromagnetic spectrum (Figure 3.6) and therefore, selection of the technique depends on the process and material of interest, for example, ultraviolet (UV) spectrometry analyses electronic transitions whilst, Infra-red (IR) uses lower energy light to probe vibrations and even secondary structures of materials.

3.2.2.1. Fourier transform infrared spectroscopy (FTIR)

FTIR is a convenient, non-destructive technique and is used for both qualitative analysis, like identification of molecules in the sample, and quantitative analysis such as concentration of the individual component in the sample (*Smith, 2011*). Academic, quality control / quality assurance and forensic laboratories are frequently use the technique as an integral part for the identification and characterisation of the substances.

Infrared absorption pattern is unique for every substance as bonds within a compound has a different frequency of vibration. The infrared spectrum is divided into various regions consisting of Near-IR region which ranges between 14,000-4,000 cm^{-1}, Mid-IR region which ranges between 4,000-400 $cm^{-1}$and Far-IR ranges between 400-4 cm^{-1}. Mid-IR region is the most widely used region for IR instrumentation (*Smith, B., 2011*).

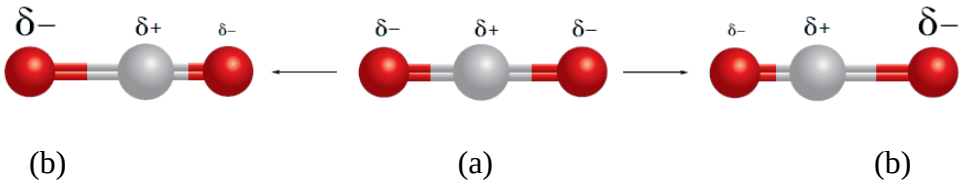

Figure 3.7 (a) No permenant dipole moment due to symmetric stretching, (b) temporary dipole moments due to assymmetric stretching.

In order for a molecule to be IR active there must be a change in electric dipole moment of the molecule. For example, the asymmetric stretching (Figure3.7b) of carbon di oxide generate a net charge in dipole moment and will produce a

peak in IR spectra whereas in symmetric stretching (Figure 3.7a) both oxygen atoms are moving away from carbon and the net dipole moment cancel out each other and no peaks will appear.

Figure 3.8 FTIR spectrophotometer (Lab source)

FTIR measures the intensity of an absorbed infrared radiation at a particular wavelength when molecule of a substance undergoes a net change in dipole moment resulted from its vibrational or rotational motion (*Kong, and YU, 2007*). Each peak observed in a spectrum correlates to the molecular structure as specific bonds have a specific vibrational infrared region thus provide qualitative or quantitative information about the material. FTIR mainly consists of an IR source, the interferometer, a laser, and a detector. Figure 3.9 illustrates the basic components located within the instrumentation.

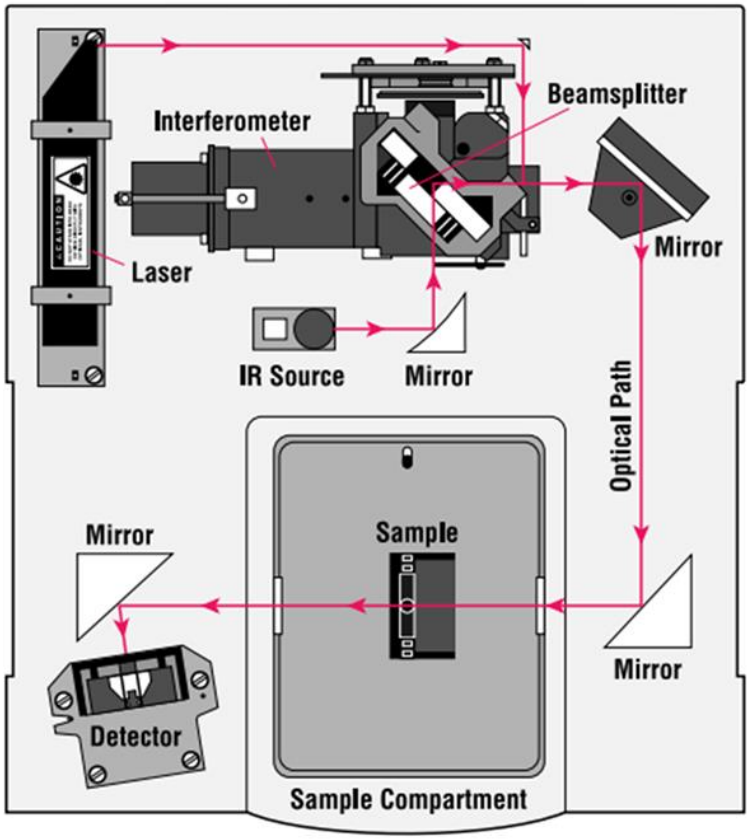

Figure 3.9 Lay out of fourier transform infrared spectrometer (http://mmrc.caltech.edu/FTIR/FTIRintro.pdf).

3.2.2.2. Raman spectroscopy

Raman spectroscopy is a vibrational spectroscopy which is very sensitive to molecular geometry. The technique relies on inelastic scattering which was discovered in 1928 by Chandrasekhara Venkata Raman. The analysis requires a very small sample with little or no sample preparation. Raman spectroscopy has a wide range of application for example, monitoring polymorphism and crystallisation (*Simonea, et. al. 2014*). Other applications include

pharmaceutical analysis (*Vankeirsbilck, et. al., 2002*) and drug interaction studies (*Mehrotra, et. al., 2013*).

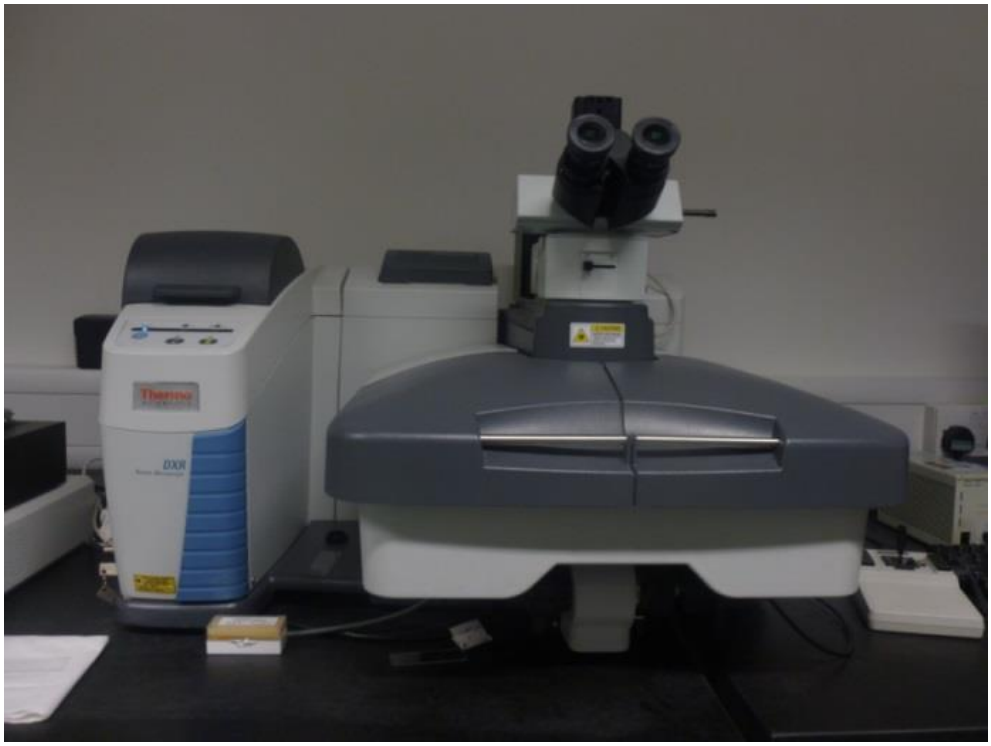

Figure 3.10 Raman spectrophotometer (Lab source)

Raman scattering or inelastic scattering occurs when a monochromatic light irradiates a sample and causes the excitation of its molecule from lower energy state to a virtual higher energy state followed by relaxation. Most of the scattered light comprises of the same incident frequency and referred as elastic or Rayleigh scattering however, when the excited molecule relaxes to a higher vibrational level than the initial level, the scattered photon will be shifted to a lower frequency and the phenomenon is known as Stokes scattering.

Conversely, when the excited molecules relax to a lower vibrational level than the initial level, the emitted photons will be shifted to a higher frequency and is called Anti-Stokes phenomenon (Figure 3.11).

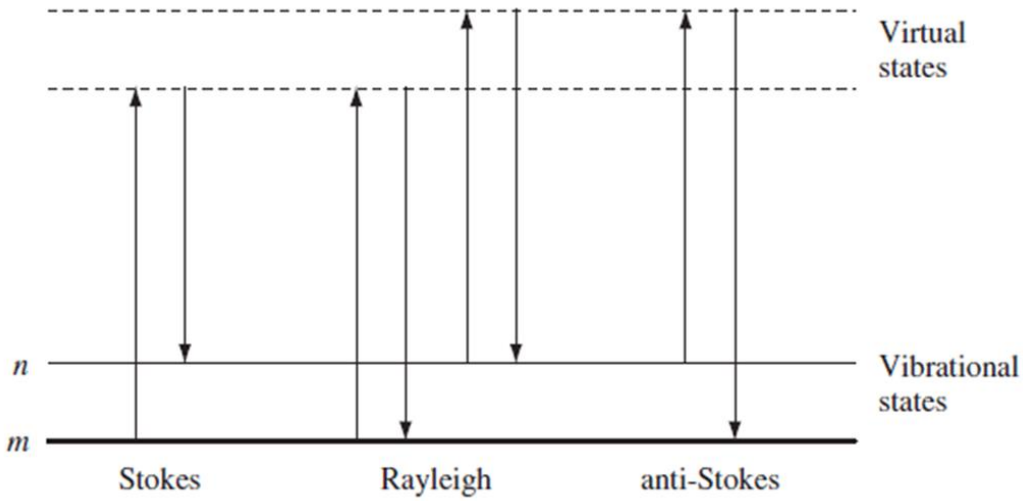

Figure 3.11. A representation of the transitions involved in Raman spectroscopy (*Smith & Dent, 2005*).

The observation of vibrational modes in the Raman spectrum is determined by the change in molecular polarisability associated with the vibration when a beam of intense radiation passes through a sample. This change in polarisability results in information regarding the molecular structures of sample. An advantage of Raman spectroscopy is that proteins in aqueous solution can be investigated in addition to their solid state because water is a weak Raman scatter. Raman spectrophotometer consists of a laser beam that has a wavelength that varies from 785nm to 532nm. A photo-detector, such as

a charged couple device (CCD), records the intensity of Raman scattering in arbitrary units by wavelength.

Fluorescence, another type of inelastic scattering, which normally overlaps with Raman spectra may be troublesome because Raman spectral landscape may be masked by even trace quantities of fluorescent material therefore fluorescence background interference should be avoided as much as possible during the detection of Raman spectra. Various strategies have been used to overcome or to reduce fluorescence interference, such as photo-bleaching, low sample temperature, drop coating deposition Raman (*Zhang et al., 2004*).

Raman spectroscopy is extremely useful in the identification and characterisation of new polymorphs (*Larkin, et al 2014*) and monitoring phase transitions as the technique is extremely sensitive to any change in the molecular geometry and variations in the intermolecular and intramolecular interactions.

3.2.2.3. Nuclear magnetic resonance spectroscopy (NMR)

NMR spectroscopy has been an important analytical tool for investigating compounds for many years. It is an excellent alternative to X-ray diffraction for compounds that are difficult to crystallise and provide quality information to elucidate the structure of molecules. Nowadays NMR is not limited to small biomolecules; current research includes the study of larger compounds and bio-macromolecules, such as proteins even in a living environment (*Sakakibara, et. al. 2009*). In addition to structural information about natural compounds, NMR

drug research generally includes characterisation of a range of its physical and chemical properties, dynamics and interactions of bio-macromolecules. The rapid development of NMR techniques has offered many new opportunities for more effective research (*López-Cebral, et al., 2014*).

NMR experiment relies on intrinsic spin properties of nuclei. The experiment is carried out in three steps which involve exposure of the sample to a constant and static magnetic field at the first place then its nucli are excited with a radio frequency pulse and finally the frequency of the emitted signals are measured. The precession of the spins is recorded during the free induction decay of the NMR experiment and converted into a frequency spectrum after Fourier transformation. The NMR active nuclei of atoms (the nucleus have an overall spin) in the sample have specific resonance frequencies when excited by the radio frequency pulse. The values of these frequencies are greatly affected by the typical nucleus and its neighbourhood atomic environment. In the strong magnetic field atomic nuclei of the sample align according to their spin and their electrons start circulating around the nucleus due to their interaction with magnetic field. The spinning of electrons creates its own magnetic field against to the applied magnetic field. The phenomenon is called shielding effect and the difference between the two fields at the nucleus is called nuclear shielding. The change in the applied magnetic field due to shielding is small and usually measured in parts per million (ppm). Several parameters can be read from the spectra which provide information about the structure of the molecule such as chemical shift which represents nature of the nucleus and describe its local

neighbourhood due to the effect of the electron configuration. Hence, all nuclei exhibit different chemical shifts which helps in their identification in the NMR spectrum. Another important parameter which provides angle information is the scalar J-coupling because it can calculate it for nuclei separated by up to three bonds and in such case the parameter is called ^{3}J coupling. The parameter indicates specifically intramolecular indirect magnetic interaction of two nuclear spins generated through the bonds between two nuclei.

In the structural analysis of organic molecules normally ^{1}H and ^{13} C NMR for the compound are obtained along with other NMR experiments outlined below.

3.2.2.3.1. ^{1}H NMR

^{1}H NMR experiment is primarily used for structural identification. In the ^{1}H NMR of a molecule, each type of proton can be deduced from a characteristic shift and its integration. The multiplicity and extent of coupling constant of the protons provides an indication of the neighbourhood and their spatial positioning (*Williams and Fleming, 2008*).

3.2.2.3.2. ^{13}C NMR

^{13}C NMR describes the chemical shifts of the carbon. The natural isotope of carbon (^{12}C) has no nuclear spin hence, to observe carbon chemical shifts ^{13}C is used to determine the number of carbons and their type.

3.2.2.3.3. Heteronuclear multiple quantum coherence (HMQC)

HMQC is a 2D ^{1}H-^{13}C experiment. In a HMQC spectrum, the ^{1}H and ^{13}C spectrum is plotted along the x-axis and y-axis, respectively. Cross-peaks show protons and carbons that are directly linked to each other (*Williams and Fleming, 2008*).

3.2.2.3.4. Nuclear Overhauser effect spectroscopy (NOESY)

^{1}D NOE experiment is useful for determination of the relative stereochemistry of a specified proton (*Williams and Fleming, 2008*). The basics of the Nuclear Overhauser effect spectroscopy is that a magnetic nucleus can interact with another magnetic nucleus through space. Thus, when one of the protons at its resonance frequency is irradiated can cause an increase in the intensity of the other proton signal(s) provided that the distance between the two protons is not more than 2-4 Å.

3.2.2.3.5. Correlation spectroscopy (COSY)

Cosy experiment is important to demonstrate ^{1}H-^{1}H connectivity. The proton shifts are plotted on both axes with the contour plot along the diagonal of the square. Cross peaks also called spin-spin coupled protons are arranged along the diagonal symmetrically. Various observations can be made in a cosy spectrum for example the correlations due to geminal (2*J*) and vicinal (3*J*) couplings (*Williams and Fleming, 2008*).

3.2.2.4.. Circular Dichroism (CD) Spectroscopy

Circular dichroism spectroscopy is a valuable, non-destructive and frequently used method for the estimation of structural properties of complex biological systems such as peptides and proteins and to follow the structural changes. The technique is also valued in measuring folding kinetics, thermal stability, binding kinetics and effect of different agents which effect structure properties of peptides and proteins (*Fiedler. et. al., 2013*).

Plane polarised light is made up of two circularly polarised components which are equal in magnitude but rotating in opposite direction and referred as left (L) and right (R) handed circularly polarized light. CD refers to the measurement of the difference in absorption of these two components by an optically active chiral chromophore (*Kelly and Price. 1997*).

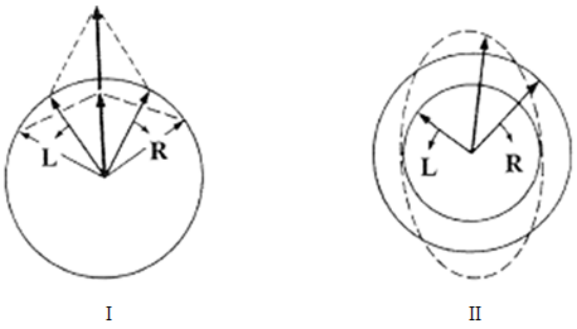

Figure 3.12 (a) The (L) and (R) circularly polarised components in (I) showing the equal magnitude and result into plane polarised radiation when combine whereas, in (II) the components are not same in amplitude and when combine generate (dashed line) elliptically polarised radiation.

The circularly polarised components, when passed through the sample, will generate either original plane due to equal absorption of the polarised light or create elliptical polarisation for the reason that the L and R components are absorbed to different magnitudes Figure 3.12 (*Kelly. et al., 2005*).

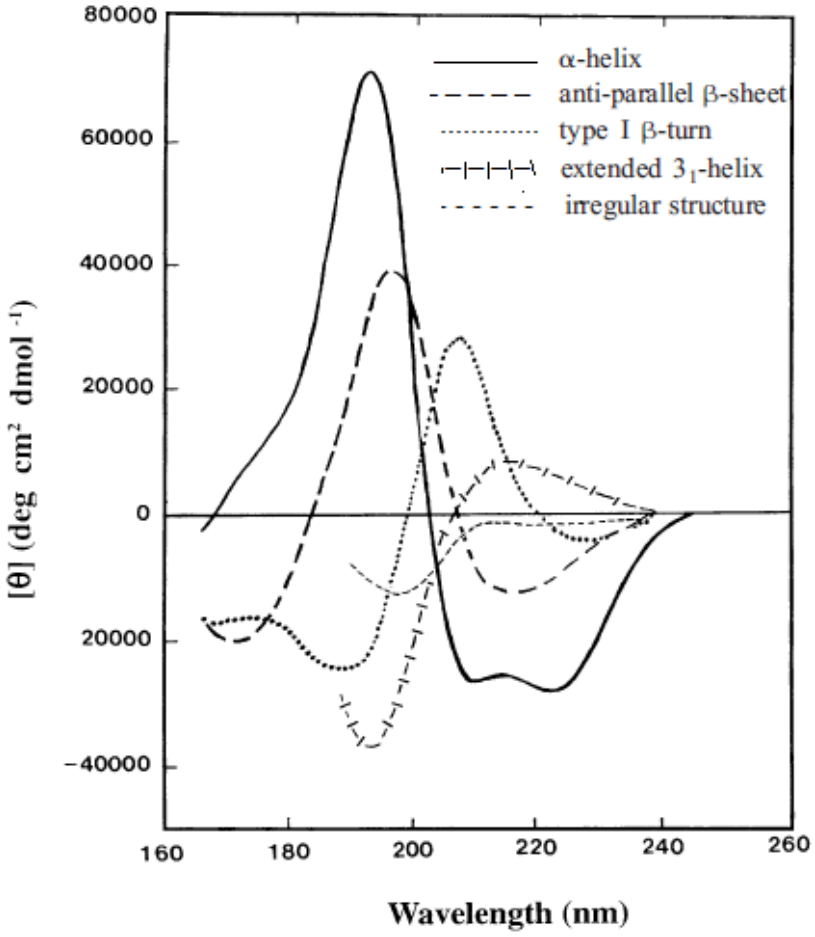

Figure 3.13 Far UV CD spectra showing different types of secondary structures (*Kelly. et al., 2005*).

Different types of secondary structures in peptide or protein, such as α-helices, β-sheets, β-turns and random coil, induce characteristic bands in the far-ultraviolet region (Figure 3.13). It is reported that α-helix give rise to a

positive band at 190 nm and two negative bands one at (π- $\pi*$ transitions) 208 nm and the other at is positioned at about (the amide n- $\pi*$) 220 nm (*Dafforn, et. al. 2004*). Other structural elements provide specific shapes and magnitudes in the CD spectrum at their specific regions.

The units for the CD spectra are in millidegrees this can be converted to mean residual ellipticity (MRME), the units of which are degrees cm^2 $dmol^{-1}$, using the equation below.

$$\theta_{MRW} = \frac{MRW.\theta}{10.l.c} \qquad 3.1$$

Where,

θ = measured ellipticity (millidegrees), c = protein concentration (mg/ml),

l = path length (cm), and MRW = protein mean residue weight.

MRW for the peptide bond is calculated from the following formula;

$$MRW=M/(N-1) \qquad 3.2$$

Where,

M is the molecular mass of the peptide chain and N is the number of amino acids. Number of peptide bonds is N-1.

3.2.3. Microscopic methods

Various microscopic techniques below have been used to determine the morphology of the materials prepared during the studies discussed in the thesis.

3.2.3.1. Polarised light microscopy

Most crystals are birefringent (difference between high and low refractive index which occurs when a refracted ray experience a retardation in speed of light) therefore, plane polarised light microscopy is of significant advantage as compared to bright field microscopy for the observations of crystal growth or selection of a quality crystal for single crystal X-ray diffraction studies. There are few exceptions which impose little limitation to use this phenomenon as a test for crystallinity for instance, crystalline materials representing high symmetry systems may not display birefringence because of having only one vibration direction and refractive index for example cubic crystals. Similarly, organic fibres or liquid crystals show this property of birefringence although they are not fall into the definition of classic crystals.

The construction of the microscope is such that polarising filters are fixed above and below the sample stage. The incident light is constrained by the first polariser to vibrate in one plane only, and the polariser above the sample is rotated to a 90 degree angle forming a position in which the polarisers are crossed. This geometry allows only the light that is rotated by the sample and is transmitted to the eyepiece. The field of view will appear dark when an amorphous materials are looked through cross-polarisers, whereas,

polycrystalline materials or crystals will cause the refraction of light and will be easily viewed.

3.2.3.2. Scanning electron microscopy (SEM)

SEM is a non-destructive tool to develop three-dimensional images at higher level of magnification using a high-energy beam of electrons (*Lawes, 1987*).The SEM is used in many different areas of research and industry like pharmacy, biology, agriculture, conductors and electronics (*Kiesow, et. al. 2003; Leamy, 1982*) for a variety of applications. SEM permits identification and analysis of solid bulk specimen, allowing for the surface topography, morphology and electrical conductivity etc.

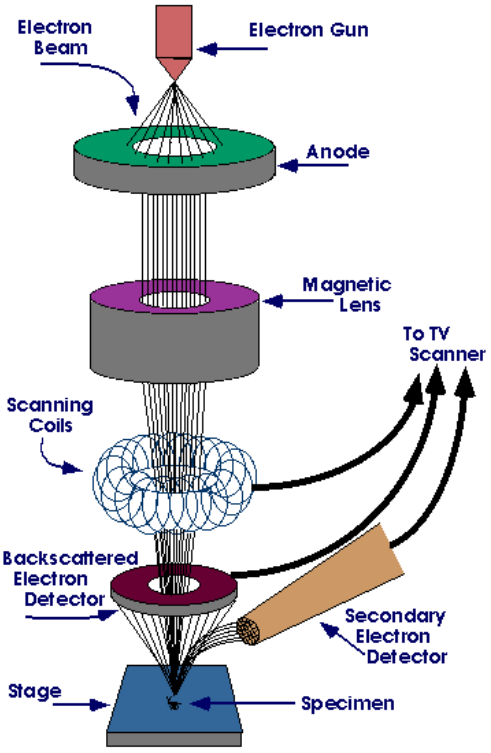

Figure 3.14 Scanning Electron Microscope Components (http://www.purdue.edu/rem/rs/sem.htm.

Figure 3.14 shows the main construction components of SEM which includes, electron source produced from the cathode of an electron 'gun' which is either a tungsten wire or a lanthanum hexaboride rod (*Lee, 1993*), electron lenses comprise of condenser and objective lenses sample stage, detector scintillator/photomultiplier, specimen current detectors, and data output device.

SEM uses a high energy beam of electrons which is applied to the sample under vacuum. The voltage of the electron beam is manipulated to generate a clear image with high resolution. The electron beam travels through the column to the condenser lenses which reduce the diameter of the beam and the scanning coils control the focused electron beam over the sample. The coils also play role in targeting the electron beam to the centre of the objective lens which further shrinks the diameter of the beam and direct the electrons to a minimum spot size on the sample (*Lawes, 1987*). The electron beam when accelerate onto the focused atoms of the sample cause collisions which result into an elastic or inelastic scattering. The scattering results in signals which are used for imaging and quantitative information of the sample.

Figure 3.15 illustrates the typical signals used for imaging, which include secondary electrons, backscattered electrons, auger electrons, and photoelectrons (*Hayat, 1975*). The detector collects the radiation and converts it into an electrical signal which is amplified to a significant magnitude that will display an image of the sample (*Lee, 1993*).

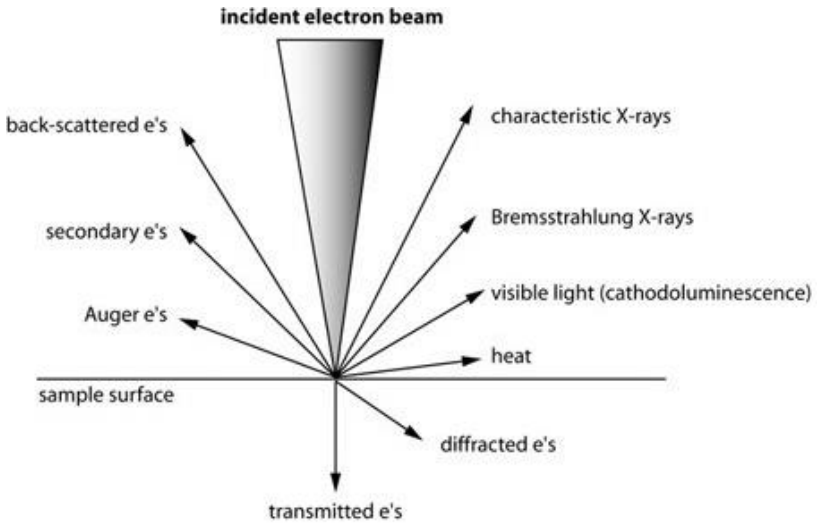

Figure 3.15 Types of beam-specimen interactions (*Henry, 2012*)

SEM technique requires electrically conductive samples. The sample is mounted on a stub by means of a double-stick adhesive carbon tape (*Beane, 2004*). The materials which are not conductive are coated with a conductive material like carbon or gold, with a device called a "sputter coater". The experimental and sample consideration should be taken in to account to select the coating material and coating thickness so that it should not cause interference with the imaging or analysis (*Hayat, 1975*).

3.2.3.3. Atomic force microscopy (AFM)

The concept of AFM was presented for the first time in 1986 (*Binnig and Quate, 1986*). Atomic Force Microscopy is a surface biophysical probe which has now having increased use in physical sciences and biological sciences for topographical imaging and force measurements. (*Last, et.al., 2010*). The technique is useful to investigate a broad range of materials i.e. plastic, metals,

glasses, semiconductors, and soft biological material like cell wall and bacteria. AFM provides a high resolution three dimensional image of the surface on a nano scale, by measuring forces between a probe and surface.

The probe is fixed on a flexible cantilever (a sharp tip). The cantilever come in contact with the surface of the sample in various modes. In a traditional AFM, there are three operating modes used to get image and those are; **contact mode** where the probe is in constant contact with the sample surface (*Weisenhorn, et al., 1989*), **tapping-mode**, the cantilever is oscillated through the sample surface at its resonance frequency maintaining a constant oscillation amplitude (*Putman. et. al.1994*) and **non-contact mode**, the oscillating probe at its resonant frequency does not contact the sample surface, but instead kept at a distance within the long-range van der Waals attractive forces of the probe-sample interaction during surface scanning (*Luthi. et. al.1994*).

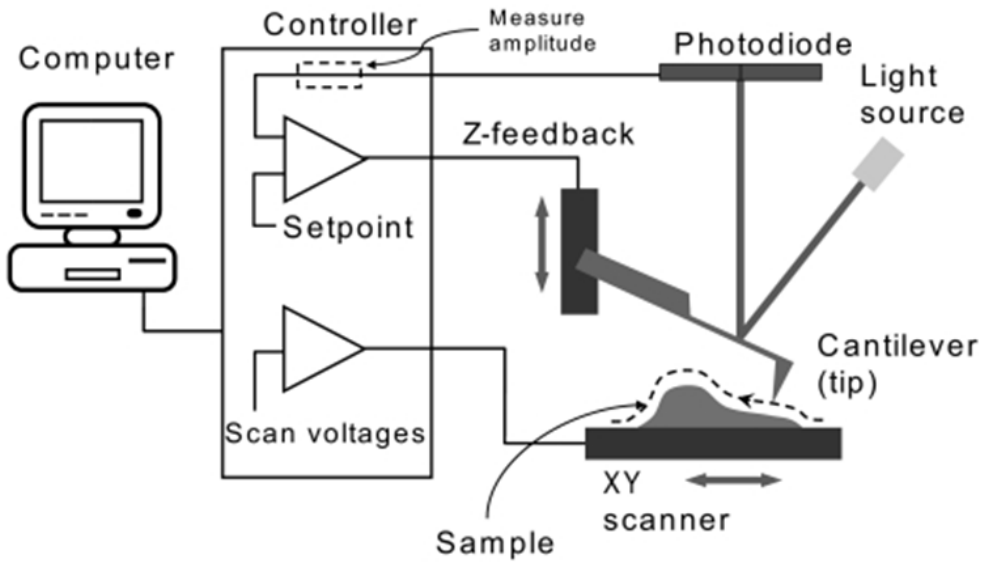

Figure 3.16 Schematic representation of the AFM set up (*Last, et.al. 2010*).

A probe attached to a cantilever is scanned over the sample surface to acquire a topographical image. The movement of the cantilever is controlled through a piezoelectric ceramic scanner which work on an electronic feedback mechanism. While the probe is scanning across the sample a laser beam is bounced off the back of the cantilever onto a position sensitive photodiode detector and small change in cantilever is measured through an atomic-scale sensitivity optical lever system. The measured cantilever deflections are processed by the system to generate an image of the surface topography (Figure 3.16).

3.2.4. Laser diffraction for particle analysis

Laser diffraction technique is a reliable and commonly used method for particle size analysis in many applied areas such as ceramics, food, cosmetics and particularly in pharmaceutical industry (*Syvitski, 1991*). Laser light scattering technique measure the intensity of a scattered laser light beam when it strikes on a sample. Various particulate related factors like optical properties, shape and size affect the scattered light intensity at different directions (*Merkus, 2009*). Particle size, shape and distribution has significant importance in product development and quality control as it directly affects the bulk properties, processability, dissolution and stability of the intermediates and end product.

The laser diffraction technique is based on the principle that particles of a given sample passing through a laser beam will diffract light at an angle inversely proportional to particle size (*Ozer, et .al., 2010*). As seen in figure

3.17, larger particles causes light scattering at narrow angles with high intensity while light scattering at wider angles with low intensity are associated with small particles.

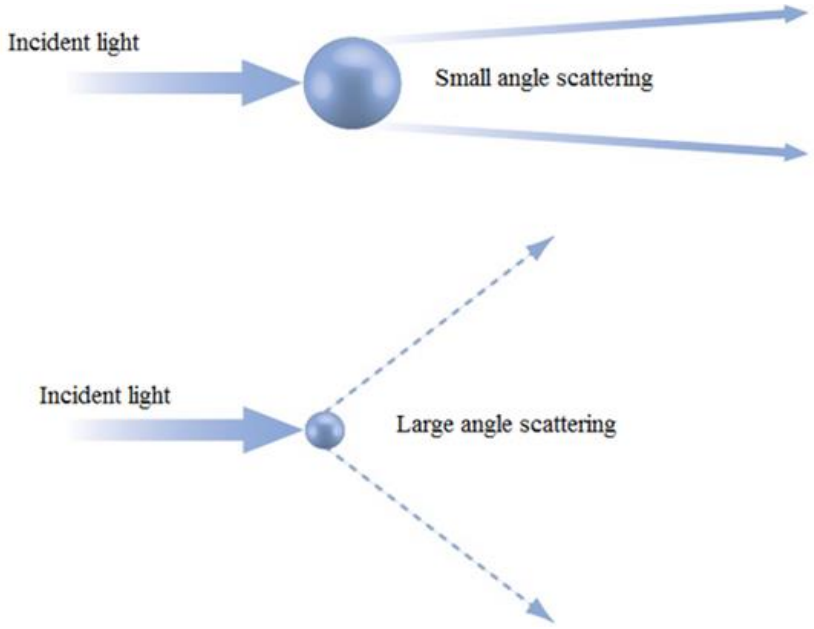

Figure 3.17 Scattering of light from small and large particles (*Rawle, 2012*)

The sample preparation requires the dispersion of sample in a gas or a liquid and the intensity of the angular scattering light are recorded and particle size and distribution is calculated based on Mie theory of light (*Washington, 1992*).

A laser diffraction instrument (Figure 3.18) comprises of a laser light source, suitable detectors to determine the intensity at different angles of the remaining light and the scattered light from various sized particles. Lastly, the computer software process the signals an interface and calculate the particle size and its distribution.

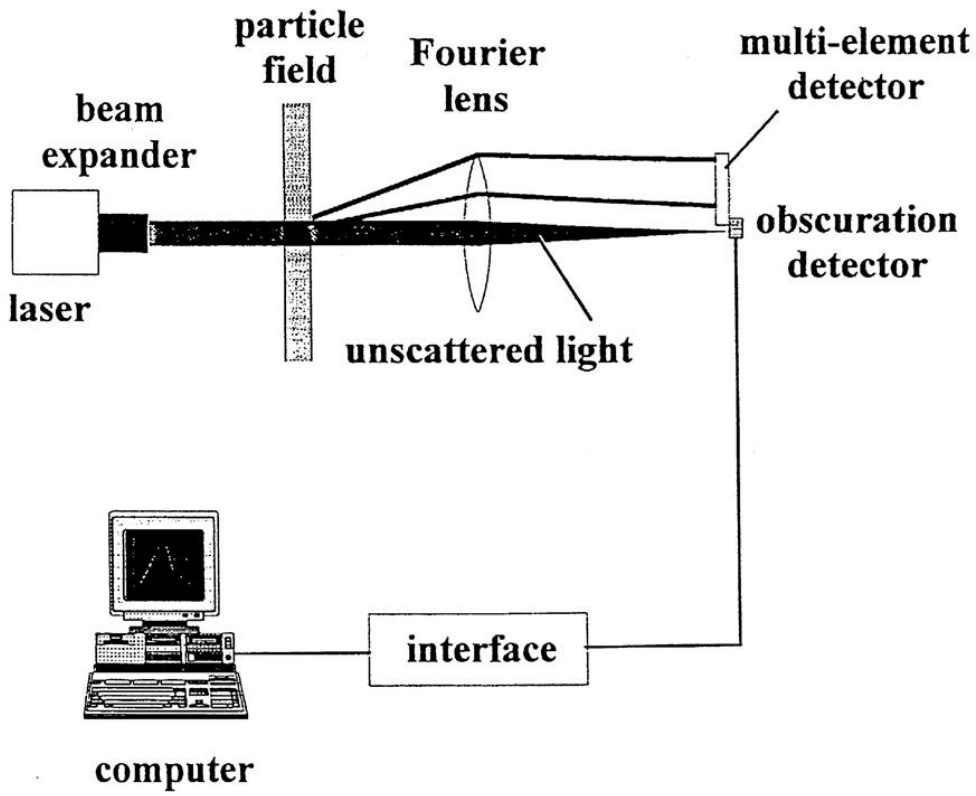

Figure 3.18 Typical laser diffraction particle size analyser (*Ma,et al., 2000*)

Laser diffraction scattering technique can measure wide range of particle size ranging from 0.1μm -3,000μm and both dispersed segregated and agglomerated particles can be analysed within 0.01-30 seconds (*Kippax, P. 2007*).

3.2.5. Crystallography

Crystallography is defined as the "Science dealing with the system of forms among crystals, their structure, and their forms of aggregation" (*Webster, 1983*). Investigating structural properties of crystalline materials by acquiring its three dimensional molecular structure through X-ray diffraction is the subject of study in many research areas of chemistry, material sciences

(*Gorfman. 2014*), biological sciences (*Smyth and Martin. 2000*) and many others. The year 2014 is declared as the International Year of Crystallography by United Nations to commemorate the hundred years of the discovery of X-ray crystallography since the pioneering work in crystallography commenced by William Henry Bragg and William Lawrence Bragg in 1913.

3.2.5.1. Diffraction experiment for crystal structure analysis

X-rays are the electromagnetic radiations and are generated by bombardment of electrons on a metal plate for example tungsten, molybdenum, copper etc. and each metal gives a characteristic wavelength (Figure 3.19). The X-ray wavelength generated by molybdenum is 0.71073 Å and that of copper is 1.54184 Å are commonly used as X-ray source depending upon their suitability to be diffracted by atoms in the crystal (*Clegg, 2006*).

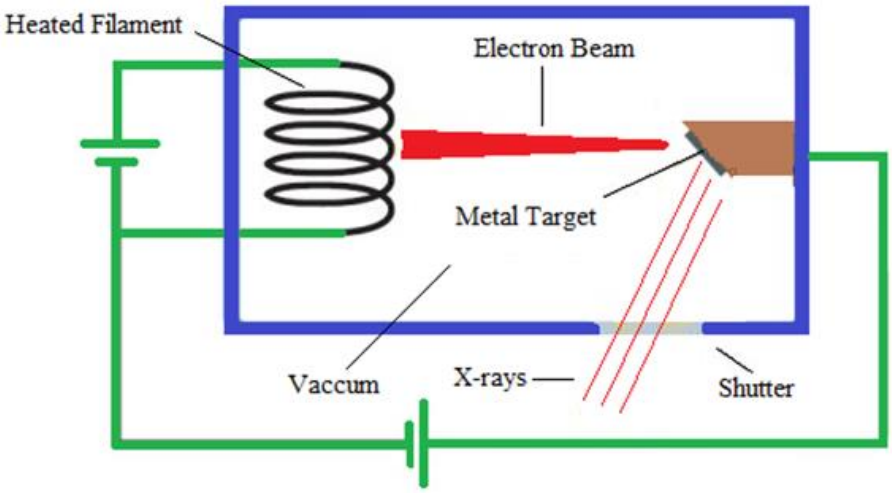

Figure 3.19 Schematic diagram of the X-ray production.

The X-rays are of comparable wavelength to interatomic distances observed in crystalline materials and form the basis to study crystalline solids by X-ray diffraction techniques. When an intense beam of monochromatic X-rays strikes a crystalline sample (powder or single crystal), the beam is scattered in particular angles with different intensities. This phenomenon is known as diffraction. The scattered X-rays can be recorded with a detector as a spot giving a unique diffraction pattern (Figure 3.20). The regular array of spots and their corresponding intensities generate information on the unit cell parameters, the coordinates of the atoms in the asymmetric unit and the space group. The characteristic diffraction pattern is then used to explain structural information about the atomic arrangement and molecular features to understand observed physico-chemical properties.

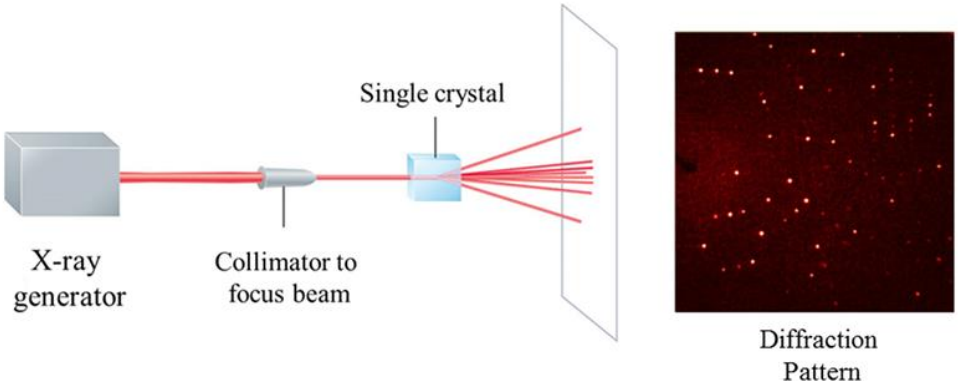

Figure 3.20 Schematic representation of an X-ray beam entering a crystal. The diffracted X-rays produce a diffraction pattern.

3.2.5.2. Crystal

A crystalline solid is composed of atoms, molecules or ions stacked in a systematic way giving rise to repeating three dimensional long range order structures. The crystal structure are generally described by the contents of the unit cell and the repeating pattern of it in all three dimensions. The repeating pattern is represented by symmetry and to explain the symmetry crystal lattice is obtained by taking all equivalent points in the structure exhibiting a regular pattern of identical points which are related to each other by translational symmetry.

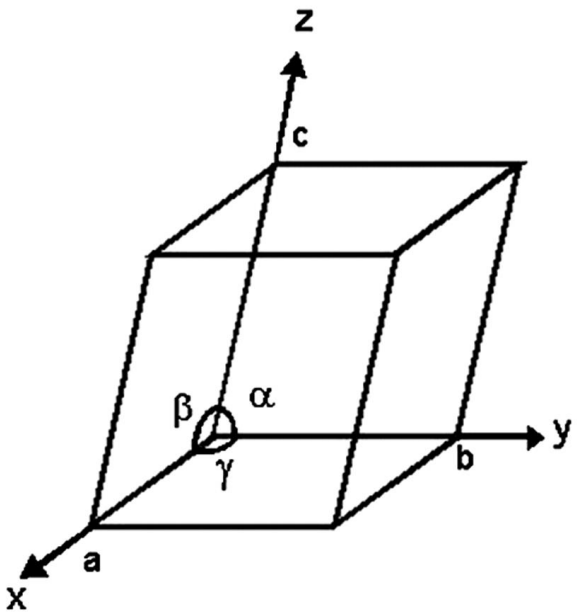

Figure 3.21 A unit cell

In other words the lattice may be defined as an array of points in space in which each point is identical in surrounding and orientation. In ideal crystal the repeating unit of a crystal lattice is known as unit cell. A unit cell can be

explained by three lattice vectors: **a, b, c** or with constant axial lengths *a, b,*and *c* in angstroms (Å) and interaxial angles α, β and γ (Figure 3.24).

The general recommendations is to select a unit cell with shortest possible three sides of equal length and their interaxial angles near to 90° however, internal symmetry in the unit cell restrict the number of unit cell choices. These restrictions in choosing a unit cell geometry categorise the crystal structures into seven different types known as crystal systems shown in Table 3.1.

Table 3.1 Crystal systems and unit cell restrictions.

Crystal system	Axial Lengths	Axial Angles	Cell Type
Triclinic	$a \neq b \neq c$	$\alpha \neq \beta \neq \gamma$	*P*
Monoclinic	$a \neq b \neq c$	$\alpha = \gamma = 90^o, \beta > 90^o$	*P , C*
Orthorhombic	$a \neq b \neq c$	$\alpha = \beta = \gamma = 90^o$	*P, C, I, F*
Trigonal	$a = b = c$	$\alpha = \beta = \gamma \neq 90^o$	*P, I*
Tetragonal	$a = b \neq c$	$\alpha = \beta = \gamma = 90^o$	*P*
Hexagonal	$a = b \neq c$	$\alpha = \beta = 90^o\ \gamma = 120^o$	*P*
Cubic	$a = b = c$	$\alpha = \beta = \gamma = 90^o$	*P, I, F*

In each crystal system the lattice point within the unit cell may be arranged in different ways. The combination of unit cell centring and crystal system defines the 14 lattice types also called the Bravais lattices (Table 3.1). Unit cell where the lattice points are present at the corners is called primitive (P) but when the lattice points are on corners as well as centred on opposite pair of faces (A, B, C) or on all faces (F) they are called face centred . Lastly, body centred (I) are assigned to those in which the lattice points are on the corners

and in the centre of the unit cell body. In the crystalline solid, the individual molecules within the asymmetric unit are described by one of the 230 unique space groups (*Clegg, W. 2006*). These space groups are based on the symmetry elements like inversion centres, rotation axes, mirror planes and together with internal translations such as screw axes and glide planes making 230 possibilities of grouping these symmetry elements within the lattices

3.2.5.3. The Bragg equation

The diffraction of X-rays by a crystal lattice arises from the constructive interference of X-rays scattering and recombination. For a constructive interference it is necessary that the path differences of the X-rays diffracted by a lattice plane and subsequent lattice plane(s) below must be a whole number of wavelengths. The angle in which this interference is constructive is correlated by Bragg's law equation (3.3).

$$n\lambda = 2d \sin \theta \qquad \text{Eq. 3.3}$$

where,

λ is the incident beam and θ (°) is the scattering angle of the diffracted beam. With known value of wavelength λ and measured scattering angle θ, the interplanar distance d can be calculated, as shown in Figure 3.25.

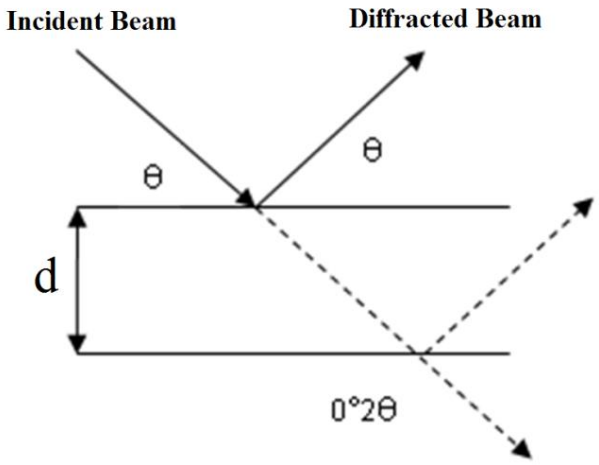

Figure 3.22 Schematic representation of Bragg Equation.

3.2.5.4. Crystal structure determination

3.2.5.4.1. Growing crystals

Growing single crystals is the first step in X-ray crystal structure determination followed by data collection leading to structure solution.

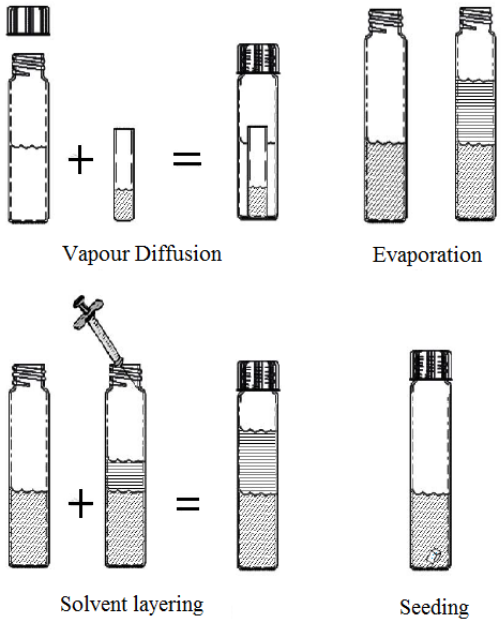

Figure 3.23 Scheme of crystal growing techniques.

Growing diffraction quality crystals is a science of patience as it often met with challenges like crystal stacking or twinning etc. The preparation of quality crystals depends on many factors like concentration, solubility, temperature, and last but not the least luck. There are several methods (Figure 3.26) proved effective in crystal growing, including, vapour diffusion, evaporation, solvent layering, and seeding.

3.2.5.4.2. Data collection

An X-ray diffractometer is used to collect crystal data. A schematic illustration of a typical diffractometer can be seen in Figure 3.24.

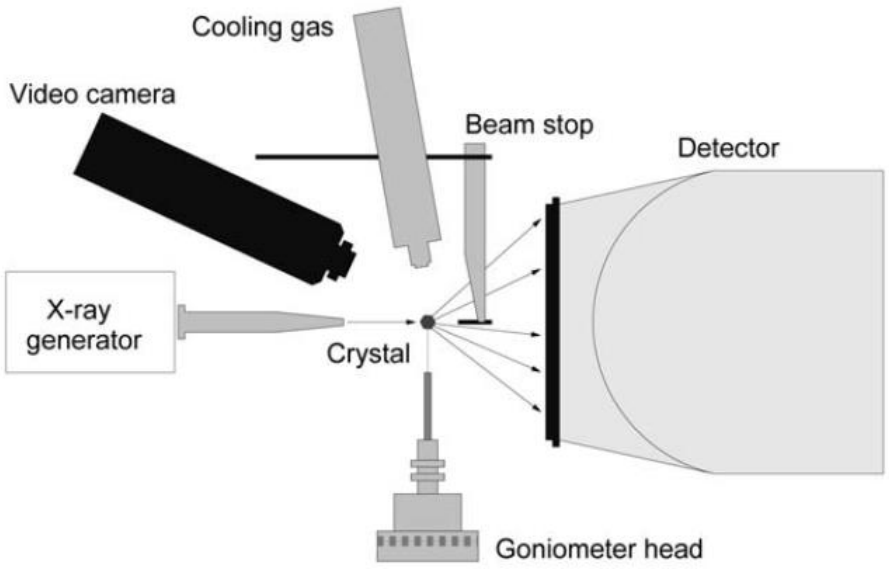

Figure 3.24 Schematic of an X-ray diffractometer. (*Kooijman, H. 2005*)

It is essential to focus X-ray beam through a crystal fixed on a goniometer head and to make sure that a beam stop is positioned in between the crystal and the

detector in order to prevent non-diffracted X-rays directly hitting the detector. The detector records the position and intensity of the diffracted X-ray beams. A video camera is used to aid in centring of the crystal and lastly a cryostream is placed on top of the crystal to control the temperature to lower the thermal vibrations and stabilize air sensitive crystals.

After the crystal is centred, the shutter is opened and X-ray beam hits the crystal, the crystal scatter the diffracted radiations into a characteristic pattern based on Bragg's Equation (Eq 3.3). The diffracted X-rays are recorded on a charge coupled device (CCD) area detector in the form of spots of different sizes and intensities referred as reflections. In case of an amorphous or polycrystalline material dark rings will be produced instead of spots (Figure 3.25).

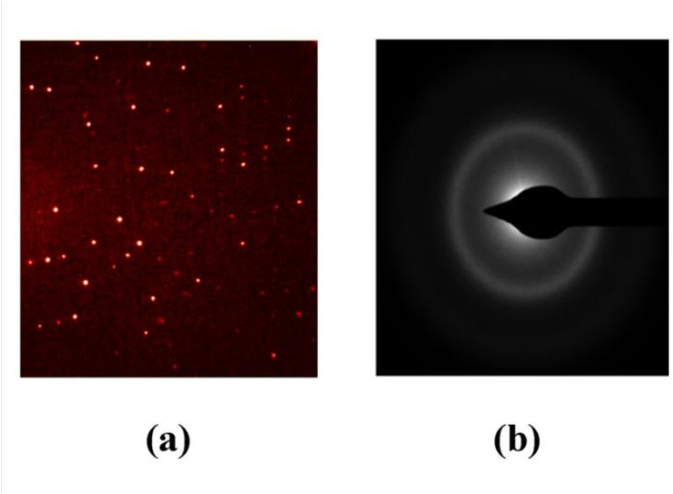

Figure 3.25 Images of (a) single crystal and (b) an amorphous material.

A crystal can give a good data if the experimental parameters are programmed properly for instance, exposure time etc., as many factors are important to get a

quality data of the reflections. A full crystal data is recorded as the crystal is rotated in a pre-determined manner through various orientations around three rotational angles; Omega, Kappa, and Phi.

With few initial frames unit cell and crystal system can be determined followed by a full data set. If the data is poor or if the cell parameters are of known starting material then the experiment is terminated.

Thousands of reflections are recorded from a crystal giving information about its intensity (*I*), standard uncertainty (σ (*I*)) and its orientation matrix which relates the diffractometer axis to the unit cell axes. The measured intensities of each reflection are converted to an observed structural amplitude $|F_0|$, and are assigned a structure factor, *F* which represent the amplitude and phase (Clegg, 1998):

$$F\,(hkl) = |\,F\,(hkl)| \cdot \exp[i\Phi(hkl)] \qquad \text{Eq. 3.4}$$

Once the diffraction data has been measured, the data reduction process generates a unique, corrected, and scaled data set. Data reduction produces a list of *hkl* indices with their intensity |F*h,k,l*| and errors σ(F*h,k,l*). Using this list the crystal structure can be solved by generating electron density map, from the reverse Fourier transform of the diffraction pattern. Here, the electron density (ρ) is visualised from the recombination of diffracted beams. For each position *xyz* from each reflection *hkl* in a unit cell of volume, V (Clegg, 1998);

$$\rho(xyz) = 1/v\sum_{h,k,l} |\,F\,(hkl)| \cdot \exp[i\Phi(hkl)] \cdot \exp[-2\pi i(hx+ky+lz)] \qquad \text{Eq. 3.5}$$

The limitation in diffraction pattern is that relative phases cannot be directly measured and without it equation 3.5 is unusable. This is called “phase problem” (*Clegg, 2006*). To overcome this issue various methods can be used but two of them are commonly employed and those are Patterson synthesis and Direct methods. “Patterson method” is generally preferred for solving crystal structures of molecules which contain heavy atoms. In this method initial model is built by determining the correct positions of the heavy atoms and then further refined by identifying all other atomic positions calculated through electron density map to solve the structure. ‘Direct methods’ is the approach which is commonly used and popular. The method is performed by selecting the most intense reflections and working out the probable relationships between their phases and then utilising a trial-and-error approach to find the best combination.

3.2.5.4.3. Refining the structure

Refining the crystal structure means to apply several numerical parameters for the atomic position, vibrational motion and other typical structural properties like bond angles and distances that gives the best fit to the observed data to build a more complete model of the crystal. The residual factor, or R-factor, is a parameter used to measure the fit of the model to the observed diffraction data and reported as a percent. The lower R-factor generally attributed to a best fit model. The R-factor is calculated (Eq. 3.6) by the summation of the observed structure factors (Fo) minus the calculated structure factors (Fc),

divided by the summation of the observed structure factors Fo).

$$R = \frac{\sum[|Fo| - |Fc|]}{\sum|Fo|} \qquad \text{Eq.3.6}$$

When the structural model is refined to a satisfactory stage then a crystallographic information file (cif) is created for scientific communication. This is a simple text file that contains details of the parameters applied in the X-ray diffraction data collection along with complete information about the distinct atom model.

3.3 References

Beane, R. (2004. Using the Scanning Electron Microscope for Discovery Based Learning in Undergraduate Courses. *Journal of Geoscience Education*. 52(3), 250-253**.**

Binnig, G., & Quate, C.F. 1986. Atomic Force Microscope. *Physical Review Letters. Vol. 56.* (9), 930-933.

Brittain, H.G. (1995). Physical Characterization of Pharmaceutical Solids. Ed. (Drugs and the Pharmaceutical Sciences Series 70), Marcel Dekker, Inc.,(ISBN 0-8247-9372-2).

Clas, S.D., Dalton C.R., & Hancock, B.C. (1999). Differential scanning calorimetry: applications in drug development. *Pharmaceutical Science & Technology Today*. *2*(8), 311-320.

Clegg, W. (1998). Crystal structure determination. Oxford University Press, Oxford.

Clegg, W. 2006. Crystal Structure Determination. New York:Oxford University Press.

Dafforn, T.R., Rajendra, J., Halsall, D.J., Serpel, L.C., & Rodger, A. (2004). Protein Fiber Linear Dichroism for Structure Determination and Kinetics in a Low-Volume, Low-Wavelength Couette Flow Cell. *Biophysical Journal.* 86. 404–410.

Fiedler, S., Cole, L., & Sandro, K.S. (2013). Automated Circular Dichroism Spectroscopy for Medium-Throughput Analysis of Protein Conformation. *Analytical Chemistry.* 85. 1868−1872.

Giacovazzo, C., Monaco, H.L., Artioli, G., Viterbo, D., Ferraris, G., Gilli, G., Zanotti, G., & Catti, M. (2002). Fundamentals of Crystallography, 2nd (ed.), Oxford.University Press, New York.

Gorfman, S. (2014). Sub-microsecond X-ray crystallography: techniques, challenges, and applications for materials science. *Crystallography Reviews.Vol. 20*, 3.

Henry, D. (2012). http://serc.carleton.edu/17272

Hayat, M.A. (1975). Principles and Techniques of Scanning Electron Microscopy. Vol. 4. Van Nostrand Reinhold Company: New York.

Hollas, J. M. (1996). Modern Spectroscopy, 3rd ed., John Wiley & Sons, New York.

Kelly, S.M. & Price, N.C. (1997).The application of circular dichroism to studies of protein folding and unfolding. *Biochimica et Biophysica Acta* . 1338, 161–185.

Kelly, S.M., Jess, T.J., & Price N.C. 2005. How to study proteins by circular dichroism. *Biochimica et Biophysica Acta*. 1751, 119 – 139.

Kiesow, A., Füting, M., & Heilmann, A. (2003). Environmental Scanning Microscopy - Applications in Pharmacy and Agriculture. *Microscopy and Microanalysis. Vol.9*, Suppl S03, 488-489.

Kippax, P. (2007). Aspects of particle sizing in pharmaceutical manufacturing. *Pharma.* 46-48.

Kong, J. & YU, S. (2007). Fourier transform infrared spectroscopic analysis of protein secondary structures. *Acta Biochimica et Biophysica Sinica*. *39*(8), 549–559.

Kooijman, H. (2005). Interpretation of Crystal Structure Determinations version 2.3 Utrecht University:Undergraduate course notes.

Larkin, P.J., Dabros, M., Sarsfield, B., Chan, E., Carriere, J.T. & Smith B.C. (2014). Polymorph Characterization of Active Pharmaceutical Ingredients (APIs) Using Low-Frequency Raman Spectroscopy. *Applied Spectroscopy. 68.* 7, 758-776.

Last, J.A., Paul, R.P., Nealey, P.F., & Murphy, C.J. (2010).The Applications of Atomic Force Microscopy to Vision Science. *Investigative Ophthalmology and Visual Science. 51*(12), 6083–6094.

Lawes, G. (1987). Scanning electron microscopy and X-ray microanalysis, ed. A. James. Chichester: John Wiley and Sons.

Leamy, H.J. (1982). Charge collection scanning electron microscopy. *Journal of Applied Physics*. 53, R51.

Lee, R. (1993). Scanning electron microscopy and X-ray microanalysis. New Jersey: Prentice-Hall, Inc.

Liu, F., Wu, J., Chen, K., & Xue, D. (2010). Morphology Study by Using Scanning Electron Microscopy in Microscopy: Science, Technology, Applications and Education (ed) Mendez-Vilas, A., & Diaz, J. Formatex Research Center. Badajoz, Spain.

López-Cebral, R., Martín-Pastor, M., Seijoa, B., &Sanchez, A..(2014). Progress in the characterization of bio-functionalized nanoparticles using NMR methods and their applications as MRI contrast agents. *Progress in Nuclear Magnetic Resonance Spectroscopy*. 79. 1–13.

Luthi, R., Meyer, E., Howald, I., Haefke, H., Anselmetti, D., Dreier, M., …. & Guntherodt, H.J. (1994). Progress in Non-Contact Dynamic Force Microscopy. Journal of Vacuum Science and Technology B. 12, 1673-1676.

Ma, Z., Merkus, H.G., de Smet, J.G.A.E., Heffels, C., & Scarlett B. (2000). New developments in particle characterization by laser diffraction: size and shape. *Powder Technology. 111*(1–2), 66-78.

Mehrotra, R., Jangir, D.K., Agarwal, S., Ray, B., Singh, P., & Srivastava A.K. (2013). Interaction Studies of Anticancer Drug Lomustine with Calf Thymus DNA using Surface Enhanced Raman Spectroscopy. MAPAN-*Journal of Metrology Society of India. 28*(4), 273–277.

Merkus, H.G. (2009). Particle Size Measurements. Springer.

Ozer, M., Orhan, M., & Isik, N.S. (2010). Effect of particle optical properties on size distribution of soils obtained by laser diffraction. *Environmental & Engineering Geoscience, Vol. XVI* (2), 163–173.

Putman, C.A.J., Vanderwerf, K.O., de Grooth, B.G., Vanhulst N.F., & Greve, J. (1994). Tapping Mode Atomic Force Microscopy in Liquid. *Applied Physics Letters*. 64, 2454-6.

Pyramides, G., Robinson, J.W., & Zito, S.W. (1995). The combined use of DSC and TGA for the thermal analysis of atenolol tablets. *Journal of Pharmaceutical and Biomedical Analysis. 13*(2), 103-110.

Sakakibara, D., Sasaki, A., Ikeya, T., Hamatsu, J., Hanashima, T., Mishima, M., …. & Ito, Y. (2009). Protein structure determination in living cells by in-cell NMR spectroscopy. *Nature*. Vol 458, 5.

Seo, Y., & Jhe, W. (2008). Atomic force microscopy and spectroscopy. *Reprts on Progress in Physics*. 71,016101.

Simonea, E., Saleemia, A.N., &Nagy, Z.K. (2014). Application of quantitative Raman spectroscopy for the monitoring of polymorphic transformation in crystallization processes using a good calibration practice procedure. *Chemical Engineering Research and Design* . 92, 594-611.

Smith, B. (2011). Fundamentals of Fourier transform infrared spectroscopy. Second ed., Boca Raton: CRC Press.

Smith, E., & Dent, G. (2005). Modern Raman Spectroscopy– A Practical Approach. John Wiley & Sons Ltd, The Atrium, Southern Gate, Chichester,West Sussex, England.

Smyth, M.S. & Martin, J. H.J. (2000). X-Ray-crystallography. *Molecular Pathology. 53* (1), 8-14.

Syvitski, J. (1991). Principles, methods, and application of particle size analysis. Cambridge University Press. Cambridge.

Vankeirsbilck, T., Vercauteren, A., Baeyens, W., &Van der Weken, G. (2002). Applications of Raman spectroscopy in pharmaceutical analysis. Trends in Analytical Chemistry. 21, 12.

Washington, C. (1992). Particle Size Analysis in Pharmaceutics and Other Industries: Theory and Practice. New York: Ellis Horwood.www.mt.com/ta-handbooks

Webster, M. (1983). Websters Ninth New Collegiate Dictionary, Merriam Webster.

Weisenhorn, A.L., Hansma, P.K., Albrecht, T.R., &Quate, C.F. (1989). Forces in Atomic Force Microscopy in Air and Water. *Applied Physics Letters*. 54, 2651-3.

Williams, D., &Fleming, I. (2007). Spectroscopic methods in organic chemistry. 6(Ed.).McGraw-Hill. UK.

Zhang, D., Mrozek, M.F., Xie, Y., & Ben-Amotz, D. (2004). Chemical Segregation and Reduction of Raman Background Interference Using Drop Coating Deposition. *Applied Spectroscopy. 58* (8), 929-933.

Zhang, G., Watanabe, T., Yoshida, H., &Kawai, T. (2003). Phase Transition Behavior of Nylon-66, Nylon-48, and Blends. *Polymer Journal. 35*(2), 173-177 .

.

CHAPTER 4

Co-crystallisation of homochiral amino acids.

4.1. Introduction

Amino acids are the nitrogen containing organic compounds and have a common atomic arrangement that constitute the amino acid backbone. The groups that make up the amino acid backbone are amino group, alpha carbon and carboxylic acid group. Other than amino group and a carboxylic acid group, an R group or side chain and hydrogen atom are also bonded to the alpha carbon (Figure 4.1).

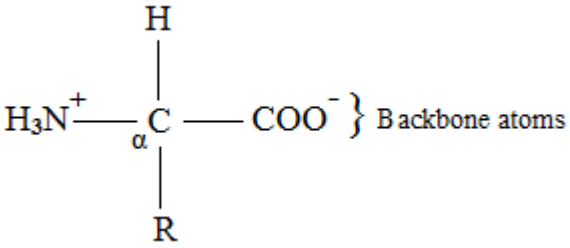

Figure 4.1 General chemical structure of a single amino acid

Amino acids are also called “building blocks” as in peptide or protein formation they are held together by an amide bond also called a peptide bond. The bond links the amino group of one amino acid with the carboxyl group of the second amino acid which results in a linear chain having an amino group at one end and a carboxyl group at the other end (Figure 4.2). It is the R group or the side chain which differentiates the twenty amino acids found in proteins. The side chains not only classify the amino acids such as hydrophobic, hydrophilic, polar, acidic or basic but also have a range of physico-chemical

properties that affect the behaviour of the protein molecules due to inter or intra molecular interactions of amino acid residues (*Nelson & Cox, 2000*)

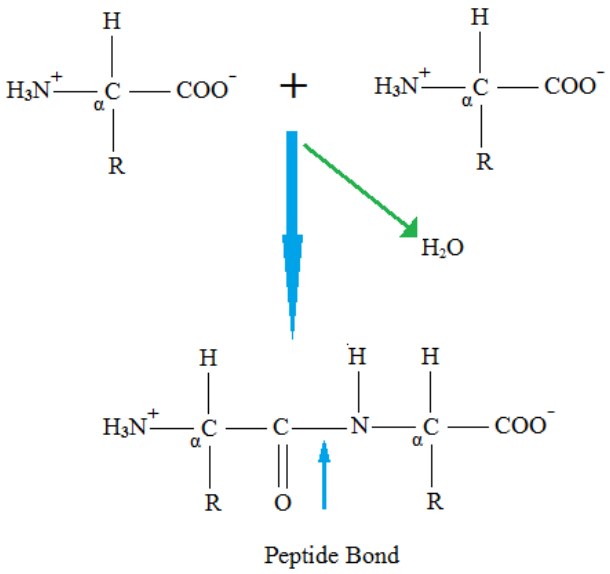

Figure 4.2 Schematic representation of a peptide bond formation.

Amino acids present in the biological systems are chiral in nature with the exception of Glycine which is achiral because its side chain comprises of two hydrogen atoms. Another interesting fact is that all these amino acids are in the L enantiomeric form. The D / L assignment to amino acids is due to the position at which the amino group is bonded with the alpha carbon. Based on a Fischer projection (*Moreno, 2011*) in an L-amino acid, the carboxylic acid group is positioned at the top and the R group at the bottom of the alpha carbon whereas, the amino group is on the left side of the carbon (Figure 4.3). In a D-amino acid the only difference is that the amino group is placed on the right side of the alpha carbon.

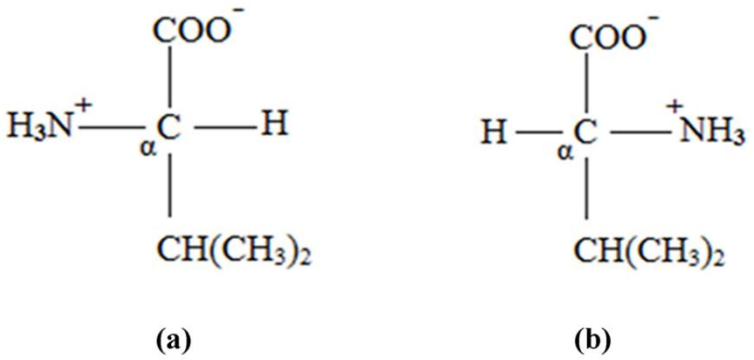

Figure 4.3 The Fischer projection of a). L-Valine b). D-Valine.

The polymerisation of amino acid build up the structural and functional properties of a protein and are directed by the sequence in which amino acid residues interact within the protein (primary structure) and fold into its three dimensional form (tertiary structure). From primary to tertiary structure there is an intermediate form known as secondary structures which dictate the pattern of aggregation or folding of proteins. The most common secondary structures are the alpha helix and beta pleated sheet.

Amino acids are involved in forming enzymes (*Liu, 2008*) and other body tissue that are necessary in a wide variety of chemical and biochemical reactions vital in performing life processes (*Wagenmakers, 1998, Zhu, et al., 2011*).

Valine, leucine, and isoleucine are formed with aliphatic side chains and are known as hydrophobic amino acids. These amino acids are also referred to as branched chain amino acids (BCAAs) for the reason, that in their side chain,

three carbon atoms in valine and four carbon atoms in leucine and isoleucine are attached with the skeletal carbon atom in a nonlinear fashion (Figure 4.4).

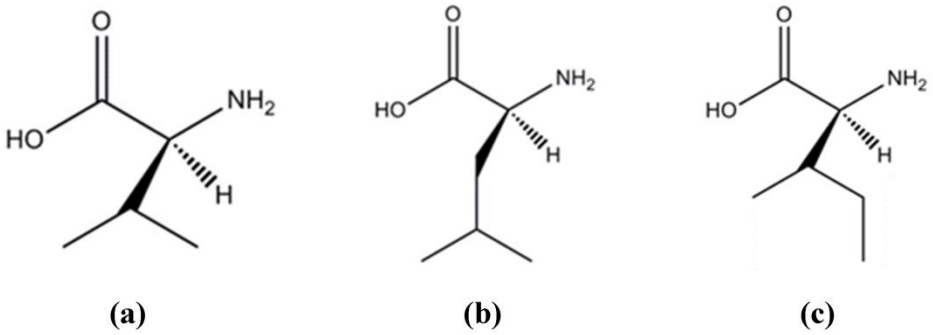

Figure 4.4 Structural form of (a) L-Valine (b) L-Leucine (c) L-Isoleucine.

BCAAs are essential in protein synthesis and important in regulating the protein synthesis (*Karlsson et.al., 2004; Blomstrand et. al., 2006*). Hydrophobic amino acids create hydrophobic pockets in water-soluble proteins and greatly influence protein folding process as they have less chance to interact with the aqueous environment (*Hernández et al., 2009*). BCCAs also play important role in the stability of proteins and phospholipid bilayers (*Tamm, 2005*).

In literature, the crystal structures of branched chain hydrophobic amino acids are reported as pure enantiomers (*Torii & Iitaka, 1970; Harding and Howiesont, 1976; Torii and Iitaka, 1971*) or racemates (*Mallikarjunan & Rao, 1969; Blasio et. al., 1975; Benedett et. al., 1973*). All these reported crystal structures have head- to-tail sequences in which all the α- amino groups and all the carboxylate groups of the molecules are in close proximity to establish

hydrogen bonding arrangement similar to that of a polypeptide. Many studies have reported aggregation pattern of crystalline amino acids complexes and their correlation with polypeptide to understand biologically relevant and important interactions (*Saraswathi & Vijayan, 2001*).

These biologically active molecules have high potential for creating co-crystals as the amine and carboxylic acid functional groups are well-known and used in the formation of co-crystals (*Tilborg et al., 2014*). Co-crystallisation methods have been used to prepare complexes of two different hydrophobic amino acids but these studies have been limited to the crystallisation of D and L-enantiomers in most of the studies reported but it is not a rule of thumb that enantiopure co-crystals are formed only when a D-L combination is present as in literature a co-crystal of R,R-cyclohexanediol and R,R-tartaric acid is described (*Thorey et.al., 2010*). The crystal structures of complexes involving Valine and Leucine (*Dalhus & Gorbitz, 1999*) and Isoleucine series with Valine and Leucine (*Dalhus & Gorbitz, 1999*) were presented but all these complexes were co-crystallised involving amino acids with opposite chirality. Co-crystals of naturally occurring amino acids with the same handedness i.e. L-, L- or D-, D-, have not been reported despite the fact that many peptides show homochirality and their formation is preferred over the heterochiral peptide (*Zhou et al., 2005*). The 1:1 co-crystals of a complex between N-Boc-L-Pro-L-Val-OCH3 and N-Boc-LPro-C$^{\beta}$L methylated-L-Val-OCH3 is reported and supports the formation of co-crystals between peptides of the same chirality (*Trikha et al., 1990*). The complex formation of homochiral molecules

is also supported based on study reported by Burchell et al., 2008, wherein they reported a co-crystal of a dipeptide L-alanyl-L-valine and amino acid L-alanine.

Aggregation behaviour of branched chain amino acids in crystalline state can be categorised into three main classes that is I, II and III (*Dalhus and Gorbitz, 1999*). These classes are based on their unique hydrogen bonding pattern for example in class I, the D and L amino acid complexes are interrelated by crystallographic or pseudo-glide planes whereas, crystallographic or pseudo-inversion is observed in class II between the molecules.

The crystal structures of amino acids and their complexes have been studied under various conditions (*Dittrich et al., 2012; Funnell et al., 2013; Abagaroa et al., 2013; Minkov et al., 2012*) and provided useful information about molecular interaction and their properties. The basic understanding of intermolecular interactions of these compounds may be used to inform scientists who are interested in using these materials in various applications, such as chiral separations, stability and storage of drugs. The focus of the present work is to investigate the formation of amino acid co-crystals of L-Valine, L-Leucine and L-Isoleucine and to determine the solid-state structure of these novel forms.

4.2. Experimental

4.2.1. Materials

All the starting materials were of reagent grade and were purchased commercially from Sigma–Aldrich. Deionised water from a MilliQ water purification unit was used for crystallisation experiment. All reagents were used as received without further purification however, the powder X-ray diffraction pattern (PXRD), Differential scanning calorimetry (DSC) and Thermalgravimetry analysis (TGA) thermograms and FTIR and Raman spectrum of the reagents were recorded for comparison with the complexes of the amino acids. The reagents used in the study are listed in Table 4.1.

Table 4.1 Key compounds studied in this work, including melting point and molecular weight.

Compound	**Molecular weight (g mol^{-1})**	**Melting point (°C)**
L-Valine	117.15	295 - 300
L-Leucine	131.17	> 300
L-Isoleucine	131.17	288

Table 4.2 Complexes of L-L- Amino acids.

Complex	**Amino acids**
Compound 1	Leucine - Isoleucine
Compound 2	Valine - Leucine
Compound 3	Valine - Isoleucine

4.2.2. Methods

Polycrystalline powders and single crystals of amino acids complexes listed in Table 4.2 were prepared by solid state grinding and solution crystallisation methods respectively.

4.2.2.1. Mechanical grinding

The equimolar amount [(104.35mg:104.39mg), (90.10mg:100.35mg) and (89.99mg:100mg)] of L-Leucine and L-IsoLeucine (1), L-Valine and L-Leucine (2) L-Valine and L-Isoleucine (3) respectively, were ball milled (Retsch Mixer Mill model MM400) for 30 minutes at the rate of 20 Hz. The communised powder samples were analysed using various techniques for co-crystal formation described later in the chapter.

4.2.2.2. Crystal growth of amino acids complexes by slow evaporation

Aqueous solutions of the amino acid complexes (1, 2 and 3) were prepared by weighing equimolar amounts [(50.15mg:50.10mg), (45.35mg:50.80mg) and (45.40mg:50.85mg)] of the selected amino acids of compound 1, 2 and 3 in a 10 ml vial respectively. Then 5 ml of purified water was added to the respective vials. The solutions were then magnetically stirred for few minutes to dissolve the contents of the vials. The solutions were filtered through 0.22μm filter paper to avoid any undissolved particles of the constituents of the complexes which may act as a seed to affect the crystallisation of the amino acids complexes. After filtration the vials were capped and a few holes were

punched into the caps in order to induce slow evaporation. The vials were left undisturbed for two weeks to crystallise at room temperature.

4.2.2.3. Crystal growth of amino acids complexes by solvent diffusion

For co-crystallisation by solvent diffusion method same procedure was followed as mentioned in slow evaporation method except that after filtration the vials without caps were placed in a jar containing a solvent which is miscible with the water but function as an anti-solvent for the reacting substances and their complexes. The complexes crystallised after three weeks and further left over for another week to get proper size single crystals.

The crystals were generally of good quality as the crystals extinguished and brightened satisfactorily when rotated in plane-polarized light.

4.2.3. Characterisation of amino acids complexes.

4.2.3.1. Differential scanning calorimetry (DSC).

DSC measurement was carried out using a Mettler Toledo Model DSC 822 with auto sampler and liquid nitrogen cooling system. The sample powder sizes in between 2 – 6 mg were weighed into a 40 μl aluminium pan, which was then hermetically sealed with a pinhole in the lid and heated under nitrogen purge. The temperature range was 40 °C to 340 °C at a heating rate of 10°C min^{-1}. The temperature and heat flow of the DSC instrument was calibrated with indium and zinc. Mettler Toledo STARe software was used to analyse the data and the thermogram obtained were compared with the one obtained with the pure components of the co-crystals.

4.2.3.2. Thermogravimetric analysis (TGA)

To measures the change in mass of a sample on heating were determined by TGA (Mettler Toledo Model TGA / SDTA 851). Samples were prepared by carefully weighing between 10 and 15 mg of each sample into a 70 µl crucibles and were heated over the temperature range of 25°C to 340°C at a constant heating rate of 10°C min^{-1}.

4.2.3.3. Fourier transform infrared spectroscopy (FTIR).

Fourier Transform Infrared (FT-IR) spectra were collected using Smart iTR Nicolet iS10 spectrophotometer (Thermo Scientific). The spectra were recorded in the range of 4000 to 400cm^{-1} at an instrument spectral resolution of 4cm^{-1} (20 scans per spectrum). The spectra were visualised and analysed with OMNIC^{TM} software (version 8.1) (Thermo Scientific). The spectra were compared with the pure compounds to confirm the co-crystal formation.

4.2.3.4. Raman spectroscopy

Raman studies were under taken on the ball milled samples and single crystals of the amino acids complexes (1, 2 and 3) and were compared with their parent components. Raman spectra were collected using DXR Raman instrument (ThermoScientific, Madison, USA) with a DXR 532nm laser with maximum laser power of 10mW. Raman spectra in the shift region of 50-3400 cm-1 was collected at a spectral resolution of 5 cm-1 (1-10 second exposure) using 10/20x objective with 50µm aperture to focus the laser beam. All the spectra were analysed with OMNIC^{TM} software (version 8.2) (Thermo Scientific).

4.2.3.5. Powder X-ray diffraction (PXRD)

Polycrystalline samples prepared through ball mill were analysed by XRPD for fingerprinting. Approximate 20-50 mg of samples were mounted on 28 well plate supported on a polyimide (Kapton, 7.5 μm thickness) film. Data were collected on a Bruker AXS D8-Advance transmission diffractometer. The diffractometer was equipped with θ/θ geometry, primary monochromated radiation (Cu Kα1, λ= 1.54056 Å), a Vantec 1-D position sensitive detector (PSD) and an automated multi-position *x-y* sample stage. Data were obtained in the range 4-35° 2θ with a 0.015° 2θ step size and 1 s step-1 count time. The identification of the co-crystals formation was performed by comparing the powder diffraction patterns with those of the pure materials.

4.2.3.6. Single crystal X-ray diffraction (SXD)

X-ray diffraction intensities for compound 1were collected at I19 at Diamond Light Source (*Project MT7150*) whereas, compound 2 and 3 by the National Crystallography service (*Coles & Gale, 2012*). X-ray diffraction intensities for 2 were collected with Mo-Kα radiation on a Bruker KAPPA Apex II CCD diffractometer equipped with an Oxford Cryosystems Cryostream-*Plus* variable-temperature device operating at -150 °C (*Cosier and Glazer, 1986*). Absorption corrections were carried out using the multiscan procedure *SADABS* (*Sheldrick, 2004*, based on the procedure described by *Blessing, 1995*). The structures were solved by direct methods (*SIR-92, Altomare A et. al, 1993*) and refined by full-matrix least-squares against F ($I > 3\sigma$) using all data (*CRYSTALS, Betteridge P. W et. al, 2003*). Due to the wavelength of the

source (0.71073 Å) the chirality of the amino acids was assumed to be as stated by the manufacturer however the molecules were consistent with each other in the model i.e. both molecules were in the L-enantiomer.

4.2.3.6.1. Crystal structure refinements

The basic amino acid backbone (CO-C-N) and the first carbon of the chain was easily observed and used as the basic starting model for the refinements. From the difference map extra peaks were observed that were of the correct geometry to be assigned to be the components of a specific amino acid. Once the two molecules were identified further difference maps were used to find subsequent atoms that could only be assigned to a second component. These different components were assigned part numbers. The bond distances of the carbon side-chains (for compounds 1 and 2) were restrained to be similar to those found in the Cambridge Structural Database. Thermal similarity and vibrational restraints were also applied. The parts were given values of 50% occupancy and allowed to refine. Compound 1 and 2 gave occupancy values that differed slightly and the values quoted in the thesis are average values with a standard deviation. Compound 3 was more straight forward with the refinement remaining at 50% for one of the molecules in the asymmetric unit. In this case once the occupancy was established the parts were not competitively refined. All hydrogen atoms attached to carbon atoms were geometrically placed and those participating in hydrogen bonding i.e. hydroxyl hydrogens were found in the difference map. All non-H atoms were modelled with anisotropic displacement parameters.

4.3. Results and Discussion

4.3.1. Differential scanning calorimetry (DSC)

The DSC thermograms were shown in Figure 4.5 a, b and c for the compound 1, 2 and 3 respectively. The melting point, onset and endset values of the samples of the co-crystal complexes along with the pure reacting components were presented in Table 4.3.

Table 4.3 Onset, endset and melting point values for L-Valine, L-Leucine, L-Isoleucine and their complexes (Compound 1, 2 and 3).

Compound Name	Onset Value °C	Endset Value °C	Melting point °C
L-Valine	250.91	301.98	294.86
L-Leucine	274.19	308.89	303.02
L-Isoleucine	253.86	295.00	286.76
Compound 1	263.77	307.78	301
Compound 2	278.78	312.94	304.99
Compound 3	263.79	297.90	291.79

The values of the amino acid complexes were compared to their respective parent components i.e. L-Valine, L-Leucine and L-Isoleucine and found different thus indicate the formation of co-crystal.

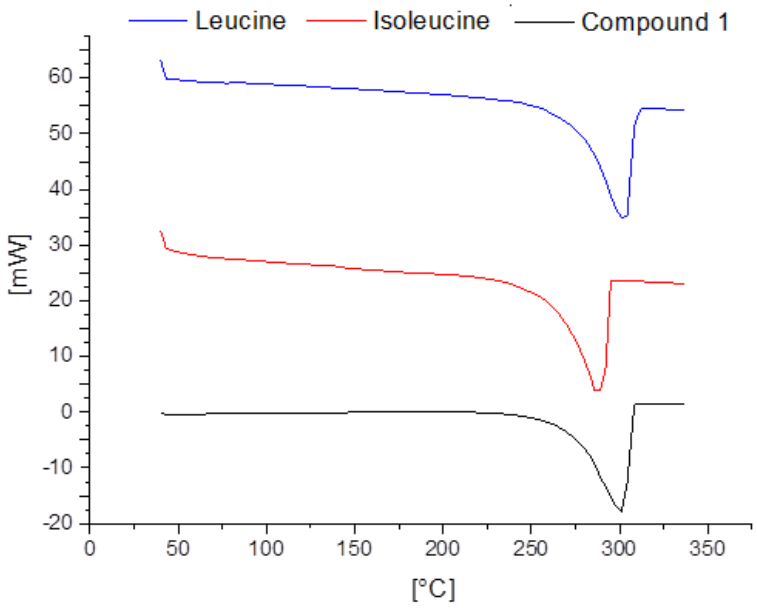

Figure 4.5a DSC thermogram for compound 1.

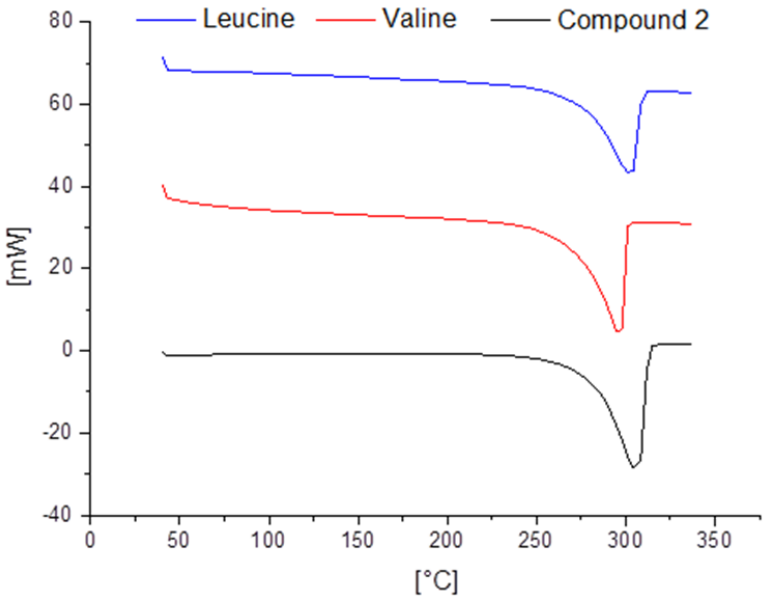

Figure 4.5b DSC thermogram for compound 2.

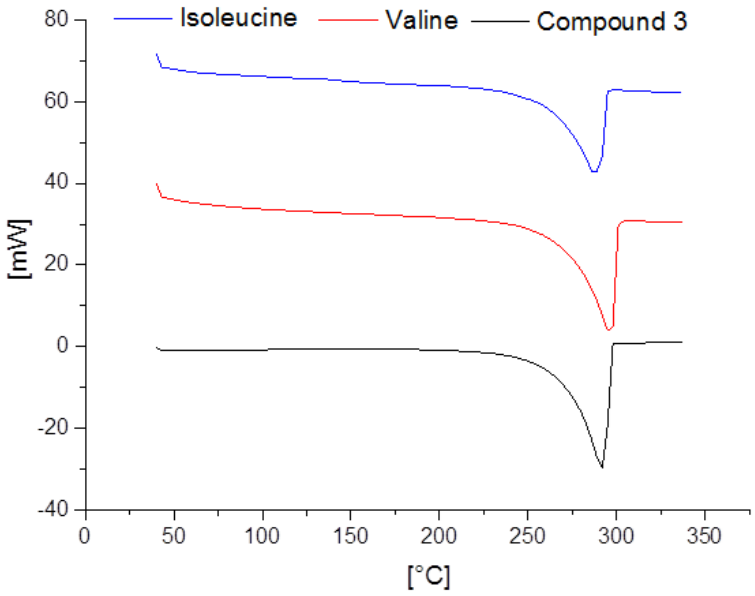

Figure 4.5c DSC thermogram for compound 3.

4.3.2. Thermogravimetric analysis (TGA)

TGA curves of the amino acid complexes are presented in Figure 4.6a, b and c for the compound 1, 2 and 3 respectively.

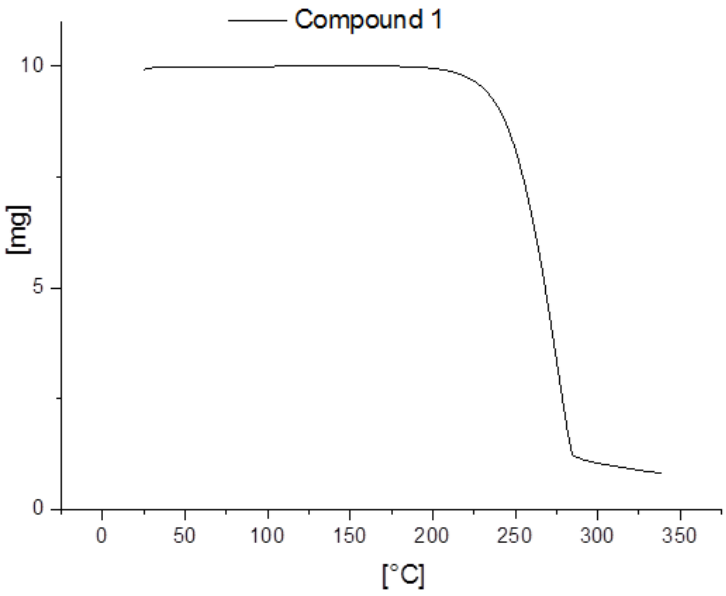

Figure 4.6a TGA curve for compound 1.

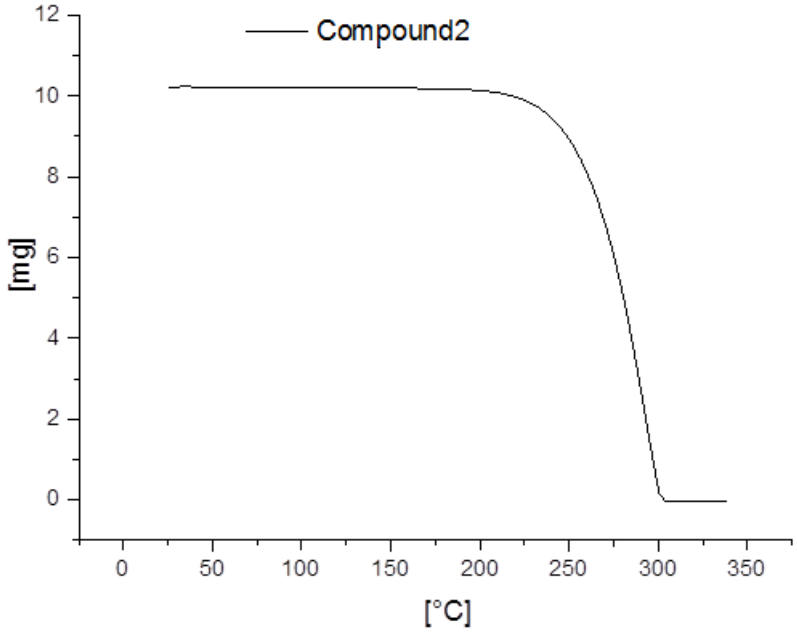

Figure 4.6ba TGA curve for compound 2.

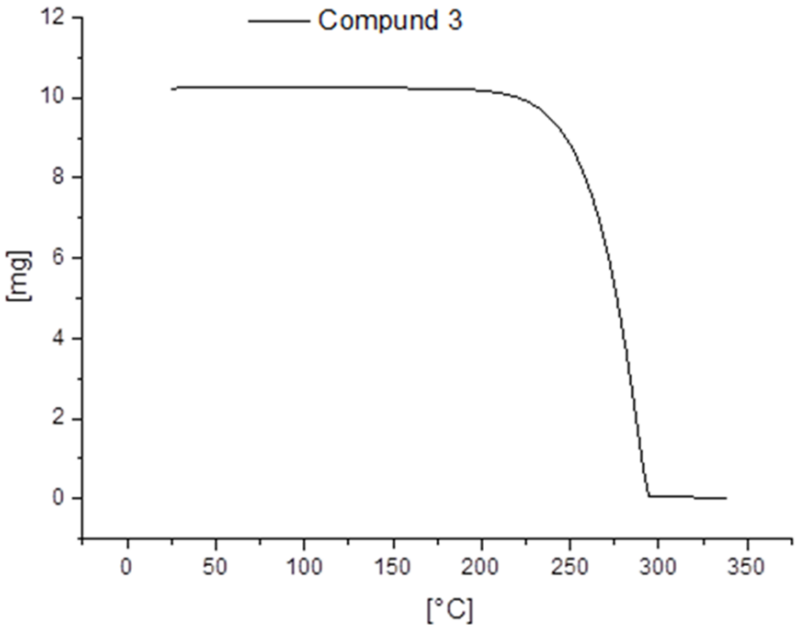

Figure 4.6c TGA curve for compound 3.

The powder samples of all the amino acid complexes observed a typical one stage TGA curve and show no residues of any of the reacting components thus indicating complex formation. The TGA curves showed an insignificant mass loss which may be due to moisture but significant mass loss was observed for all the compounds just before their thermal decomposition.

4.3.3. Fourier transform infrared spectroscopy (FTIR).

The FTIR spectroscopy was carried out on ball milled samples of compound 1, 2 and 3 to analyse the samples as a prospective new materials. Infra-red spectra of amino acids have typical broad NH stretching band between 3300-3500cm^{-1} and low frequency 1580-1650cm^{-1} NH bending bands. Asymmetric and symmetric CO stretching bands were observed at lower wavenumbers at 1000-1260cm^{-1} and 1760-1670cm^{-1} respectively and generally overlay with NH bending bands. The IR spectrum of the compound 1, compound 2 and compound 3 were comparable to the reacting constituents of the respective complexes and superimpose a large number of closely related bands in spectral range. It seemed very problematic to recognize and to assign the characteristic bands of the amino acids complexes when compared with the L-Valine, L-leucine and L-Isoleucine spectra. There were some deviations observed in the peak intensities and shifts mainly in the characteristic wavenumber regions in the range from 700 – 1700 cm^{-1} presented in Figure 4.7, 4.8 and 4.9 for the compound 1, 2 and 3 respectively. It is difficult to figure out convincingly that the compound 1, 2 and 3 were co-crystals as it may be an additive effect of the physical mixture of the two reacting components of the complex.

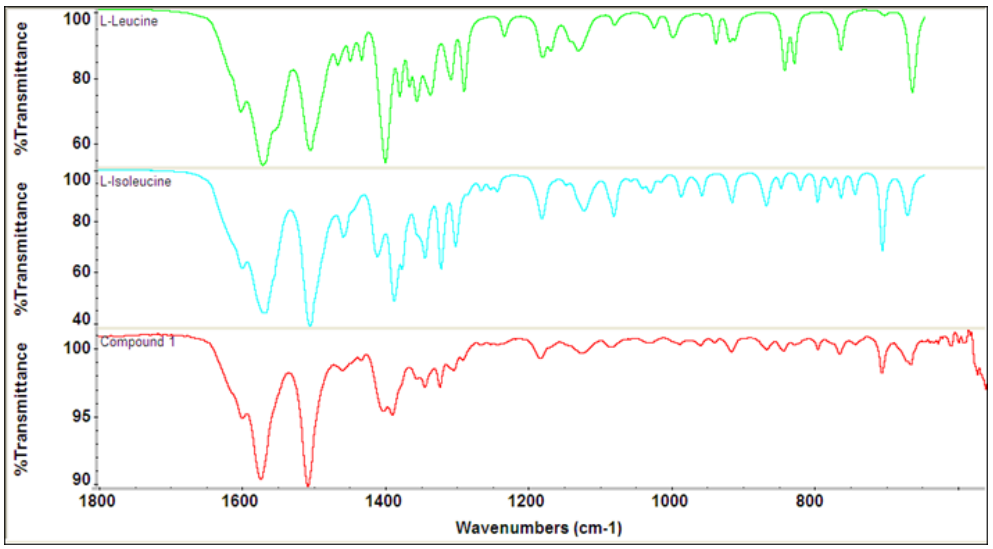

Figure 4.7 FTIR Spectra of L-Leucine, L-Isoleucine and Compound 1 in the characteristic wavenumber region of 700 - 1800cm^{-1}

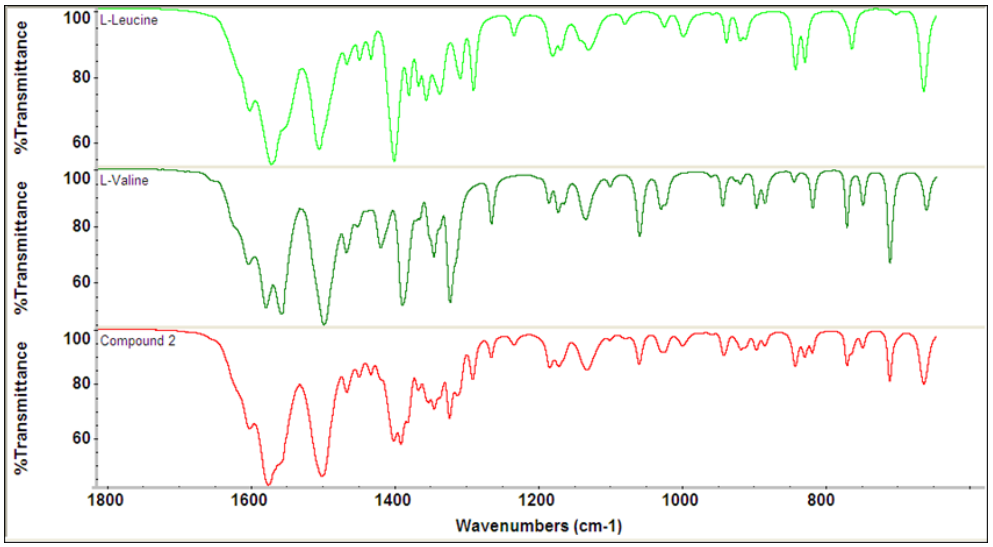

Figure 4.8 FTIR Spectra of L-Leucine, L-Valine and Compound 2 in the characteristic wavenumber region of 700 - 1800cm^{-1}

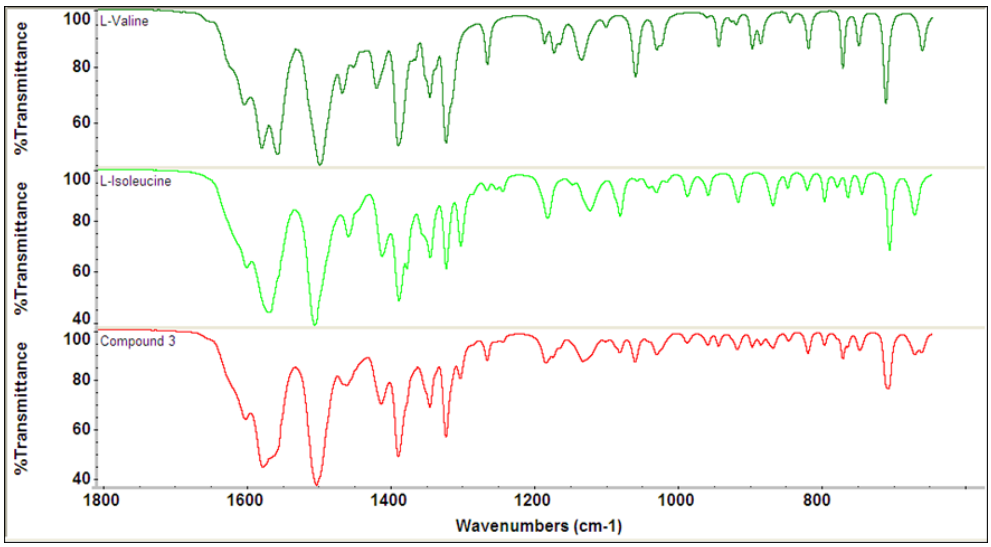

Figure 4.9 FTIR Spectra of L-Valine, L-Isoleucine and Compound 3 in the characteristic wavenumber region of 700 - 1800cm^{-1}

4.3.4. Raman spectroscopy

Raman shift also called the "fingerprint region" contains the majority of the Raman bands used to identify a specific material. Each amino acid spectrum is unique although very complex. In order to get evidence that powders of amino acid complexes prepared by ball mill were co-crystals, raman spectrum of single crystal of the compound 1, 2 and 3 (Figure 4.10), grown by the slow evaporation method and characterised through single crystal X-ray diffraction, were collected.

The Raman spectra of the pure amino acids, ball milled powder samples and their single crystals in the 600–1800cm^{-1} spectral region is presented in Figure 4.11, 4.12 and 4.13 for compound 1, 2 and 3 respectively. This is a complex

but characteristic region, where many bands related with a specific material are observed.

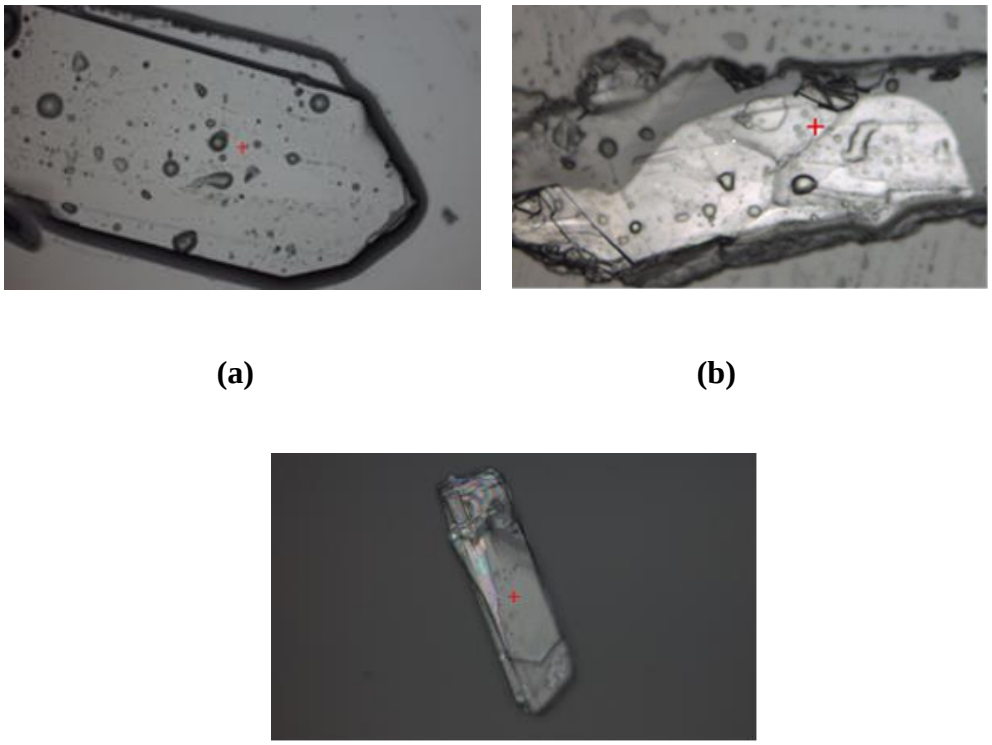

(a) **(b)**

(c)

Figure 4.10 Single crystals of compounds a) 1, b) 2 and c) 3.

With regards to amino acids most of the bands in the region 1300 – 1375cm^{-1} are related with deformations of CH whereas spectral region between 1380cm^{-1} and 1420cm^{-1} and 1450cm^{-1} and 1500cm^{-1} are assigned to symmetric and asymmetric bending of CH_3. The bands observed at 1500-1650cm^{-1} are assigned to stretching vibrations of COO and usually overlap with bending vibration of NH_3. It is worthwhile to mention that amino acids under investigation were very similar and closely related to each other in their crystal structure.

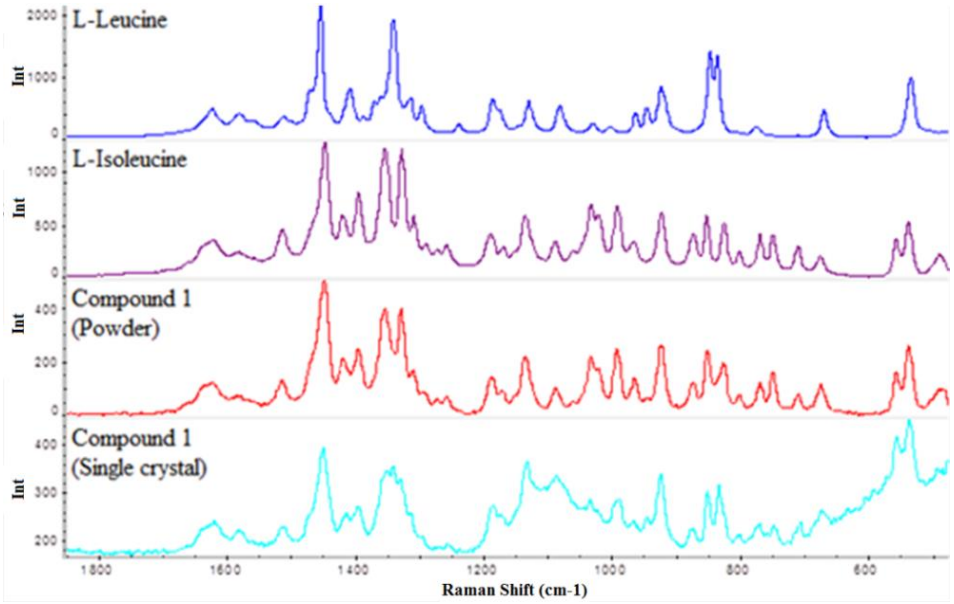

Figure 4.11 Raman spectra in the finger print region of L-Leucine, L-Isoleucine and compound 1 (powder & single crystal).

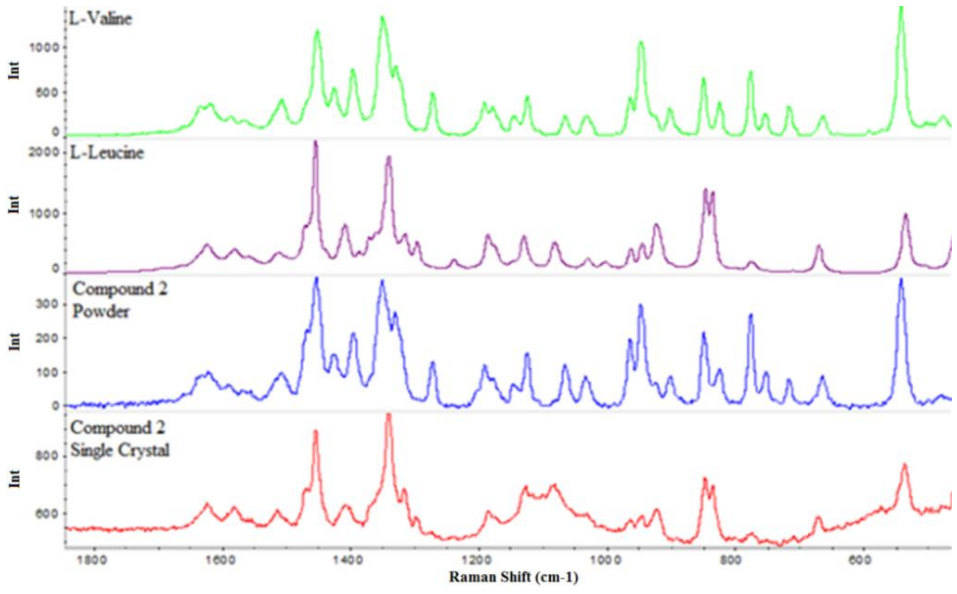

Figure 4.12 Raman spectra in the finger print region of L-Valine, L-Leucine and compound 2 (powder & single crystal).

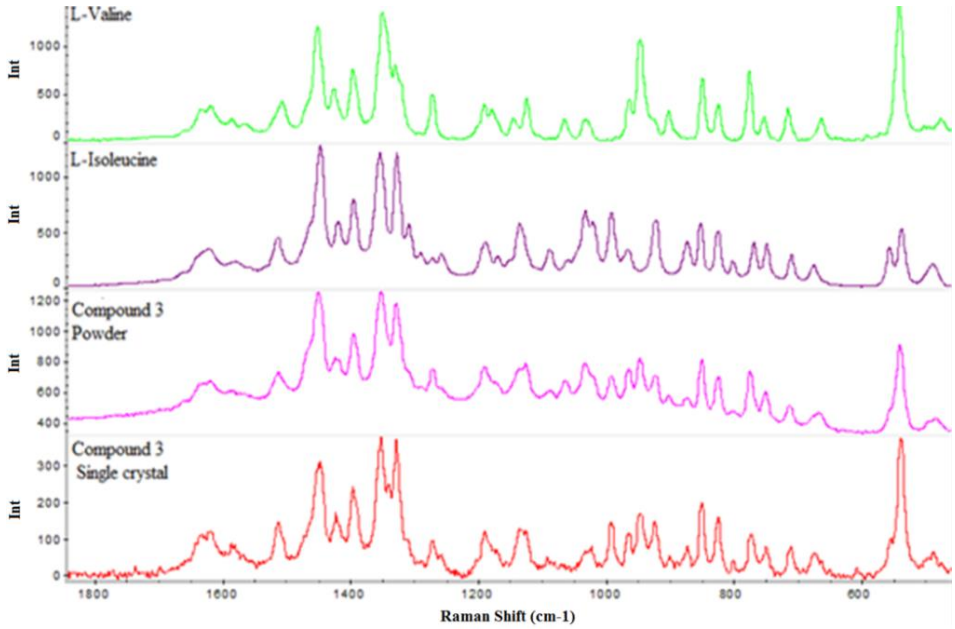

Figure 4.13 Raman spectra in the finger print region of L-Valine, L-Leucine and compound 3 (powder & single crystal).

The similarity of the most characteristic absorption bands clearly points to similar coordination characteristics in all co-crystals with respect to their constituents suggesting that the single crystals of the amino acid complexes contain both reacting components in the crystal structures.

4.3.5. Powder X-ray diffraction (PXRD)

Powder X-ray diffraction is a rapid and extensively used analytical technique to identify and characterise the crystalline materials. PXRD pattern of ball milled samples of amino acid complexes referred as compound 1, 2 and 3 appeared to be the physical mixture of the contributing amino acids suggesting

that ball milling has not created co-crystals. The diffraction pattern of all the amino acid complex has shown characteristic peaks related with their respective contributing parent components. In compound 1 (Figure 4.14) peaks can be observed at 6 and 6.5 (2θ) which are specific to L-Leucine and L-Isoleucine respectively. Similarly peaks at 6 and 7.5 (2θ) in compound 2 (Figure 4.15) are attributed to L-Leucine and L-Valine respectively and in compound 3 (Figure 4.16) peaks characteristic of L-Isoleucine and L-Valine can be identified at 6.5 and 7.5 (2θ) respectively thus confirming the presence of both components in the respective powder samples and indicates the presence of the starting materials.

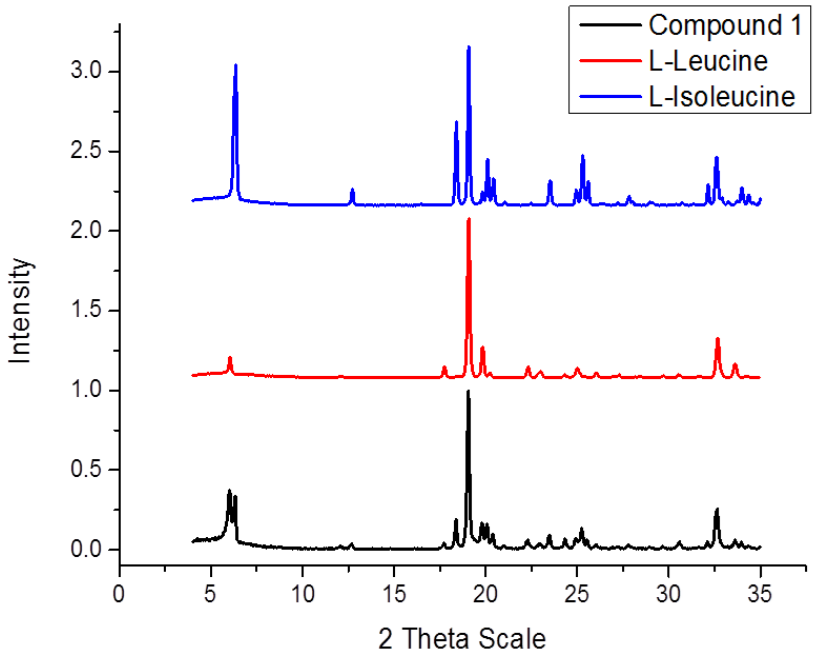

Figure 4.14 PXRD pattern of L-Leucine, L-Isoleucine and Compound 1

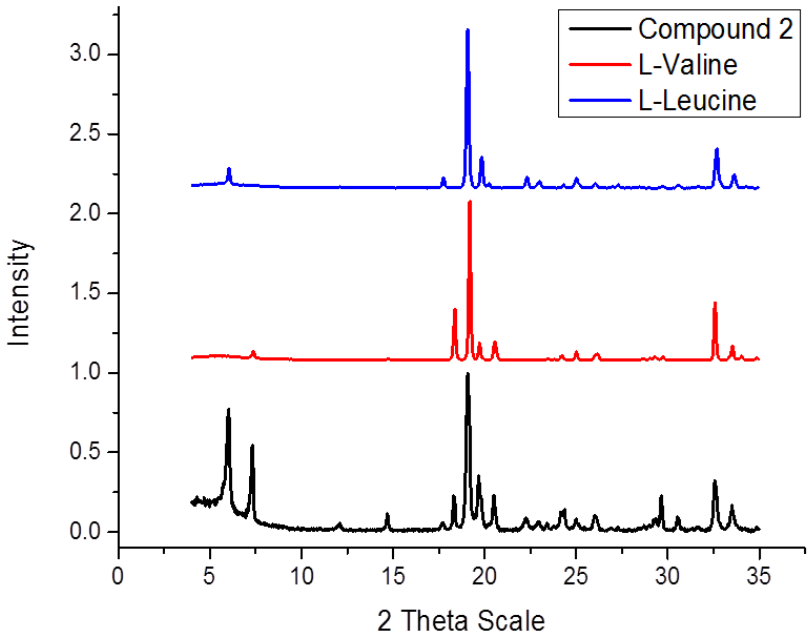

Figure 4.15 PXRD pattern of L-Leucine, L-Valine and Compound 2

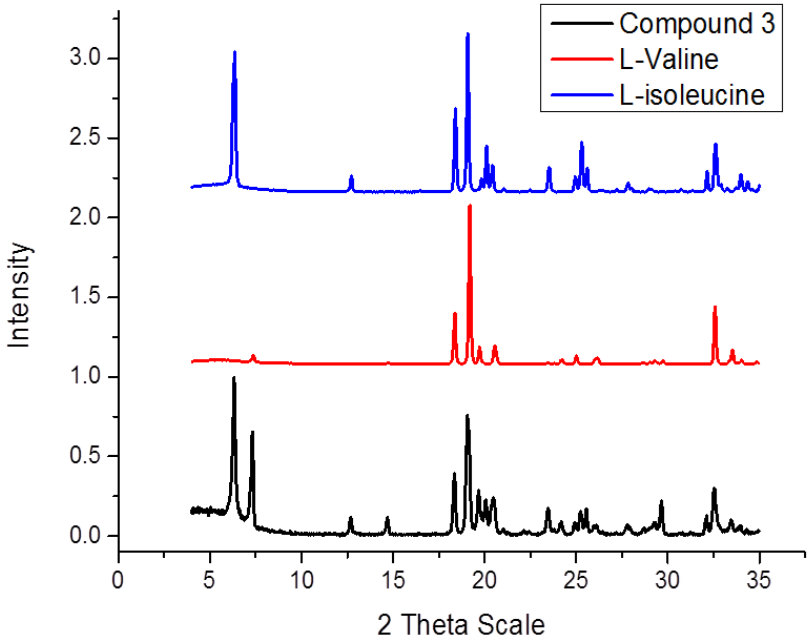

Figure 4.16 PXRD pattern of L-Valine, L-Isoleucine and compound 3

4.3.6. Single crystal X-ray diffraction (SXD)

The diffraction quality single crystals of compound 1, 2 and 3 were grown by slow evaporation. The single crystal diffraction data were collected and novel unit cell parameters were observed for the three compounds. The crystal data were refined and crystal structure revealed new crystalline forms which are presented in Table 4.4 for the compound 1, 2 and 3 and compared with their respective constituents.

4.3.6.1. Structural analysis of co-crystals

Though the reacting constituents are in stoichiometric ratios in the crystallisation step, however, the percentage composition of each constituent in the crystal is not stoichiometric showing disorder in the crystal structures. Many crystals of each compound were randomly chosen for structure determination and analysis of their structures revealed that there is no significant variation present in the proportion of the constituents within the crystals of each compound suggesting co-crystals are orderly disordered. The percentage composition in compound 1 is 59(2)% isoleucine; compound 2 is 61(3)% leucine and compound 3 is 75% valine. At ambient conditions the compounds 1 and 2 crystallise in $P2_1$ whilst compound 3 crystallise in C2 monoclinic space symmetry group and all compounds comprises of two molecules in the asymmetric unit. Asymmetric unit of amino acids complex are presented in figure 4.17 for compound 1, figure 4.18 for compound 2 and figure 4.19 for compound 3.

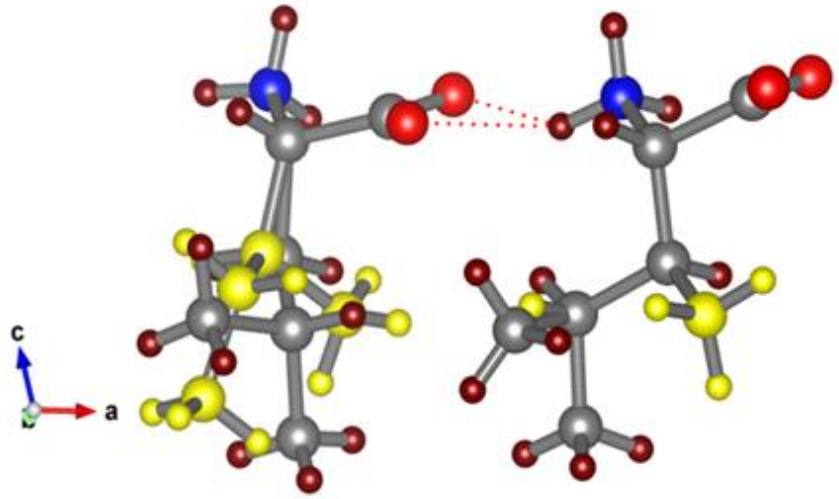

Figure 4.17 Asymmetric unit of compound 1. The disordered component Isoleucine is colour coded yellow. General atom colours: Grey, carbon; blue, nitrogen; red, oxygen; and brown, hydrogen.

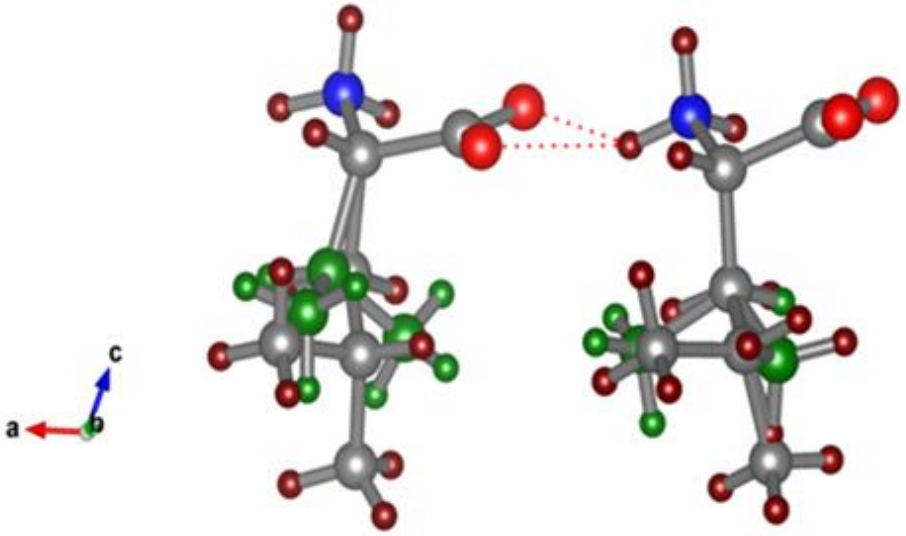

Figure 4.18 Asymmetric unit of compound 2. The disordered component Valine is colour coded green. General atom colours: Grey, carbon; blue, nitrogen; red, oxygen; and brown, hydrogen.

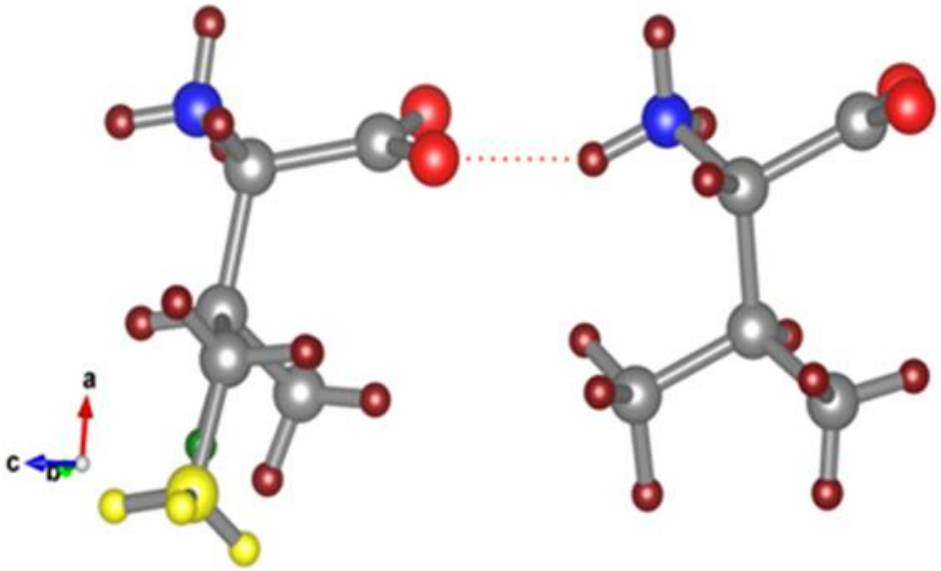

Figure 4.19 Asymmetric unit of compound 3. The disordered component Isoleucine is colour coded yellow. General atom colours: Grey, carbon; blue, nitrogen; red, oxygen; and brown, hydrogen.

The molecular packing in all three amino acid complexes is also very closely related and crystal structure of these compounds is separated into distinct hydrophilic and hydrophobic layers (Figure 4.20 (1), 4.21 (2) and 4.22 (3). Like other hydrophobic amino acids, crystal structures can be described in terms of head-to-tail sequences in which the α-amino group and the α-carboxylate groups of neighbouring molecules are engage in hydrogen bonding while the side chains are involved in van der Waals interactions only and were stacked linearly back to back. Each layer in the bi-layer arrangement comprises two hydrogen atoms of the polarised amino group while the third hydrogen atom of the amino group involve in establishing a hydrogen bond linking pairs between the two layers.

Table 4.4 Unit cell parameters for compound 1, 2 and 3 compared with their contributing constituents L-Valine, L-Leucine and L-Isoleucine.

	Compound 1 (LIL)	Compound 2 (VL)	Compound 3 (VIL)	L-Valine[a]	L-Leucine[b]	L-Isoleucine Form- I[c]	L-Isoleucine Form-II[d]
Space group	$P2_1$	$P2_1$	C2	P21	$P2_1$	$P2_1$	$P222_1$
a	9.633(5) Å	9.596(6) Å	26.142(6) Å	9.682(2) Å	9.562(2) Å	9.681(5) Å	13.89(6) Å
b	5.281(3) Å	5.281(4) Å	5.2621(12) Å	5.247(1) Å	5.301(1) Å	5.301(3) Å	20.17(5) Å
c	14.669(7) Å	14.486(13) Å	9.688(2) Å	11.930(2) Å	14.519(3) Å	13.956(6) Å	5.35(9) Å
alpha	90	90	90	90	90	90	90
beta	104.410(4)	109.328(5)	96.961(7)	90.57	94.20(2)	96.16	90
gamma	90	90	90	90	90	90	90

a) Dalhus & Gorbitz, (1996). b) Gorbitz & Dalhus, (1996). c) Gorbitz & Dalhus, (1996). d) Khawas, (1970).

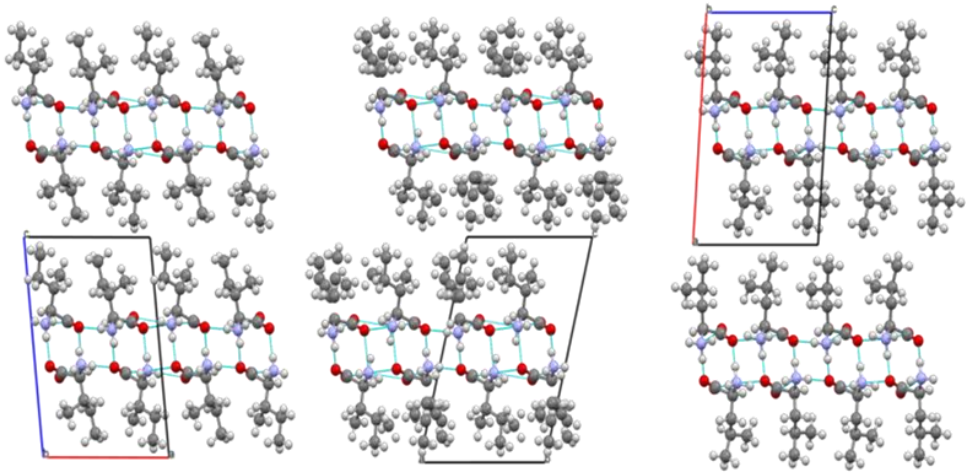

Figure 4.20 The packing diagrams for compound 1. The central structure is the co-crystal with the pure components at either side, Iso-leucine to the left and Leucine to the right.

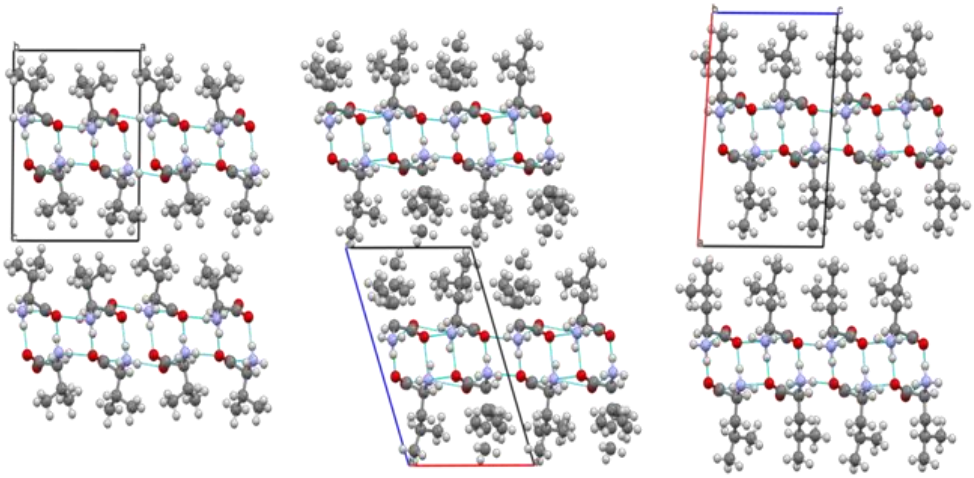

Figure 4.21 The packing diagrams for compound 2. The central structure is the co-crystal with the pure components at either side. Valine to the left and Leucine to the right.

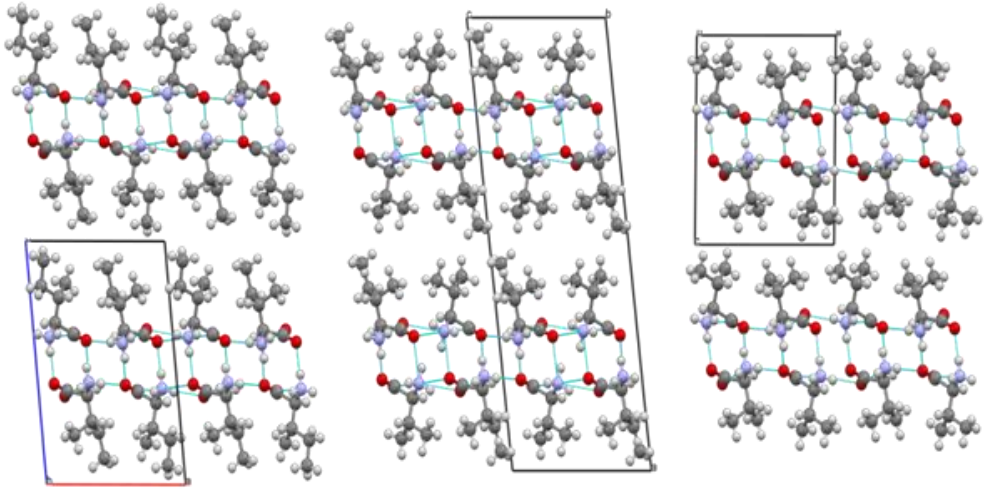

Figure 4.22 The packing diagrams for compound 3. The central structure is the co-crystal with the pure components at either side. Iso-leucine to the left and Valine to the right

4.3.6.2. Hydrogen bonding and conformational analysis of co-crystals.

4.3.6.2.1. Hydrogen bonding

Hydrogen-bond parameters of the amino acid co-crystals are given in Table 4.5 for the compounds 1, 2 and 3. The hydrogen-bond patterns of these co-crystals are apparently very similar and closely related to those observed previously for L-Valine (*Dalhus & Gorbitz, 1996*), L-Leucine (*Gorbitz & Dalhus, 1996*) and L-Isoleucine (*Gorbitz & Dalhus, 1996*) wherein the nitrogen atom in each molecule is linked by four oxygen atoms at short distances in the range of 2.759(6)Å–2.999(6)Å for compound 1, 2.748(13)Å – 3.001(13)Å for compound 2 and 2.765(10)Å–3.025(10)Å for compound 3. The two amino hydrogen atoms of each molecule will join the molecules to form a layer while

the remaining amino hydrogen bonds are involved in linking the single layer to form bilayer structures which are separated from each other by the hydrophobic tail group (Figure 4.23).

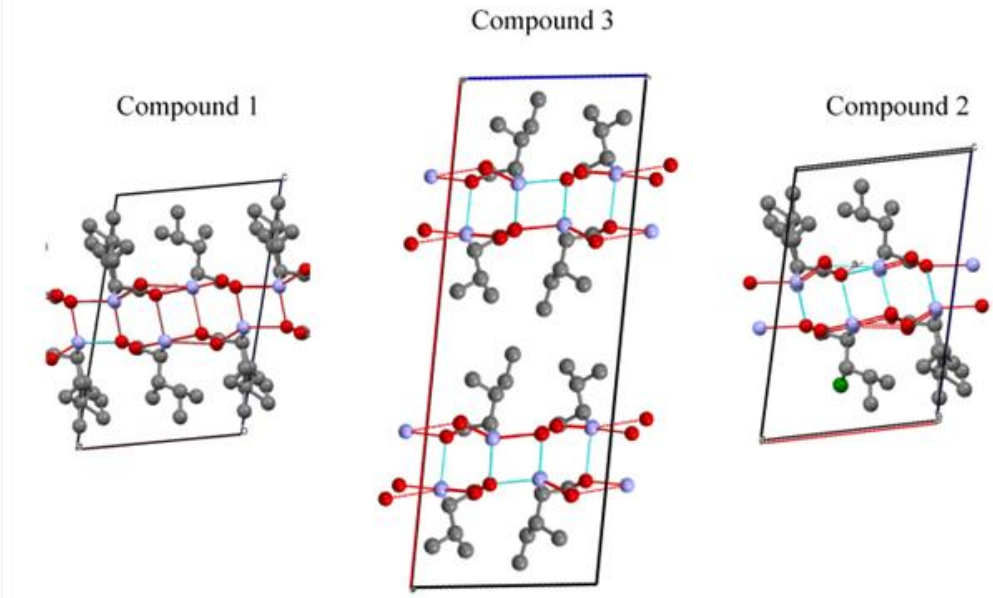

Figure 4.23 Hydrogen bonding patterns in Compound 1, 2 and 3.

Table 4.5 Hydrogen-bonding geometry for compound 1, 2 and 3.

D—H----A	D—H Å	H----A Å	D----A Å	D—H----A º
Compound 1				
N11 . H111 . O12	0.950	2.253	2.999(6)	134.77(5)
N11 . H111 . O22	0.950	2.168	2.974(6)	141.91(5)
N11 . H112 . O12	0.950	1.864	2.763(6)	156.89(5)
N11 . H113 . O21	0.950	1.920	2.851(6)	165.95(5)
N12 . H123 . O11	0.895	1.866	2.759(6)	175.26(5)
N12 . H122 . O11	0.929	1.966	2.808(6)	149.84(5)
N12 . H121 . O22	0.906	1.962	2.854(6)	168.06(5)
Compound 2				
N11 . H111 . O12	0.949	2.278	3.001(13)	132.45(9)
N11 . H111 . O22	0.949	2.131	2.967(13)	146.20(9)
N11 . H112 . O12	0.948	1.851	2.748(13)	156.99(9)
N11 . H113 . O21	0.948	1.926	2.859(13)	167.77(9)
N12 . H121 . O11	0.948	1.821	2.757(13)	168.70(11)
N12 . H122 . O11	0.948	1.935	2.812(13)	152.97(10)
N12 . H123 . O22	0.948	1.972	2.876(13)	158.84(9)
Compound 3				
N11 . H113 . O12	0.904	1.885	2.788(10)	176.15(19)
N11 . H112 . O12	0.904	1.885	2.788(10)	176.15(19)
N11 . H114 . O21	0.900	1.968	2.856(10)	168.50(17)
N12 . H121 . O11	0.951	2.296	3.025(10)	132.83(15)
N12 . H121 . O21	0.951	2.121	2.920(10)	140.78(18)
N12 . H122 . O11	0.954	1.901	2.765(10)	149.35(18)
N12 . H123 . O22	0.952	1.924	2.856(10)	165.89(18)

4.3.6.2.2. Conformational analysis

In recent time conformational properties of amino acids and peptides is not restricted to the backbone structures because many modern techniques like NMR and crystallography can be used to investigate the side chain conformations which play a significant part in biological activity (*Hanchen, et al., 2013*). There are two areas in which the conformation will play a significant role i) the basic amino acid backbone and ii) the hydrophobic tail groups of each amino acid.

The analysis of the structures is complicated by the fact that the numbering schemes from the literature and our structures are different. In this section I have tried to match the molecules with respect to their conformations rather than their labelling. The conformation of the backbone skeleton in compound 1, 2 and 3 are determined by the intermolecular hydrogen-bond interactions between the amino group and carboxylic group shows a bifurcated N-H···O=C hydrogen bond which further become stable by a cis-COOH interaction. The torsion angles of the co-crystals of amino acids back bone are in good agreement with their reacting components that is L-Valine, L-Leucine and L-Isoleucine crystals (Table 4.6). Whilst compounds 1 and 2 have similar values for their conformations, compound 3, at first glance, appears to have radically different conformations but this is just a consequence of matching the conformations of the side chains. If the torsion angles are swapped for each molecule the conformations are closely related to pure L-Valine and L-Isoleucine.

Table 4.6 Torsion angles of the molecular skeleton of amino acid co-crystals (1, 2, 3) and their parent components L-Valine, L-Leucine and L-Isoleucine.

	Atoms involved in torsion				Compound 1	Compound 2	Compound 3	Valine[a]	Leucine[b]	Isoleucine[c]
	Atom1	Atom2	Atom3	Atom4						
Molecule 1	O11	C11	C21	N11	-37.5(2)	-35.5(4)	-19.7(6)	-42.8(1)	-32.3(1)	-41.4(2)
	O21	C11	C21	N11	145.5(2)	146.5(3)	164.8(4)	139.5(1)	150.2(1)	141.5(2)
Molecule 2	O12	C12	C22	N12	-25.8(2)	-25.13	-42.2(6)	-17.5	-26.8(1)	-19.0(2)
	O22	C12	C22	N12	156.43	155.36	139.5(5)	164.7(1)	155.4(1)	164.1(1)

a) Dalhus & Gorbitz, (1996). b) Gorbitz & Dalhus, (1996). c) Gorbitz & Dalhus, (1996).

In amino acids the side chain conformation is mainly defined by the dihedral angle χ_1 around the Cα-Cβ-bond and can adopt different conformations in the solid-state. Figure 4.24 present predominant configurations highlighted with in a box that were noticed about the Cα-Cβ-bond in the tail groups of the most stable conformers of L-Valine, L-Leucine and L-Isoleucine structures in gas phase (*Cocinero, et al., 2006*).

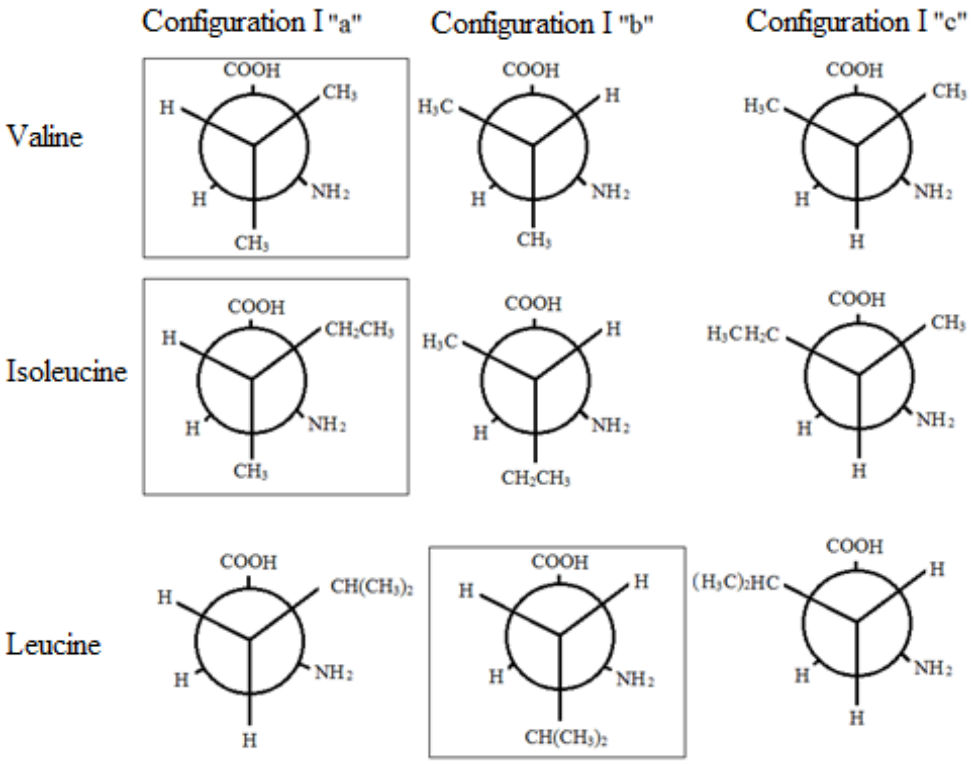

Figure 4.24 Newman projections around the Cα-Cβ-bond in the side chains of the most stable conformers (within box) of valine, isoleucine and leucine (*Cocinero, et al., 2006*).

4.3.6.2.2.1. Compound 1

The co-crystal comprises of two molecules in the asymmetric unit. Each molecule has a disorder in its tail group causing a change in molecular conformation when observed at rotation around Cα-Cβ-bond with respect to that observed in pure enantiomers of L-Leucine and L-Isoleucine crystal structures.

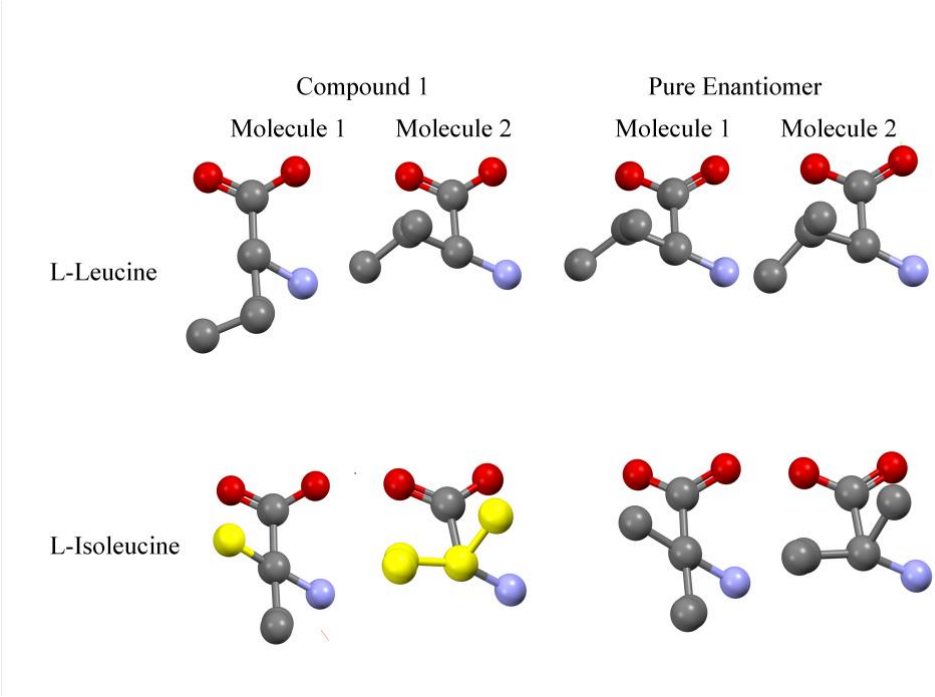

Figure 4.25 Observed configurations for rotation about the Cα-Cβ-bond in the side chains of the conformers of molecules in the asymmetric unit of compound 1, pure enantiomer L-leucine and L-Isoleucine. The yellow atoms represent the disordered isoleucine component in the structure.

L-Leucine in compound 1 observed two conformations in the asymmetric unit that is *gauche*$^{(+)}$ and *trans* for molecule 1 and 2 respectively (Figure 4.25)

whereas, in pure enantiomer crystal structure of L-Leucine (*Gorbitz & Dalhus, 1996*) both molecules in the asymmetric unit exhibit *trans* position for rotation around the Cα-Cβ-bond.

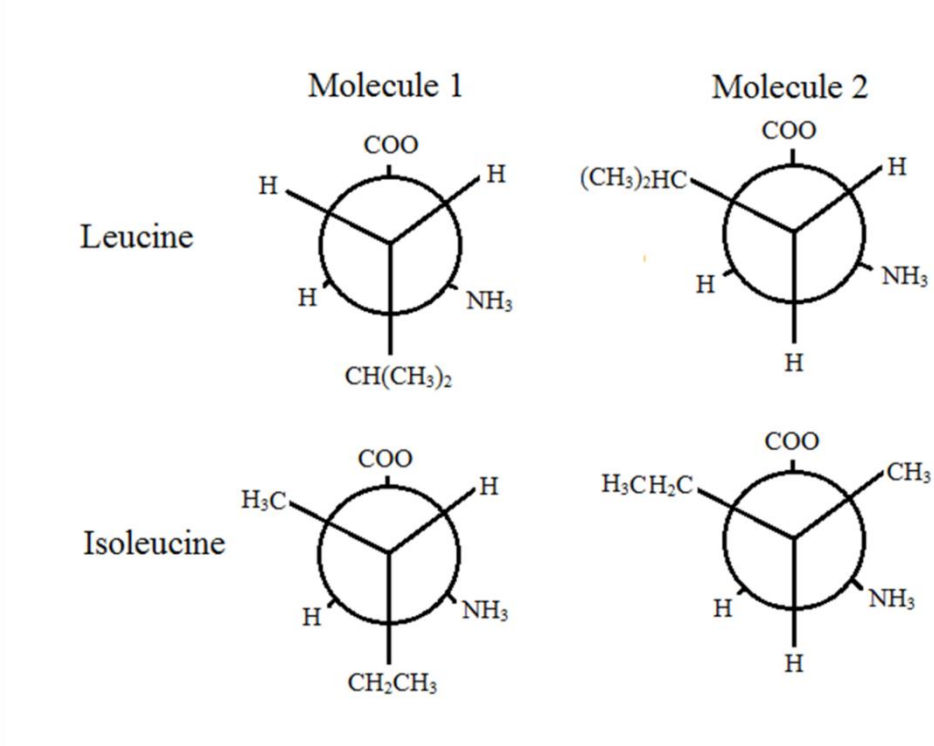

Figure 4.26 Newman projections of the observed configurations for rotation about the Cα-Cβ-bond in the side chains of the conformers of molecules in the asymmetric unit of compound 1.

The Newman projection of the tail groups in compound 1 is presented in Figure 4.26 which shows that the L-Leucine tail moiety in *gauche*$^{(+)}$ conformation in the compound 1 exhibit a stable conformation (1b) unlike with the pure enantiomer in which both molecules present relatively less stable conformation (1c) (Figure 4.24). Similarly, molecule of the L-Isoleucine, in

which an ethyl and methyl group are bonded to the Cβ, exhibits a conformation in which the tail group is observed in the *trans* and *gauche*$^{(+)}$ position equating to the most stable conformation (1a) . Molecule 2 is observed in the relatively less stable conformation (1c) where the ethyl and methyl substituents are present in the *gauche*$^{(+)}$ and *gauche*$^{(-)}$ position, respectively (Figure 4.24). The change in L-Leucine conformation in molecule 1 may be due to the competing tail group of L-Isoleucine exhibiting a less stable conformation compared to L-Leucine which presents the most stable conformation. The numbering scheme of the atoms present in the asymmetric unit is shown in Figure 4.27 along with torsion angles tabulated in Table 4.7 for compound 1. Torsion angle of the respective components reveal the extent of conformational diversity of side chains of the amino acids co-crystals and are compared with their respective parent constituent in crystal structure.

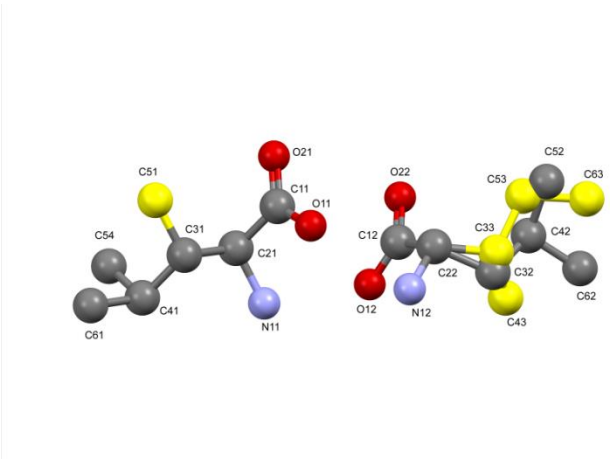

Figure 4.27 Numbering scheme of atoms in compound 1. The disordered L-Isoleucine moiety is coded in yellow colour.

Table 4.7 Torsion angles of L-Leucine and L-Isoleucine in co-crystal (compound 1) and in their parent crystal structure.

Atoms involved in torsion						
L-Leucine residue in co-crystal						
	Atom1	Atom2	Atom3	Atom4	Compound 1	L-Leucine
Molecule 1	C11	C21	C31	C41	-177.6(2)	69.8(1)
	C21	C31	C41	C54	-80.58	71.0(2)
	C21	C31	C41	C61	-178.18	-166.9(1)
Molecule 2	C12	C22	C32	C42	65.3(4)	63.3(1)
	C22	C32	C42	C52	66.2(5)	64.6(1)
	C22	C32	C42	C62	-172.1(4)	-174.3(1)
L-Isoleucine residue in co-crystal						
	Atom1	Atom2	Atom3	Atom4	Compound 1	L-Isoleucine
Molecule 1	C11	C21	C31	C41	-177.6(2)	-177.4(2)
	C11	C21	C31	C51	57.75	57.9(2)
	C21	C31	C41	C61	-178.2(3)	-176.3(2)
Molecule 2	C12	C22	C33	C43	-49.42	-43.0(2)
	C12	C22	C33	C53	77.31	82.5(2)
	C22	C33	C53	C63	173.91	178.3(2)

4.3.6.2.2.2. Compound 2

The asymmetric unit of compound 2 contains two molecules with disorder in the side chain as shown in Figure 4.30. The conformations of L-Valine and L-Leucine side chain are shown in Figure 4.28 and torsion angles in comparison with the pure enantiomers of L-Valine and L-leucine are tabulated in Table 4.8.

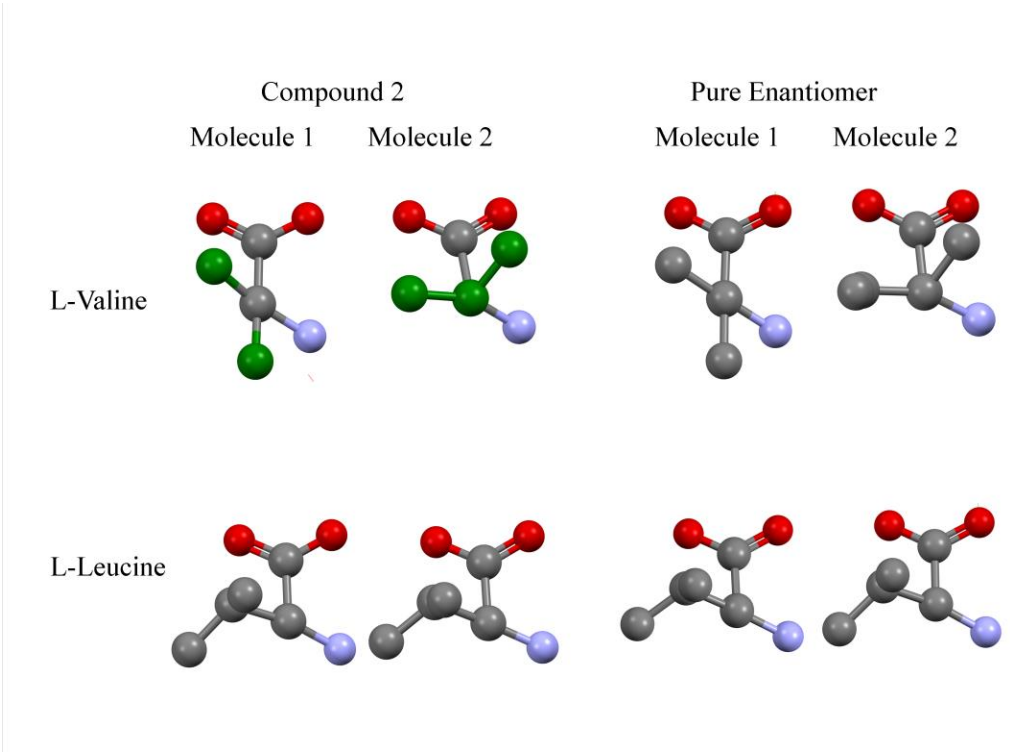

Figure 4.28 Observed configurations for rotation about the Cα-Cβ-bond in the side chains of the conformers of molecules in the asymmetric unit of compound 2, pure enantiomer L-Valine and L-leucine.

The two methyl groups in the tail group bifurcated at Cβ of L-Valine are at *gauche*$^{(+)}$ and *trans* position in molecule 1 and on Newman projection the molecule represent (Ib) showing a relatively stable configuration as compared

to molecule two in which (Ic) configuration is observed due to *gauche*$^{(+)}$ and *gauche*$^{(-)}$ positions of the methyl groups (Figure 4.29). The molecular packing of L-Valine side chain in compound 1 is very similar to its corresponding pure enantiomer (Dalhus & Gorbitz, 1996). In case of L-Leucine the both molecules in the asymmetric unit show a *trans* position of the tail rotation around the Cα-Cβ-bond which is equivalent to the conformation in pure L-Leucine crystal structures (*Dalhus & Gorbitz, 1996*). Both molecules of L-Leucine exhibit Ic configurational state when compared with the gas phase structure of L-Leucine.

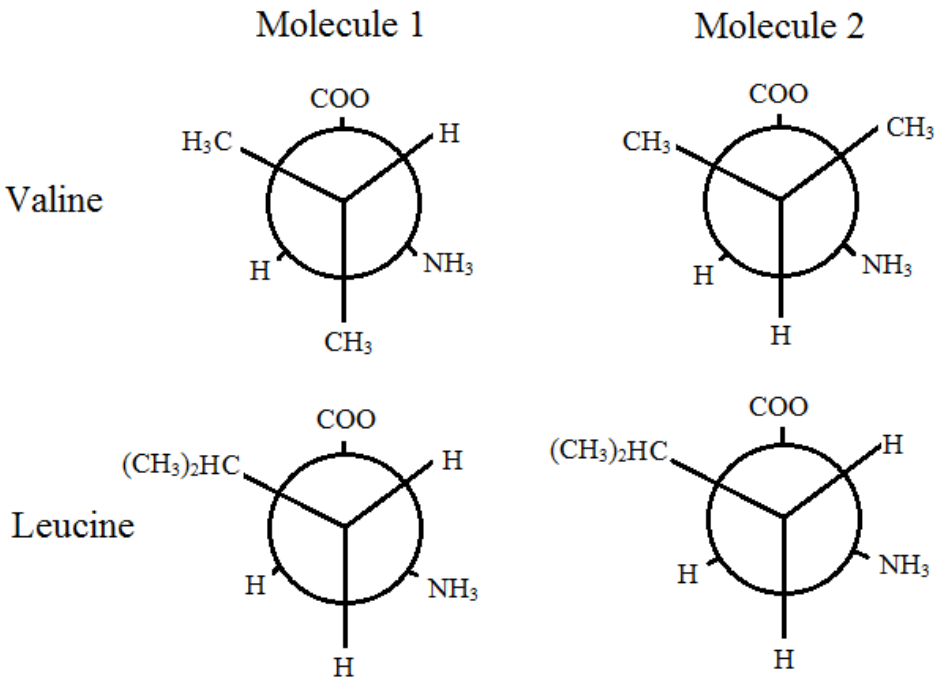

Figure 4.29 The observed configurations for rotation about the Cα-Cβ-bond in the side chains of the conformers of molecules in the asymmetric unit of compound 2.

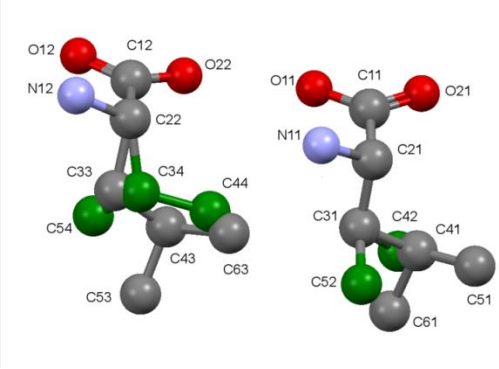

Figure 4.30 Numbering scheme of atoms in compound 2. The disordered L-Valine moiety is coded in green colour

Table 4.8 Torsion angles of L-Valine and L-Leucine in co-crystals (compound 2) and in their parent crystal structure.

Atoms involved in torsion						
L-Valine residue in co-crystal						
	Atom1	Atom2	Atom3	Atom4	Compound 2	L-Valine
Molecule 1	C11	C21	C31	C42	50.7(9)	58.6(1)
	C11	C21	C31	C52	179.1(7)	-178.5(1)
Molecule 2	C12	C22	C34	C44	75.25	83.6(1)
	C12	C22	C34	C54	-49.60	-41.3(1)
L-Leucine residue in co-crystal						
	Atom1	Atom2	Atom3	Atom4	Compound 2	L-Leucine
Molecule 1	C21	C31	C41	C51	71.2(9)	64.63(13)
	C21	C31	C41	C61	-167.9(7)	-174.2(12)
Molecule 2	C22	C33	C43	C53	65.79	71.0(15)
	C22	C33	C43	C63	-174.73	-166.8(14)

4.3.6.2.2.3. Compound 3

The preferred orientation of the side chain of L-Valine molecules in compound 3 is in close agreement with that observed for the pure L-Valine crystal structure (Dalhus & Gorbitz, 1996) and the conformational behaviour around the Cα-Cβ-bond is in *gauche*$^{(+)}$ and *trans* position in molecule 1 and *gauche*$^{(+)}$ and *gauche*$^{(-)}$ in molecule 2 of the asymmetric unit (Figure 4.31).

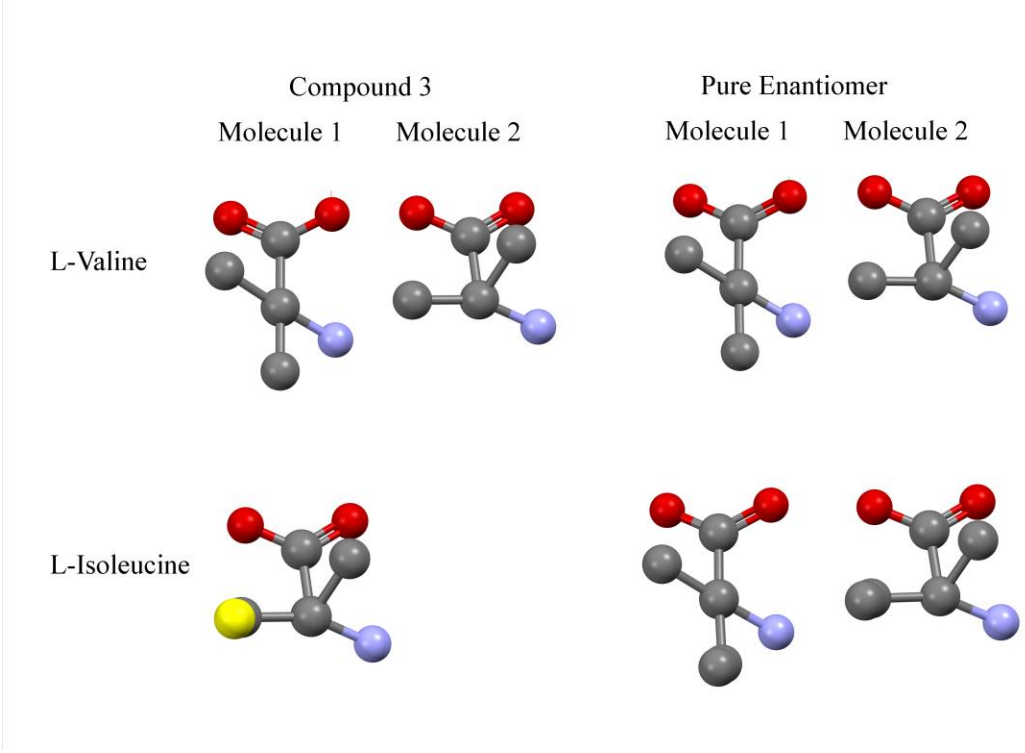

Figure 4.31 Observed configurations for rotation about the Cα-Cβ-bond in the side chains of the conformers of molecules in the asymmetric unit of compound 3, pure enantiomer L-Valine and L-Isoleucine.

The conformations of Isoleucine residue which is disordered within one molecule of the asymmetric unit in compound 3 and conformational preference is in *trans* state which is equivalent to one of the molecules in the asymmetric

unit of pure Isoleucine crystal structure (*Gorbitz & Dalhus, 1996*). There is no significant deviation observed in the torsion angles between the structures of Isoleucine in co-crystal and pure Isoleucine crystal structure.

In comparison with the gas phase structure of L-Valine (*Lesarri et al., 2004*) and L-Isoleucine (*Lesarri et al., 2005*) it is observed by plotting Newman projection that L-Valine exhibits two conformational states that is Ib and Ic which are relatively high energy conformers whereas L-Isoleucine observed Ic configuration (Figure 4.32). It is interesting to notice that the same configuration is observed by these two aliphatic amino acids in their pure enantiomeric solid state. The full description of the side chain torsion angles are given in Table 4.9 for comparison and numbering scheme of the atoms in the unit cell is given in Figure 4.33.

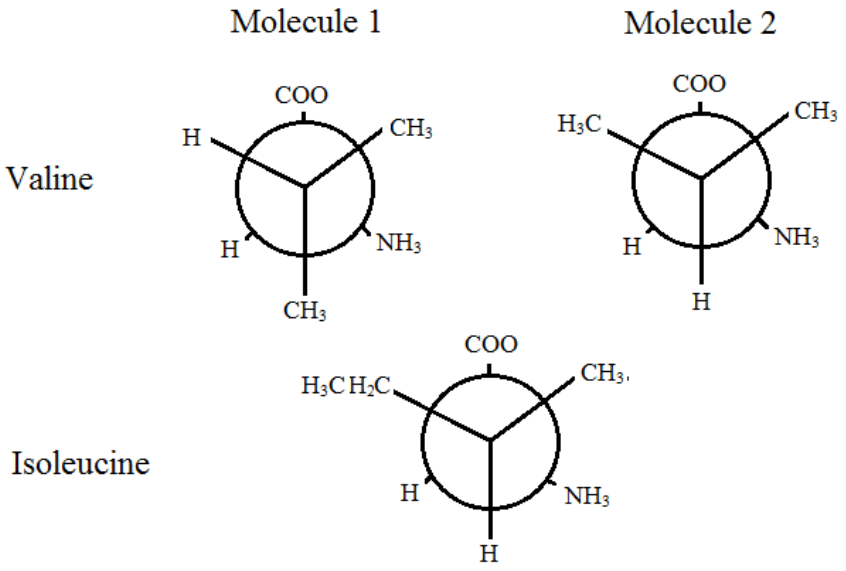

Figure 4.32 The observed configurations for rotation about the Cα-Cβ-bond in the side chains of the conformers of molecules in the asymmetric unit of compound 3.

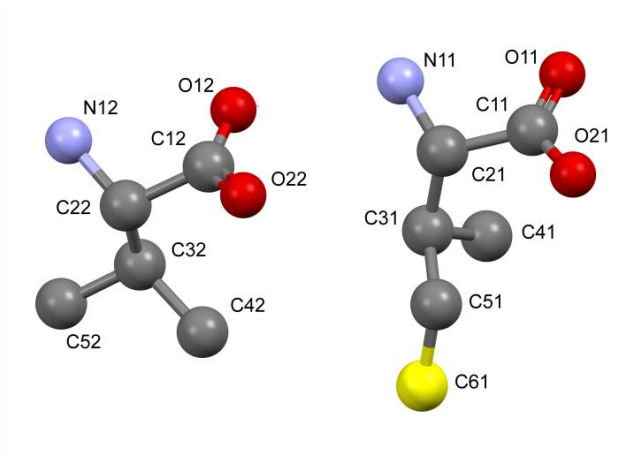

Figure 4.33 Numbering scheme of atoms in compound 3. The disordered L-Isoleucine moiety is coded in yellow colour.

Table 4.9 Torsion angles of L-Valine and L-Isoleucine in co-crystals (compound 3) and in their parent crystal structure.

Atoms involved in torsion						
L-Valine residue in co-crystal						
	Atom1	Atom2	Atom3	Atom4	Compound 3	L-Valine
Molecule 1	C11	C21	C31	C41	-41.1(6)	-41.3(1)
	C11	C21	C31	C51	82.6(6)	83.6(1)
Molecule 2	C12	C22	C32	C42	56.7(6)	58.6(1)
	C12	C22	C32	C52	-180.0(5)	-178.5(1)
L-Isoleucine residue in co-crystal						
	Atom1	Atom2	Atom3	Atom4	Compound 3	L-Isoleucine
Molecule 1	C11	C21	C31	C41	-41.1(6)	-43.0(2)
	C11	C21	C31	C51	82.6(6)	82.5(2)
	C21	C31	C41	C61	179.1(7)	178.3(2)

4.4. Summary

Novel co-crystals of homochiral Leucine:Isoleucine (compound 1), Valine:Leucine (compound 2) and Valine:Isoleucine (compound 3) were prepared using the conventional technique of solvent evaporative crystallisation. Co-crystals were formed through equimolar addition of the reacting components in water. The co-crystals were investigated through various analytical techniques like PXRD, DSC, FTIR and Raman spectroscopy. Crystal structures of these multi-component systems were determined by single crystal X-ray diffraction and the structures were probed to understand the structural and conformational arrangement of the molecules within the crystal lattice. The crystal structures of the amino acids complexes revealed that the molecules adopt a similar conformation and packing in contrast to their parent crystal structures except in compound 1.

4.5 References

Abagaroa, B.T.O., Freire, P.T.C., Silva, J.G., Meloa, F.E.A., Lima Jr, J.A., Filho, J.M., & Pizani, P.S. (2013). High pressure Raman scattering of dl-leucine crystals. *Vibrational Spectroscopy. 66*, 119–122.

Altomare, A., Cascarano, G., Giacovazzo, C., & Guagliardi, A. (1993). Completion and refinement of crystal structures with SIR92. *Journal of Applied Crystallography*. *26*, 343-350.

Benedett, E., Pedone, C., & Sirigu. (1973). The Crystal Structure of DL-Isoleueine and Structural Relations between Racemic and Optically Active Pairs in some Aminoacids. *Acta Crystallography. B29*, 730.

Betteridge, P.W., Carruthers, J.R., Cooper, R.I., Prout, K., & Watkin, D.J. (2003). CRYSTALS Version 12: Software for Guided Crystal Structure Analysis. *Journal of Applied Crystallography. 36*, 1487-1487.

Blasio, B., Pedone, C., and Sirigu. (1975). DL-Leucine. *Acta Crystallography. B 31*, 601.

Blessing, R.H. (1995). An Empirical Correction for Absorption Anisotropy. *Acta Crystallography. A. 51*, 33-38.

Blomstrand, E., Eliasson, J., Karlsson, H.K., & Köhnke,. R. (2006). Branched-chain amino acids activate key enzymes in protein synthesis after physical exercise. *The Journal of Nutrition*. 136, 269S–273S.

Burchell, T.J., Soldatov, D.V., & Ripmeester J.A. (2008). Crystal structure of the co-crystal ALA-VAL.ALA.H2O: A layered inclusion compound. *Journal of Structural Chemistry. 49*(1), 188-191.

Cocinero, E.J., Lesarri, A., Grabow, J.U., Lopez, J.C., & Alonso, J.L. (2007). The Shape of Leucine in the Gas Phase. ChemPhysChem. 8, 599 – 604.

Coles, S.J. & Gale, P.A. (2012). Changing and challenging times for service crystallography. *Chemical Science*. 3, 683-689.

Cosier, J. & Glazer, A.M. (1986). A Nitrogen-Gas-Stream Cryostat for General X-ray Diffraction Studies. *Journal of Applied Crystallography.19*, 105-107.

Dalhus, B. & Gorbitz, C.H. (1999). Molecular aggregation in crystalline 1:1 complexes of hydrophobic D- and L-amino acids. I. The L-isoleucine series. *Acta Crystallographica. B* 55, 424-431

Dalhus, B. & Gorbitz C.H. (1999). Molecular aggregation in selected crystalline 1:1 complexes of hydrophobic D- and L-amino acids. III. The L-leucine and L-valine series. *Acta Crystallographica. C. 55*, 1547-1555.

Dalhus, B. & Gorbitz, C.H. (1996). Crystal Structures of Hydrophobic Amino Acids. I. Redeterminations of L-Methionine and L-Valine at 120 K. *Acta Chemica Scandinavica. 50*, 544-548.

Dittrich, B., Pfitzenreuter, S., & Hubschle, C.B. (2012). On QM/MM and MO/MO cluster calculations of all-atom anisotropic displacement parameters for molecules in crystal structures *Acta Crystallographica. A. 68*, 110-116.

Funnell, N.P., Dawson, A., Marshall, W.G., & Parsons, S. (2013). Destabilisation of hydrogen bonding and the phase stability of aniline at high pressure. *CrystEngComm, 15*(6), 1047-1060.

Gorbitz, C.H., & Dalhus, B. (1996). Redetermination of L-Leucine at 120 K. *Acta Crystallographica . C. Crystal Structure Communications. 52*, 1754.

Gorbitz, C.H., & Dalhus, B. (1996). L-Isoleucine, Redetermination at 120 K. *Acta Crystallographica. C. Crystal Structure Communications. 52*, 1464-1466.

Hanchen, A., Rausch, S., Landmann, B., Toti, L., Nusser, A., & Sssmuth R.D. (2013). Alanine Scan of the Peptide Antibiotic Feglymycin: Assessment of Amino Acid Side Chains Contributing to Antimicrobial Activity. *ChemBioChem*. *14*, 625 – 632.

Harding, M.M., & Howiesont, R.M. (1976). L-Leucine. *Acta Crystallography. B 32*, 633.

Hernández, B., Pflüger, F., Nsangou, M., & Ghomi, M. (2009). Vibrational Analysis of Amino Acids and Short Peptides in Hydrated Media. IV.

Amino Acids with Hydrophobic Side Chains: L-Alanine, L-Valine, and L-Isoleucine. *Journal of Physical Chemistry B , 113*, 3169–3178.

Karlsson, H.K., Nilsson, P.A., Nilsson, J., Chibalin, A.V., Zierath, J.R., & Blomstrand, E. (2004). Branched-chain amino acids increase $p70^{S6k}$ phosphorylation in human skeletal muscle after resistance exercise. *American journal of Physiology. Endocrinology Metabolism. 287*(1), E1-7.

Khawas, B. (1970). An X-ray study of L-isoleucine. *Acta Crystallographica. B. 26*, 1385.

Lesarri, A., Cocinero, E.J., Lopez, J.C., & Alonso, J.L. (2004). The Shape of Neutral Valine. *Angewandte Chemie International Edition.* 43, 605 – 610.

Lesarri, A., Sanchez, R., Cocinero, E.J., Lopez, J.C., & Alonso, J.L. (2005). Coded Amino Acids in Gas Phase: The Shape of Isoleucine. *Journal of American Chemical Society.* 127, 12952-12956.

Liu, M., Nauta, A., Francke, C., & Siezen, R.J. (2008). Comparative Genomics of Enzymes in Flavor-Forming Pathways from Amino Acids in Lactic Acid Bacteria. *Applied and Environmental Microbiology. 74* (15), 4590–4600.

Mallikarjunan, M., & Rao, S.T. (1969). Crystal Structure of DL-Valine. *Acta Crystallographica. B.25*, 296;

Minkov, V.S., Boldyreva, E. V., Drebushchak, T. N., and Gorbitz, C. H. (2012). Stabilizing structures of cysteine-containing crystals with respect to variations of temperature and pressure by immobilizing amino acid side chains. *CrystEngComm, 14*, 5943–5954

Moreno, L.F. (2011). Understanding Fischer Projection and Angular Line Representation Conversion. *Journal of Chemical Education. 89*,175–176.

Nelson, D.L., & Cox, M.M. (2000). Lehninger Principles of Biochemistry; Worth Publishers: New York.

Project MT7150. Collected via the I19 Rapid access service at Diamond Light Source.

Saraswathi, N.T., & Vijayan, M. (2001). X-ray studies on crystalline complexes involving amino acids and peptides. XXXVIII. Crystal structures of the complexes of L-arginine and L-histidine with glutaric acid and a comparative study of amino acid-glutaric acid complexes. *Acta Crystallographica Section B Structural Science. B57*, 842-849

Sheldrick G. M. (2004). SADABS Version 2004-1. Bruker-AXS, Madison, WI.

Tamm, L. K. (2005). Protein-Lipid Interactions: From Membrane Domains to Cellular Networks Wiley-VCH Verlag GmbH & Co. KGaA, Weinheim.

Tilborg A, Norberg B, Wouters J. (2014). Pharmaceutical salts and cocrystals involving amino acids: A brief structural overview of the state-of-art. *European Journal of Medicinal Chemistry 74*, 411-426.

Thorey, P., Bombicz, P., Szilágyi, I.M., Molnár, P., Bánsághi, G., Székely, E., Simándi, B., Párkányi, L., Pokol, G., Madarász, J. (2010). Co-crystal of (R, R)- 1, 2-cyclohexanediol with (R, R)-tartaric acid, a key structure in resolution of the (±)- trans-diol by supercritical extraction, and the related ternary phase system. *Thermochimica Acta*. 497, 129–136

Torii K and Iitaka Y. (1970). The Crystal Structure of L-Valine. *Acta Crystallographica. B.*26, 1317.

Torii K and Iitaka Y. (1971). The Crystal Structure of L-Isoleucine. *Acta Crystallographica. B.*27, 2237.

Trikha, J., Patel, H.C., & Singh T.P. (1990). Structure of a 1:1 Complex between N-Boc-L-Pro-L-VaI-OCH3 (I) and AT-Boe-L-Pro-Ca-Methylated-L-Val-OCH3 (II). *Acta Crystallographica. C.46*, 74-78.

Wagenmakers A.J. (1998). Protein and amino acid metabolism in human muscle. *Advances in Experimental Medicine and Biology*. 441, 307-19.

Zhou, Y., Oostenbrink, C., Gunsteren, W.F.V., Hagen, W.R., De Leeuw, S.W., & Jongejan, J.A. (2005). Relative stability of homochiral and heterochiral dialanine peptides. Effects of perturbation pathways and force-field parameters on free energy calculations. *Molecular Physics.103*(14), 1961–1969.

Zhu, G., Zhu, X., Fan, Q., & Wan, X. (2011). Raman spectra of amino acids and their aqueous solutions. *Spectrochimica Acta Part A*. 78. 1187–1195.

CHAPTER 5

Bulk preparation of amino acid co-crystals.

This work was done in collaboration with Ulrich Schacht and Jan Sefcik, Department of Chemical and Process Engineering, University of Strathclyde.

5.1. Introduction

Manufacturing of most pharmaceutical products comprises on crystalline materials such as pharmacologically active pharmaceutical ingredients (API) and inactive ingredients (excipients) and involves a crystallisation step. Crystallisation is a most commonly used and important method of separation and purification of solid state finished products and intermediates in the bulk, fine chemicals, food, and pharmaceutical industries (*Myerson, 2002*).

Crystallisation processes in the pharmaceutical manufacturing units are generally managed to prepare crystalline substances with controlled purity, size, shape, and polymorphic form in high yield. The control of crystal morphology and crystal habit is crucial for the finished pharmaceutical product, as these can not only affect downstream processes like filtration, drying, and particle size reduction but also influence the product effectiveness such as stability, dissolution rate and solubility. The crystalline phase purity and yield of the product are also very important parameters in the crystallisation process design in order to ensure that the product fall within quality control specifications and to get maximum production. In order to avoid high economic penalty of manufacturing an out of specification product, understanding of the parameters and conditions required to fabricate crystals with controlled properties is crucial in process design (*Jones, 2002; Mullin, 2002*). Theory of crystallisation can broadly be divided in two stages: nucleation and crystal growth (*Mullin, 1993; Tung, et al. 2009*) and Figure 5.1

shows a schematic diagram describing the course of a typical crystallisation process.

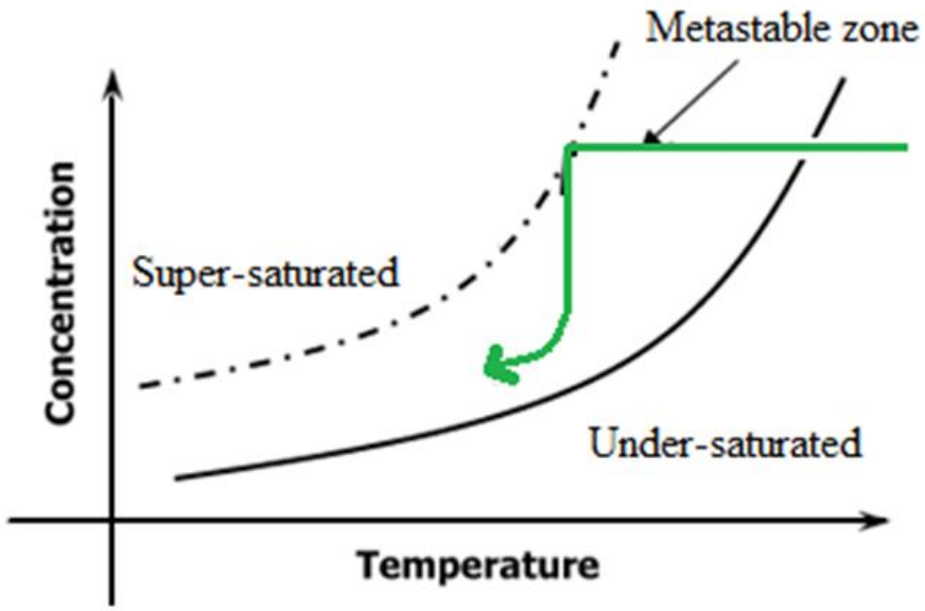

Figure 5.1 General schematic of a typical solution cooling process. Showing super-solubility curve (dot-dash line), solubility curve (solid line) and coloured arrow showing cooling process from supersaturation to saturation state.

Normally, creation of a supersaturated condition is the first requirement for spontaneous nucleation and between the supersaturated and solubility curves exists a metastable zone, which provides a labile region of driving force for the formation of nuclei. However, spontaneous nucleation is unlikely to occur in the metastable zone. At some point near to supersaturation nucleation takes

place followed by crystal growth thus causing the decrease in concentration of the compound in the solution.

The solubility of a substance in a solution can be determined by various methods for example a commonly employed method is the gravimetric method but it is difficult to measure precisely its supersaturated value or the metastable zone width. The rate of creating supersaturation, impurities in the solution, fluid dynamics etc. all effect supersaturation and metastable zone condition (*Ulrich and Strege. 2002*) and these values will vary if any change is applied such as crystalliser's or reactor's conditions or even switching from small laboratory scale to large scale bulk preparation. The shifting from laboratory scale crystallisations to bulk preparation is imperative to increase the rate of production but is often met with challenges like phase purity, e.g. formation of hydrates/solvates, polymorphism etc. Many scale-up methodologies have been investigated in detail focussing on the effects such as, rotational speed of impellor, stirred tank Reynolds number, ratio of impellor to vessel diameters, etc., in crystalliser design and process (*Lawton, et al., 2009*). Due to the number of variables and the challenges of keeping a set of parameters constant there is a limited understanding of the scale up process in a stirred tank crystalliser (STC) especially as some of these parameters are product specific and hence are not translatable to other systems. Furthermore it is also important to gain a better understanding of the effect of mixing on crystallisation to ensure the optimum conditions for scale up (*Genck, 2003*)**.** Due to the smaller scale, laboratory experiments do not, generally, suffer from mixing gradients that plague industrial scale operations therefore the products are well mixed. In

larger scale environments it is observed that there is variation in mixing within a vessel. Efficient mixing occurs at and around the impeller regions whereas, inefficient mixing take place elsewhere (*Rielly, et al., 2001; Xie, et al., 2007*), thus causing problems in linearly scaling-up processes. From a crystallisation process point of view, mixing gradients have direct impact on crystallisation process as they will cause variation in concentration within a solution, e.g. the supersaturation and metastable zone widths will differ in different parts of the vessel. Cooling crystallisation from solution is dependent on optimum heat transfer and is difficult to maintain the specific area per unit volume for heat transfer with scale. The decrease in heat transfer area and other factors like non-uniform mixing on scale up of STCs makes cooling profiles (e.g., linear or parabolic) potentially problematic to implement in any industrial batch STC. Nonetheless open- and closed loop control of batch crystallisation processes have been reported (*Gron, et al.2003; Nagy & Braatz 2004; Liotta & Sabesan, 2004*).

For many decades batch crystallisation has been a standard in pharmaceutical industries and the finished product is achieved using cooling, anti-solvent, or reactive crystallization techniques (*Beckmann, 2013*). Despite a good understanding of batch crystallisation processes and actually being used in practice, industries are still facing problems of batch-to-batch variation as well as major issues in the other related unit operations such as filtration and drying in processing of the finished material (*Randolph & Larson, 1988*). Although the batch crystallisation processes look straightforward and simple in operation there are still large problems to overcome in obtaining and optimising

reproducible properties of the materials like particle shape and size, particle size distribution, polymorphism. All these properties are very critical in defining the later processes in product development like filtration, drying and formulation which ultimately affect the performance of the final product (*Nyvlt, 1992*). Other issues within a batch is the presence of out-of-specification crystals which may then require additional processes like milling and recrystallization which can add time and cost to processing (*Nyvlt, 1977*). Industries still prefer batch crystallisation because the process ensures a higher yield of the product as compared to continuous process. The former process operates at equilibrium while later works on the principle of steady state *(Chen, et al 2011*). Recent research has shown that high product yield, comparable to the batch yield, can be obtained by designing and optimisation of continuous crystallisation process such as recycling the mother liquor in appropriately designed crystallisers such as mixed-suspension, mixed-product removal crystalliser (*Wong, et al., 2012*). Developing and designing continuous crystallisation have been recognized in recent years as key processes for improved way of manufacturing materials and that there is a high potential to use these methods in the chemical and pharmaceutical industries (*Chen, et al.,2011; Alvarez and Myerson, 2010*).

Continuous manufacturing in recent years has become a popular area of research in both academia and industry as it offers significant advantages over batch manufacturing for example, reliability in quality, reduction in production cost, shorter down time, ease of scale up and achieving operating parameters not achievable in discontinuous or batch processes. (*Poechlauer, et al., 2012,*

Pellek and Arnum, 2008; Swichtenberg, 2008; Vervaet & Remon 2005; Gron, et al., 2003; Liu, et al.,1997;Plumb. 2005).

For pharmaceutical crystallisation the three main types of continuous crystallisers are: mixed-suspension, mixed-product removal (MSMPR) crystallisers in single or multiple stage configurations; plug flow reactors (PFR); and oscillatory baffled crystallisers (OBC) (*Wong, et al., 2012*). The most common types of continuous crystallisers are continuous mixed-suspension, mixed-product removal (MSMPR) and plug-flow reactor (PFR) crystallisers (*Randolph & Larson, 1988*). Both types of crystallisers were studied extensively over the years for the determination of nuclei formation and rate of growth of nuclei in crystallisation systems (*Nyvlt, J., 1977.; Lawton, et al.,2009.; Hanley and Mischike,1978*). The MSMPR crystallisers are advantageous for low conversion with long residence time (*Quon, et al.,2012***)** and the PFR being preferred for fast growing crystals with short residence times (*Alvarez and Myerson 2010*). In a continuous crystallisation set up, a steady state or equilibrium is achieved when the flow of materials into the crystalliser becomes equal to the out flow of materials and the amount of those materials in the crystalliser become constant. The ratio of the amount of materials in the crystalliser to the flow rate (in or out) is called residence time.

The system being studied here (Figure 5.2) combines several technologies which have been individually investigated and reported for batch or semi-continuous operation in literature. For example, methods such as jet mixing (*Choi, 2005*), hot solution into cold anti-solvent (*Dalvi and Dave., 2009*),

ultrasound to enhance cleaning of equipment (*Fuchs, 1995; Narducci, et. al. 2011*).

The aim of this chapter is to investigate experimentally continuous stirred tank crystalliser to perform a continuous anti-solvent crystallisation for multi-component system and to evaluate the advantages of continuous crystallisation for bulk preparation of amino acid co-crystals with emphasis on particle size distribution, purity and yield.

5.2. Experimental

5.2.1. Materials.

The materials used in the study include reagent grade L-Valine, L-Leucine and L-Isoleucine which were purchased commercially from Sigma-Aldrich Company, Ltd. (Gillingham, UK) and used as received. Deionised water from a MilliQ water purification unit was used for crystallisation experiment. The powder X-ray diffraction pattern, differential scanning calorimetry, thermalgravimetry analysis, FTIR and Raman spectrum of the reagents were recorded for comparison with the bulk powders of complexes of the amino acids prepared by continuous crystallisation method.

5.2.2. Methods

5.2.2.1. Stirred tank crystalliser for continuous flow system

The scheme of the experimental setup (Figure 5.2) consisted of;

- Glass-jacketed crystallisers (V3) with independent temperature control and overhead mechanical stirring.
- Ismatec external gear pumps (MCP-Z) with magnetically coupled pump head (P1) Watson-Marlow 520S peristaltic pump (P2) to maintain a constant mixing ratio of stream 1: stream 2.
- heat exchanger (E1 and E2) to warmed the fluid to achieve a desired saturation level.
- Nozzles used to control the flow rates of stream.
- Neslab Rte Refrigerated Bath Circulator.
- PTFE syringe filter with 0.2-µL pore size.

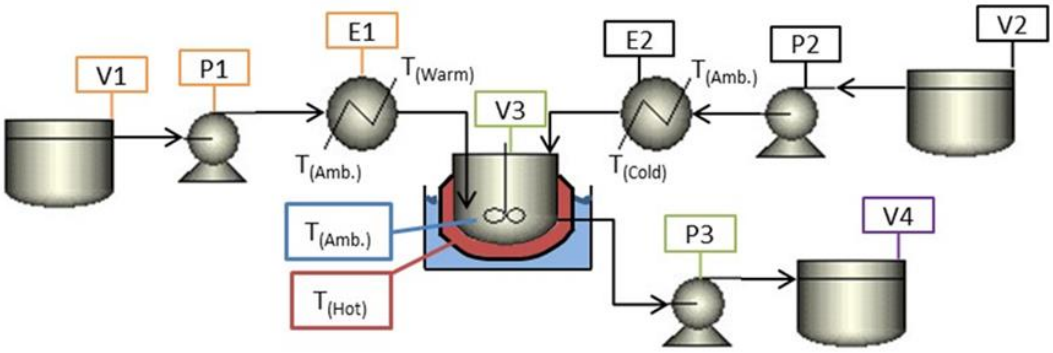

Figure 5.2 The set-up of the continuous flow system. P1-3 represent pumps, V1-3 are the vessels, V3 is the crystalliser where the crystals are formed. E1&2 are the heat exchangers ensure that the flow is at ambient and cold temperatures, respectively.

5.2.2.1.1. Solution preparation and operating conditions for continuous crystallisation.

For all the crystallisation runs, the equimolar quantities of the amino acids were carefully weighed and dissolved in purified water quantity sufficient. The solutions were filtered before subjecting to the process. The summaries of the operating conditions and sample preparation are given in Table 5.1 and Table 5.2 respectively.

Table.5.1 Operating parameters for continuous flow system (Figure 5.2).

Operating parameters	Values	
m_1 [g/min]	5	
m_2 [g/min]	95	
m_{Total} [g/min]	100	
$V_{Injection\ Nozzle}$ [m/s]	2.57	
T_1 [°C]	45	
T_2 [°C]	3.4 – 4.5	
T_{Bulk} [°C]	16 - 24	
C_{aq} for L-Amino Acids [mg (amino acids)/g (solution)]	LIL	27.2977
	VL	34.0412
	VIL	40.3405

Table 5.2 Solution preparation of amino acid co-crystals (Compound 1, Compound 2 and Compound 3).

Solution no.	Amino Acid	$m_{(amino\ acid)}$ [g]	N	$m_{(Solution)}$ [g]	$c_{(Solution)}$ [$mg/g_{(Solution)}$]
Compound 1					
1 - Aq.	Leucine	14.4286	0.110		13.6488
	Iso-Leucine	14.4287	0.110	1057.1	13.6489
Compound 2					
1 - Aq.	Valine	24.6021	0.209		16.0601
	Leucine	27.5448	0.210	1531.9	17.9811
Compound 3					
1 - Aq.	Valine	12.3016	0.1047		19.0320
	Iso-Leucine	13.7731	0.1050	646.4	21.3085

5.2.2.1.2. Procedure.

Anti-solvent continuous crystallisation experiments for all the compounds were performed using the continuous crystallisation apparatus described in Figure 5.3. During operation a warm solution (47 – 49 °C) of amino acids [stream 1 (m_1)] was jet injected through a submerged stainless steel nozzle into the bulk solution of the crystalliser (V3) at a flow rate of 5 g/min controlled by an Ismatec external gear pumps (MCP-Z) with magnetically coupled pump head (P1). The heat exchanger (E1) warmed the fluid to a saturation level of 40-50% of the saturation concentration (maximum solubility) at ambient temperature. Nozzles with two different internal diameters (0.2 and 0.6 mm) were used to control the flow rates of stream 1 (jet injection velocities 1.1 – 8.0 m/s) into the bulk solution. Cold anti-solvent Isopropanol [stream 2 (m_2)] entered the crystalliser (V3) through Marprene tubing, falling from the top of the vessel. The flow rates of stream 2 were delivered and controlled by a Watson-Marlow 520S peristaltic pump (P2) so that a constant mixing ratio of stream 1: stream 2 was maintained. The resulting mixing temperature in V3 for any given ratio was always recorded to be well below the ambient temperature hence ensuring supersaturation.

5.2.2.2. The Crystal 16® reactor for solubility studies

The Crystal16® is a bench top multiple reactor station gaining popularity among pharmaceutical research scientists and pharmaceutical companies because of its simplicity in use and wide range of applications including

solubility studies (*Sistla, et. al. 2011*) and crystallisation studies (*Kulkarni . et al. 2012*).

The apparatus is consisting of four independently heated Aluminium reactor blocks and is a compact bench top setup (Figure 5.3). The crystallisation platform can hold (4 x 4) standard HPLC glass vials which allow running 16 experiments in parallel. These reactor blocks are electrically heated and cooled by a sequence of Peltier elements and a cryostat. The nitrogen gas is purged into the system to avoid condensation of water on the reactor blocks and electronics during experimental runs.

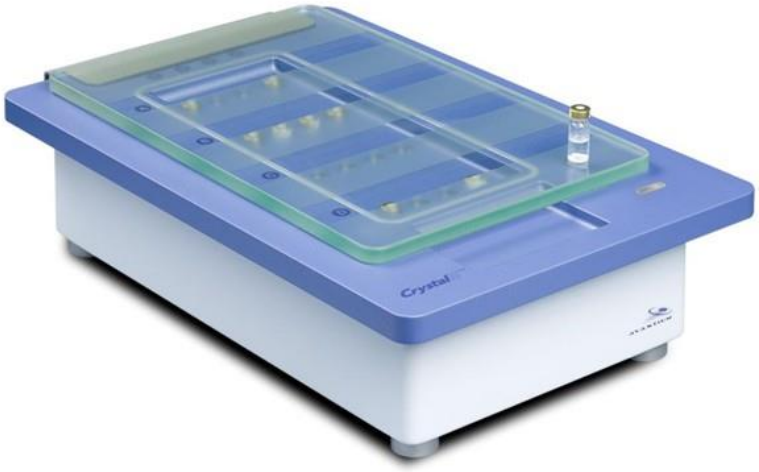

Figure 5.3 Crystallisation bench top system (*Crystal16*®).

Four independent and individually programmable temperature zones combine magnetic stirring and turbidity measurements within each reactor to monitor

changes in state as a function of time and temperature. Solubility data were generated by determination of clear and cloud points by measuring turbidity.

A clear point is the point at which dispersed solid material dissolves completely giving 100% transmittance and the solubility curve of a substance consists of a series of clear points. The cloud point means a point at which the dissolved solid first appears in a solution causing a decrease in transmittance from 100% to no transmittance. The metastable limit curve consists of a series of 'cloud points'.

Crystal Clear software package is used to transform the data produced by the Crystal 16® and can be used to construct solubility curves.

5.3. Powder (product) characterisation

5.3.1. Phase analysis- X-ray powder diffraction

A small quantity (10 - 50 mg) of each crystallised sample was analysed using transmission foil XRPD. Data collected on a Bruker AXS D8-Advance transmission diffractometer equipped with θ/θ geometry, primary monochromated radiation (Cu-Kα1 λ = 1.54056 Å), a Bruker Vantec 1D position sensitive detector (PSD) and an automated multi-position x-y sample stage. Samples were ground lightly before being mounted on a 28 position sample plate supported on a polyimide (Kapton, 7.5 μm thickness) film. Data were collected from each sample in the range 4 – 35 ° 2θ with a 0.015 ° 2θ step size and 1 sec. count time.

5.3.2. Fourier transform infrared spectroscopy

Infrared spectroscopy was conducted using a ThermoFisher Nicolet iS10 spectrometer. Data were collected on the pure amino acids, mixtures of amino acids and the co-crystals formed from the anti-solvent bulk production. The spectra were visualised and analysed with OMNIC^{TM} software (version 8.1) (Thermo Scientific).

5.3.3. Differential scanning calorimetry

DSC analysis was carried out using a Mettler Toledo Model DSC 822 with auto sampler and liquid nitrogen cooling system. The sample powder prepared by weighing in between 3.35 – 5.23 mg into a 40 µl aluminium pan, which was then hermetically sealed with a pinhole in the lid and heated under nitrogen purge. The temperature range was 40 °C to 340 °C at a heating rate of 10°C min^{-1}. The temperature and heat flow of the DSC instrument was calibrated with indium and zinc. Mettler Toledo STARe software was used to analyse the data and the thermogram obtained were compared with the one obtained with the pure components of the amino acid complexes.

5.3.4. Scanning electron microscopy studies

The gold coated sample was analysed by a Hitachi Field Emission Scanning Electron Microscope (FE-SEM) SU6600, Japan). Sample preparation for SEM imaging involved pipetting a few drops of crystal slurry from the crystalliser outlet tube onto a PTFE filter membrane. The solvent quickly dispersed into the filter membrane without adversely affecting the product crystals in terms of

caking or other crystal changes. The area of the filter membrane containing the crystals was cut out and stuck onto a little piece of conductive carbon tape on top of a SEM sample holder. In the final step the entire sample holder, including the crystals on the filter membrane, was coated with a thin layer of gold using Edwards S150 Sputter Coater.

5.3.5. Particle size distribution studies

A Malvern Mastersizer (APA2000, Malvern Instruments Ltd., UK) was used to measure the mean particle size distribution of co-crystal powder samples. The instrument was conditioned with mother-liquor from the crystallisation experiment and zeroed to account for background scattering. The sample crystal slurries from the crystalliser outlet tube were pipetted into the Mastersizer sample container unit until the instrument indicated that the optimum solid concentration had been achieved for a measurement. The refractive index of 1.65 was used for the measurement and data analysis (*Brydson, 1999*).

5.3.6. Solubility studies of the co-crystals

Solubility studies of the co-crystals were carried out using the Crystal 16® (Avantium Technologies BV. Netherlands) with an accelerated thermal cycle in water: isopropanol (95:5) mixed solvent system.

5.3.7. Powder flow and compressibility measurements

The test was carried out by using the Powder Tapped Density Tester (Copley Scientific, Nottingham, UK). The apparatus (figure 5.4) has a constant rate of

250 ± 15 taps per minute and has a constant set drop of 3 ± 0.2 mm. The test was performed, with little modification due to limitation of sample quantities, according to the method described in the European Pharmacopoeia 7th edition.

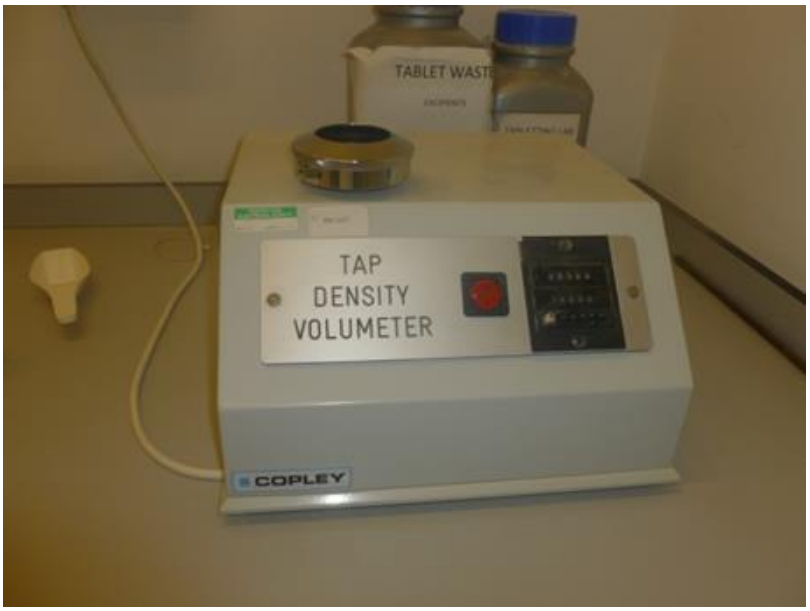

Figure 5.4 Tap density volumeter.

First of all, the cylinder was filled with one of the powder samples and during the filling it was made sure that the cylinder is approximately in a 45-degree angle by attaching it to a stand. The powder was gently poured in and the cylinder was slowly moved to an upright position afterwards. The cylinder was placed carefully onto the weighing scale to prevent the powder from sagging by avoiding sudden movements. The net mass (M) was measured and read the corresponding volume to the nearest graduated unit for the determination of the bulk volume V_0. In case of uneven surface, the highest and lowest surface points were observed and estimated the mean volume. The filled graduated cylinder was secured in the support of the apparatus. Then carried out

respectively 50, 250 and 500 taps, each time followed by reading the apparent volume in the same way as described above. The tapped volumes V_{50}, V_{250} and V_{500} were obtained. V_{500} was recorded as the tapped volume as the difference between V_{250} and V_{500} was insignificant and was less than 1mL (Ph.Eur.7th Ed.). Using these data we calculate the tapped and bulk density values for each of the powders. The equations used are the following:

$$\rho Bulk = M / V_0 \quad (5.1)$$

where,

ρBulk = Bulk density (g/mL), M = Mass (g),

V_0 = Bulk volume (mL)

$$\rho Tapped = M / V_{500} \quad (5.2)$$

where,

ρTapped = Tapped density (g/mL), M = Mass (g),

V_{500} = Tapped volume (mL)

The Carr's index or compressibility index doesn't really describe the flowability, but rather the relationship between bulk and tapped densities. It differentiates well between cohesive and free-flowing powders. For the determination of the Carr's index CI we use the following formula (*Staniforth, 2007*).

$$CI = ((\rho Tapped - \rho Bulk) / (\rho Tapped) \times 100) \quad (5.3)$$

Where, CI = Carr's Index

ρTapped = Tapped density (g/mL)

ρBulk = Bulk density (g/mL)

Table 5.3 Relationship between powder flowability and percentage compressibility range (*Staniforth , 2007*).

% Compressibility range	Flow description
5--15	Excellent (free flowing granules)
12--16	Good (free flowing powdered granules)
18--21	Fair (powdered granules)
23--28	Poor (very fluid powders)
28--35	Poor (fluid cohesive powders)
35--38	Very poor (fluid cohesive powders)
> 40	Extremely poor (cohesive powders)

Since the Hausner ratio is linked with friction among the particles, it is a way to forecast powder flowability. For the determination of the Hausner ratio HR we use the following formula:

$$HR = (\rho Bulk / \rho Tapped) \quad (5.4)$$

Where, HR = Hausner ratio

ρBulk = Bulk density (g/mL)

ρTapped = Tapped density (g/mL)

5.4. Results and Discussion

5.4.1. Phase analysis- X-ray powder diffraction

The product from the anti-solvent crystallisation was subject to analysis through X-ray powder diffraction to verify the production of the co-crystal. Figure 5.5 (top) contains the X-ray powder diffraction patterns of all the bulk samples and confirms the identity of the co-crystals. The simulated patterns of the reacting components (generated by using their respective cell parameters) are of structures at -153.15 °C & -150.15 °C as reported in literature and hence the peaks will be shifted towards slightly higher 2 theta values compared with the data collected at ambient temperature due to the reduction in the cell parameters at low temperature. It was apparent during grinding process that the crystals were not conducive to a good powder and the powder patterns suffer from broadening and preferred orientation (*cf.* the ratio of heights between the peak at 6.5°vs those at ~19° 2θ in patterns Figure 5.5d with Figure 5.5e & f). A Pawley fit of Compound 1 is shown in Figure 5.5(bottom) together with a comparison with the pure compounds, a mixture and a simulated powder pattern from the cell parameters of the respective co-crystal. The powder patterns are slightly broad due to the grinding process but this was common with other preparative methods such as grinding under solvent or

liquid N_2. The results of the fit confirm that for the powder of Compound 1 it is largely the co-crystal phase but there is some small component that can be attributed to isoleucine (re. small peaks at 12.5° and 24.4°). Pawley fits and comparisons of Compounds 2 and 3 can be found in Figure 5.6 and 5.7, respectively, and show that in both instances the co-crystal was made in pure form; the differences being attributed to slight misfits in the peak fitting.

5.4.2. Infrared spectroscopy

To complement the powder diffraction data, and to verify that the powder from the bulk crystallisation was in the same ratio as the single crystal determination, the two peaks representative of the constituent amino acids were highlighted and their peak height ratios were calculated. These were compared with the IR from the single-crystal co-crystal and the pure components as well as a mixture. For this analysis prominent peaks from each component were used and their ratios taken as a measure of the quantities of each component within the powder, for example, in compound 1, the stretching of leucine (846) and wagging of isoleucine (800) are strong vibrations in their respective spectra but they are both prominent in the single crystal of the co-crystal (Figure 5.8). A well-mixed 50:50 powder of both components was also analysed as a measure of whether a mixture of the components was crystallised as opposed to the co-crystal. Table 5.4 shows the peak height and peak area ratios of these observed for the three different co-crystals and their parent compounds. These ratios clearly show that the co-crystal was produced rather than the mixture of the two components.

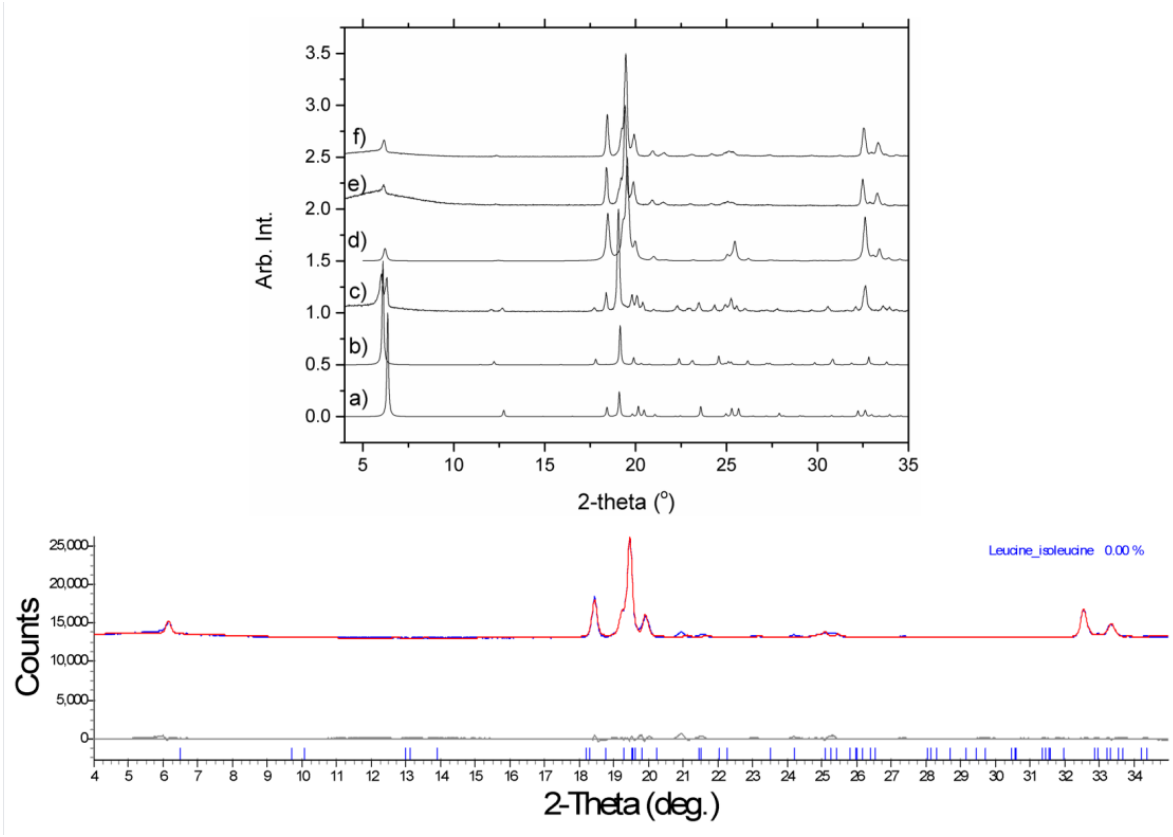

Figure 5.5 Top) A comparison of the diffraction data from bulk preparation with known forms. a) simulated patterns of isoleucine b) simulated patterns of leucine c) mixture from slurry experiment d) simulated patterns of co-crystal from SXD data with preferred orientation (001) direction e) Bulk product after 3 mins f) Bulk product after 100 mins. Bottom) Pawley fit of bulk product using co-crystal parameters.

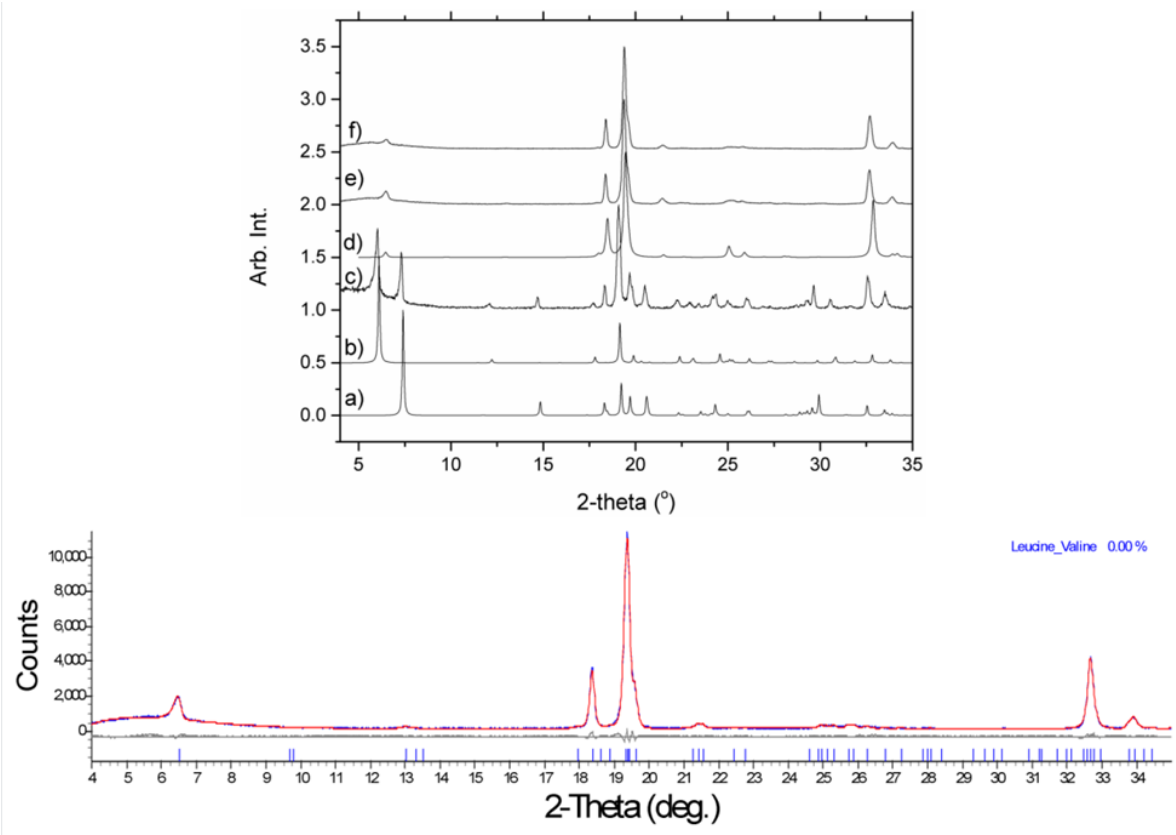

Figure 5.6 Top) A comparison of the diffraction data from bulk preparation with known forms. a) simulated patterns of valine b) simulated patterns of leucine c) mixture from slurry experiment d) simulated patterns of co-crystal from SXD data with preferred orientation (001) direction e) Bulk product after 3mins f) Bulk product after 100mins. Bottom) Pawley fit of bulk product using co-crystal parameters.

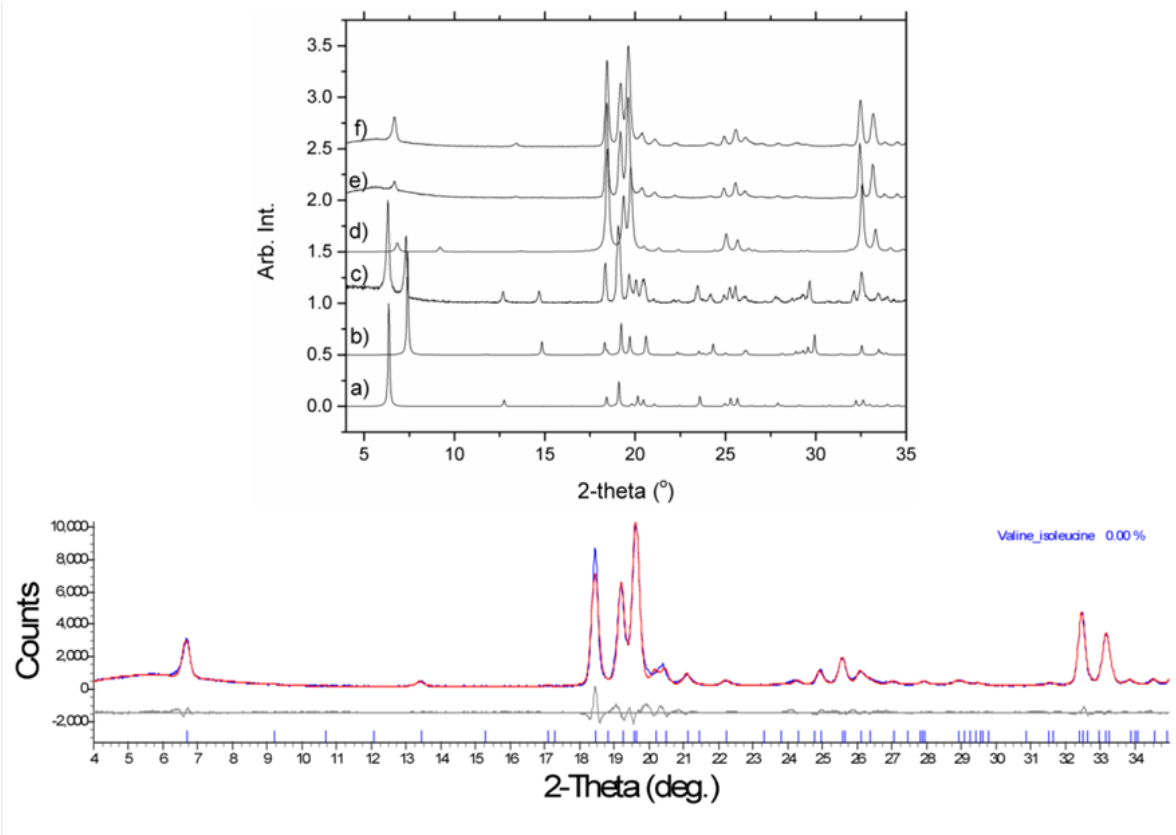

Figure 5.7 Top) A comparison of the diffraction data from bulk preparation with known forms. a) simulated patterns of isoleucine b) simulated patterns of valine c) mixture from slurry experiment d) simulated patterns of co-crystal from SXD data with preferred orientation (100) direction e) Bulk product after 3 mins f) Bulk product after 100 mins. Bottom) Pawley fit of bulk product using co-crystal parameters.

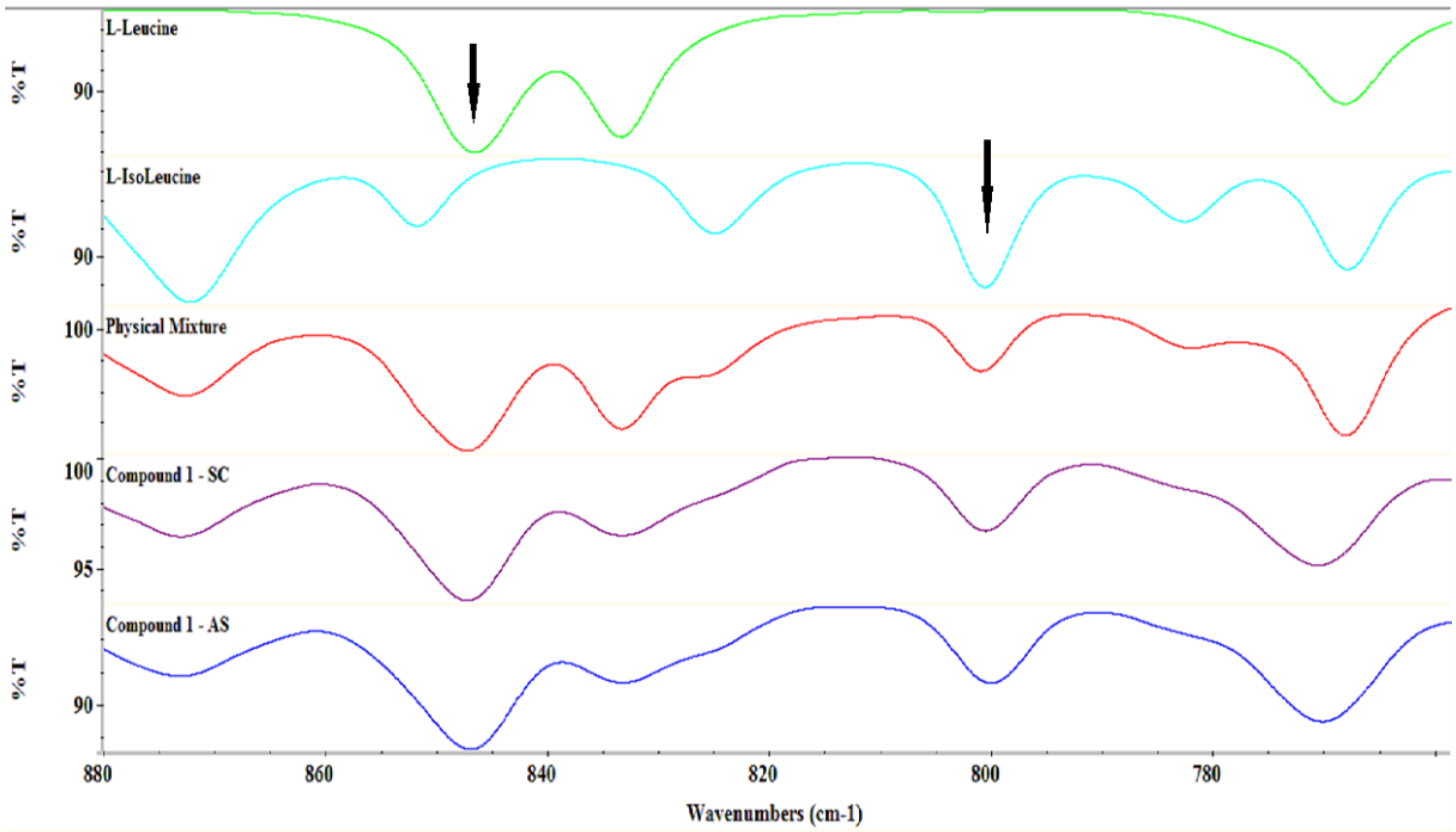

Figure 5.8 FTIR spectrum of prominent peaks of pure L-Leucine, L-Isoleucine, well mixed 50:50 physical mixture of both components, L-Leucine-L-Isoleucine single crystal and bulk powder of compound 1 used for the analysis of peak height and peak area ratios.

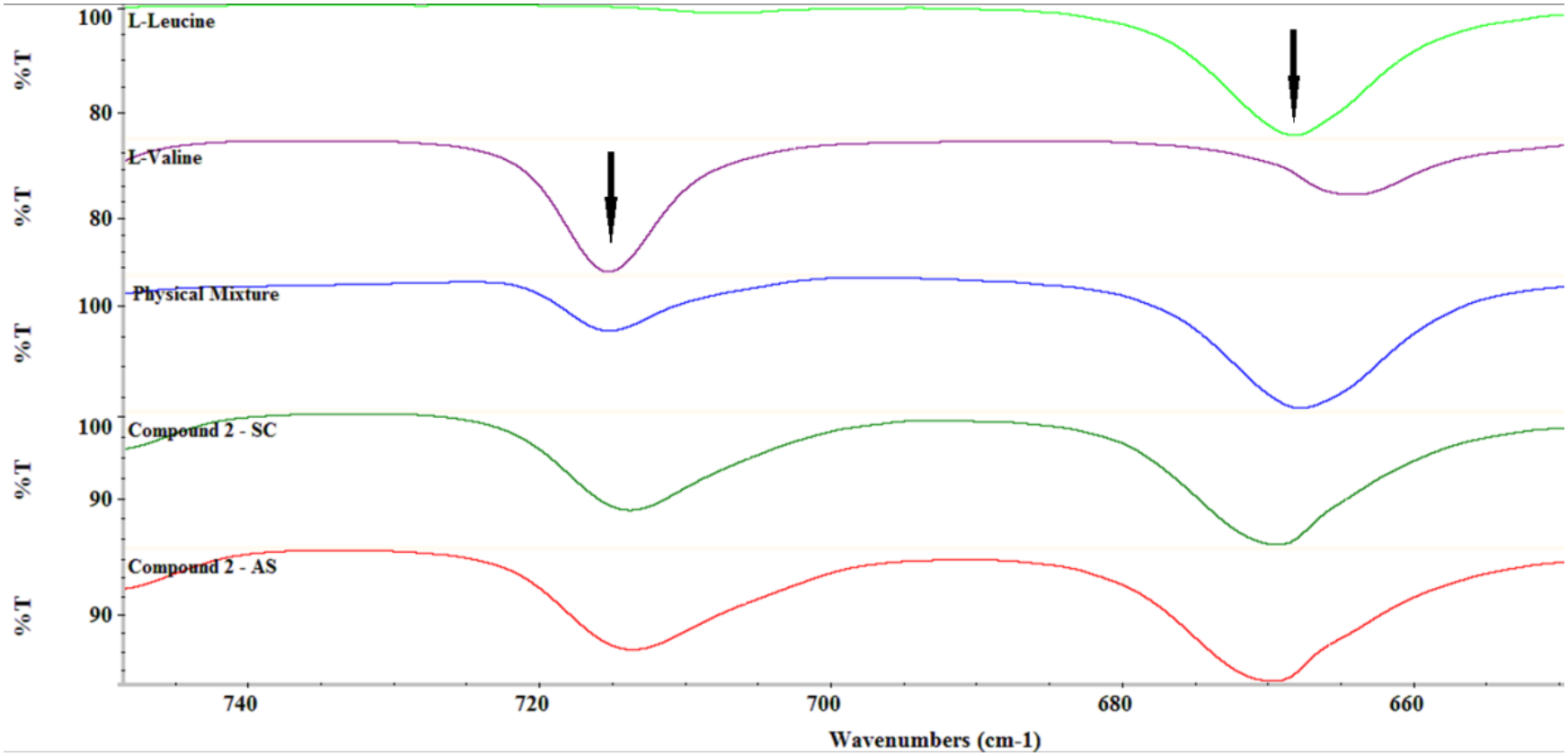

Figure 5.9 FTIR spectrum of prominent peaks of pure L-Leucine, L-Valine , well mixed 50:50 physical mixture of both components, L-Valine –L-Leucine single crystal and bulk powder of compound 2 used for the analysis of Peak height and peak area ratios.

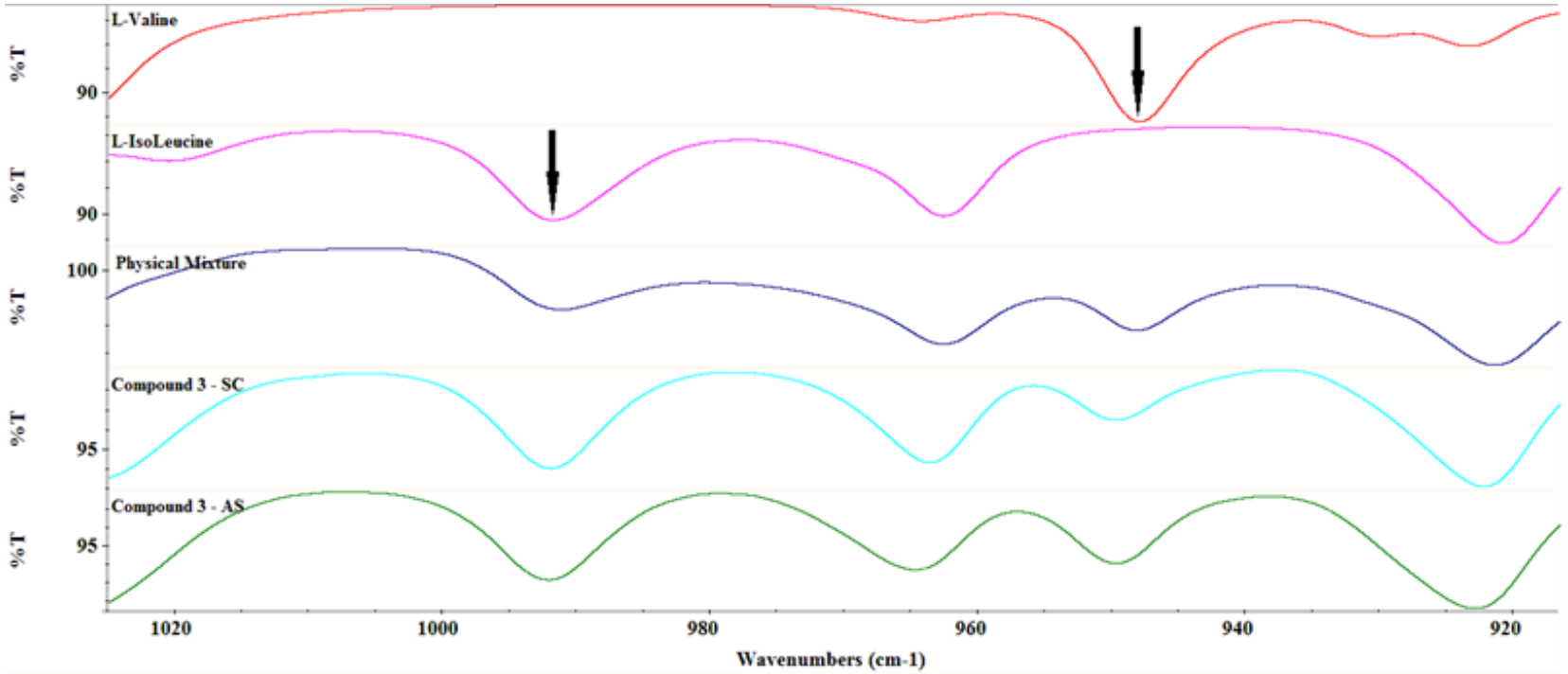

Figure 5.10 FTIR spectrum of prominent peaks of pure L-Valine, L-Isoleucine, well mixed 50:50 physical mixture of both components, L-Valine-l-Isoleucine single crystal and bulk powder of compound 3 used for the analysis of peak height and peak area ratios.

Table 5.4 Peak height (PH) and peak area (PA) ratios.

Compound 1 (LIL)						
	Peak Height	Peak Area	Peak Height	Peak Area	Peak Height	Peak Area
	833 cm^{-1}		847 cm^{-1}		Ratio	
Physical Mixture	4.78	25.28	7.94	72.15	1.66	2.85
Anti-Solvent	1.53	8.60	7.59	73.75	4.96	8.57
Single Crystal	1.07	6.34	4.58	42.45	4.28	6.69
Compound 2 (VL)						
	Peak Height	Peak Area	Peak Height	Peak Area	Peak Height	Peak Area
	669 cm^{-1}		715 cm^{-1}		Ratio	
Physical Mixture	21.44	316.23	8.35	78.23	2.56	4.04
Anti-Solvent	16.67	251.55	12.98	185.13	1.28	1.36
Single Crystal	15.20	227.91	11.57	157.07	1.31	1.45
Compound 3 (VIL)						
	Peak Height	Peak Area	Peak Height	Peak Area	Peak Height	Peak Area
	949 cm^{-1}		992 cm^{-1}		Ratio	
Physical Mixture	3.40	21.56	3.99	37.48	1.17	1.74
Anti-Solvent	3.18	23.28	4.80	48.47	1.50	2.07
Single Crystal	2.03	14.38	4.87	47.84	2.40	3.33

5.4.3. Differential scanning calorimetry (DSC)

The thermal behaviour of the co-crystals in contrast to the individual components was studied by analysing DSC thermal data presented in Table 5.5. DSC data of compound 1 (Figure 5.11), compound 2 (Figure 5.13) and compound 3 (Figure 5.15) shows endothermic peak at 296.65°C, 303.08°C and 288.71°C for compound 1, 2 and 3 respectively. The thermal profile of co-crystals was distinct and indicates the formation of novel multi-component phase. This single endothermic transition suggest the anhydrous form of the co-crystals which is evident from the thermal gravimetric analysis shown in Figure 5.12, 5.14and 5.16 for the compound 1, 2 and 3 respectively.

Table 5.5 Onset, end set and melting points of L-Valine, L-Leucine, L-Isoleucine and their corresponding complexes.

Compound	**Onset (°C)**	**Endset (°C)**	**Melting point (°C)**
L-Leucine	274.19	308.89	303.02
L-Isoleucine	253.86	295.00	286.76
L-Valine	250.91	301.98	294.86
LIL Comp. 1	251.36	302.10	296.65
VL Comp. 2	267.09	311.07	303.08
VIL Comp. 3	248.88	294.27	288.71

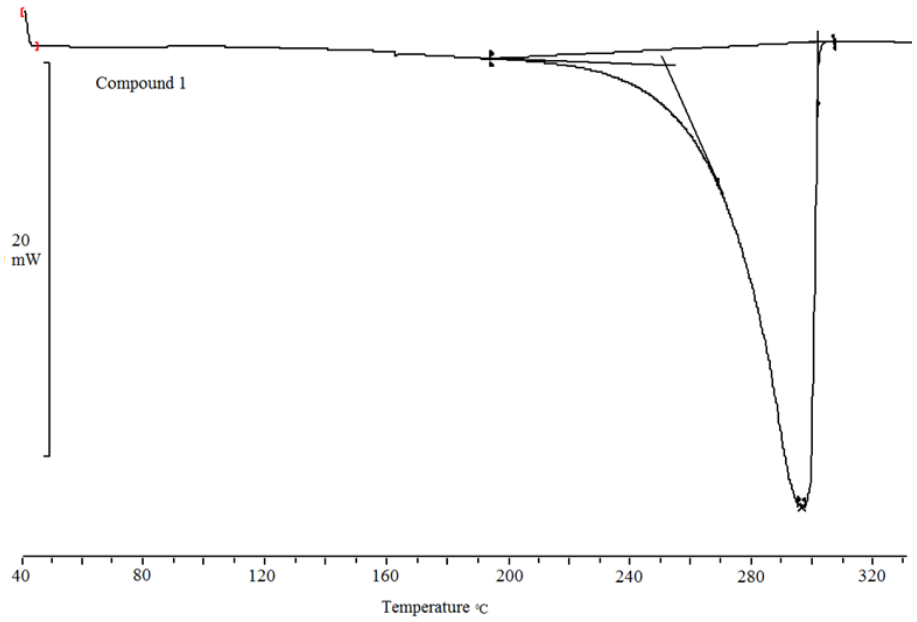

Figure 5.11 DSC heating curves for compound 1 (LIL co-crystals) prepared from Anti-solvent crystallisation.

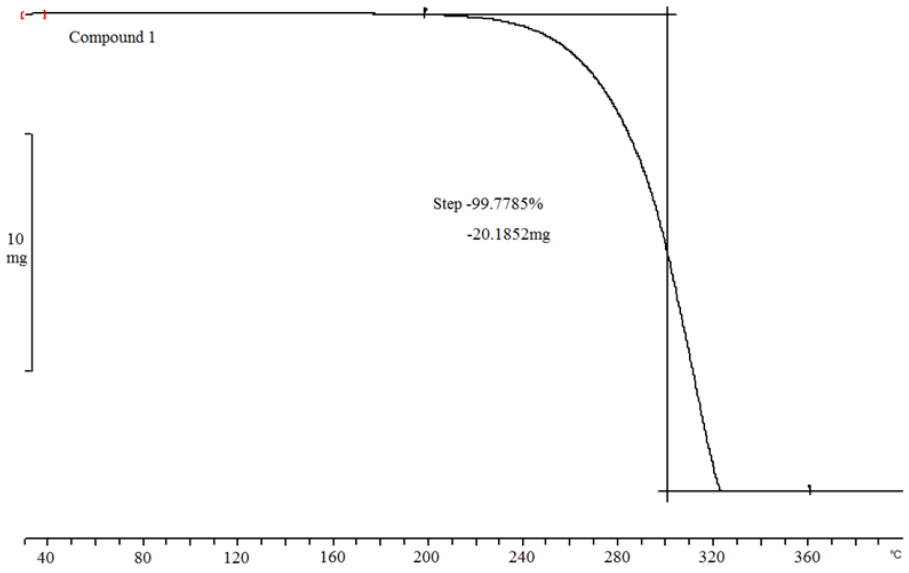

Figure 5.12 TGA trace for compound 1 (LIL cocrystals) prepared from Anti-solvent crystallisation

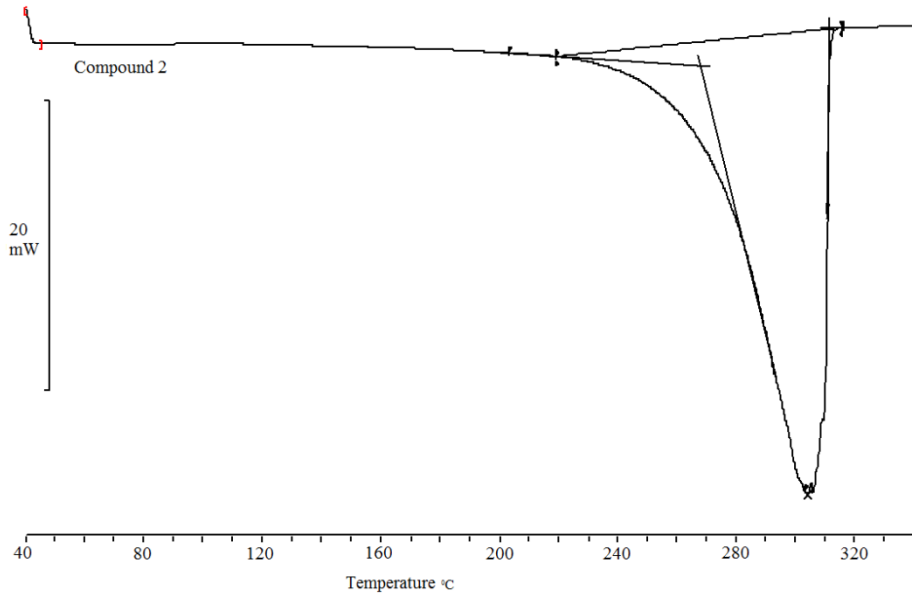

Figure 5.13 DSC heating curves for compound 2 (VL co-crystals) prepared from Anti-solvent crystallisation.

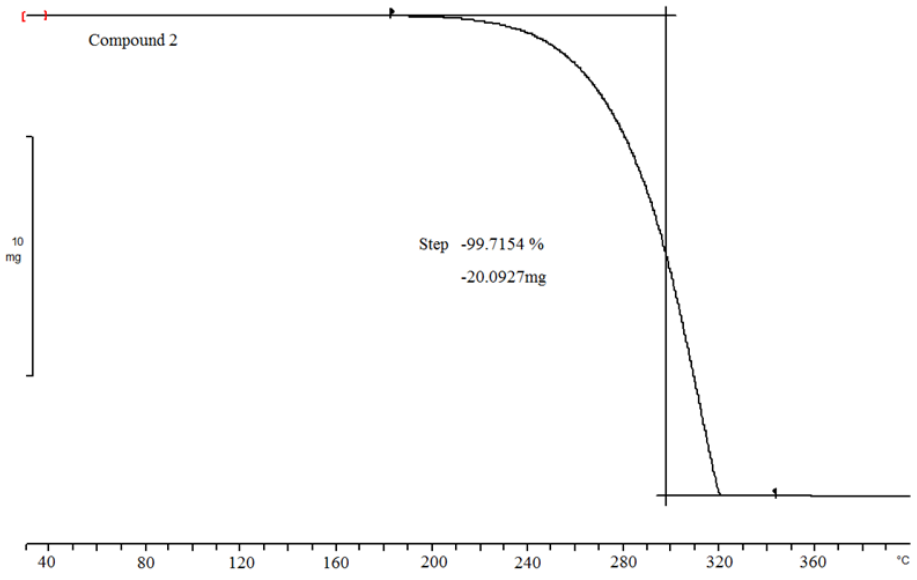

Figure 5.14 TGA trace for compound 2 (VL cocrystals) prepared from Anti-solvent crystallisation

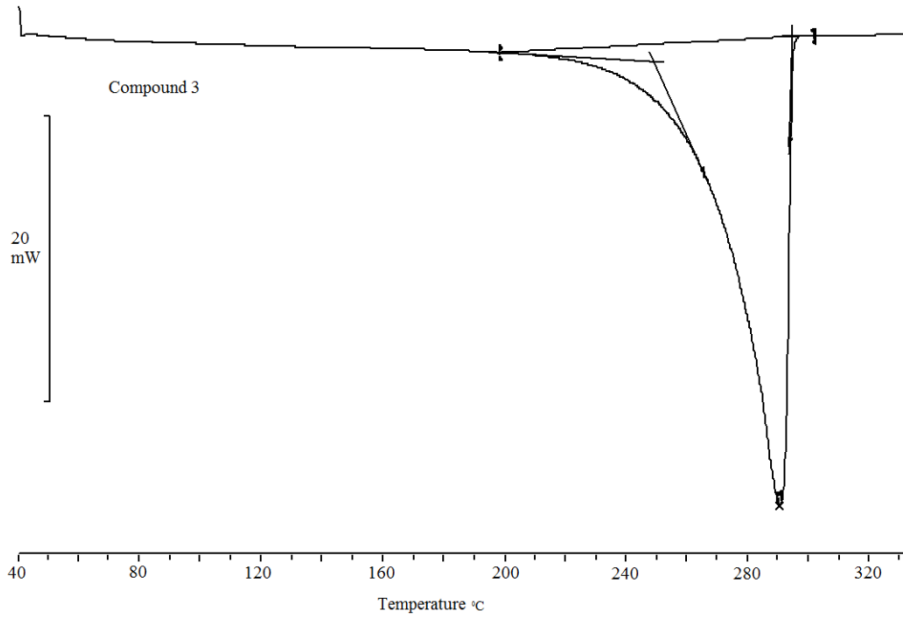

Figure 5.15 DSC heating curves for compound 3 (VIL co-crystals) prepared from Anti-solvent crystallisation.

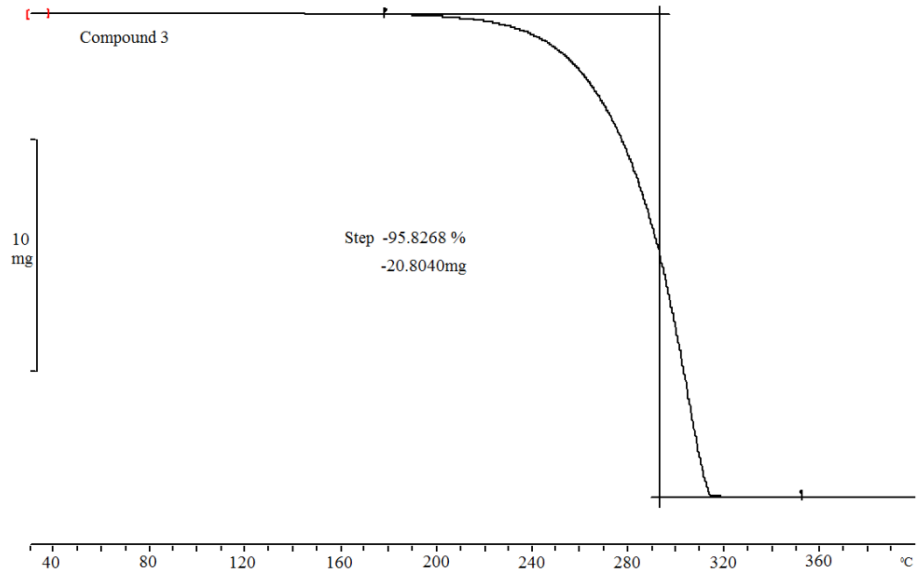

Figure 5.16 TGA trace for compound 3 (VIL cocrystals) prepared from Anti-solvent crystallisation

5.4.4. Scanning electron microscopy studies

SEM images of prepared co-crystals are presented in Figure 5.17, 5.18 and 5.19 for compound 1, 2 and 3 respectively. The images show that the product is of uniform particles and are having plate-like morphology.

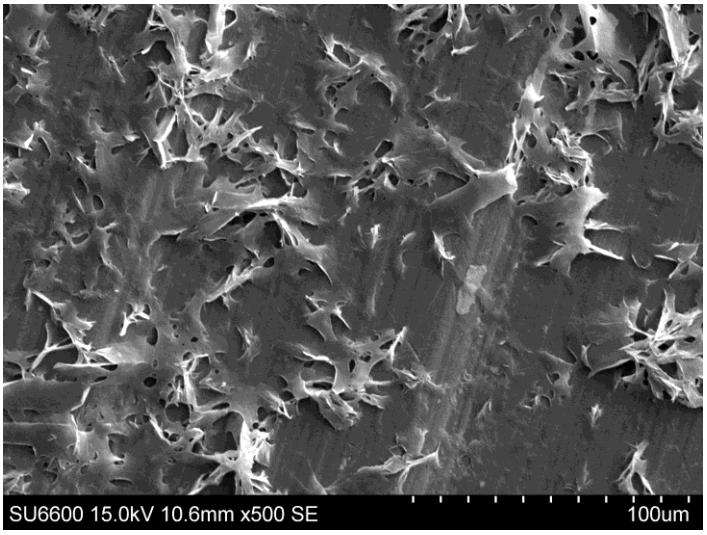

Figure 5.17 SEM image of compound 1.

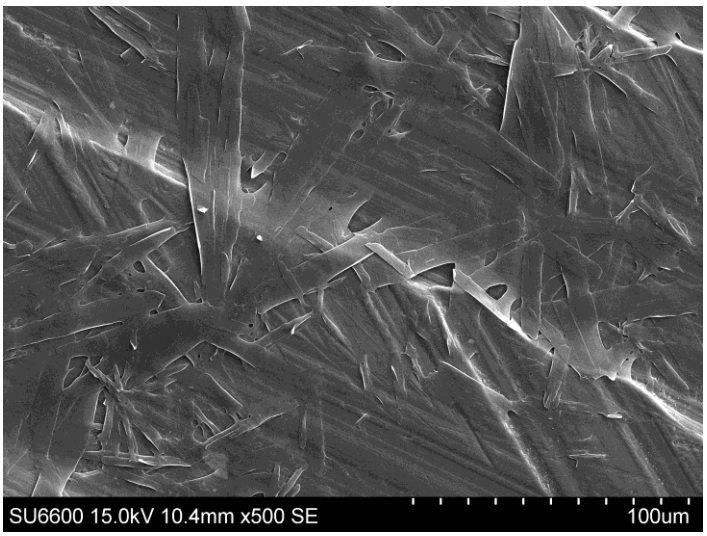

Figure 5.18 SEM image of compound 2.

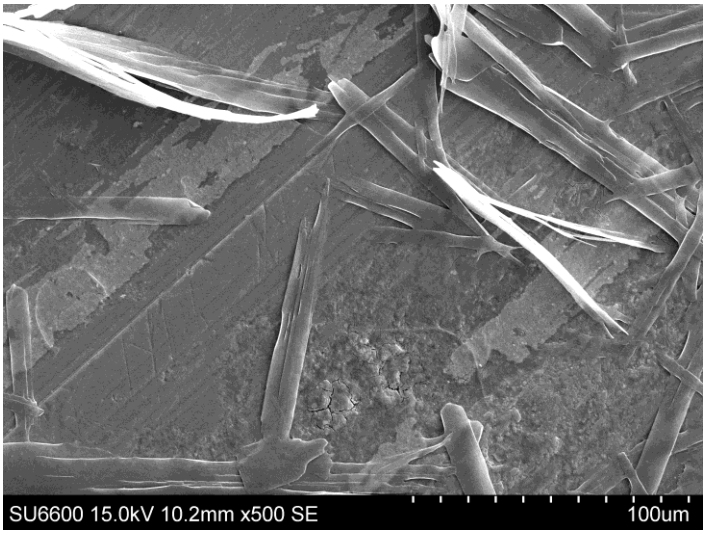

Figure 5.19 SEM image of compound 3.

5.4.5. Co-crystal yield

The percentage yield of compound 1, 2 and 3 can be seen in Table 5.6, 5.7 and 5.8, respectively. The yields for each of the co-crystal systems have reached a steady-state of 67.8% for compound 1, 50.3% for compound 2 and 67.3 for compound 3 after experimental running times of 30 minutes, 3 minutes and 10 minutes (Figure 5.20, 5.21 and 5.22), respectively. It is worth to mention here that in all the experimental runs the residence time was kept constant at 0.5 minutes. Whilst these yields are good these may be improved by varying the solvent:antisolvent ratio but for the purposes of this study these results were sufficient to obtain enough material for further identification and characterisation.

Table 5.6 Crystal yield of compound 1 at various experimental run time.

Time [min]	1	3	10	30	100
Practical Yield [%]	0.0	3.0	24.6	67.8	72.2

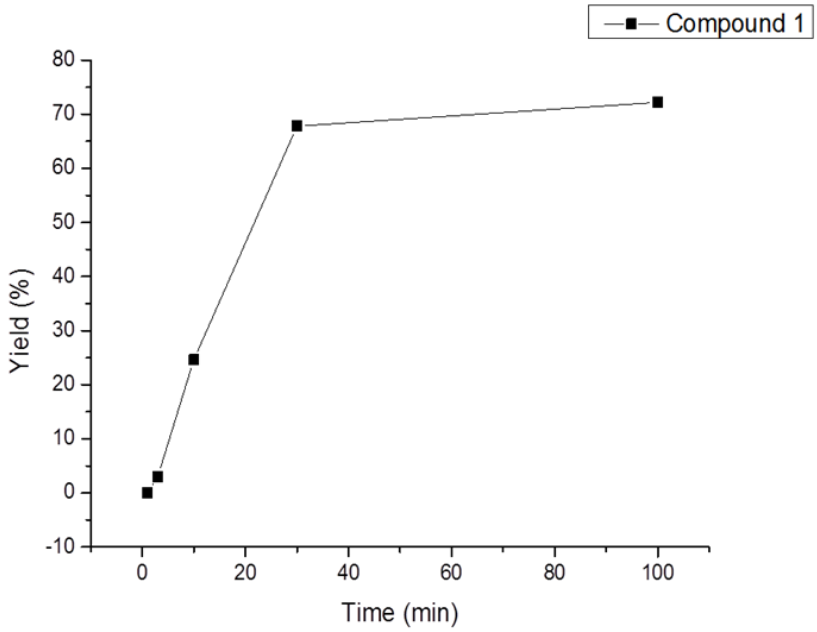

Figure 5.20 The crystal yield of compound 1 at pre-determined time interval. The graph showing steady state at 30 minutes.

Table 5.7 Crystal yield of compound 2 at various experimental run time.

Time [min]	1	3	10	30	100
Practical Yield [%]	4.0	50.3	50.6	53.8	54.9

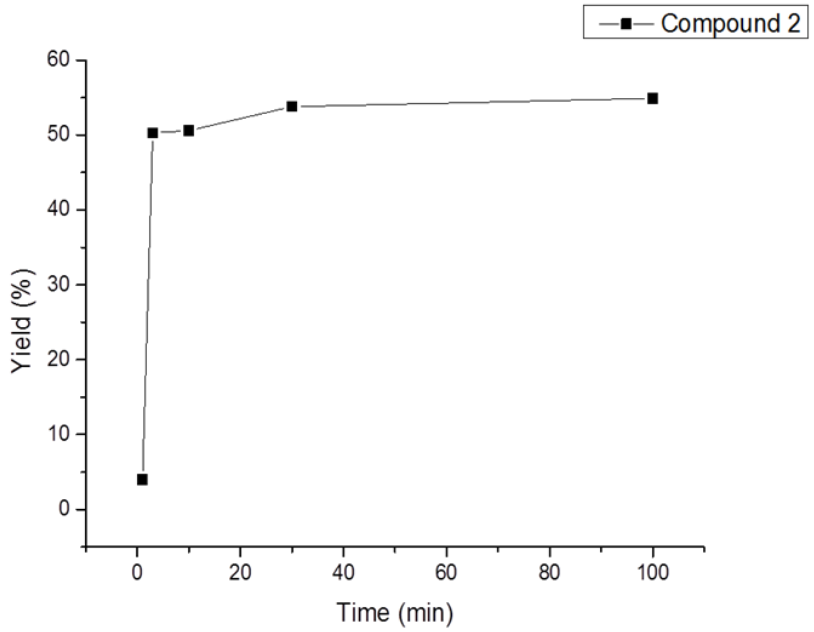

Figure 5.21 The crystal yield of compound 2 at pre-determined time interval. The graph showing steady state at 3 minutes.

Table 5.8 Crystal yield of compound 3 at various experimental run time.

Time [min]	1	3	10	30	100
Practical Yield [%]	3.4	26.3	67.3	67.7	70.8

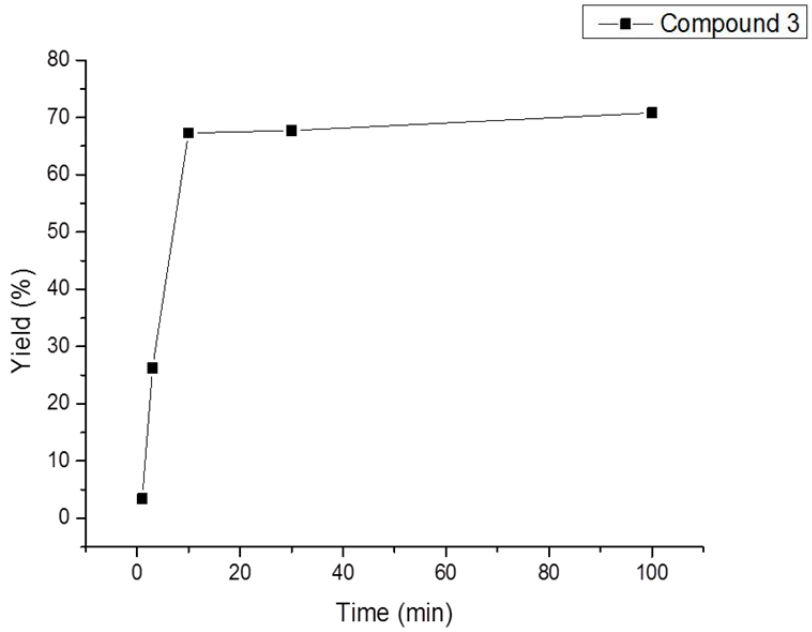

Figure 5.22 The crystal yield of compound 3 at pre-determined time interval. The graph showing steady state at 10 minutes.

5.4.6. Partical size distribution of amino acids complexes

The particle size for compound 1, 2 and 3 (Figure 5.23, 5.24 and 5.25 respectively) showed a slight bimodal distribution in which the proportion of smaller crystallites reduced over the course of the experiment. The highest proportions of each co-crystal were centred around 40, 25, 50 µm for compounds 1, 2 and 3, respectively.

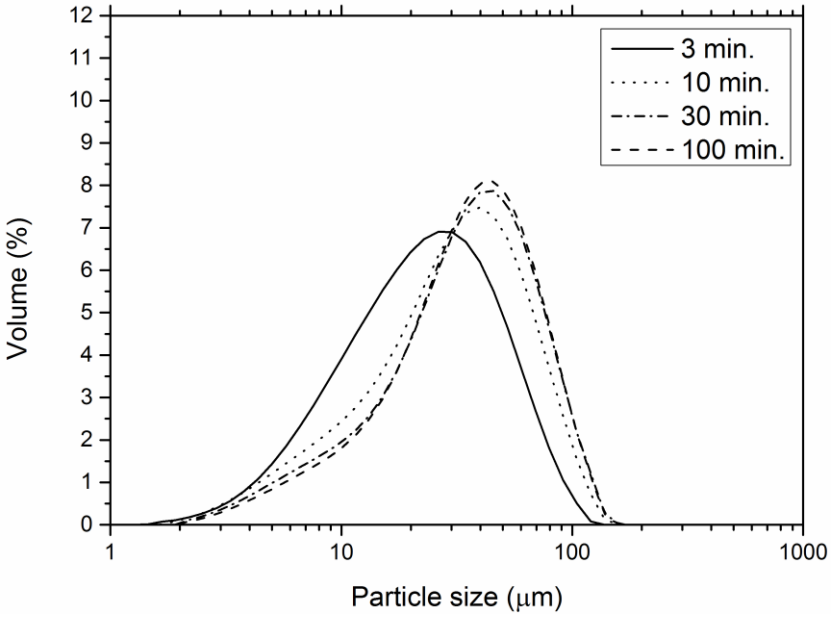

Figure 5.23 The particle size distribution of compound 1 of all the samples recovered after pre-determined time interval. The time represents the overall running time of the experiment.

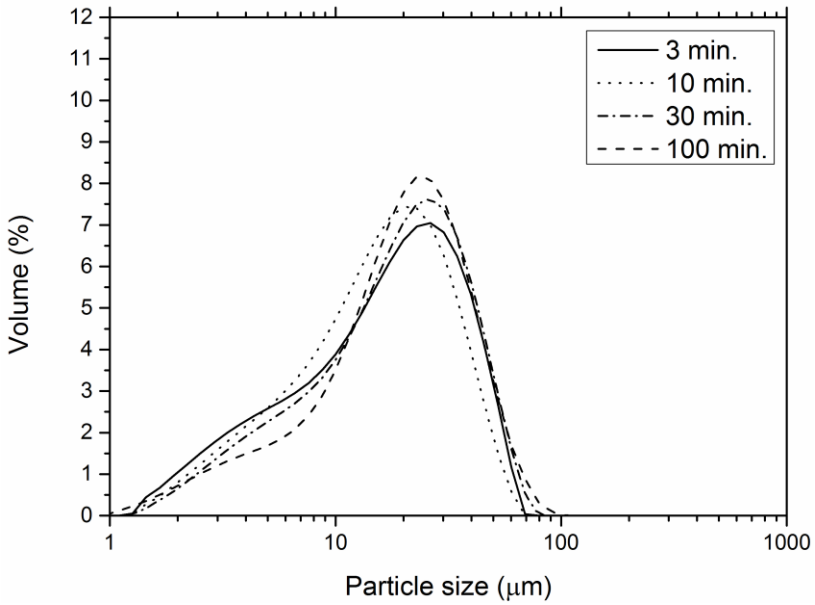

Figure 5.24 The particle size distribution of compound 2 of all the samples recovered after pre-determined time interval. The time represents the overall running time of the experiment.

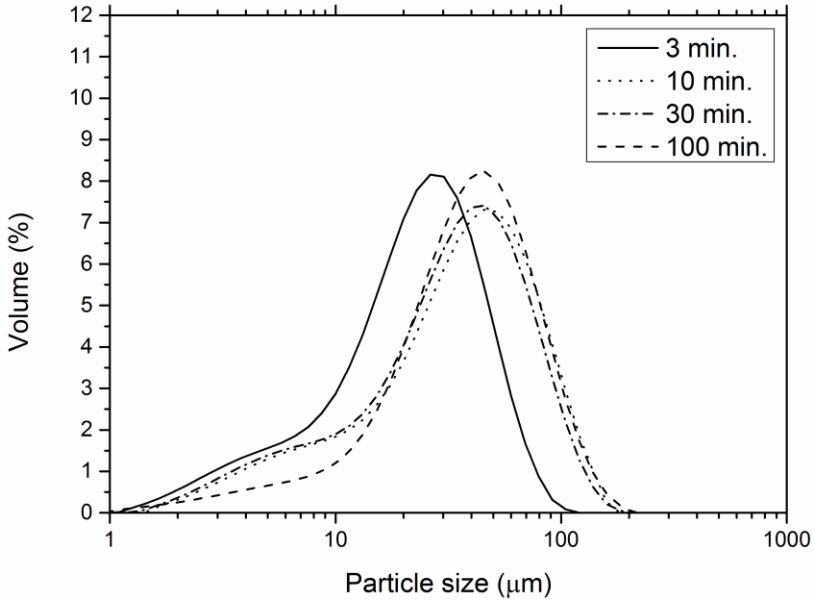

Figure 5.25 The particle size distribution of compound 3 of all the samples recovered after pre-determined time interval. The time represents the overall running time of the experiment.

5.4.7. Solubility studies of amino acids complexes

The solubilities of the co-crystals showed slight variations compared to the pure compounds in a 95:5 w/w water: isopropanol mixture. This solvent system was used as there were wettability issues with only water as the solvent.

Compounds 1 (Figure 5.26) and compound 3 (Figure 5.28) show similar solubilities to one of the parent compounds which is perhaps not surprising given that they possess a slightly higher portion of the more soluble compound in the lattice.

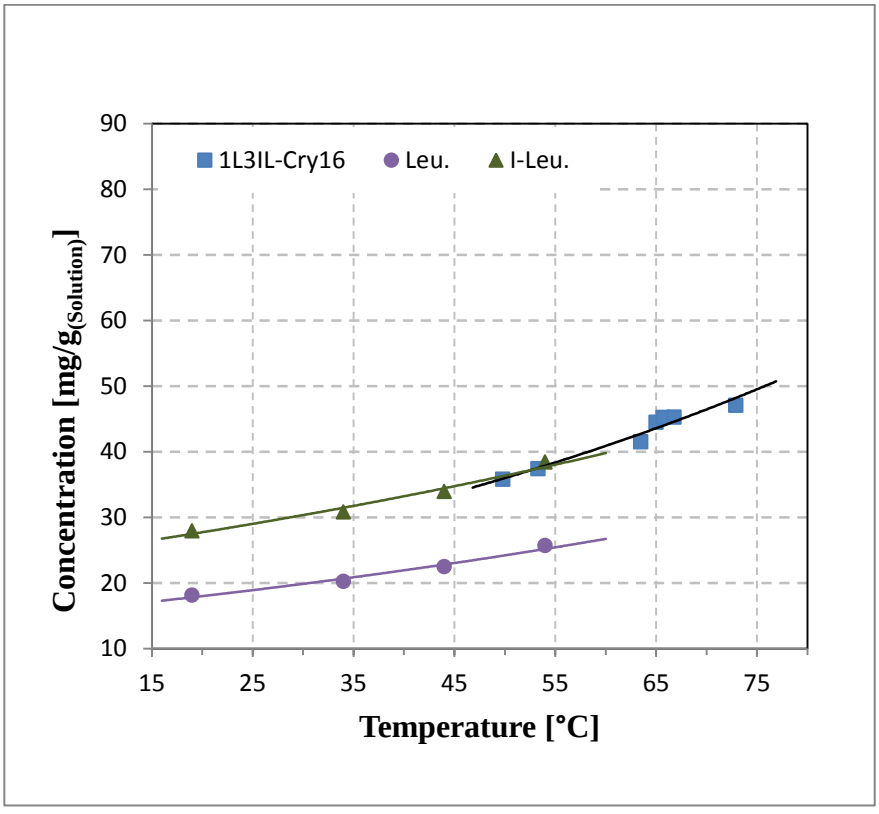

Figure 5.26 Solubility of Leucine, Isoleucine and compound 1 in a 95:5 w/w water: isopropanol mixture

The solubility of Compound 2 (Figure 5.27) is interesting in that it sits between the solubilities of the pure compounds. In this structure leucine is the main component and so it can be seen that by adding valine into the structure the solubility is greatly enhanced.

In all cases the solubility line for the co-crystals has a steeper gradient than the pure components and in the case of compounds 1 and 3 the solubilities exceed the pure components at higher temperatures (>55°C).

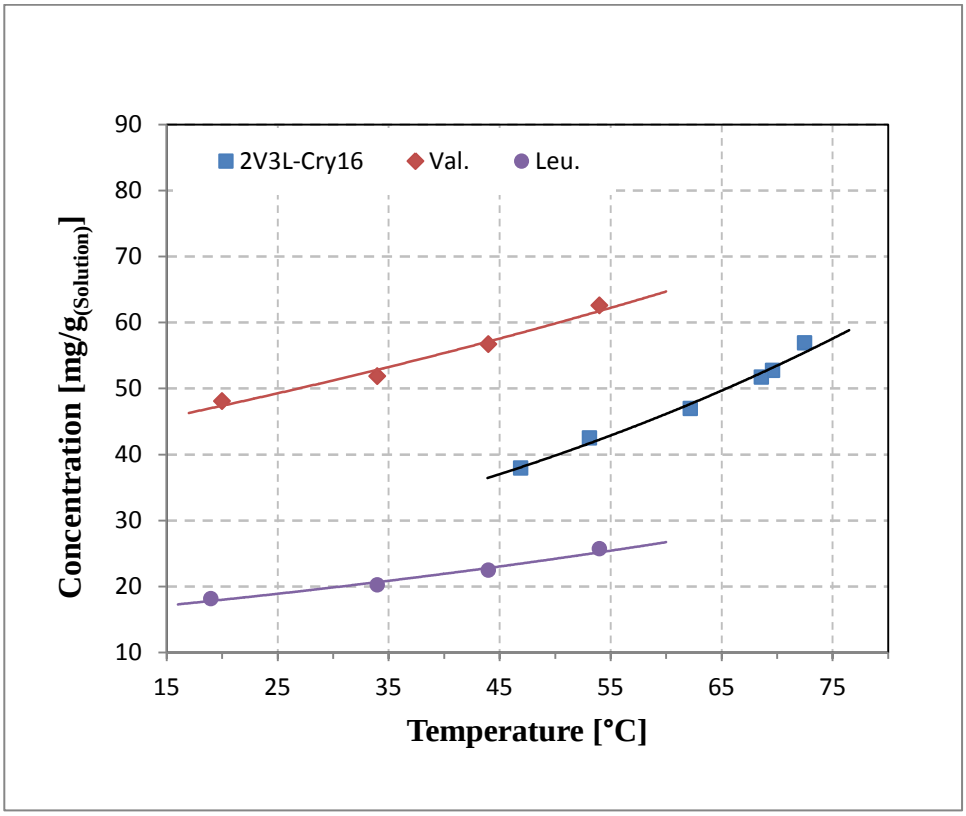

Figure 5.27 Solubility of Leucine, Valine and compound 2 in a 95:5 w/w water: isopropanol mixture

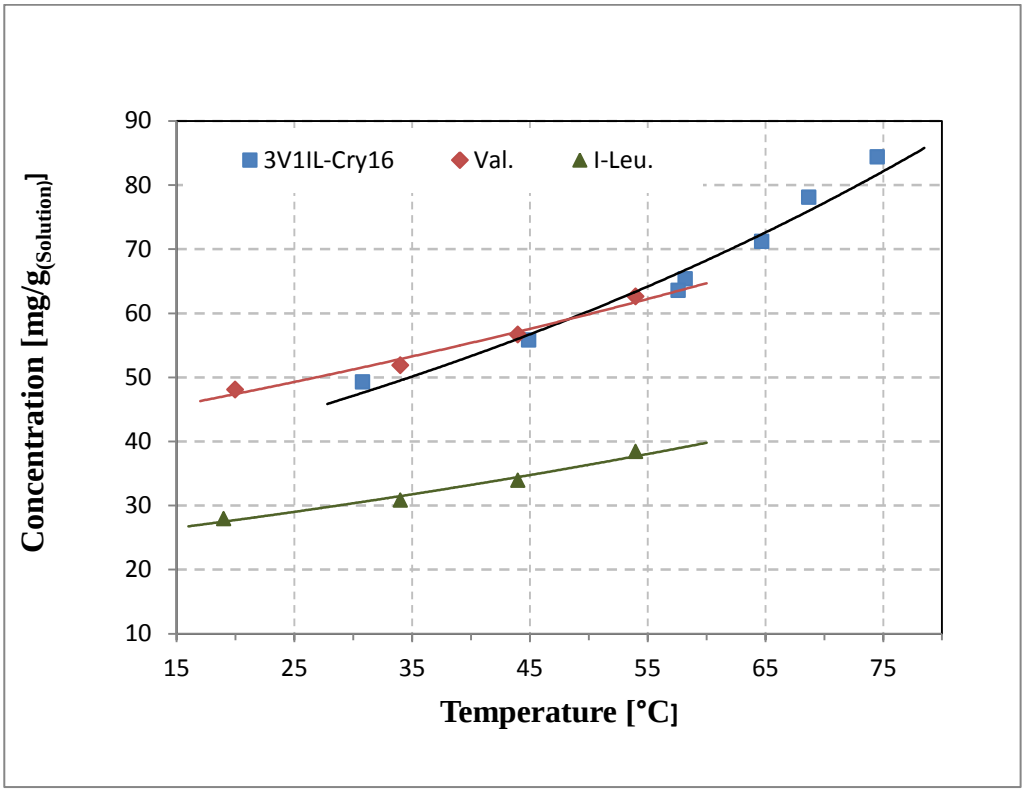

Figure 5.28 Solubility of Leucine, Valine and compound 3 in a 95:5 w/w water: isopropanol mixture

5.4.8. Powder flow measurements of amino acids complexes

During the manipulation of the co-crystalline material it was apparent that they were more resistant to "dusting" than the pure amino acids. In order to measure this phenomenon flowability and compressibility measurements were made on the materials. Table 5.9 indicates that the new compounds have a higher cohesiveness due to the poorer flowability (Hausner ratios >1.19) and higher compressibility (Carr's index >17%) than the parent compounds which results in less dusting as alluded to in the patent and in our own observations.

Table 5.9 The flowability and compressibility of the powders measured using the Carr's index (CI) and Hausner Ratio (HR).

Compound	Densities (ρ)		Density derivatives	
	ρBulk (g/mL)	ρBulk (g/mL)	CI (%)	HR
L-valine	0.4070	0.4669	12.83	1.15
L-leucine	0.5057	0.5739	11.87	1.13
L-isoleucine	0.5484	0.5934	7.58	1.08
Compound 1	0.1665	0.2219	24.95	1.33
Compound 2	0.1802	0.2181	17.38	1.21
Compound 3	0.1605	0.2078	22.76	1.29

5.5. Summary

The majority of the active pharmaceutical ingredients and excipients are generally prepared by solution crystallisation method in batch mode. In recent time continuous crystallisation is considered as a promising method or process to improve the bulk production of pharmaceutical materials. Co-crystals of amino acids L-Leucine, L-Isoleucine and L-Valine were successfully prepared by a rapid and continuous anti-solvent crystallisation method. The anti-solvent nucleation unit was designed in such a way that the warm solution of pre-mixed amino acids is injected into cold anti-solvent. Operating parameters were optimised for a better control of the continuous crystallisation and production of the co-crystals. The process design was having a reproducible control over phase purity, particle size and process yield. The co-crystals have

shown change in their physico-chemical properties like flowability, compressibility and solubility which may be exploited during product development, dosage form design and manufacturing.

5.6. References

Alvarez, A. J., & Myerson, A.S. (2010). Continuous Plug Flow Crystallization of Pharmaceutical Compounds. *Crystal Growth & Design.* 5, 2219−2228.

Beckmann W. (2013). Crystallization - Basic Concepts and Industrial Applications.Wiley-VCH: Weinheim.

Brydson, J. A. (1999). Plastics Materials. 7th edn, Butterworth-Heinemann.

Chen, J., Sarma, B., Evans, J. M. B., & Myerson, A.S. (2011). Pharmaceutical Crystallization. *Crystal Growth & Design.* 11, 887−895.

Choi Y.J., Chung S.T., Oh, M., & Kim, H.S. (2005). Investigation of Crystallization in a Jet Y-Mixer by a Hybrid Computational Fluid Dynamics and Process Simulation Approach. *Crystal Growth & Design. 5*(3), 959 – 968.

Dalvi, S.V., & Dave R.N. (2009). Controlling particle size of a poorly water-soluble drug using ultrasound and stabilizers in antisolvent precipitation. *Industrial & Engineering Chemistry Research*. 48 7581–7593.

Fuchs, F.J. (1995). Ultrasonic Cleaning: Fundamental Theory and Application. *NASA Conference Publication*.

Genck, W. J. (2003). Optimizing Crystallizer Scaleup. *CEP Mag*. 36–44.

Gron, H., Borissova, A., & Roberts, K.J. (2003). In-Process ATR-FTIR Spectroscopy for Closed-Loop Supersaturation Control of a Batch

Crystallizer Producing Monosodium Glutamate Crystals of Defined Size. *Industrial & Engineering Chemistry Research*. 42, 198–206.

Gron, H., Mougin, P., Thomas, A., White, G., & Wilkinson, D. (2003). Dynamic In-Process Examination of Particle Size and Crystallographic Form under Defined Conditions of Reactant Supersaturation as Associated with the Batch Crystallisation of Monosodium Glutamate from Aqueous Solution. *Industrial & Engineering Chemistry Research*. 42, 4888–4898.

Hanley, T.R., & Mischike, R.A. (1978). A Mixing Model for a Continuous Flow Stirred Tank Reactor. *Industrial & Engineering Chemistry Fundamentals*. 17, 51−58.

Jones, A.G. (2002). Crystallization Process Systems; Butterworth-Heinemann: Oxford, UK.

Kulkarni, S.A., McGarrity, E. S., Meekesc, H., & Horst, J.H. (2012). Isonicotinamide self-association: the link between solvent and polymorph nucleation. *Chemical Communications*. 48, 4983–4985.

Lawton, S., Steele, G., Shering, P., Zhao, L., Laird, I., & Ni, X-Wei. (2009). Continuous Crystallization of Pharmaceuticals Using a Continuous Oscillatory Baffled Crystallizer. *Organic Process Research & Development.* 13, 1357–1363.

Liotta, V., & Sabesan, V. (2004). Monitoring and Feedback Control of Supersaturation Using ATR-FTIR to Produce an Active Pharmaceutical

Ingredient of a Desired Crystal Size. *Organic Process Research & Development.*8, 488–494.

Liu, D.H.F., Liptak, B.G., & Bouis, P.A. (1997). Environmental Engineers' Handbook, 2nd ed.; Lewis Publishers, Inc.: Stamford, CA, U.S.A.

Mullin, J.W. (2002). Crystallization, 4th ed.; Butterworth-Heinemann: Oxford, UK.

Mullin, J. W. (1993). Crystallisation; Butterworth-Heinnemann: Woburn, MA.

Myerson, A.S. (2002). Handbook of Industrial Crystallization, 2nd ed.;Butterworth-Heinemann: Boston, MA.

Nagy, Z.K., & Braatz, R.D. (2004). Open-Loop and Closed-Loop Robust Optimal Control of Batch Processes Using Distributional and Worst-Case Analysis. *Journal of Process Control.* 14, 411–422.

Narducci, O., Jones A.G., & Kougoulos, E. (2011). Continuous crystallization of adipic acid with ultrasound. *Chemical Engineering Science.* 66, 1069-1076.

Nyvlt, J. (1992). Design of Crystallizers; CRC Press: Boca Raton, FL.

Nyvlt, J. (1977). Solid-liquid equilibria; Elsevier: Amsterdam, Holland.

Pellek, A., & Arnum, P.V. (2008). Continuous Processing: Moving with or against the Manufacturing Flow. *Pharmaceutical Technology. 9*(32), 52–58.

Plumb, K. (2005). Continuous processing in the Pharmaceutical Industry. Changing the Mind Set. Trans IChemE, Part A, *Chemical Engineering Research and Design*, *83*(A6): 730–738

Poechlauer, P., Manley, J., Broxterman, R., Gregertsen, B., & Ridemark, M. (2012). Continuous Processing in the Manufacture of Active Pharmaceutical Ingredients and Finished Dosage Forms: An Industry Perspective. *Organic Process Research & Development.*16, 1586−1590.

Quon, J. L., Zhang, H., Alvarez, A., Evans, J., Myerson, A. S., & Trout, B. L. (2012). Continuous Crystallization of Aliskiren Hemifumarate. *Crystal Growth & Design.* 6, 3036−3044.

Randolph, A.D., & Larson, M.A. (1988). Theory of Particulate Process: Analysis and Techniques of Continuous Crystallization, 2nd ed.; Academic Press: Toronto, Canada.

Rielly, C.D., & Marguis, A.J. (2001). A Particle's Eye View of Crystallizer Fluid Mechanics. *Chemical Engineering Science.* 56, 2475–2493.

Kulkarni, S.A., McGarrity, E. S., Meekesc, H., & Horst, J.H. (2012). Isonicotinamide self-association: the link between solvent and polymorph nucleation. *Chemical Communications*. 48, 4983–4985.

Sistla, A., Wu, Y., Khamphavong, P., & Liu, J. (2011). Medium-throughput hydrate screening using the Crystal 16™ *Pharmaceutical Development and Technology*. *16*(2), 102–109.

Staniforth, J.N. (2007). Powder flow. In:Aulton M.E. (Ed): Pharmaceutics. The design and manufacture of medicines, 3rd Ed. Churchill Livingstone, Edinburgh, UK, pp.168-179.

Swichtenberg, B. (2008). Moving Beyond the Batch. *Pharmaceutical Manufacturing. 7*(1), 24–26.

Tung, H.-H., Paul, E.L., Midler, M., & McCauley, J.A. (2009). Crystallisation of Organic Compounds. An Industrial PerspectiVe; Wiley: New York.

Ulrich, J., & Strege, C. (2002). Some aspects of the importance of metastable zone width and nucleation in industrial crystallisers. *Journal of Crystal Growth.* 237-239. 2130–2135.

Vervaet, C., & Remon, J.P. (2005). Continuous Granulation in the Pharmaceutical Industry. *Chemical Engineering Science. 60* (14), 3949–3957.

Wong, S.Y., Tatusko, A.P., Trout, B.L. & Myerson, A.S. (2012). Development of Continuous Crystallization Processes Using a Single-Stage Mixed-Suspension, Mixed-Product Removal Crystallizer with Recycle. *Crystal Growth & Design.* 12, 5701−5707.

Xie, L., Rielly, C.D., Eagles, W., Ozcan-Taskin, G. (2007). Dispersion of Nano-Particle Clusters Using Mixed Flow and High Shear Impellers in Stirred Tanks. *Chemical Engineering Research & Design 85* (A5), 676–684.

CHAPTER 6

Host–guest complexation of β-cyclodextrin with c(RGDfV)

6.1. Introduction.

The phenomenon of molecular complexation is one of the growing fields of importance in supramolecular chemistry in general. This area of research attracted scientists particularly from chemistry, biology and material sciences to develop and regulate the distinct supramolecular structures and investigate their properties and functionalities (*Aida et. al., 2012*). The supramolecular inclusion complex involves noncovalent intermolecular interactions mainly hydrogen bonding, $\pi - \pi$ stacking and hydrophobic interactions between the interacting materials and mostly represents a host-guest type of interaction. Many molecular complex forming agents such as cyclodextrins, curcubituril, calixarenes etc., have been studied for their wide range of applications (*Wang, et al., 2013*).

β-Cyclodextrin (β-CD) belongs to a series of cyclic oligosaccharides. The β-CD is prepared by enzymatic degradation of starch and composed of seven units of (α-1, 4)-linked α-D-glucopyranose (*Szejtli. 1998*).

The structural representation of β-CD look like a conical cylinder or truncated cone due to its $^4C_1$ chair conformation of the glucose unit (Figure 6.1). The secondary hydroxyl groups, the O(2)-H and O(3)-H)) are on the wider opening of the cone whereas, primary hydroxyl groups, O(6)-H are present on its opposite side. The core of the cavity is relatively hydrophobic where C-3 CH groups and C-5 CH groups are situated (*de Oliveira et al. 2011; Garcia et al., 2014*).

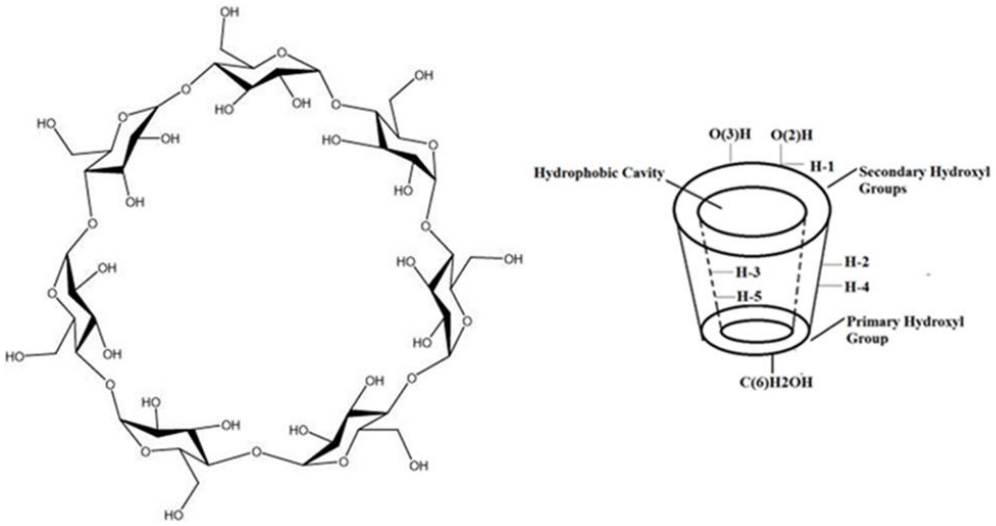

Figure 6.1 The chemical structure and shape of β-cyclodextrin.

β-CD is popular among the cyclodextrins as it is a safe molecule for human use (*Stella & He, 2008*). Chemical structure of β-CD is capable to host, partially or completely, hydrophobic molecules into its interior hydrophobic cavity to form an inclusion complex. This amasing character of the β-CD to entrap guest molecules may significantly alter or used to tune the physical, chemical and biochemical properties of the guest molecule (*Szejtli J. 2004; Yuan Z et al, 1999*). β-CD based molecular complexes have been exploited in many fields which include pharmaceuticals (*Loftsson and Brewster, 2010; Hu, et al., 2012*), biotechnology (*Singh, et al,2002*), food (*Szente, and Szejtli, 2004; Astray, et al, 2009; Liu, et al., 2013*) and cosmetics (*Buschmann and Schollmeyer, 2002; Al-Rawashdeh et al 2013*).

β-CD complexes present an important and considerable supramolecular system and is a very attractive strategy in improving the drug properties like systemic availability , enhancement in solubility, stability, masking odour, and controlled release of active pharmaceutical ingredients from the dosage form (*Tiwari et al., 2010; Zhou et al.,2012; Kurkov and Loftsson 2013*). Cyclodextrins are stable entities and are not affected in the gastric environment or in the small intestine making them suitable as a host molecule for those drugs which are hydrolysed or unstable in stomach or small intestine including peptides and proteins (*Yeguas, et al., 2011*).

Most pharmaceuticals form 1:1 complexes with cyclodextrin (Figure 6.2) however, the stoichiometry and stability of cyclodextrin based host-guest inclusion complexes are affected by the shape, volume, and polarity of guest molecules (*Rekharsky and Inoue, 1998*).

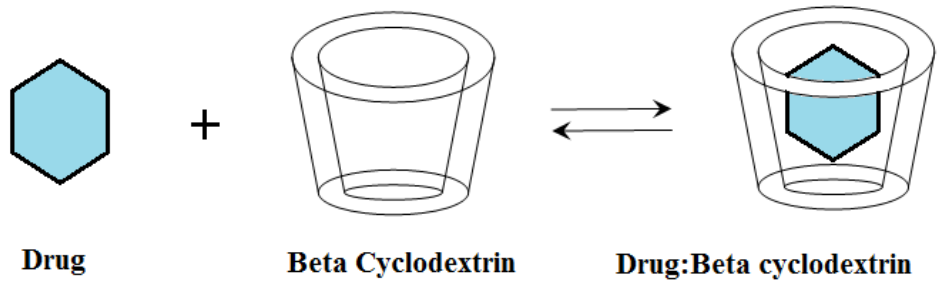

Figure 6.2 A schematic representation of 1:1 complex between a drug molecule and beta cyclodextrin at equilibrium.

The potential of peptides in drug development is gaining considerable importance in recent times because of the recognition that proteins can have high potency and specificity at the site of action which consequently leads to fewer side effects (*Craik et al., 2013*). Peptide-based pharmaceuticals have disadvantages such as poor biological stability, inadequate membrane permeability, instability, rapid plasma clearance, immunogenicity etc.,(*Irie and Uekama 1999*) and their high production cost. With all advantages and disadvantages, preparation and evaluation of the biologics in clinical trials are growing over the last few years (*Kaspar, & Reichert, 2013*) and therefore, additional strategies should be explored to enhance solubility, stability, protection from conformational changes, to improve uptake, permeability and targeting.

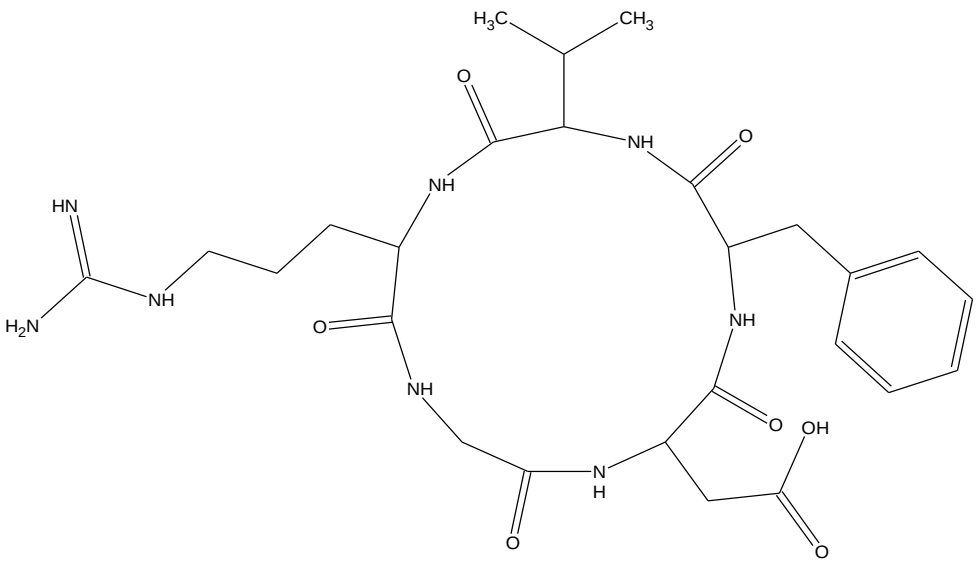

Figure 6.3 Chemical structure of a c(RGDfV).

The c(RGDfV), (Figure 6.3), has demonstrated the ability to inhibit the growth of glioblastoma and other tumors by blocking αvβ3 and αvβ5 integrin activation. The integrins αvβ3 and αvβ5 are over expressed on both glioma cells and tumor vasculature and Clingitide is the first integrin inhibitor in clinical Phase III development for oncology. (*Reardon et.al.,2008; Reardon et. al.,2011*).

Cyclodextrins have considerable applications related to peptide and protein delivery as their interaction may affect the aqueous solubility, permeability of the mucous membrane and stability of the biological macromolecules ragainst proteolysis. Interaction of peptides and cyclodextrin in several respects, such as receptor-ligand binding (*Bekos et al,1996*) and modification of response in the human body (*Lula, et al, 2011*) have been examined. It has been demonstrated that insulin forms a complex with beta-cyclodextrin which consequently influences the drug loading and absorption (*Jerry et al., 2001*) and in another study an enhancement of bioavailability was observed when insulin : sulphobutyl ether beta-cyclodextrin complex was given subcutaneously to rats (*Tokihoro et al., 2000*).

In this work, we report the study of the c(RGDfV) and its association with β-CD using a number of techniques to characterise the complex and obtain information regarding peptide and its interaction with β-CD to understand the setting of this supramolecular complex. The analytical techniques that have been used to investigate host-guest complex formation of β-CD and c(RGDfV) include differential scanning calorimetry, fourier transform infra-red

spectroscopy, circular dichroism and powder X-ray diffraction. Nuclear magnetic resonance spectroscopy (NMR) was used to determine their structures. ^{1}H-^{1}H COSY (Correlated Spectroscopy) experiments was used to correlate self-aggregation of a free peptide molecule and its complex with β-cyclodextrin. In addition, ^{1}H-^{1}H NEOSY (Nuclear overhauser effect Spectroscopy) experiments have been used to gain insight into interactions between cyclodextrin and guest molecules. The experiments were also carried out to grow crystals of the inclusion complex and crystals of c(RGDfV) to get a better understanding of their structures by single crystal X-ray diffraction technique. During crystallisation of c(RGDfV), it was observed that the penta peptide c(RGDfV) undergoes self-assembly to form a hydrogel which was evident by AFM images.

6.2. Experimental

6.2.1. Materials

Two batches (B-1 and B-2) of c(RGDfV), were obtained from China Peptide® Limited., China, and β-cyclodextrin was obtained from Sigma Aldrich, UK. Milli-Q® water (Lab Source) and DMSO-*d*6 from Sigma, were used in sample preparation. All reagents were used as received. The PXRD, DSC, TGA, FTIR and Raman spectrum of the solid materials were recorded for comparison with the inclusion complex of the pentapeptide with the β-cyclodextrin, prepared by freeze drying method.

6.2.2. Methods

6.2.2.1. Preparation of physical mixture of c(RGDfV) and β-CD

c(RGDfV) (B-1) (10.3mg) and β-CD (20.4 mg) were accurately weighed and mixed to prepare a physical mixture (molar ratio of 1:1). The components were gently triturated for few minutes to get a well-mixed product of the two ingredients.

6.2.2.2. Preparation of c(RGDfV) and β-CD inclusion complex

The solid-state c(RGDfV) (B-1): β-CD inclusion complex was prepared in a 1:1 molar ratio using the freeze-drying method. First β-CD (30.5mg) was dissolved in sufficient water in a vial then equimolar quantity (15.5mg) of peptide was dispersed and the solution was stirred at room temperature for 24 hours. After stirring, the resultant solution was filtered and frozen at −80°C. The freeze product was subjected to freeze-drying.

6.2.2.3. Stock solutions of c(RGDfV) and β-CD

10mM of β-CD and 10mM of c(RGDfV) (B-1 and B-2) stock solution were prepared in DMSO-*d*6 and used in nuclear magnetic resonance (NMR) experiments of each solution.

6.2.2.4. Stock solutions of c(RGDfV) batch B-2 and β-CD for complex formation

In order to study the complexation process between c(RGDfV) (B-2) and β-CD in solution, stock solution (10mM) of each reactant in DMSO-*d*6 was prepared.

Based on these equimolar solutions, a rack of 5 clean glass tubes was assembled and a series of five samples containing both the c(RGDfV) (B-2) and β-CD molecules were prepared. This was achieved by mixing the two solutions to constant volume at varying proportions to achieve a molar ratio of 1:3, 1:2, 1:1, 3:1and 2:1 for β-CD and c(RGDfV) (B-2).

6.2.2.5. Crystallisation of c(RGDfV) batch B-1

6.2.2.5.1. Crystallisation by evaporation

Crystallisation by slow evaporation is a most commonly used technique for growing crystals of small and macromolecules.

5 ml glass vials were used for the crystallisation experiments. Peptide solution was prepared by dissolving 1mg - 2mg of pentapeptide in 1ml - 3 ml of different organic solvent or co-solvent (Table 6.1). The glass vials containing the peptide solution were sealed with plastic lid. Few holes were made in the plastic lid by means of a sharp thin needle to allow very slow evaporation of the solvent. The conditions for slow evaporation were maintained at a constant room temperature and without any physical disturbance. The experimental vials were monitored on a regular basis to observe any change or crystal formation.

6.2.2.5.2 Crystallisation by vapour diffusion

Crystallisation by vapour diffusion method was carried out by dissolving 1mg of the peptide in 1 ml of purified water in a small vial. The vial was then placed inside a wide mouth jar that contains an appropriate volume of the solvent in

which the peptide is insoluble. The jar is then tightly capped and sealed and secured at a location where it was not disturbed. Solvent vapour from the outer jar diffuses into the inner vial containing the peptide solution, creating supersaturation conditions for peptide in the solution causing it to grow as crystals.

Table 6.1 Solvents used for the c(RGDfV) batch B-1crystallisation

Solvent / Co-solvent	c(RGDfV) (mg/ml)
Water	2 mg/ml
Methanol	0.5 mg/ml
Ethanol	0.5 mg/ml
Acetonitrile	0.5 mg/ml
DMF	1 mg/ml
DMSO	1 mg/ml
Water:Methanol (4:1),(1:1),(1:4)	1 mg/ml
Water:Ethanol (4:1),(1:1),(1:4)	1 mg/ml
Water:DMSO,(4:1)	1 mg/ml

6.2.2.5.3. Crystallisation by using Crystal Screen2

Biological macromolecules are complex molecules and are difficult and time consuming to crystallise by conventional method such as slow evaporation crystallisation. Very often macromolecule crystallisation experiments are not successful due to many challenges to optimise conditions required for nucleation and crystal growth. Crystal screen 2 is a reagent kit developed by Hampton Research (Figure 6.4) for determination of preliminary crystallisation conditions of macromolecules. The screen contains 48 formulated reagents using the salts, polymers, organics and buffers. The details of the reagents of Crystal Screen 2 can be found in Appendix 1.1.

Figure: 6.4 Crystallisation screen reagents with 24 well VDX plate

Hanging Drop Vapour Diffusion method is used in Crystal Screen 2 and is the commonly employed method of crystallisation of macromolecules.

The sample is prepared in purified water and a concentration of 5 to 25 mg/ml of sample is recommended. The chances of crystallisation are significantly

affected by the sample purity and free from any amorphous or unnecessary additives.

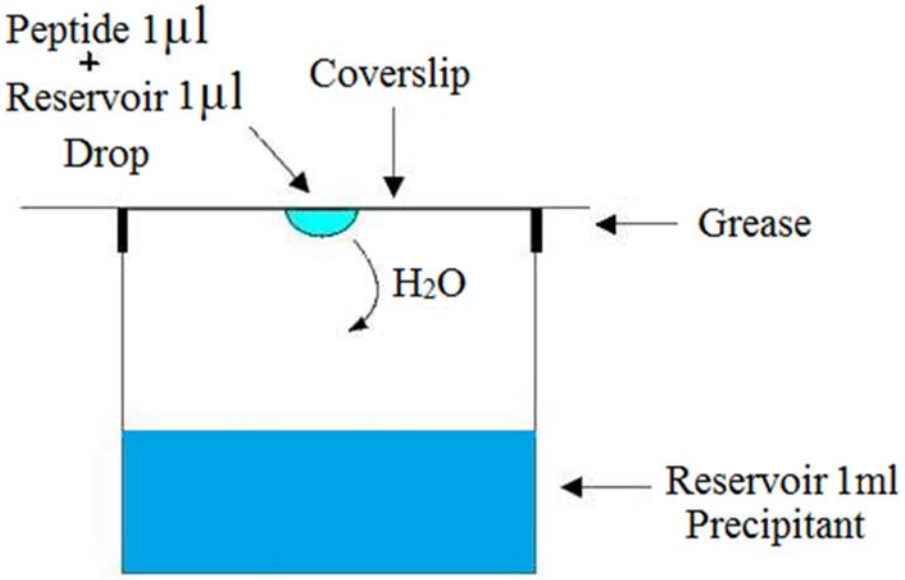

Figure 6.5 Cross section of a reservoir in the VDX plate.

Thin coats of cover slide sealant is applied to the upper edge of each of the (24 * 2) well plates and then with clean pipet tip add 1 ml of the Crystal Screen reagent 1 into well A1. Similarly, add reagent 2 in well A2 and repeat the procedure for all remaing reagents using a clean pipet tip for each reagent to prevent reagent contamination. Next is to pipet 1 µl - 2 µl of the peptide sample onto a siliconised cover slip which is followed by adding equal amount of the well solution into the sample droplet. The peptide and reservoir solution is then carefully mixed avoiding any air bubbles and foaming. The cover slip is quickly and gently inverted over the well and sealed without disturbing the drop of the mixture (Figure 6.5). Two sets of crystal screen are generally

prepared and incubate at different temperature, one set of plates at room temperature and the second set at 4°C. The crystallisation plates are then left undisturbed in a vibration free environment. Water in the drop will evaporate which result into an increase of peptide concentration which may lead to crystal formation of the peptide.

Once the screen is set up, it is important to record the observation by examining the drops under a stereo microscope for comparison purposes. It is worth to examine the drops each day for a couple of week and then once a week unless records indicate the practice of no use. Observations should indicate whether the drop is clear or any change significant to record, precipitate formation, and or crystals. Following sets of screens were prepared;

6.2.2.5.3.1 Screen 1

In each reservoir (well), 1 ml of the crystallisation reagent (Hampton research reagent solution) was placed. Then 2 µl of the peptide sample (2.5 mg/ml) was pipetted onto a clean siliconised cover slide which is then followed by adding 2 µl of the reservoir solution. The peptide and reservoir solution were carefully mixed avoiding any air bubbles. The cover slide is then very gently inverted without disturbing the drop of the mixture over the well and sealed. The screen was then left undisturbed at room temperature.

6.2.2.5.3.2 Screen 2

Similar procedure to screen 1 was adopted with the exception that the screen plate was placed at controlled temperature (4°C)

6.2.2.5.3.3 Screen 3

Similar procedure to screen 1 was adopted with the exception that the peptide concentration used was 5 mg/ml.

6.2.2.6. Crystallisation of β-CD: c(RGDfV) inclusion complex

6.2.2.6.1. Crystallisation by evaporation.

Approximately 5mg of stoichiometric (1:1) quantity of c(RGDfV) (B-1) and β-CD were weighed accurately into a glass vial and dissolved in ~5mL of deionised, distilled water with stirring until all solid had dissolved. The solution continued to be stirred at room temperature for 24 hours and the solution was filtered through standard-grade filter paper. The vial was then capped with perforated lid to allow slow evaporation.

6.2.2.6.2. Crystallisation by vapour diffusion.

Same procedure as used in crystallisation by evaporation method was employed with the exception that the vial without lid is placed in another jar containing anti-solvent. The jar was then placed in a location free from any disturbance.

6.2.2.7 c(RGDfV) hydrogel preparation in water

To explore whether the pentapeptide had different gel formation behaviour, a range of samples (2, 3, 5and 8 mg/ml) of the c(RGDfV) were prepared by dissolving the weighed quantities of c(RGDfV) in 1 ml of deionised water,

vortex mixing was carried out for 15 seconds and left to equilibrate for 24 hours at room temperature.

6.3. Instrumentation

6.3.1. Differential scanning calorimetry (DSC)

DSC plots were obtained using dynamic DSC (DSC 822e, Mettler Toledo, UK). Samples were prepared by carefully weighing between 2.31 and 6.03 mg of each sample into a 40 µl aluminium pan, which was then hermetically sealed with a pinhole in the lid. An empty pin-holed 40 µl aluminium pan was used as a reference. Both pans were subjected to a nitrogen atmosphere. The pans were then heated at a rate of 10 °C/min from 40 °C to 340 °C. The temperature and heat flow of the DSC instrument was calibrated with indium and zinc. The results were analysed using Mettler STAR software.

6.3.2. Fourier transform infrared spectroscopy (FTIR).

Fourier Transform Infrared (FT-IR) spectra were collected using Smart iTR Nicolet iS10 spectrophotometer (Thermo Scientific). The spectra were recorded in the range of 4000 to 400 cm^{-1} at an instrument spectral resolution of 4 cm^{-1} (20 scans per spectrum). The spectra were visualised and analysed with OMNIC^{TM} software (version 8.1) (Thermo Scientific). The spectra were compared with the pure compounds to confirm the co-crystal formation.

6.3.3. Powder X-ray diffraction (PXRD)

A small quantity (10 - 50 mg) of each sample were mounted on 28 well plate supported on a polyimide (Kapton, 7.5µm thickness) film. Data were collected

on a Bruker AXS D8-Advance transmission diffractometer equipped with θ/θ geometry, primary monochromated radiation (Cu Kα1, λ= 1.54056 Å), a Vantec 1-D position sensitive detector (PSD) and an automated multi-position *x-y* sample stage. Data were collected in the range 4-35° 2θ with a 0.015° 2θ step size and 1 s step-1 count time. The identification of the co-crystals formation was performed by comparing the powder diffraction patterns with those of the pure materials.

6.3.4. Circular dichroism (CD)

CD spectra of c(RGDfV) and its inclusion compound solutions were recorded using a JASCO spectrophotometer model J-720 at 298 K with a 0.1cm path length cell cuvette. Wavelengths were measured from 190 to 320nm with 0.5 nm step resolution, sweep speed of 100nm min^{-1} and bandwidth of 0.1nm. The spectra, an average of 6 scans, were processed with JASCO software. Solvent spectral subtraction was performed from the CD spectra using software. For comparison of CD spectra the output is converted to mean residue molar ellipticity (MRME).

6.3.5. NMR spectroscopy.

NMR experiments were recorded on a JEOL (JNM LA400) 400 MHz. ^{1}H NMR experiment was carried out for all compounds and was used as the primary means of structural identification. In the ^{1}H NMR, the chemical shifts and integration indicate the number of each type of protons present in the molecule, the multiplicity and extent of coupling constant gives an idea of the adjacent protons and their spatial proximity. The ^{1}H NMR and ^{1}H-^{1}H COSY

contour maps were used in determining complex formation. ^{1}H -^{13}C (one bond) (HSQC) and ^{1}H -^{13}C long range (2-3 bond) (HMBC) correlations were also recorded.

After Fourier transformation and baseline correction, the diffusion dimension was processed. NMR data were processed and analysed with the Bruker XWINNMR software package (version 3.5), Delta and Mnova NMR software, version 9.

6.3.6 Atomic force microscopy

The AFM images were collected by scanning the mica surface in air at ambient temperature by using a Multimode 8 scanning probe microscope (Digital Instruments, Santa Barbara, CA, USA). The AFM measurements were obtained using calibrated Scan Asyst-air probes. The images were obtained from freshly prepared samples.

6.4. Results and Discussion

6.4.1. Differential scanning calorimetry

DSC has been shown to be a very useful tool in the identification of solid-state interactions between host and guest molecules. The melting point of the guest molecules generally changed to a different temperature or may disappeared when it form an association with the host molecules (*Nicolescu et al., 2010*). Figure 6.6 explains the DSC thermogram of β-CD, pentapeptide, the physical mixtures and corresponding freeze dried inclusion complex.

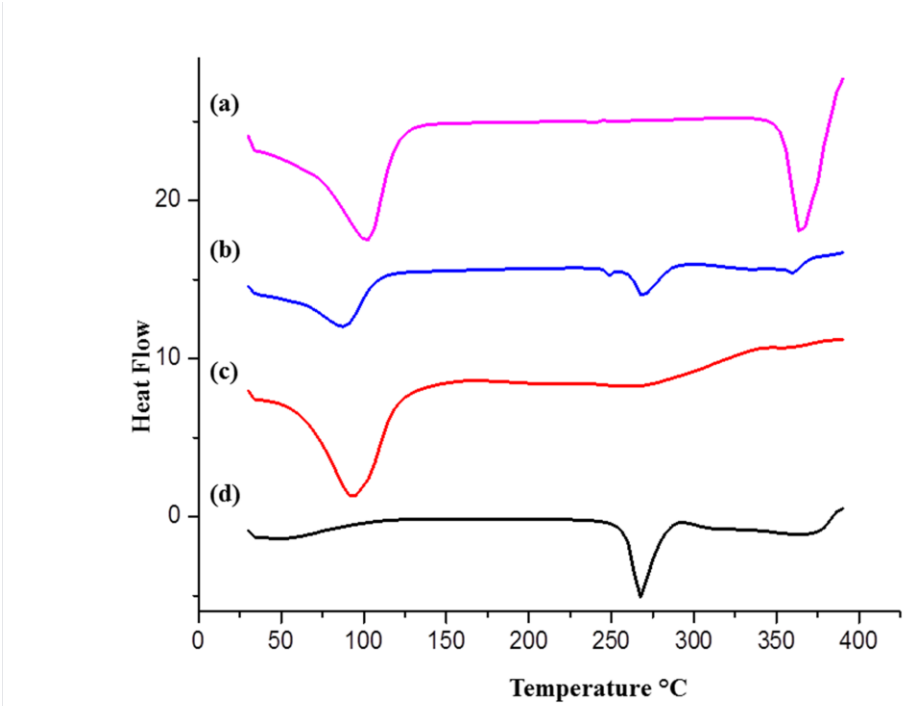

Figure 6.6 DSC plots of (a) betacyclodextrin, (b) physical mixture (1:1), (c) inclusion complex and (d) c(RGDfV)

The c(RGDfV) thermal curve was typical and was characterised by an endothermic peak assigned to its melting point. The DSC plot of β-CD showed two endothermic peaks. A wide and endothermic effect in the 100°C–130°C range which may be attributed to dehydration while the other observed in the 360°C–370°C range is related with the decomposition of β-CD. The thermogram of the physical mixture displayed the broad endothermic effects due to the β-CD dehydration process and the pentapeptide melting peak slightly shifted from its original position indicating interaction. The endotherm did not appear as a sharp peak which could be ascribed to the weak molecular interactions between the pentapeptide and β-CD. Similar behaviour was

observed in the albendazole-modified β-CD system (*Garcia et al., 2014)*. The thermogram of the inclusion complex showed a very broad endothermic event characteristic of c(RGDfV) with significantly reduced intensity than that of physical mixture, thus suggesting a complex formation.

6.4.2. Powder X-ray diffraction

X-ray powder diffraction patterns of β-CD, c(RGDfV) (B-1) and the corresponding complex of c(RGDfV) with β-CD are shown in Figure 6.7. β-CD showed many intense and sharp peaks explaining its crystalline solid state whereas the pattern of pentapeptide with no peaks reveals its amorphous nature. Physical mixture of the pentapeptide with β-CD showed characteristic peaks similar to the β-CD indicating that the crystallinity of β-CD did not change significantly during physical mixing of the two components. The reduced intensity or disappearance of some peaks of β-CD in the presence of the pentapeptide could be affixed to the dilution and trituration effect. The inclusion complex of pentapeptide with β-CD prepared by the freeze drying method presents few undefined, broad, dispersed peaks with low intensities. This pattern of the inclusion complex is observed in many previous studies (*Banchero, et al., 2013*).

The PXRD pattern of the inclusion complex indicates significant interaction of the pentapeptide with β-CD as few extra diffraction peaks at diffraction angle 2θ 14° and 17° for instance can be observed which are not related with the β-CD. These results support the formation of a new material via inclusion complex.

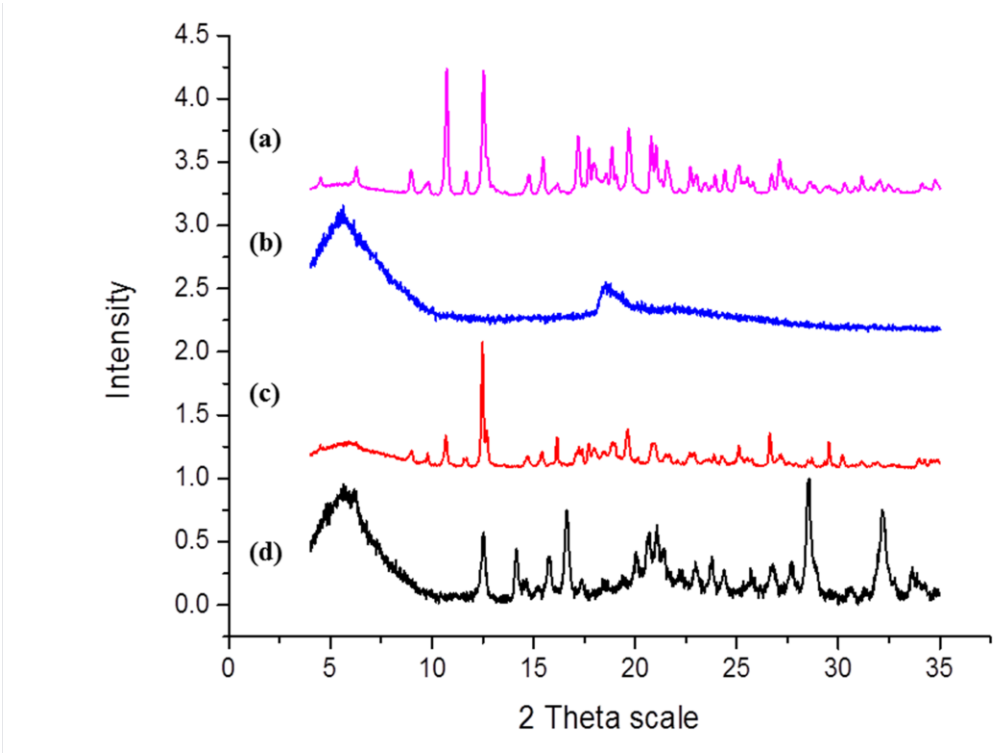

Figure 6.7 PXRD patterns of (a) β-CD (b) c(RGDfV) , (c) physical mixture and (d) inclusion complex via freeze drying.

6.4.3. Fourier tranform infrared studies

The FT-IR spectra of c(RGDfV) (B-1), β-CD, physical mixture and inclusion complex of c(RGDfV) and β-CD are presented in Figure 6.8. The spectra of both the inclusion complex and the physical mixture were largely dominated by the vibrational bands of the cyclodextrin molecule. There were some differences in the spectra of the inclusion complex from parent spectra, i.e., c(RGDfV) and β-CD and the corresponding physical mixture.

The IR spectra of β-CD (Figure 6.9) showed prominent absorption bands at 3331cm^{-1} for O-H stretching vibrations, 2925cm^{-1} C-H stretching vibrations,

1152cm^{-1} for C-C stretching vibration and 1020cm^{-1} for O-H bending vibration. The distinctive peaks found in pure pentapeptide (Figure 6.10) spectrum include the C=O stretching vibration located at 1634cm^{-1} whereas, the N-H stretching vibrations appeared at 3267cm^{-1} .

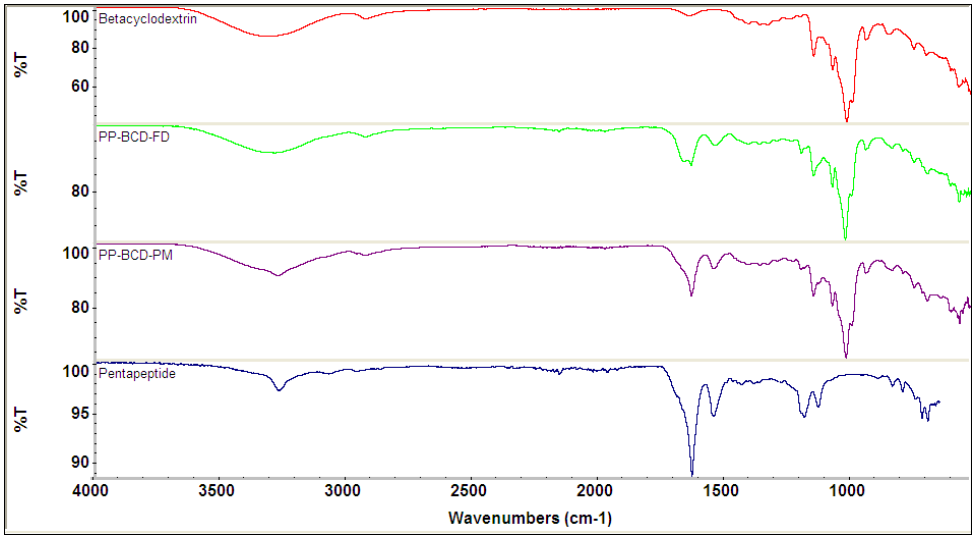

Figure 6.8 The FT-IR spectra of c(RGDfV) (B-1), β-CD, physical mixture and freeze dry inclusion complex of c(RGDfV) and β-CD.

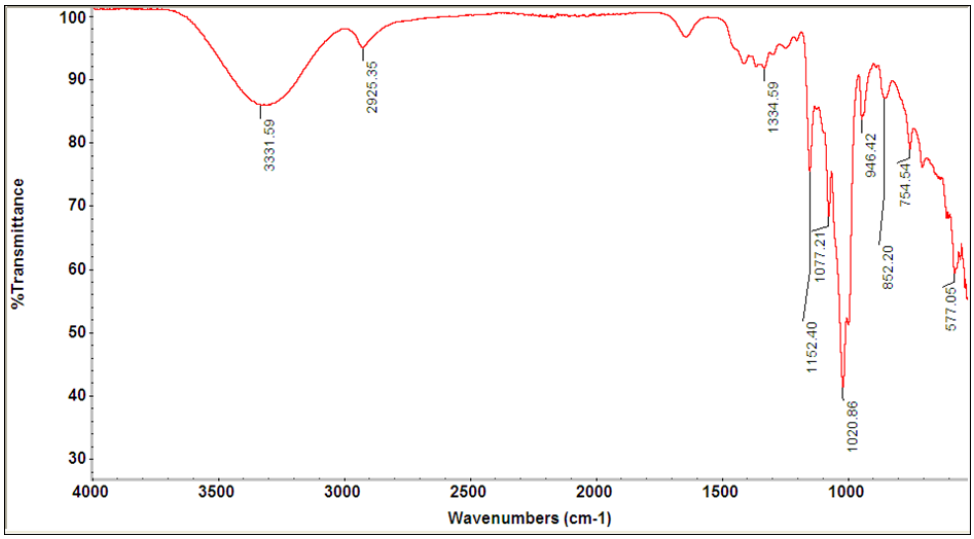

Figure 6.9 The FT-IR spectra of β-CD.

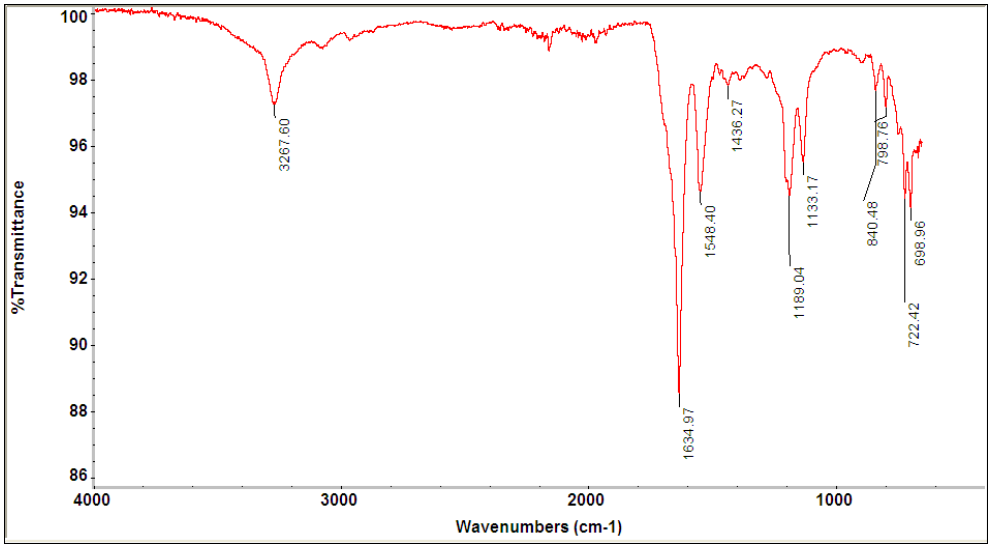

Figure 6.10 The FT-IR spectra of c(RGDfV) (B-1).

In the IR spectrum of c(RGDfV) and β-CD physical mixture (Figure 6.11), the peaks assigned to parent component can easily be identified indicating a mixture containing c(RGDfV) along with the complex forming agent. The slight shifting of peaks with reduction in relative intensities can be attributed to complementary mixing and dilution effects.

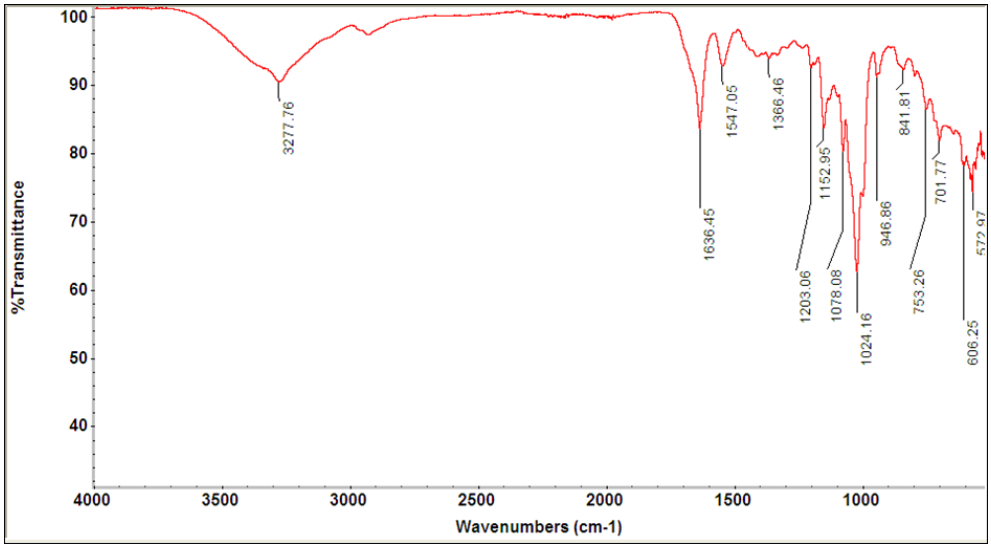

Figure 6.11 The FT-IR spectra of physical mixture of c(RGDfV) (B-1) & β-CD.

In the freeze dried sample of the prospective inclusion complex, the whole spectrum of c(RGDfV) is significantly affected indicating strong interaction with the betacyclodextrin (Figure 6.12).

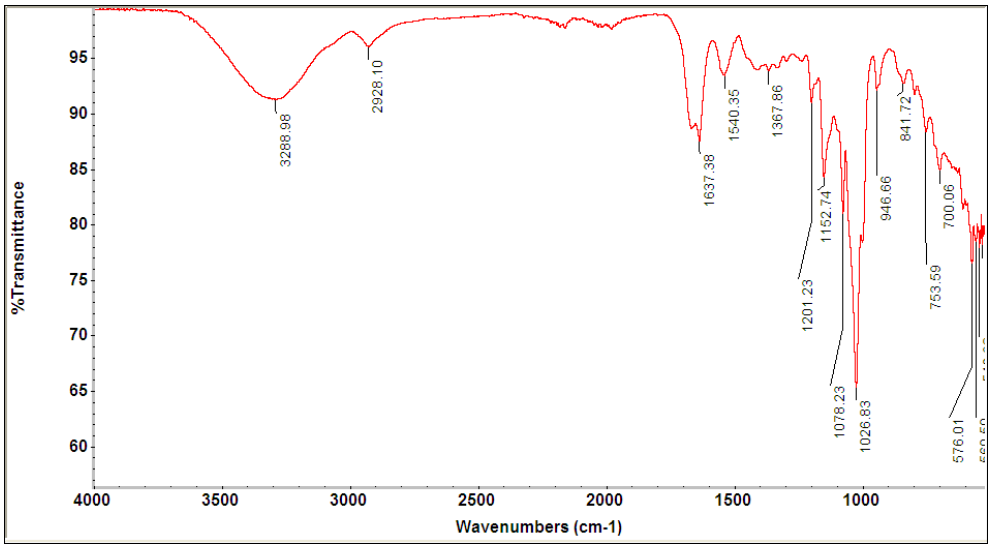

Figure 6.12 The FT-IR spectra of inclusion complex of c(RGDfV) (B-1) and β-CD

In c(RGDfV): β-CD freeze dry complex, the N−H stretching band, which in the free peptide is located around at 3290 cm^{-1}, is almost masked which might be due to strong interaction between c(RGDfV) and the hydroxyl groups of β-CD or swamped by the O–H stretch of β-CD . In the amide regions free c(RGDfV) shows two peaks located at 1634 cm^{-1} and 1548cm^{-1}, whereas, in peptide–β-CD, amide I and II bands undergo significant broadening, and the band located at 1634cm^{-1} in the free c(RGDfV) now shows two peaks one at 1668cm^{-1} and the other at 1637cm^{-1} indicating the change in C=O environment of the c(RGDfV) and supporting interaction with β-CD complex formation.

6.4.4. Circular dichroism spectroscopy

The CD spectra of c(RGDfV) recorded with and without β-cyclodextrin are shown in Figure 6.11. In aqueous solution, the spectrum of c(RGDfV) presented two negative bands at 208 and 215nm and under the same conditions, the spectrum of c(RGDfV) / β-CD in solution showed the same profile observed for the free c(RGDfV) in solution but with less negative ellipticities indicative of interaction between the two components (Figure 6.13). The difference in the intensity of c(RGDfV) in the presence of β-CD is mainly ascribed to the different orientation or inclusion of hydrophobic residue(s) of the peptide molecule in the β-CD cavity. Similar effect that is reduction in intensities was observed in the inclusion complex between vasoactive peptide angiotensin-(1–7) (Ang-(1–7)) with β-CD (*Lula, et al., 2007*).

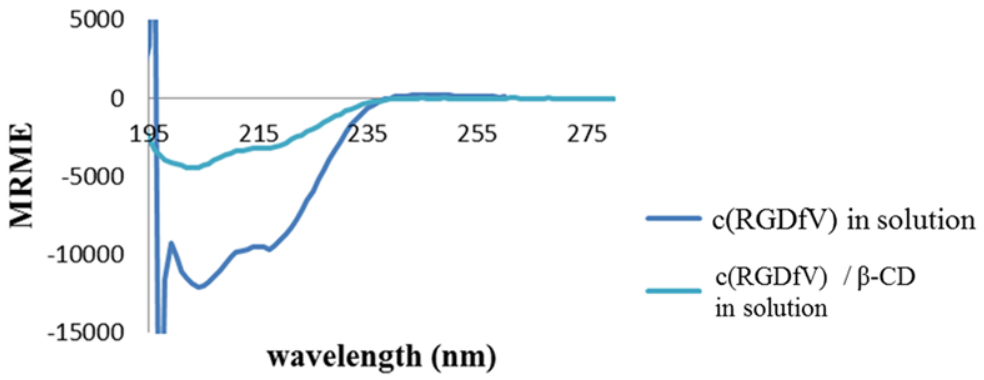

Figure 6.13 Circular dichroism spectra of c(RGDfV) and c(RGDfV): β-CD in aqueous solution.

6.4.5. NMR spectroscopy

β-CD cavity can host a hydrophobic molecule as a whole or the hydrophobic residue of a polar molecule by replacing the water molecules which are inside the cavity. The host - guest interaction may lead to the partial or complete entry of the guest molecule hence, altering the properties of the guest molecule. The complex formation can be observed through NMR experiment by measuring the chemical shifts of host (β-CD) and guest (c(RGDfV) protons both in complex state as well as in their native state. ^{1}H NMR spectra of pure components and β-CD: c(RGDfV) mixture in a 1:1 molar ratio is presented in Figure 6.14.

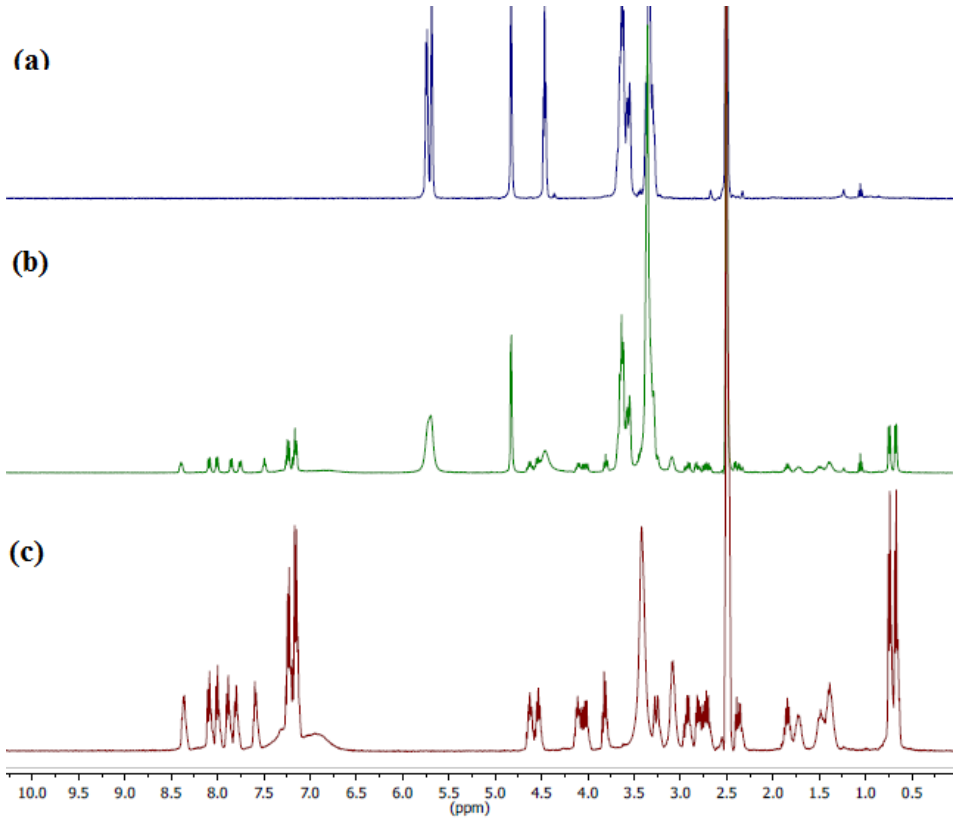

Figure 6.14 ^{1}H NMR spectra of a) β-CD b). c(RGDfV): β-CD inclusion complex and c), c(RGDfV) (B-1) in DMSO-d6 at 400 MHz.

The chemical shift changes of the protons H3 and H5 of β-CD which are present inside the cavity of β-CD are indicative that a guest molecule is encapsulated or not. The guest is partially included if Δδ H3 > Δδ H5 and when Δδ H3 ≤ Δδ H5, a complete inclusion inside the cavity takes place (*Greatbanks & Pickford, 1987*).

The NMR experiment shows that inclusion complex between c(RGDfV) and the β-CD is formed and can be observed by analysing the differences between the proton chemical shifts of c(RGDfV) and β-CD. The chemical shifts of the hydrogen atoms of β-CD and c(RGDfV) (B-1) compared with their complex are summarized in Table 6.2 and 6.3 respectively.

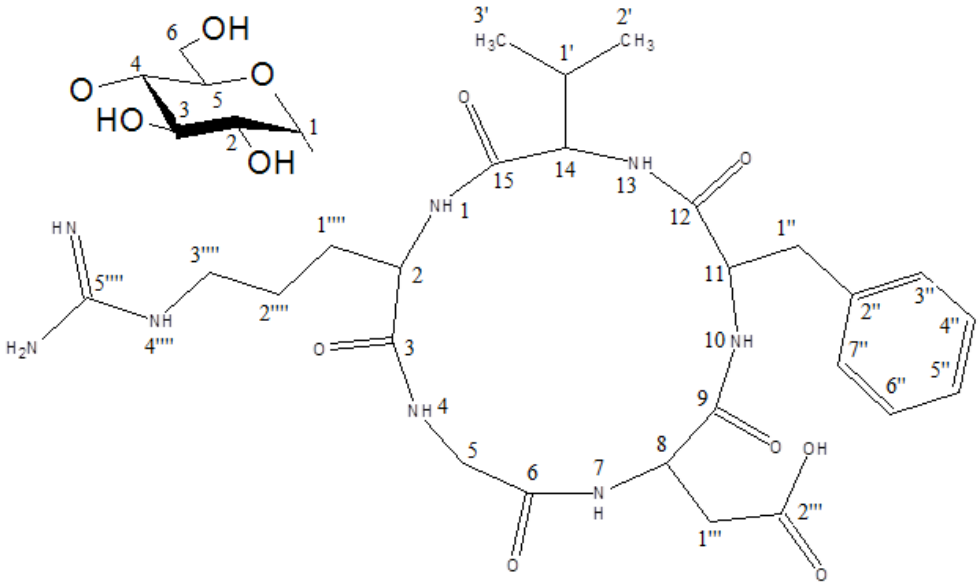

Figure 6.15 Molecular structures of c(RGDfV) and β-CD with numbering scheme.

Table 6.2 Chemical shifts (ppm) for the proton of β-CD in the free and complex states.

Position	β-CD δfree (ppm)	c(RGDfV): β-CD δcomplex (ppm)	Δδ(ppm)
	H	H	H
1	4.83 J = 4Hz	4.83 J = 4Hz	0.00
2	3.30 (m)	3.64 (m)	0.34
3	**3.63 (m)**	**3.56 (m)**	**-0.07**
4	3.28 (m)	3.31 (m)	0.03
5	**3.56(m)**	**3.35 (m)**	**-0.21**
6	3.63 (m)	3.64 (m)	0.01
2-OH	5.74 (d, J=8 Hz)	5.71 (br,s)	
3-OH	5.69 (d, J=4 Hz)	5.71 (br,s)	
6-OH	4.47 (d, J1=4 Hz) (J2=8 Hz)	------	

Table 6.3 Chemical shifts (ppm) for the proton of c(RGDfV) (B-1) in the free and complex states.

Position	c(RGDfV) δfree (ppm)		c(RGDfV): β-CD δcomplex (ppm)		Δδ(ppm)
	H	C	H	C	H
1	**7.80(NH)**	**---**	**7.76(NH)**	**---**	**-0.04**
2	4.11	52.7	4.11	52.6	---
3	---	171.8	---	171.7	---
4	**8.36(NH)**	**---**	**8.38 (NH)**	**---**	**0.02**
5	4.03	43.7	3.26, 4.05	43.6	0.02
6	---	170.1	---	170.0	---
7	**8.08(NH)**	**---**	**7.98 (NH)**	**---**	**-0.1**
8	4.63	49.4	4.65	49.4	0.02
9	---	170.5	---	170.4	---
10	**8.01(NH)**	**---**	**7.98 (NH)**	**---**	**-0.03**
11	4.53	54.6	4.56	54.5	0.03
12	---	171.3	---	171.2	---
13	**7.88(NH)**	**---**	**7.86 (NH)**	**---**	**-0.02**
14	3.82	60.8	3.82	60.7	---
15	---	171.7	---	171.6	---
1’	1.84	30.2	1.86	30.1	0.02
2’	0.67	18.8	0.69	18.7	0.02
3’	0.74	19.8	0.76	19.7	0.02

Table 6.3 continued…Chemical shifts (ppm) for the proton of c(RGDfV) (B-1) in the free and complex states.

Position	c(RGDfV) δfree (ppm)		c(RGDfV): β-CD δcomplex (ppm)		Δδ(ppm)
	H	C	H	C	H
1''	2.81,2.92	37.8	2.82, 2.93	37.7	0.01
2''	---	137.9	---	137.8	---
3''	7.15	129.7	7.16	129.6	0.01
4''	7.24	128.7	7.24	128.6	---
5''	7.25	126.8	7.17	126.7	-0.08
6''	7.24	128.7	7.24	128.6	---
7''	7.15	129.7	7.16	129.6	0.01
1'''	2.73	35.4	2.38, 2.74	35.3	0.01
2'''	---	172.3	---	172.1	---
1''''	1.48,1.72	28.9	1.50, 1.71	28.8	0.02, -0.01
2''''	1.39	26.0	1.43	25.9	0.04
3''''	3.08	40.8	3.10	40.7	0.02
4''''	**7.59(NH)**	---	**7.52 (NH)**	---	**-0.07**
5''''	---	157.2	---	157.1	---

It can be seen from Table 6.3 that the chemical shifts of most peaks are affected showing that significant change in the moleclar environment has taken place, but as the chemical shift differences in hydrophobic group that is

the phenyl and valine side chain of c(RGDfV) are also observed conforming the penetration of these in the β-CD cavity. The aromatic protons H-5" and H-3" and H-7" (Table 6.2) are shifted downfield about 0.08 ppm, 0.01 ppm and 0.01 ppm respectively whereas, both methyl proton signals of Valine, i.e. H-2' and H-3', (Table 6.3) are shifted upfield about 0.02ppm. The evidence of inclusion complex is supported by the chemical shift differences observed in proton H-3 and proton H-5 of the β-CD which are preseant in the hydrophobic cavity. The magnitude of chemical shift of proton H-5 (Δδ -0.21ppm) which is greater than the magnitude of proton H-3 (Δδ-0.07ppm) shown in Table 6.2 clearly indicates that inclusion complex is formed.

6.4.5.1. Structure of the Inclusion Complex

The NMR result indicates that c(RGDfV) and β-CD interact through hydrogen bonds, favouring the formation of a supramolecular structure. Based on chemical structure, (RGDfV) can penetrate the β-CD cavity in three orientations: 1) the Phenyl residue, 2) the hydrophobic chain of valine and 3) both the phenyl and valine side chain. The ^{1}H NMR chemical shift assignment of β-CD: (RGDfV) was performed by a sequential strategy using COSY to understand the host–guest interactions and to establish the self-aggregation state of pentapeptide (Figure 6.17). The inner diameter of β-CD is 6-6.5Å (*Del Valle, 2004*), and the size of the β-CD cavity being suitable to accommodate a phenyl group. Since the protons of the phenyl residue and methyl groups of valine show chemical shift differences (Table 6.3) between free c(RGDfV) and

complexed c(RGDfV): β-CD therefore, it is assumed that both the phenyl ring and isopropyl group of valine are inserted into the cavity of β-CD.

In addition, the changed environment of N-H is also evident from chemical shift difference (Table 6.3) suggesting strong interaction between c(RGDfV) and β-CD. The squashing of the secondary hydroxyl groups, the O(2)-H and O(3)-H) and disappearance of primary hydroxyl groups, O(6)-H in β-CD (Figure 6.14) demonstrate its strong hydrogen bonds formation with the polar side chains of arginine and aspartic acid in c(RGDfV) molecule. On the basis of chemical shift observations and the above discussions, the proposed structure of β-CD complex with c(RGDfV) is presented in Figure 6.16.

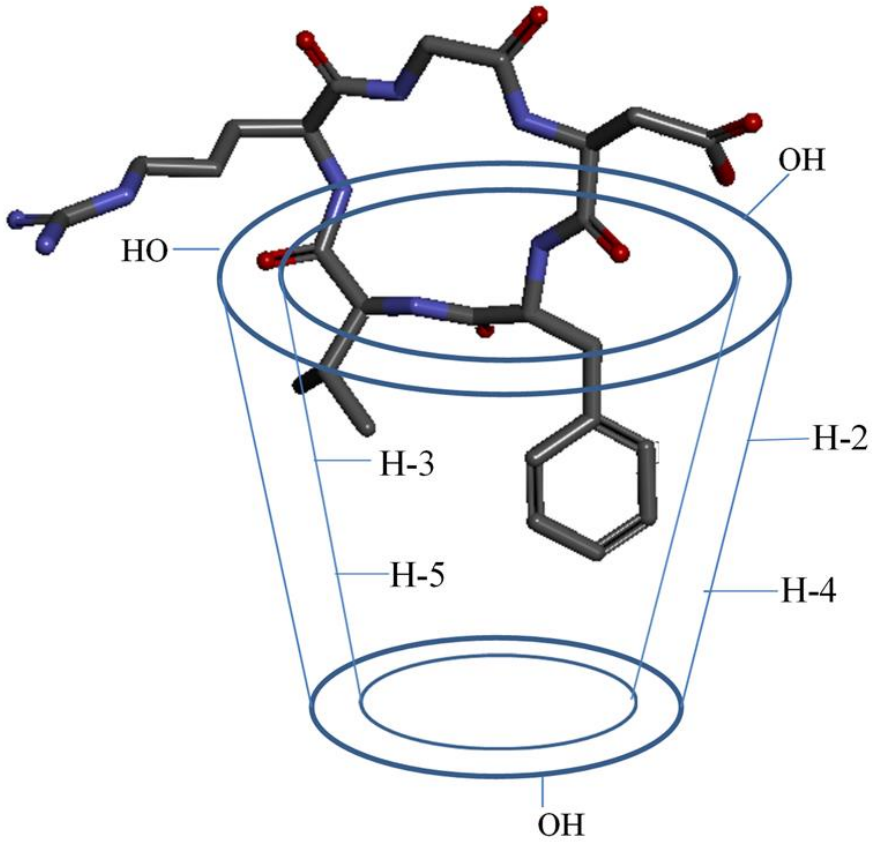

Figure 6.16 Possible inclusion geometry of β-CD with c(RGDfV) batch 1.

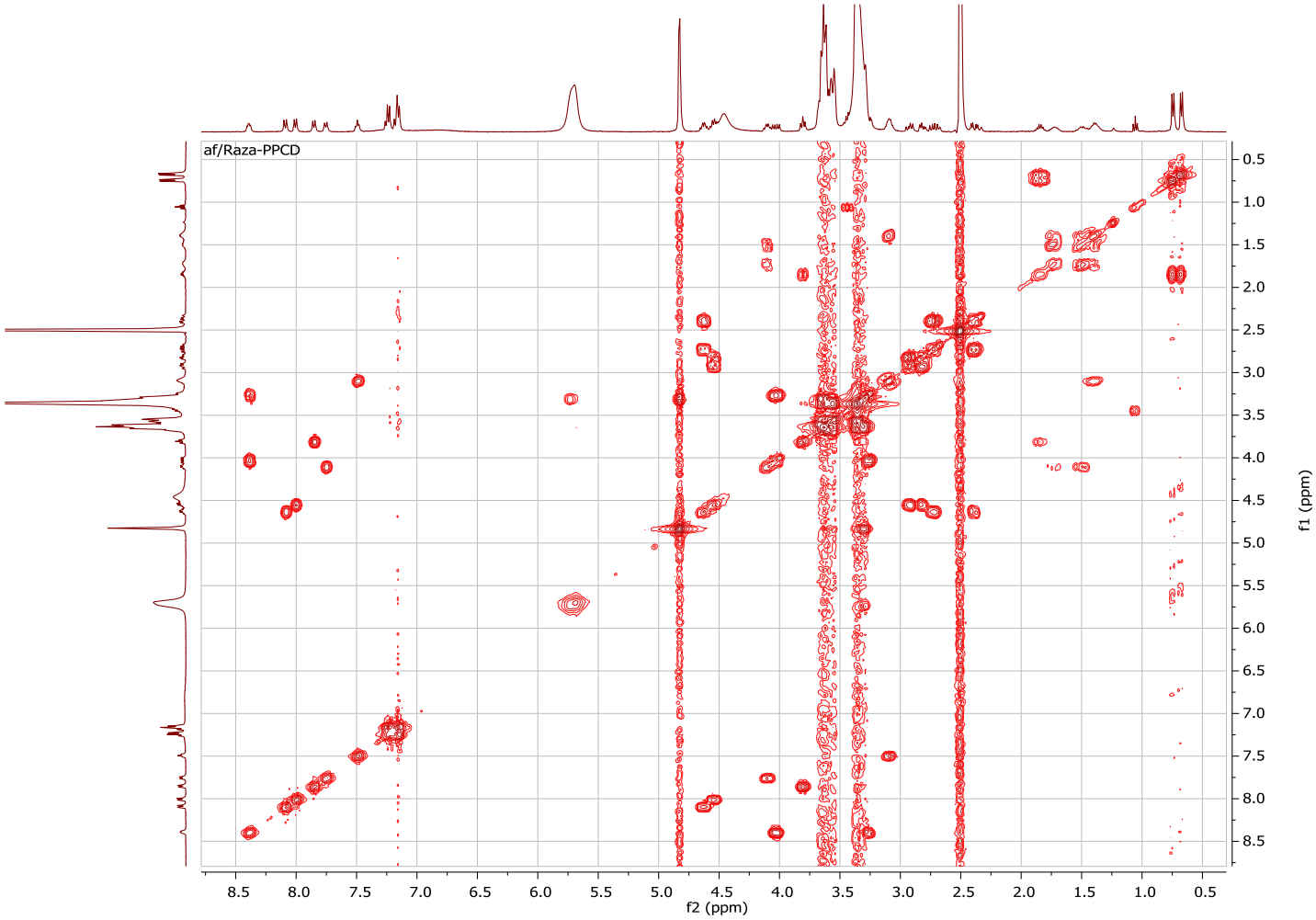

Figure 6.17 COSY counter map of c(RGDfV) (B-1): β-CD complex.

6.4.5.2. Batch to Batch variation or Conformational polymorphism

In order to study the association process between β-CD and c(RGDfV) another batch (B-2) of c(RGDfV) was purchased from the same supplier as the batch (B-1) was totally exhausted during the experiments. The certificate of analysis provided by the supplier was in agreement with the previous batch but it was surprising that the results of ^{1}HNMR and ^{13}CNMR presented in Figure 6.18 and Figure 6.19 respectively of the new batch (B-2) in comparison with the old batch (B-1) were showing different chemical shifts (Table 6.4) indicating a conformational difference between the two batches.

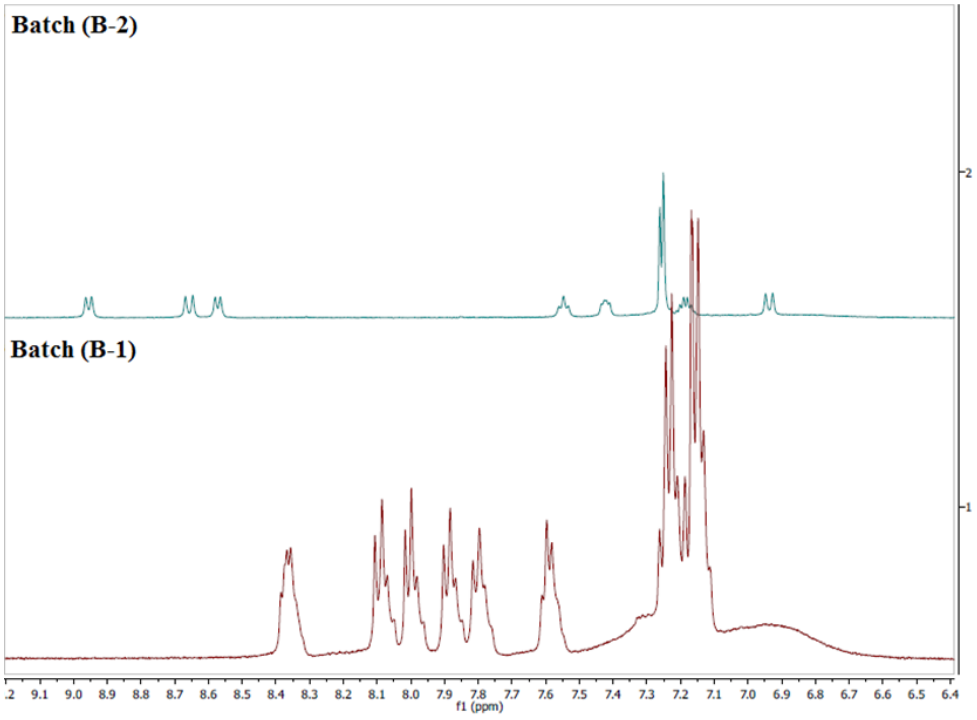

Figure 6.18 ^{1}H NMR spectra of c(RGDfV) batch (B-2) & batch (B-1).

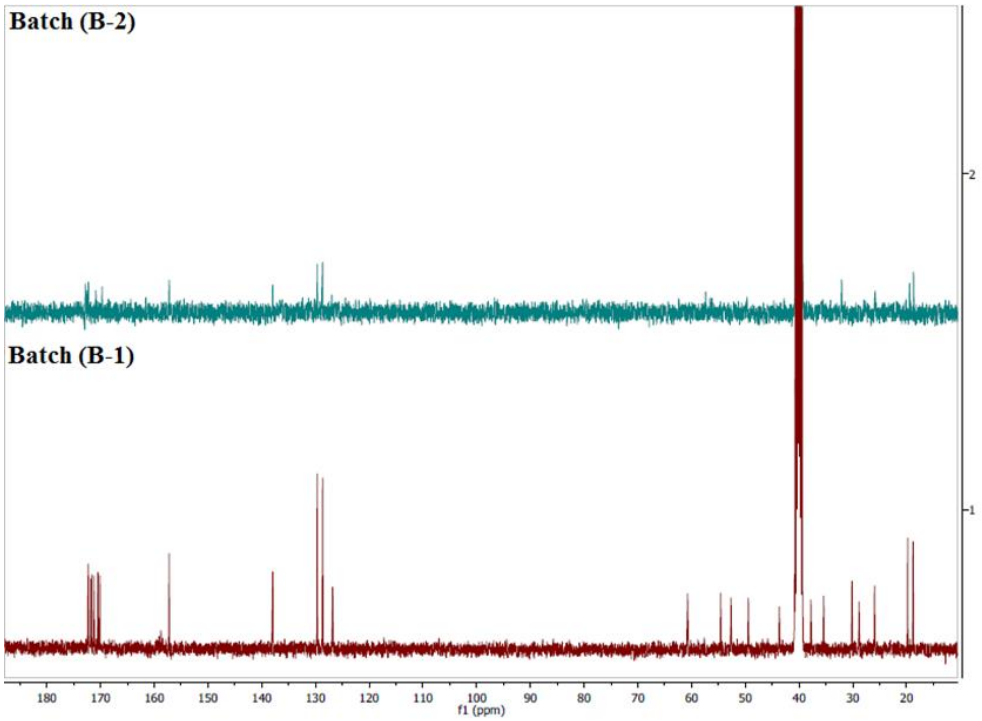

Figure 6.19 ^{13}C NMR spectra of c(RGDfV) batch (B-2) & batch (B-1).

The ^{1}H NMR and ^{13}C NMR spectrum clearly indicating that the two batches of c(RGDfV) although have the same configuration but they have different conformations.

To study the complex formation process of β-CD and c(RGDfV) batch (B-2), the same quantities and procedure used for the batch (B-1) was adopted. ^{1}H NMR spectra of pure components and c(RGDfV): β-CD mixture in a 1:1 molar ratio is shown in Figure 6.20. ^{1}H NMR signals were assigned using the same procedures adopted for the batch (B-1).

Table 6.4 Chemical shifts (ppm) for the proton and carbon of c(RGDfV) B-1 and B-2.

Position	c(RGDfV) New Batch (B-2) δ (ppm)		c(RGDfV) Old batch (B-1) δ (ppm)	
	H	C	H	C
1	8.59	---	7.80	---
2	3.83	56.8	4.11	52.7
3	---	173.2	---	171.8
4	7.42 (NH)	---	8.36(NH)	---
5	3.89, 3.63	43.0	4.03	43.7
6	---	173.0	---	170.1
7	8.64 (NH)	---	8.08(NH)	---
8	4.62	49.9	4.63	49.4
9	---	172.8	---	170.5
10	8.95 (NH)	---	8.01(NH)	---
11	4.29	56.7	4.53	54.6
12	---	170.2	---	171.3
13	6.93 (NH)	---	7.88(NH)	---
14	4.05	58.0	3.82	60.8
15	---	173.2	---	171.7
1’	1.62	32.6	1.84	30.2

Table 6.4 continued…..Chemical shifts (ppm) for the proton and carbon of c(RGDfV) B-1 and B-2.

Position	c(RGDfV) New Batch (B-2) δ (ppm)		c(RGDfV) Old batch (B-1) δ (ppm)	
	H	C	H	C
2’	0.66	19.2	0.67	18.8
3’	0.57	20.0	0.74	19.8
1’’	2.89, 2.78	36.5	2.81, 2.92	37.8
2’’	---	138.0	---	137.9
3’’	7.25	129.6	7.15	129.7
4’’	7.26	128.7	7.24	128.7
5’’	7.16	127.4	7.25	126.8
6’’	7.26	128.7	7.24	128.7
7’’	7.25	129.6	7.15	129.7
1’’’	2.44, 2.73	36.2	2.73	35.4
2’’’	---	171.9	---	172.3
1’’’’	1.66, 1.66	28.1	1.48, 1.72	28.9
2’’’’	1.52	26.2	1.39	26.0
3’’’’	3.10	41.0	3.08	40.8
4’’’’	7.55 (NH)	---	7.59(NH)	---
5’’’’	---	157.3	---	157.2

The NMR experiment for the new batch (B-2) were very surprising because there was no significant difference observed between the protons chemical shifts of c(RGDfV) and β-CD in their free and complexed state showing no complex formation between c(RGDfV) and the β-CD. In order to verify that the batch c(RGDfV) (B-2) may form inclusion complex at a different molar ratio than the batch c(RGDfV) (B-1), ^{1}H NMR spectra were collected for a series of five samples containing both the c(RGDfV) (B-2) and β-CD molecules with constant volume at varying proportions. The results are shown in Figure 6.21 and the chemical shifts are presented in Table 6.6. The results showed that the c(RGDfV) (B-2) form no inclusion complex in any of the tested molar ratio with the β-CD. The chemical shifts of the protons of β-CD and c(RGDfV) (B-2) compared with their complex are summarized in Table 6.5 and 6.6 respectively.

The NMR experiments with batch (B-2) of c(RGDfV) indicates that the molecule adopts a different conformation in solution as compared to batch (B-1) of c(RGDfV). This change in conformation might also be one of the reasons that the new batch (B-2) of c(RGDfV) could not make any complex with the beta-cyclodextrin due to their strong intramolecular hydrogen bonding as compared to intermolecular bonding with the host molecule.

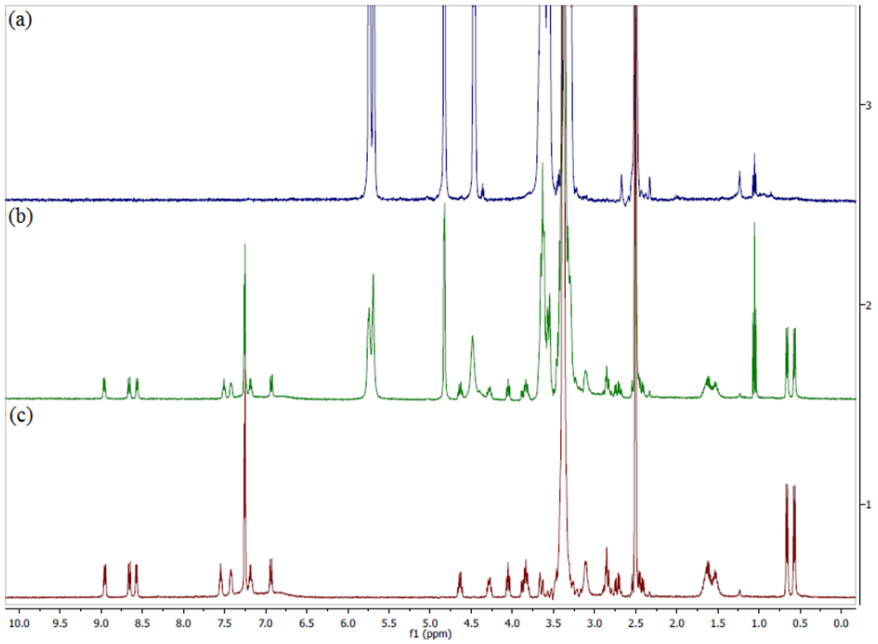

Figure 6.20 ^{1}H NMR spectra of a) β-CD, b) c(RGDfV): β-CD inclusion complex and c), c(RGDfV) (B-2) in DMSO-d6 at 400 MHz.

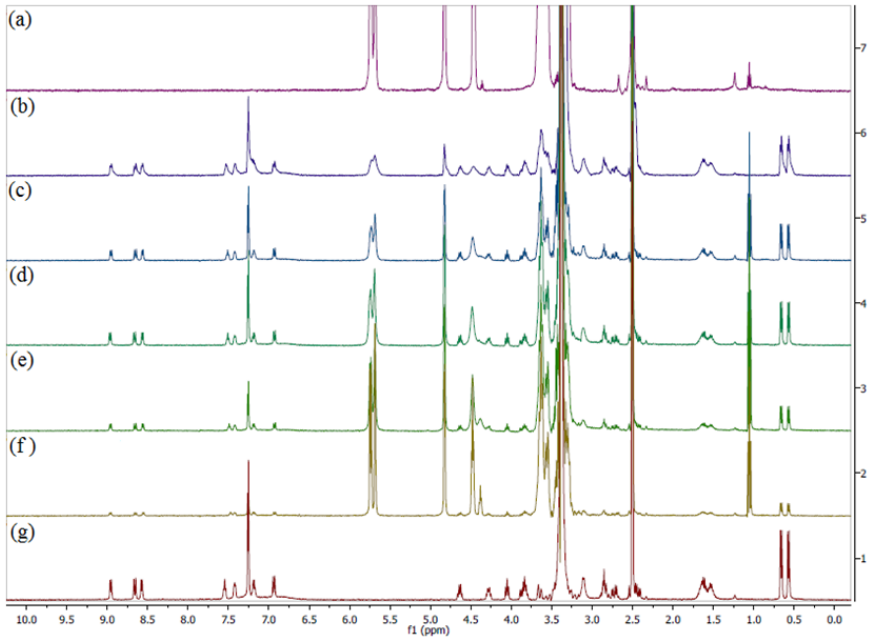

Figure 6.21 ^{1}H NMR spectrum of a) pure β-CD , c(RGDfV): β-CD mixture at molar ratio b) 3:1, c) 2:1, d) 1:1, e) 1: 2, f) 1:3, and g) pure c(RGDfV) (B-2).

Table 6.5 Chemical shifts (ppm) for the proton of β-CD in the different molar ratios of c(RGDfV (B-2) and β-CD.

Position	c(RGDfV): β-CD (3:1) δcomplex (ppm)	c(RGDfV): β-CD (2:1) δcomplex (ppm)	c(RGDfV): β-CD (1:1) δcomplex (ppm)	c(RGDfV): β-CD (1:2) δcomplex (ppm)	c(RGDfV): β-CD (1:3) δcomplex (ppm)
	H	H	H	H	H
1	4.83 J = 4Hz	4.82 J = 4Hz	4.82 J = 4Hz	4.83 J = 4Hz	4.82 J = 4Hz
2	3.30 (m)	3.32 (m)	3.32 (m)	3.31 (m)	3.32 (m)
3	3.62 (m)	3.64 (m)	3.64 (m)	3.64 (m)	3.62 (m)
4	3.31 (m)	3.32 (m)	3.32 (m)	3.31 (m)	3.32 (m)
5	3.38 (m)	3.38 (m)	3.38 (m)	3.38 (m)	3.38 (m)
6	3.63 (m)	3.63 (m)	3.63 (m)	3.63 (m)	3.63 (m)
2-OH	5.74	5.74	5.74	5.74	5.73
3-OH	5.69	5.68	5.68	5.68	5.69
6-OH	4.48	4.48	4.48	4.48	4.48

Table 6.6 Chemical shifts (ppm) for the proton of c(RGDfV) (B-2) in the different molar ratios of c(RGDfV (B-2) and β-CD.

Position	c(RGDfV): β-CD (3:1)	c(RGDfV): β-CD (2:1)	c(RGDfV): β-CD (1:1)	c(RGDfV): β-CD (1:2)	c(RGDfV): β-CD (1:3)
	H	H	H	H	H
1	8.56 (N-H)	8.57 (N-H)	8.56 (N-H)	8.56 (N-H)	8.56 (N-H)
2	3.83	3.83	3.83	3.83	3.82
3	---	---	---	---	---
4	7.41 (NH)	7.41 (NH)	7.42 (NH)	7.41 (NH)	7.41 (NH)
5	3.68, 3.87	3.67, 3.87	3.67, 3.87	3.66, 3.87	3.65, 3.86
6	---	---	---	---	---
7	8.65 (NH)	8.65 (NH)	8.65 (NH)	8.65 (NH)	8.64 (NH)
8	4.65	4.64	4.65	4.65	4.64
9	---	---	---	---	---

Table 6.6 continued…..Chemical shifts (ppm) for the proton of c(RGDfV) (B-2) in the different molar ratios of c(RGDfV (B-2) and β-CD.

Position	c(RGDfV): β-CD (3:1)	c(RGDfV): β-CD (2:1)	c(RGDfV): β-CD (1:1)	c(RGDfV): β-CD (1:2)	c(RGDfV): β-CD (1:3)
	H	H	H	H	H
10	8.95 (NH)	8.96(NH)	8.95(NH)	8.96(NH)	8.95(NH)
11	4.29	4.26	4.29	4.29	4.29
12	---	---	---	---	---
13	6.93 (NH)	6.93 (NH)	6.93 (NH)	6.93 (NH)	6.93 (NH)
14	4.07	4.06	4.06	4.07	4.06
15	---	---	---	---	---
1’	1.61,1.60	1.60, 1.61	1.60, 1.60	1.61, 1.61	1.61, 1.60
2’	0.68	0.67	0.67	0.67	0.61
3’	0.58	0.58	0.58	0.58	0.56

Table 6.6 continued….Chemical shifts (ppm) for the proton of c(RGDfV) (B-2) in the different molar ratios of c(RGDfV (B-2) and β-CD.

Position	c(RGDfV): β-CD (3:1)	c(RGDfV): β-CD (2:1)	c(RGDfV): β-CD (1:1)	c(RGDfV): β-CD (1:2)	c(RGDfV): β-CD (1:3)
	H	H	H	H	H
1''	2.86	2.85	2.86	2.87	2.86
2''	---	---	---	---	---
1'''	2.74, 2.45	2.75, 2.46	2.73, 2.45	2.73, 2.45	2.73, 2.44
2'''	---	---	---	---	---
1''''	1.67	1.65	1.65	1.66	1.66
2''''	1.54	1.54	1.54	1.54	1.53
3''''	3.10	3.11	3.10	3.11	3.10
4''''	7.54 (NH)	7.49(NH)	7.50 (NH)	7.51 (NH)	7.52 (NH)
5''''	---	---	---	---	---

6.4.6. Crystallisation of the c(RGDfV): β-CD inclusion complex.

Attempts to crystallise the inclusion complex c(RGDfV): β-CD and growing a single crystal via solution crystallisation methods were proved unsuccessful in almost every experiment and in most cases pure β-CD crystals were obtained (Figure 6.22). In one case crystals of pentapeptide and betacyclodextrin were obtained via vapour diffusion method (Figure 6.23) which was then analysed through Raman and showed both component in the crystal but surprisingly having no X-ray diffraction (Figure 6.24).

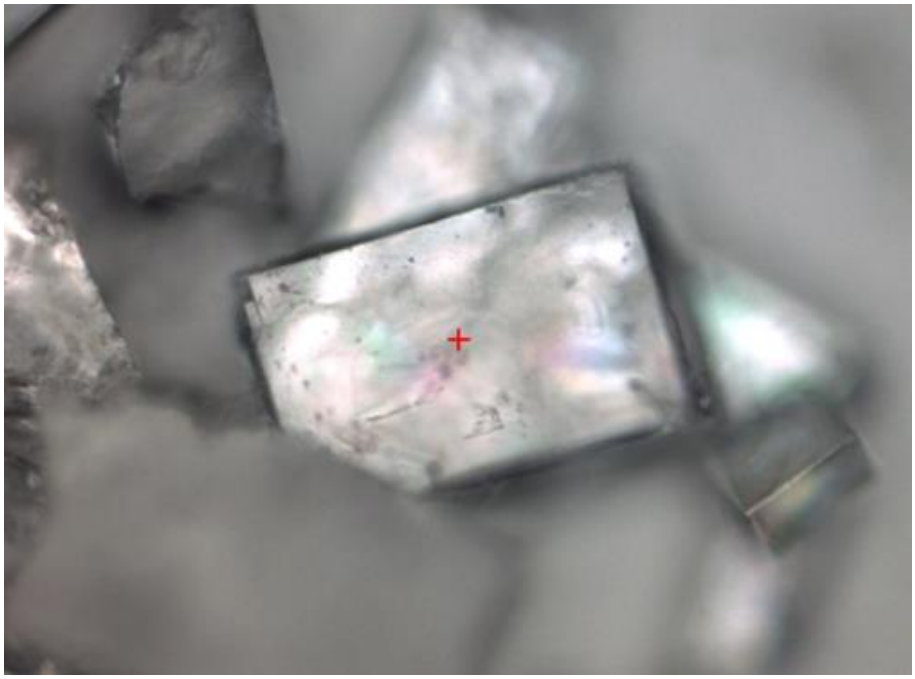

Figure 6.22 Single crystal of β-CD.

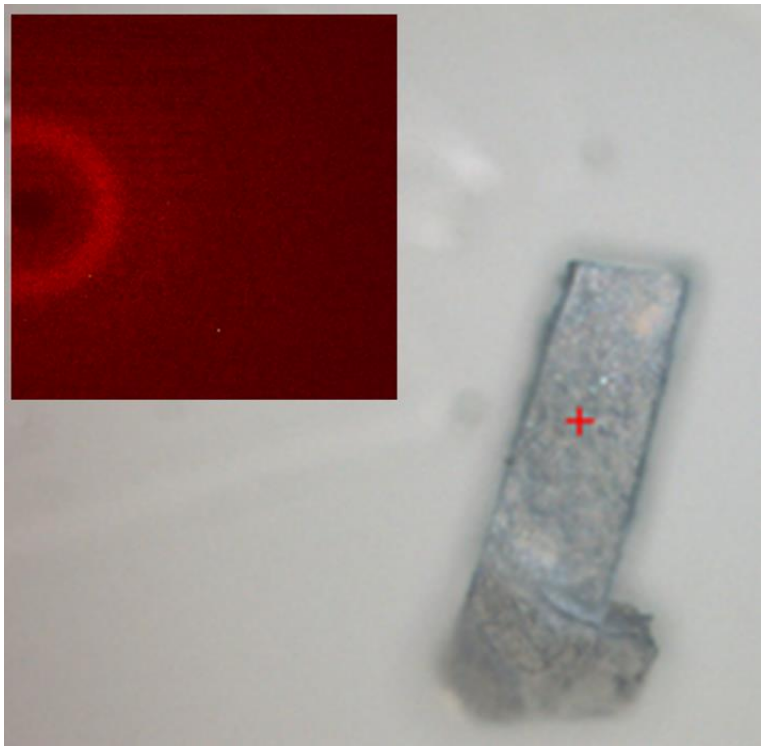

Figure 6.23 Single crystal of c(RGDfV) (B-1): β-CD complex showing no X-ray diffraction (inset).

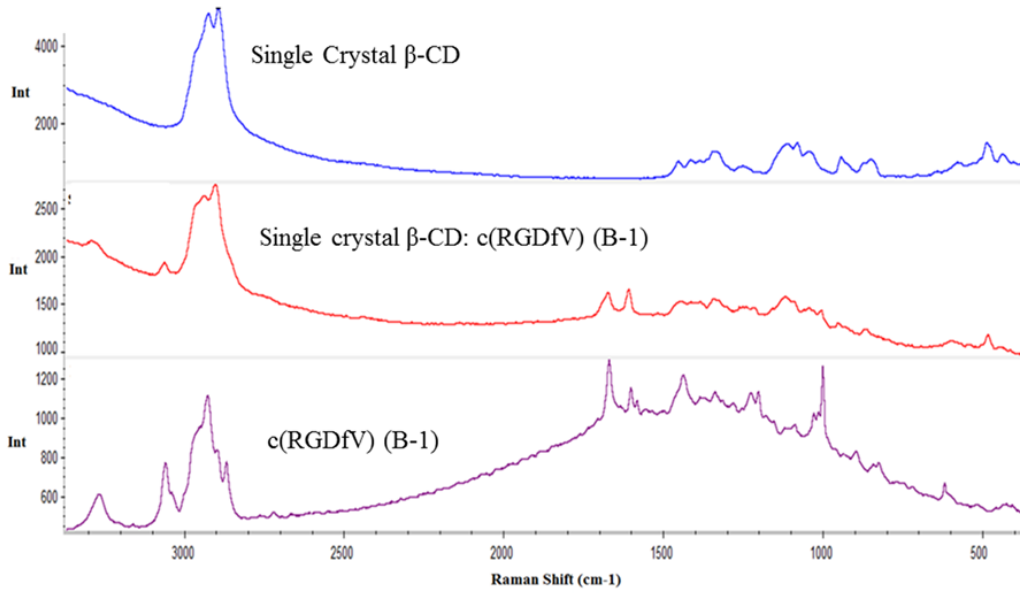

Figure 6.24 Raman spectrum of single crystal of β-CD, single crystal of inclusion complex and c(RGDfV) (B-1) raw material.

6.4.7 Crystallisation of c(RGDfV) batch (B-1).

In case of c(RGDfV), most of the crystallisation setup under various conditions it is observed that the peptide instead of crystallising out undergo some gel formation particularly in the aqueous medium whereas in other organic solvent it forms flakes. In couple of experiments single crystal were obtained (Figure 6.25 and Figure 6.26). The Raman spectrum were collected which when compared with the raw material of c(RGDfV) confirms that these crystals are of c(RGDfV). Similarly crystallites of c(RGDfV) were obtained from the acetonitrile and from Raman spectrum it is evident that they are representative of c(RGDfV) (Figure 6.27). The surprising part of the crystals was that none of them showed any X-ray diffraction.

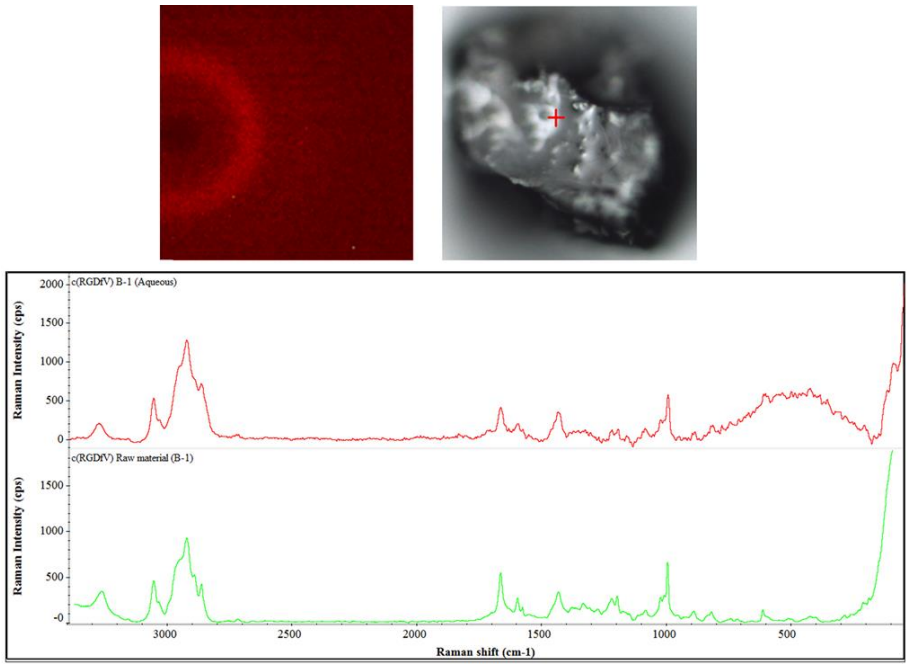

Figure 6.25 Single crystal of c(RGDfV) B-1grown from water showing no X-ray diffraction whereas, Raman spectrum of the same is comparable with the raw material.

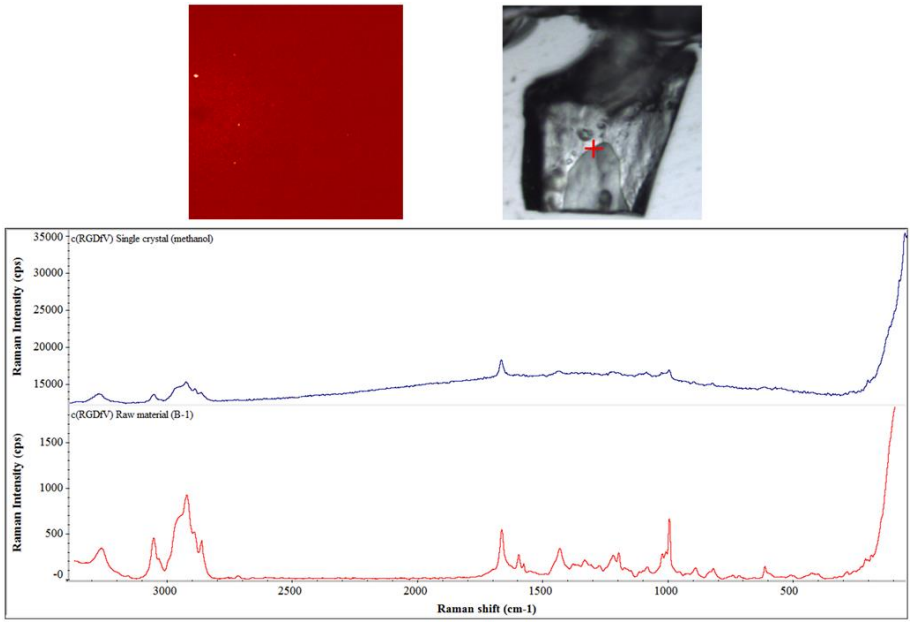

Figure 6.26 Single crystal of c(RGDfV) B-1grown from methanol showing insignificant X-ray diffraction whereas, Raman spectrum of the same is comparable with the raw material.

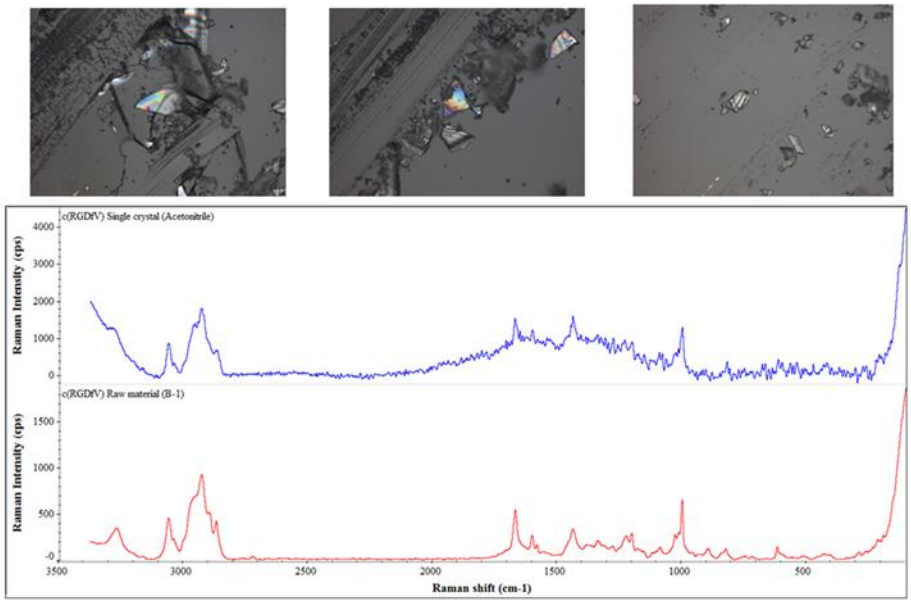

Figure 6.27 Crystallites of c(RGDfV) B-1grown from acetonitrile. Raman spectrum of these crystallites comparable with the raw material.

6.4.7.1 Crystal Screen 2™

Hampton crystallisation kit is an extensive crystallisation screen specially meant for the crystallisation of macromolecules. The three screens were monitored over a good period of time but unfortunately no crystal suitable for study was obtained. In crystal screen 1 most of the experimental conditions have shown clear drops and no change was observed. Based on screen 1 observations the concentration of the peptide was increased to overcome the assumption that crystal formation is not achieved due to low concentration of peptide. With the increase concentration either phase separation or precipitates formation is observed in few experimental setups but no crystal was formed. Some of the images from the screen are presented in Figure 6.28.

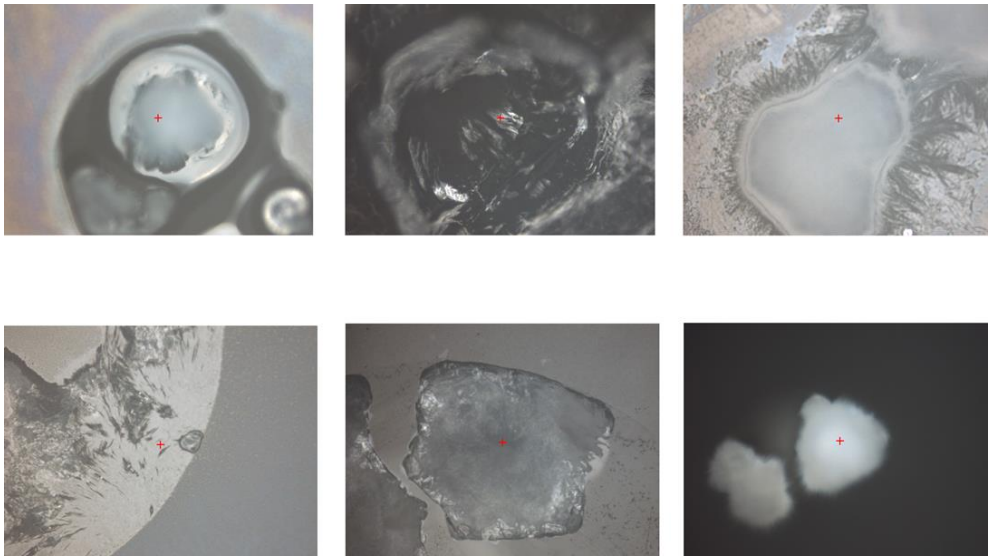

Figure 6.28 Images of different crystallisation screens showing various patterns of behaviour of c(RGDfV).

6.4.8 Self-assembly of c(RGDfV) to form hydrogel formation

The c(RGDfV) self-assembles to form a soft hydrogel. Samples were made according to the procedure described in methods, section 6.2.2.7. Figure 6.29 shows images of a series of c(RGDfV) hydrogels at 2, 3, 5 and 8 mg/ml and their gelation over time. The hydrogel formation was observed in 3mg/ml, 5mg/ml and 8mg/ml.

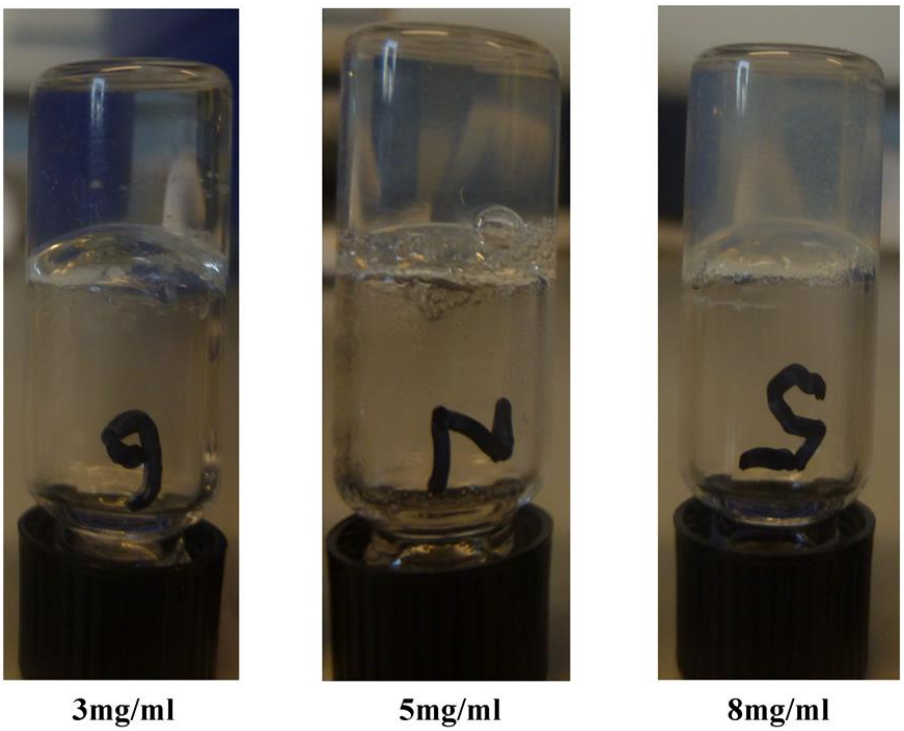

Figure 6.29 Series of c(RGDfV) hydrogels formed at 3, 5 and 8 mg/ml respectively). No flow was observed upon inversion.

The resulting hydrogels of 3mg/ml and 5mg/ml were translucent, homogeneous whereas, the peptide at 8mg/ml showed turbidity due to its insolubility at this concentration in water. All samples remained intact upon

inversion when fully formed exhibiting a cleared to a translucent, self-supporting structure. The most concentrated hydrogel (8mg/ml) was the quickest to form, taking approximately 3 to 5 min but the solution appears like a colloidal solution. The next lower concentration of c(RGDfV) (5mg/ ml) took longer to form and was fully set after 8 hours. In case of 3mg/ml the gel formation was observed over 24hours.

AFM images demonstrate evidence for self-assembly of c(RGDfV). The hydrogel with high peptide concentration 8 mg/ml showed poor self-assembly and fibres were heavily colloidal in nature (Figure 6.30) in comparison to the concentration at 5 mg/ml which gives very fine and well-organized network structures (Figure 6.31). The morphology of the hydrogel showed mesh networks of elongated fibres with diameters in a range of 30nm – 45 nm (Figure 6.32) providing clear evidence for self-assembly of peptide c(RGDfV) hydrogel.

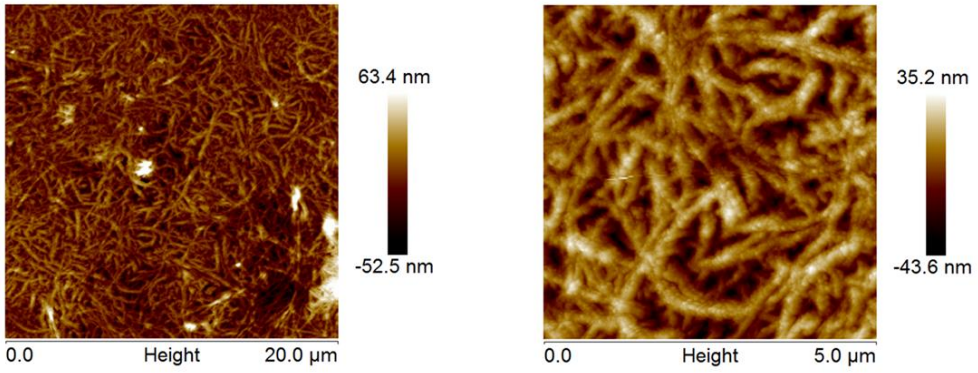

33

Figure 6.30 AFM images of c(RGDfV) at concentartion 8mg/ml.

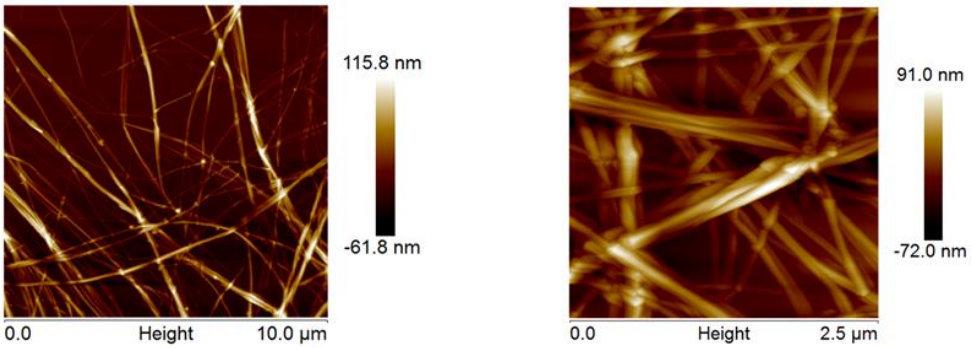

Figure 6.31 AFM images of c(RGDfV) at concentration 5mg/ml.

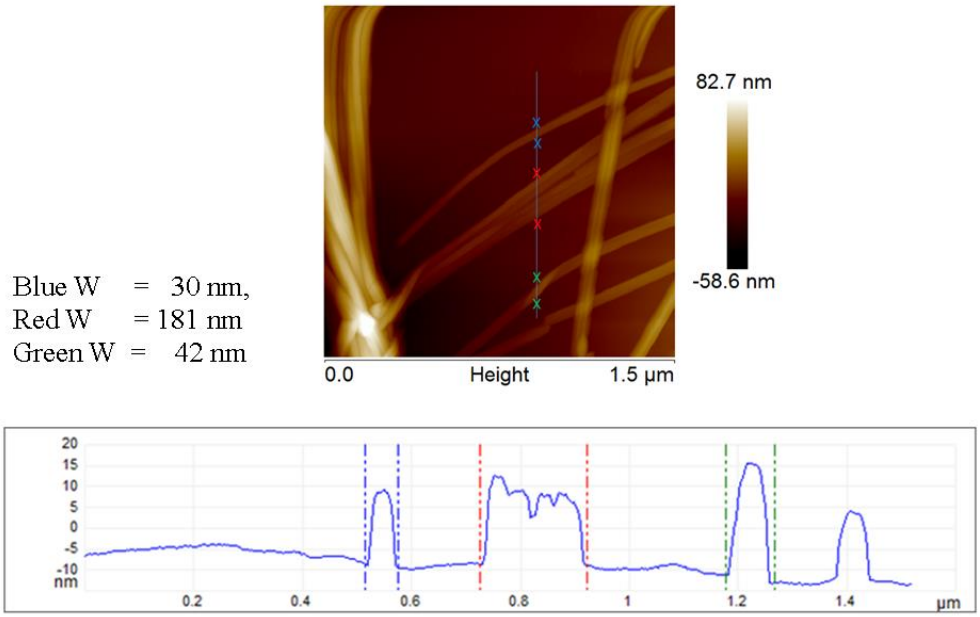

Figure 6.32 AFM image of c(RGDfV) at concentration 5mg/ml.

6.5. Summary

Complexation of the c(RGDfV) B-1penta peptide with beta cyclodextrin was accomplished by a freeze drying method. The inclusion complex was characterised by various analytical techniques including DSC, TGA, FTIR, PXRD and NMR. The structure of the inclusion complex was proposed based on NMR analysis suggesting the inclusion of both hydrophobic residues of the penta peptide molecule namely, Valine and the Phenyl side chains. The NMR analysis revealed the conformational difference between the two batches of the pentapeptide B-1 and B-2. The former batch showed no interaction with the beta cyclodextrin as observed in the NMR studies.

The pentapeptide demonstrated its ability to form hydrogel and an optimum concentration of the pentapeptide self-assemble to form well organised fibril structures as observed through AFM images. The crystallisation experiments of penta peptide alone and its inclusion complex with beta cyclodextrin to get crystals of suitable quality for X-ray diffraction studies were not successful.

6.6. References

Aida, T., Meijer, E.W., & Stupp, S.I. (2012). Functional supramolecular polymers. *Science.* 335 , 813.

Al-Rawashdeh, N.A.F., Al-Sadeh, K.S., & Al-Bitar, M.B. (2013). Inclusion Complexes of Sunscreen Agents with β-Cyclodextrin: Spectroscopic and Molecular Modeling Studies. *Journal of Spectroscopy.* Vol. 2013.

Astray, G., Barreiro, C.G., Mejuto, J.C., Otero, R.R., & Gandara, J.S. (2009). A review on the use of cyclodextrins in foods. *Food Hydrocolloids.* 23, 1631–1640.

Bekos, E.J., Gardella, J.A., & Bright, F.V. (1996). The binding of free oligopeptides to cyclodextrins, The role of the tyrosine group. *Journal of Inclusion Phenomena and Molecular Recognition in Chemistry*. 26, 185–195.

Banchero, M., Ronchetti, S., & Manna, L. (2013). Characterization of Ketoprofen/Methyl-β-Cyclodextrin Complexes Prepared Using Supercritical Carbon Dioxide. *Journal of Chemistry*. Vol. 2013.

Buschmann, H.J., & Schollmeyer, E. (2002). Applicationso of cyclodextrins in cosmetic products: A review. *Journal of Cosmetic Science*. 53, 185-191.

Craik, D.J., Fairlie, D.P., Liras, S., & Price, D. (2013). The Future of Peptide-based Drugs. *Chem Biol Drug Des.* 81, 136–147.

Del Valle, E.M.M. (2004). Cyclodextrins and their uses: a review. *Process Biochemistry.* 39, 1033–1046.

de Oliveira, V.E., Almeida, E.W.C., Castro, H.V., Edwards, H.G.M., Santos, H.F.D., & de Oliveira, L.F.C. (2011). Carotenoids and β-Cyclodextrin Inclusion Complexes: Raman Spectroscopy and Theoretical Investigation. *Journal of Physical Chemistry. A, 115* (30), 8511–8519.

Garcia, A., Leonardi, D., Salazar, M.O. & Lamas, M.C. (2014). Modified b-Cyclodextrin Inclusion Complex to Improve the Physicochemical Properties of Albendazole. Complete In Vitro Evaluation and Characterization hydrophobic cavity and a hydrophilic surface. *PLoS ONE 9*(2), e88234.

Greatbanks, D. & Pickford, R. (1987). Cyclodextrins as chiral complexing agents in water, and their application to optical purity measurements. *Magnetic Resonance in Chemistry. 25*(3), 208-215.

Hu, L., Zhanga, H., Songa, W., Gua, D. & Hu, Q. (2012). Investigation of inclusion complex of cilnidipine with hydroxypropyl-*β*-cyclodextrin. Carbohydrate Polymers. 90, 1719– 1724.

Irie, T. & Uekama, K. (1999). Cyclodextrins in peptide and protein delivery. *Advanced Drug Delivery Reviews*. 36 101–123.

Jerry, N., Anitha, Y., & Sharma, C.P. (2001). In vivo absorption studies of insulin from an oral delivery system. *Drug Delivery.* 8, 19–23.

Kaspar, A.A., & Reichert, J.M. (2013). Future directions for peptide therapeutics development. *Drug Discovery Today. 00* (00).

Kurkov, S.V., & Loftsson, T. (2013). Cyclodextrins. *International Journal of Pharmaceutics.* 453, 167–180.

Liu, B., Li, W., Zhao, J., Liu, Y., Zhu, X., & Liang, G. (2013). Physicochemical characterisation of the supramolecular structure of luteolin/cyclodextrin inclusion complex. *Food Chemistry.* 141, 900–906.

Loftsson, T., & Brewsterb, M.E. (2010).Pharmaceutical applications of cyclodextrins:basic science and product development. *Journal of Pharmacy and Pharmacology*. 62, 1607–1621.

Lula, I., de Sousa, F.B, Denadai, A.M.L., Ianzer, D., de Camargo A.C.M., R A Santos, R.A., & Sinisterra, R.D.(2011). Study of the BPP7a Peptide and its β-Cyclodextrin Complex: Physicochemical Characterization and Complete Sequence Specific NMR Assignments. Journal of Brazilian Chemical Society. Vol. 22, No. 9, 1765-1773.

Lula, I., Denadai, A.L., Resende, J.M., de Sousa, F.B., de Lima, G.F., Pilo-Veloso, D… & Sinisterra, R.D. (2007). Study of angiotensin-(1–7) vasoactive peptide and its b-cyclodextrin inclusion complexes: Complete sequence-specific NMR assignments and structural studies. *Peptides.* 28, 2199–2210.

Nicolescu, C., Arama, C., Monciu, C.M. (2010).Preparation and characterization of Inclusion Complexes between Repaglinide and β-

cyclodextrin, 2-hydroxypropyl β-cyclodextrin and randomly methylated β-cyclodextrin. *Farmacia. Vol. 58*, 1

Reardon, D.A., Fink, K.L., Mikkelsen, T., Cloughesy, T.F., O'Neill, A., Plotkin, S., …..& Nabors, L.B. (2008). Randomized phase II study of cilengitide, an integrin-targeting arginine-glycine-aspartic acid peptide, in recurrent glioblastoma multiforme. *Journal of Clinical Oncology. 26*(34), 5610-7.

Reardon, D.A., Neyns, B., Weller, M., Tonn, J.C., Nabors, L.B., & Stupp, R. (2011). Cilengitide: an RGD pentapeptide αvβ3 and αvβ5 integrin inhibitor in development for glioblastoma and other malignancies. *Future Oncology.7*(3), 339-54

Rekharsky, M.V. & Inoue, Y. (1998). Complexation Thermodynamics of Cyclodextrins. *Chemical Reviews.* 98, 1875−1917.

Singh M, Sharma R, Banerjee U.C. (2002). Biotechnological applications of cyclodextrins. Biotechnology Advances. 20, 341–359.

Stella, V.J. & He, Q. (2008). Cyclodextrins. *Toxicologic Pathology*. 36, 30-42.

Szejtli, J. (1998). Introduction and General Overview of Cyclodextrin Chemistry. *Chemical Reviews.* 98, 1743-1753.

Szejtli, J. (2004). Past, present, and future of cyclodextrin research. *Pure and Applied Chemistry. 76*(10), 1825–1845.

Szente, L., & Szejtli, J. (2004). Cyclodextrins as food ingredients. *Trends in Food Science & Technology*. 15, 137‑142.

Tiwari G., Tiwari R and Rai A K. (2010). Cyclodextrins in delivery systems: Applications. Journal of Pharmacy and Bioallied Sciences. Apr-Jun; 2(2): 72–79.

Tokihoro, K., Arima, H., & Tajiri, S. (2000). Improvement of subcutaneous bioavailability of insulin by sulphobutyl ether b-cyclodextrin in rats. *Journal of Pharmacy and Pharmacology*. 52, 911–917.

Wang L , Li L , Fan Y , and Wang H. (2013).Host–Guest Supramolecular Nanosystems for Cancer Diagnostics and Therapeutics. Advanced Materials. 25, 3888–3898

Yeguas, V., Altarsha, M., Monard, G., Lopez, R., &Ruiz-Lopez, M.F. (2011). Peptide Binding to β-Cyclodextrins: Structure, Dynamics, Energetics, and Electronic Effects. The Journal of Physical Chemistry A. 115, 11810–11817.

Yuan, Z., Zhu, M., & Han, S. (1999). Supramolecular inclusion complex formation and application of β-cyclodextrin with heteroanthracene ring cationic dyes. *Analytica Chimica Acta*. 389, 291-298.

Zhou H, Jiang L, Zhang Y, and Li J (2012). β-Cyclodextrin inclusion complex: preparation, characterization, and its aspirin release in vitro. Front. Material Science. 6(3), 259–267

CHAPTER 7

Conclusion and further work

7.1 Conclusion

Conclusion and future work is presented with reference to the experimental chapters of this thesis in the following sections.

7.1.1 Co-crystallisation of homochiral amino acids

The study revealed that co-crystals of the selected homochiral hydrophobic amino acids L-Leucine, L-Isoleucine and L-Valine can be formed by simple methods of crystallisation such as slow solvent evaporation and vapour diffusion. It was also shown in the study that a solid state grinding method to prepare the amino acids complexes of the selected series was not successful. The powdered samples were initially characterised using Raman and FTIR spectroscopy. The spectra showed a little difference compared to a mixture of the two contributing amino acids powder in the co-crystal. Single crystals of these multi-component systems prepared by solvent evaporation crystallisation technique were probed and it was evident that both constituent amino acids were present in the crystal and hence a co-crystal had been formed. Single crystals of sufficient diffraction quality showed disorder in the co-crystals and that the proportion of each constituent was not stoichiometric. However, there was no significant difference found in the proportion of the constituents although the crystals were grown from solutions of three different compositions: (1) equimolar, (2) a composition similar to that found in the crystals and (3) saturated with respect to each of the two components. The crystal structures of all the three amino acids co-crystals demonstrated that, similar to other hydrophobic amino acids, these complexes form a bi-layer arrangement which can be explained as a head to tail sequence wherein the

alpha amino group of one molecule is engaged with the alpha carboxylate group of the adjacent molecule. The conformation of the backbone skeleton in all the amino acids co-crystals is in good agreement with their parent components. There was no significant difference found in the torsion angles and intermolecular hydrogen- bond interactions. All the compounds had similar values for their conformations except in compound 1 where one molecule of Leucine in the asymmetric unit exhibited a *gauche*$^{(+)}$ conformation as compared to its parent crystal structure which adopts a *trans* conformation.

7.1.2 Bulk Preparation of amino acids co-crystals.

The work carried out in this project was to understand the initial steps towards the preparation of novel multi-component molecular complexes of L-Leucine, L-Isoleucine and L-Valine through controlled, rapid and continuous anti-solvent crystallisation method. The anti-solvent nucleation unit and the operating parameters were optimised for the continuous flow environment and a better control over rapid and reproducible production of the co-crystals. With optimised settings rapid crystallisation occurs which keeps nucleation and growth timescales as short as possible. Experiments showed that for a given mixing ratio (5 % stream 1 and 95 % stream 2) there was no difference in solid recovery behaviour when the residence time was increased from 0.5 minutes to 1 minutes or even 2 minutes. A mean residence time of 0.5 minutes was chosen for all experiments. Process control required the crystalliser vessel (V3) to be maintained at approximately ambient temperature to avoid crystal dissolution when the colder slurry warmed up after V3 withdrawal. Similarly, if the crystal slurry was above ambient temperature and cooled down after V3 withdrawal,

blockage of downstream transfer lines occurred due to nucleation and crystal growth. To achieve the desired ambient temperature in the crystal slurry, during the mean residence time of 0.5 minutes, the jacket of V3 needed to be heated substantially (55 °C). With the vessel jacket being significantly warmer than the bulk slurry, fouling of the crystalliser walls was reduced significantly. The hot jacket increased the temperature and solubility in the wall-liquid boundary layer sufficiently high so that it stayed very close to the saturation concentration. The short crystalliser mean residence time of 0.5 min., the constant flow of stream 1, stream 2 and withdrawal established a temperature gradient from the vessel wall to the vessel centre. This gradient ensured the bulk temperature only increased very little compared to the jacket therefore maintaining high supersaturation which was required for rapid crystallisation. Fouling and system blockage is a major challenge in continuous crystallisation and often leads to unwanted unit shut downs. Preventing fouling is essential and for that reason V3 was inserted into an ultrasonic bath (40 kHz, 50W), which was continuously operated during the run time of the experiment.

The powder characterisation of the bulk product revealed that the continuous anti-solvent crystallisation is a viable method for the production of amino acid complexes with high degree of purity and yield.

7.1.3 Host–guest complexation of β-cyclodextrin with c(RGDfV)

In this work, the inclusion complex of c(RGDfV) and β-CD has been prepared in aqueous media by a freeze drying method and intermolecular interactions between them was studied. The significant difference in FTIR, powder X-ray diffraction pattern and DSC thermogram of complex confirms the host-guest

inclusion complex of β-CD and c(RGDfV) of batch B-1. In addition, in ^{1}HNMR, the observed downfield chemical shift of proton H-3 and proton H-5 which are located in the cavity of β-CD suggest that in principle, the phenyl and valine residues, of c(RGDfV) of the batch B-1, which are hydrophobic groups are buried in the hydrophobic cavity of the β-CD and reveal clear evidence for inclusion phenomena. The study paved the way to investigate further this type of compound for the optimisation of its pharmacological properties and potential therapeutic use. The complex formation of c(RGDfV) B-1 with β-cyclodextrin may have the potential to modify various physico-chemical properties of the c(RGDfV) B-1 including solubility, stability and consequently, the bioavailability.

In the study it was also demonstrated that batch variation or conformational polymorphism is present in between two batches of c(RGDfV) purchased from the same supplier. The two batches showed different behaviour in the formation of inclusion complex with the β-CD and strongly suggest that the host molecule is selective with respect to the conformation of the peptide. Despite extensive efforts, our attempts to grow diffraction quality crystals of the inclusion complex and c(RGDfV) were not successful. The most significant barrier faced in the crystallisation study was the inherent nature of the c(RGDfV) to form a hydrogel. At low concentration or at saturated conditions the nuclei are not formed and the peptide molecule preferably undergoes gel formation which dominates over crystallisation process. The AFM images demonstrated that the c(RGDfV) self-assembled to form well organised structures and it will be worth it to investigate this further to see how these well

organised structures react to different stimuli and their potential use as an advanced biomaterial.

7.2 Further Work

7.2.1 Co-crystallisation of homochiral amino acids

The prospective area of further investigation of co-crystallisation of amino acids with the same chirality is to investigate other groups of naturally occurring amino acids. Extensive studies have been reported regarding co-crystallisation of acidic amino acids with organic bases and basic amino acids with organic acids resulting into co-crystals (*Gorbitz & Husdal, 1998*). One of the prospects is to study the complexes involving acidic amino acids (L-Aspartic acid, L-Glutamic acid etc.) and basic amino acids (L-Arginine, L-Histidine etc.). A comparison of the association between the crystal structures of LL amino acids and LD amino acid complexes can provide interesting details of the amino acid aggregation and the influence of chirality.

Another promising area for future work would be to explore the effects of high pressure on the co-crystals of hydrophobic amino acids, studied in this thesis. The co-crystals of hydrophobic amino acids mimic as a model system for biological membranes as these structures possess a bilayer structure similar to membranes. The exploration of the effect of pressure on multi-component systems is an area of study that has not received much attention. There have been a few studies related to the investigation of co-crystals under high pressure (*Zakharov, et al., 2013*) but no studies of the co-crystals of L-amino acids has been reported. The effect that pressure has on the side chains of these

amino acids is of particular interest as these structures possess large hydrophobic regions which can be compared to biological membranes. The interactions of the side chains in the membranes can cause changes in membrane rigidity which is key to the operation of transmembrane proteins (*Ohvo-Rekila et al., 2002*). Monitoring the changes in co-crystal structures of hydrophobic amino acids with respect to pressure will build an understanding with regards to the effect of the side chain configuration on the compressibility of each co-crystal and hence have some sense of the rigidity of the model membrane. In addition, how the packing of these chains alters with changes in components and applied forces should be studied.

7.2.2 Bulk Preparation of amino acids co-crystals.

The challenges encountered during large-scale production of co-crystals have restricted their industrial development. This thesis emphasised the anti-solvent continuous crystallisation as a potential scale-up method for co-crystals. There is a need to continue to develop more understanding in the area of continuous crystallisation with the objective of establishing continuous crystallisation as a bulk preparation method for co-crystals. Studying the influence of the operating parameters on purity and percentage yield of the product could be an interesting study subject. In addition, the learning of the nucleation mechanism of crystal formation during anti-solvent crystallisation of amino acids co-crystals would help to better govern and manage the process.

7.2.3 Host–guest complexation of β-cyclodextrin with c(RGDfV)

The following studies are proposed as being important to the further understanding of the phenomenon of inclusion complex and self-assembly of peptide to form hydrogels.

- A ^{1}H NMR and isothermal titration calorimetry studies of inclusion complex to understand binding constant.
- In-vitro and In-vivo studies of the inclusion complex may provide new development in formulation and potential therapeutic applications of the peptide molecule.

In recent years the self-assembling peptides forming hydrogels are of great interest in the field of pharmaceutical, biological and nanosciences. These materials have diversity in their applications in tissue engineering, drug delivery, bioengineering and have the potential to be employed as synthetic extracellular matrices. The following studies are important with regards to hydrogels:

1. Study of physical properties of c(RGDfV) hydrogel including gelation mechanisms and mechanical properties.
2. Investigation of the influence of different stimuli such as temperature, pH and salts on the properties of the c(RGDfV) hydrogel.

7.3 References

Gorbitz, C.H., & Husdal, J. (1998). Cocrystallizing agent for amino acids. II. The crystal structures of L-Histidine.4,5-Imidaoledicarboxylic acid(1:1) and L-Lysine.4,5- Imidaoledicarboxylic acid(1:1). *Acta Chemica Scandinavica*. 52, 218-226.

Ohvo-Rekila, H., Ramstedt, B., Leppimaki, P., &Slotte, J.P. (2002). Cholesterol interactions with phospholipids in membranes. *Progress in Lipid Research.* 41. 66–97.

Zakharov, B.A., Losev, E.A., & Boldyreva, E.V. (2013). A new high-pressure polymorph of a glycine-glutaric acid co-crystal: the same as the low-temperature form. *CrystEngComm.* 15, 1693.

APPENDIX

A.1 Crystal Screen 2™ reagent formulations.

Reagent.	Formulation
1.	2.0 M Sodium chloride, 10% w/v Polyethylene glycol 6,000
2.	0.5 M Sodium chloride, 0.01 M Magnesium chloride hexahydrate, 0.01 M Hexadecyltrimethylammonium bromide
3.	25% v/v Ethylene glycol
4.	35% v/v 1,4-Dioxane
5.	2.0 M Ammonium sulfate, 5% v/v 2-Propanol
6.	1.0 M Imidazole pH 7.0
7.	10% w/v Polyethylene glycol 1,000, 10% w/v Polyethylene glycol 8,000
8.	1.5 M Sodium chloride, 10% v/v Ethanol
9.	0.1 M Sodium acetate trihydrate pH 4.6, 2.0 M Sodium chloride
10.	0.2 M Sodium chloride, 0.1 M Sodium acetate trihydrate pH 4.6, 30% v/v (+/-)-2-Methyl-2,4-pentanediol
11.	0.01 M Cobalt(II) chloride hexahydrate, 0.1 M Sodium acetate trihydrate pH 4.6, 1.0 M 1,6-Hexanediol
12.	0.1 M Cadmium chloride hydrate, 0.1 M Sodium acetate trihydrate pH 4.6, 30% v/v Polyethylene glycol 400
13.	0.2 M Ammonium sulfate, 0.1 M Sodium acetate trihydrate pH 4.6, 30% w/v Polyethylene glycol monomethyl ether 2,000
14.	0.2 M Potassium sodium tartrate tetrahydrate, 0.1 M Sodium citrate tribasic dihydrate pH 5.6, 2.0 M Ammonium sulfate

Reagent no.	Formulation
15.	0.5 M Ammonium sulfate, 0.1 M Sodium citrate tribasic dihydrate pH 5.6, 1.0 M Lithium sulfate monohydrate
16.	0.5 M Sodium chloride, 0.1 M Sodium citrate tribasic dihydrate pH 5.6, 2% v/v Ethylene imine polymer
17.	0.1 M Sodium citrate tribasic dihydrate pH 5.6, 35% v/v tert-Butanol
18.	0.01 M Iron(III) chloride hexahydrate, 0.1 M Sodium citrate tribasic dihydrate pH 5.6, 10% v/v Jeffamine ® M-600 ®
19.	0.1 M Sodium citrate tribasic dihydrate pH 5.6, 2.5 M 1,6-Hexanediol
20.	0.1 M MES monohydrate pH 6.5, 1.6 M Magnesium sulfate heptahydrate
21.	0.1 M Sodium phosphate monobasic monohydrate, 0.1 M Potassium phosphate monobasic
0.1	M MES monohydrate pH 6.5, 2.0 M Sodium chloride
22.	0.1 M MES monohydrate pH 6.5, 12% w/v Polyethylene glycol 20,000
23.	1.6 M Ammonium sulfate, 0.1 M MES monohydrate pH 6.5, 10% v/v 1,4-Dioxane
24.	0.05 M Cesium chloride, 0.1 M MES monohydrate pH 6.5, 30% v/v Jeffamine ® M-600 ®
25.	0.01 M Cobalt(II) chloride hexahydrate, 0.1 M MES monohydrate pH 6.5, 1.8 M Ammonium sulfate
26.	0.2 M Ammonium sulfate, 0.1 M MES monohydrate pH 6.5, 30% w/v Polyethylene glycol monomethyl ether 5,000

Reagent no.	Formulation
27.	0.01 M Zinc sulfate heptahydrate, 0.1 M MES monohydrate pH 6.5, 25% v/v Polyethylene glycol monomethyl ether 550
28.	1.6 M Sodium citrate tribasic dihydrate pH 6.5
29.	0.5 M Ammonium sulfate,0.1 M HEPES pH 7.5, 30% v/v (+/-)-2-Methyl-2,4-pentanediol
30.	0.1 M HEPES pH 7.5, 10% w/v Polyethylene glycol 6,000, 5% v/v (+/-)-2-Methyl-2,4-pentanediol
31.	0.1 M HEPES pH 7.5, 20% v/v Jeffamine M-600 ®
32.	0.1 M Sodium chloride, 0.1 M HEPES pH 7.5, 1.6 M Ammonium sulfate
33.	0.1 M HEPES pH 7.5, 2.0 M Ammonium formate
34.	0.05 M Cadmium sulfate hydrate, 0.1 M HEPES pH 7.5, 1.0 M Sodium acetate trihydrate
35.	0.1 M HEPES pH 7.5, 70% v/v (+/-)-2-Methyl-2,4-pentanediol
36.	0.1 M HEPES pH 7.5, 4.3 M Sodium chloride
37.	0.1 M HEPES pH 7.5, 10% w/v Polyethylene glycol 8,000, 8% v/v Ethylene glycol
38.	0.1 M HEPES pH 7.5, 20% w/v Polyethylene glycol 10,000
39.	0.2 M Magnesium chloride hexahydrate, 0.1 M Tris pH 8.5, 3.4 M 1,6-Hexanediol
40.	0.1 M Tris pH 8.5, 25% v/v tert-Butanol
41.	0.01 M Nickel(II) chloride hexahydrate, 0.1 M Tris pH 8.5, 1.0 M Lithium sulfate monohydrate

Reagent no.	Formulation
42.	1.5 M Ammonium sulfate, 0.1 M Tris pH 8.5, 12% v/v Glycerol
43.	0.2 M Ammonium phosphate monobasic, 0.1 M Tris pH 8.5, 50% v/v (+/-)-2-Methyl-2,4-pentanediol
44.	0.1 M Tris pH 8.5, 20% v/v Ethanol
45.	0.01 M Nickel(II) chloride hexahydrate, 0.1 M Tris pH 8.5, 20% w/v Polyethylene glycol monomethyl ether 2,000
46.	0.1 M Sodium chloride, 0.1 M BICINE pH 9.0, 20% v/v Polyethylene glycol monomethyl ether 550
47.	0.1 M BICINE pH 9.0, 2.0 M Magnesium chloride hexahydrate
48.	0.1 M BICINE pH 9.0, 2% v/v 1,4-Dioxane, 10% w/v Polyethylene glycol 20,000

A.2 Crystallographic information file of compound 1, 2 and 3

Available on disk

A.3 Torsion angles of L-Valine, L-Leucine and L- Isoleucine

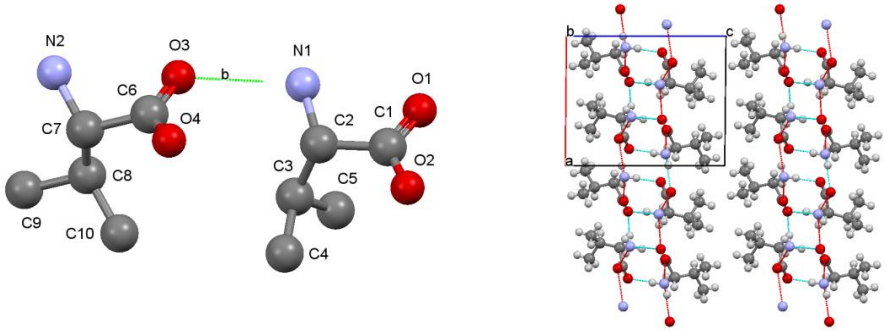

Table. Torsion angles of L-Valine in its crystal structure (Dalhus & Gorbitz, 1996).

Atom1	Atom2	Atom3	Atom4	Torsion
O1	C1	C2	N1	-17.5
O2	C1	C2	N1	164.7(1)
N1	C2	C3	C4	-154.3(1)
N1	C2	C3	C5	80.8(1)
C1	C2	C3	C4	83.6(1)
C1	C2	C3	C5	-41.3(1)
O3	C6	C7	N2	-42.8(1)
O4	C6	C7	N2	139.5(1)
N2	C7	C8	C9	-58.0(1)
N2	C7	C8	C10	179.0(1)
C6	C7	C8	C9	-178.5(1)
C6	C7	C8	C10	58.6(1)

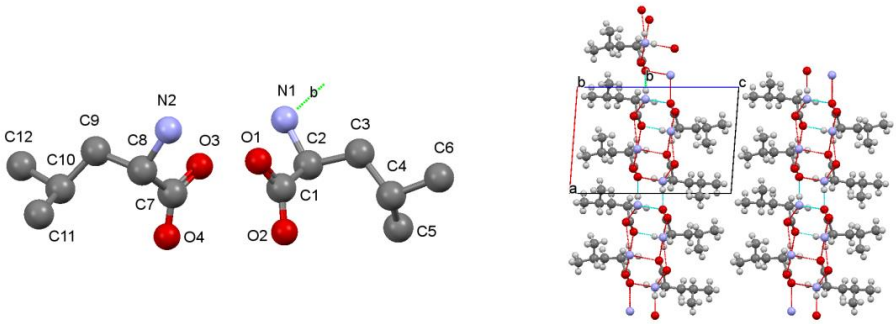

Table. Torsion angles of L-Leucine in its crystal structure (Gorbitz & Dalhus, 1996).

Atom1	Atom2	Atom3	Atom4	Torsion
O1	C1	C2	N1	-26.8(1)
O2	C1	C2	N1	155.4(1)
N1	C2	C3	C4	-176.81(9)
C1	C2	C3	C4	63.3(1)
C2	C3	C4	C5	64.6(1)
C2	C3	C4	C6	-174.3(1)
O3	C7	C8	N2	-32.3(1)
O4	C7	C8	N2	150.2(1)
N2	C8	C9	C10	-170.0(1)
C7	C8	C9	C10	69.8(1)
C8	C9	C10	C11	71.0(2)
C8	C9	C10	C12	-166.9(1)

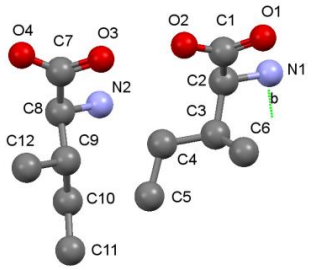

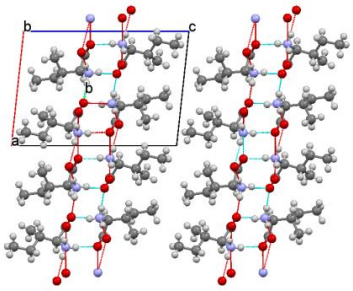

Table. Torsion angles of L-Isoleucine in its crystal structure (Gorbitz & Dalhus, 1996).

Atom1	Atom2	Atom3	Atom4	Torsion
O1	C1	C2	N1	-19.0(2)
O2	C1	C2	N1	164.1(1)
N1	C2	C3	C4	-155.0(1)
N1	C2	C3	C6	79.5(2)
C1	C2	C3	C4	82.5(2)
C1	C2	C3	C6	-43.0(2)
C2	C3	C4	C5	178.3(2)
O3	C7	C8	N2	-41.4(2)
O4	C7	C8	N2	141.5(2)
N2	C8	C9	C10	-56.9(2)
N2	C8	C9	C12	178.5(2)
C7	C8	C9	C10	-177.4(2)
C7	C8	C9	C12	57.9(2)
C8	C9	C10	C11	-176.3(2)